University of Nevada, Reno

# Time-Dependent Deflection of In-Span Hinges in Prestressed Concrete Box Girder Bridges

A dissertation submitted in partial fulfillment of the
requirements for the degree of Doctor of Philosophy in
Civil and Environmental Engineering

by

Ahmed Elsayed Youssif Akl

Dr. Mehdi Saiidi/Dissertation Advisor

May, 2015

THE GRADUATE SCHOOL

We recommend that the dissertation
prepared under our supervision by

**AHMED ELSAYED YOUSSIF AKL**

Entitled

**Time-Dependent Deflection of In-Span Hinges in Prestressed Concrete Box Girder Bridges**

be accepted in partial fulfillment of the
requirements for the degree of

DOCTOR OF PHILOSOPHY

Mehdi S. Saiidi, PhD, Advisor

David H. Sanders, PhD, Committee Member

Ahmad M. Itani, PhD, Committee Member

Ian G. Buckle, PhD, Committee Member

Sergiu M. Dascalu, PhD, Graduate School Representative

David W. Zeh, Ph. D., Dean, Graduate School

May, 2015

# Abstract

Post-tensioned multi-cell reinforced concrete bridges with in-span hinges in California have been experiencing undesirable and unexpected differential movements at expansion joints during and after construction. The deformation of in-span hinges in cast-in-place (CIP) prestressed concrete (PS) box girder bridges is referred to as "hinge curl" and is due to post tensioning forces. The difference between the elevations of the two sides of the hinge creates a bump on the road and presents a road hazard with risk to the travelling public safety. Accurate prediction of instantaneous and time-dependent deformation of superstructure in-span hinges is important to avoid mismatch at the intermediate expansion joints of bridges.

A method to estimate hinge curl was developed by the California Department of Transportation (Caltrans) through Memo to Designers (MTD) No. 11-34 and has been used in design. However, this method often leads to estimate of deformations that are different from those in the field. Hence, grinding of the superstructure at the hinge and other remedial measures are often necessary, and this results in extra cost and delay. The principal aims of this study was to evaluate the MTD method based on field measurements and analytical studies, identify the extent and sources of discrepancy between the estimated and actual "hinge curl" deflections, and propose a new method to more accurately estimate short-term and long-term hinge curl. The research presented in this dissertation consisted of six parts: (1) field measurement of hinge movements in five bridges, (2) analysis of data and comparison with the estimated movements using the current method, (3) analytical studies of the five bridges using relative simple models

utilizing software package SAP2000, (4) analytical studies of the five bridges using detailed finite element models utilizing ABAQUS, (5) analytical parametric studies of the effect of superstructure skew at abutments and horizontal curvature on the hinge curl, and (6) development of a new, practical method to improve on estimation of hinge curl.

Deflections of superstructures were measured and monitored for five bridges in the state of California during construction until bridges were opened to traffic. Temperature and relative humidity data were also collected during field measurements. The field data were analyzed and the correlation with the current method for estimating hinge curl was investigated. Hinge curls were estimated according to Caltrans MTD 11-34 with the aid of computer models developed using CTBridge software. Substantial differences between the field data and estimated hinge curls were noted due to the inaccurate boundary condition assumption and other issues determined in the current design equations. Analytical studies were conducted using two modelling approaches, stick model and finite element model, to further investigate the deformation behavior of the bridges. SAP2000 was utilized for the first modelling approach and a more sophisticated program, ABAQUS, was utilized for the second approach to capture the three-dimensional deformation behavior. Construction sequence and material time-dependent effects were modelled in both approaches. Parametric studies of the effect of skewed abutments and horizontal curvature on hinge curl were performed using the finite element approach on ABAQUS.

A new method was developed for estimating the immediate hinge curl. Modifications of the time-dependent deflection multipliers were proposed to improve prediction of the long term hinge curl. Hinge curls were calculated according to the

proposed method and compared to those measured for verification. The study validated the applicability of the proposed method for hinge curl prediction. The new method and the modifications were summarized in addition to a design example in a new proposed document with MTD format to facilitate adoption of the new method by Caltrans.

# Acknowledgements

This dissertation is based on a research project funded by the California Department of Transportation (Caltrans) through grant No. 65A0390: *Post-Tensioned Bridge Hinge Curl*. Any opinion expressed in this dissertation are those of the author and do not necessarily present the views of the sponsor. Special thanks are due to Ms. Kamal Sah, the Caltrans Research Program Manager in the initial part of the project and to Mr. Hamid Ikram, the current Caltrans Research Program Manager, for their support and advice. The interest and comments of Mr. Marc Friedheim, Ms. Sue Hida, and Mr. Juan Araya, and Mr. Don Nguyen-Tan of Caltrans are also much appreciated. The research team is indebted to the Caltrans structural representatives and other Caltrans field staff for their tremendous assistance. Specifically the following individuals are thanked for facilitating the data collection at different bridge sites: Mr. Houshang Alishahi; Mr. David Muwanes, Mr. Amir Hassoun, and Mr. Richard Julodow; Mr. Jack Rothaus, Mr. Joshua Burke, and Mr. John Lammers; Mr. Sam Singh, and Mr. Raman Guraya; Mr. Juan Torres, and Mr. Purisimo Rosal.

I would like to express my sincere gratitude and appreciation to my advisor, Dr. Mehdi Saiidi, for his advice, tireless effort, support and friendship throughout this study. Further, working with Dr. Saiidi was one of the most rewarding experiences of my life. This work would not have been possible without his guidance and encouragement. I also would like to thank Dr. Ashkan Vosooghi for the valuable comments and input he provided in this research work. His time and efforts are greatly appreciated.

I would like to extend my appreciation to Dr. David Sanders, Dr. Ahmad Itani, Dr. Ian Buckle, and Dr. Sergiu Dascalu for agreeing to serve on my committee.

I am very grateful to my family for their constant prayers and support. I would like to especially thank my parents, Dr. Sayed and Ibtesam, my first and best teachers, for their endless love, unconditional support, and encouragement. I also thank my brothers (Youssif and Mohamed) and my sister (Aya) for their continuous encouragement and help.

I thank my dear wife, Rehab, for her love and patience throughout this academic journey. Her constant sacrifice and support are what made this work achievable. I also credit my beloved daughters, Nour and Hala, for amusing me every day.

I want to thank all my friends and current/former colleagues in Reno for their social and academic support during my study, including:
Dr. Sherif Elfass, Mohammadreza Saba, Mohamed Salem, Mostafa Tazarv, Amarjeet Saini, Camila Coria, Ali Mehrsoroush, Alex Larkin, Zachary Haber, Mohammed Saeed, Emma Crossman, Mark Lattin, Mehrdad Mehraein, Brian Nakashoji, Islam Mantawy, Fatemeh Kavianipour, Ahmed Farghal, and Mahmoud Ahmad.
Special thanks go to Ahmad Saad and his family for their support and generosity.

# Table of Contents

Abstract ..... i
Acknowledgements ..... iv
Table of Contents ..... vi
List of Tables ..... xi
List of Figures ..... xiii
Chapter 1 Introduction ..... 1
1.1 Background ..... 1
1.2 Problem Statement ..... 3
1.3 Previous Research ..... 3
1.4 Objectives and Scope ..... 8
1.5 Dissertation Outline ..... 10
Chapter 2 Description of the bridges ..... 11
2.1 Introduction ..... 11
2.2 Bridge type ..... 11
2.3 In-span hinges ..... 12
2.4 Falsework ..... 14
2.5 Prestressing ..... 15
2.6 Prestressing steel ..... 16
2.7 Details of sample bridges ..... 17
2.7.1 Bridge 1: San Luis Rey River Bridge ..... 17
2.7.2 Bridge 2: N170-N5 Connector ..... 18
2.7.3 Bridge 3: Bradley Overhead ..... 20
2.7.4 Bridge 4: EB Wilshire Blvd On-Ramp OC ..... 21
2.7.5 Bridge 5: Del Paso Park Overhead ..... 22
2.7.5.1 Bridge 5EB ..... 23
2.7.5.2 Bridge 5WB ..... 25
Chapter 3 Field Measurements ..... 27
3.1 Introduction ..... 27
3.2 Data acquisition instruments ..... 28
3.3 Deflection measurement methodology ..... 29

3.3.1 Bridge 1 ..... 31
3.3.2 Bridge 2 ..... 32
3.3.3 Bridge 3 ..... 33
3.3.4 Bridge 4 ..... 34
3.4 Bridge 5 ..... 35
3.4.1 Bridge 5EB ..... 36
3.4.2 Bridge 5WB ..... 37
Chapter 4 Measured Data Analysis and Interpretation ..... 39
4.1 Introduction ..... 39
4.2 Immediate deformations ..... 39
4.2.1 Bridge 1 ..... 39
4.2.2 Bridge 2 ..... 40
4.2.3 Bridge 3 ..... 42
4.2.4 Bridge 4 ..... 42
4.2.5 Bridge 5 ..... 43
4.3 Time-dependent deformation ..... 43
4.3.1 Phase 1- before load transfer ..... 44
4.3.1.1 Bridge 1 ..... 44
4.3.1.2 Bridge 2 ..... 44
4.3.1.3 Bridge 3 ..... 45
4.3.1.4 Bridge 4 ..... 46
4.3.1.5 Bridge 5 ..... 46
4.3.2 Phase 2 - After load transfer ..... 48
4.3.2.1 Bridge 1 ..... 48
4.3.2.2 Bridge 2 ..... 49
4.3.2.3 Bridge 3 ..... 50
4.3.2.4 Bridge 4 ..... 50
4.3.2.5 Bridge 5 ..... 51
4.4 Hinge curl history ..... 51
4.4.1 Bridge 1 ..... 51
4.4.2 Bridge 2 ..... 52
4.4.3 Bridge 3 ..... 53

4.4.4 Bridge 4 ..... 53
4.4.5 Bridge 5 ..... 54
4.5 Deformation behavior of non-PS hinges ..... 55
4.6 Temperature and relative humidity effect ..... 56
4.7 Summary of field measurement findings ..... 57
Chapter 5 Comparison of Measured and MTD 11-34 Hinge Curls ..... 59
5.1 Introduction ..... 59
5.2 MTD 11-34 Method ..... 59
5.2.1 Method of calculation ..... 60
5.2.2 Development of camber diagram ..... 65
5.2.3 CTBridge analysis ..... 68
5.3 Comparison of MTD estimated and measured hinge curls ..... 69
5.3.1 Immediate hinge curl ..... 69
5.3.2 Time-dependent hinge curl ..... 70
5.3.2.1 Before load transfer ..... 71
5.3.2.2 After load transfer ..... 71
5.4 Evaluation of MTD 11-34 ..... 73
Chapter 6 Analytical Studies with Stick Models ..... 77
6.1 Introduction ..... 77
6.2 Geometry of the analytical models ..... 77
6.2.1 Superstructures and bents ..... 78
6.2.2 Tendons ..... 79
6.2.3 Falsework ..... 80
6.3 Material properties ..... 81
6.3.1 Concrete ..... 81
6.3.2 Prestressing steel ..... 82
6.3.3 Time-dependent properties ..... 82
6.4 Boundary Conditions and constraints ..... 83
6.5 Loading ..... 84
6.5.1 Load cases ..... 84
6.5.2 Construction stages ..... 85
6.6 Analytical model of the long cantilever frame ..... 85

6.7 Summary ..... 87
Chapter 7 Finite Element Analysis of Bridges ..... 88
7.1 Introduction ..... 88
7.2 Finite element modeling of bridge frames with short cantilevers ..... 88
7.2.1 Geometry ..... 88
7.2.1.1 Superstructure and bents ..... 89
7.2.1.2 Prestressing tendons ..... 89
7.2.1.3 Falsework ..... 90
7.2.2 Elements and meshing ..... 91
7.2.3 Material models ..... 91
7.2.3.1 Concrete ..... 92
7.2.3.2 Prestressing steel ..... 95
7.2.3.3 Falsework ..... 95
7.2.4 Boundary conditions and constraints ..... 95
7.2.5 Loads ..... 96
7.2.6 Analysis and loading steps ..... 97
7.3 Finite element modeling of the long cantilever frame ..... 98
Chapter 8 Comparison of Measured and Calculated Results and Parametric Studies ..... 99
8.1 Introduction ..... 99
8.2 SAP2000 analysis results ..... 99
8.3 ABAQUS analysis results ..... 101
8.4 Correlation between analytical results and field data ..... 103
8.5 Effect of geometry of bridges on the hinge curl ..... 106
8.5.1 Effect of skew angle of abutment ..... 107
8.5.2 Effect of horizontal curvature ..... 108
Chapter 9 Proposed Method for Hinge Curl Estimation ..... 109
9.1 Introduction ..... 109
9.2 Proposed method to estimate hinge curl ..... 109
9.2.1 Immediate hinge curl ..... 109
9.2.1.1 Hinge curl due to flexibility of the short cantilever support ..... 110
9.2.2 Time-dependent hinge curl ..... 115
9.2.2.1 Before load transfer ..... 116

9.2.2.2 After load transfer ..... 118
9.3 Verification of the proposed method ..... 120
9.3.1 Measured and calculated hinge curls ..... 120
9.3.2 Falsework forces ..... 123
9.4 Proposed changes to MTD 11-34 ..... 124
Chapter 10 Summary and Conclusions ..... 126
10.1 Summary ..... 126
10.2 Observations ..... 129
10.3 Conclusions ..... 131
References ..... 133
APPENDIX A ..... 279
APPENDIX B ..... 280

# List of Tables

Table 2-1 Summary of bridges ..... 138
Table 2-2 Summary of hinges ..... 138
Table 2-3 Prestressing design parameters ..... 138
Table 3-1 Field measurements schedule for Bridge 1 ..... 139
Table 3-2 Field measurements schedule for Bridge 2 ..... 139
Table 3-3 Field measurements schedule for Bridge 3 ..... 140
Table 3-4 Field measurements schedule for Bridge 4 ..... 140
Table 3-5 Field measurements schedule for Hinge 1 and Hinge 4, Bridge 5 ..... 141
Table 3-6 Field measurements schedule for Closure 1 and 2, Bridge 5EB ..... 142
Table 3-7 Field measurements schedule for Hinge 2 and 3, Bridge 5WB ..... 143
Table 4-1 Temperature and relative humidity data recorded for Bridge 1 ..... 144
Table 4-2 Temperature and relative humidity data recorded for Bridge 2 ..... 144
Table 4-3 Temperature and relative humidity data recorded for Bridge 3 ..... 144
Table 4-4 Temperature and relative humidity data recorded for Bridge 4 ..... 145
Table 4-5 Temperature and relative humidity data recorded at Hinge 1, Bridge 5EB ... 145
Table 4-6 Temperature and relative humidity data recorded at Closure 1 and Closure 2, Bridge 5EB ..... 146
Table 4-7 Temperature and relative humidity data recorded at Hinge 4, Bridge 5WB .. 147
Table 4-8 Temperature and relative humidity data recorded at Hinge 2 and Hinge 3, Bridge 5WB ..... 147
Table 5-1 Deflection of the short cantilevers due to dead load ..... 148
Table 5-2 Deflection of the short cantilevers due to prestressing force ..... 148
Table 5-3 Comparison of estimated and measured immediate hinge curl ..... 149
Table 5-4 Comparison of estimated and measured hinge curl on Day 1 ..... 149
Table 5-5 Comparison of estimated and measured time-dependent hinge curl before load transfer ..... 150
Table 5-6 Deflection of the short cantilevers due to load transfer ..... 150
Table 5-7 Calculated Adjustment “SC” for different times ..... 151
Table 5-8 Theoretical camber at hinges and deflections due to joint rotation ..... 151
Table 5-9 Hinge curl comparison after load transfer ..... 152
Table 9-1 Deflection factor values for the current and proposed methods ..... 153

Table 9-2 Comparison of immediate (Day 0) measured and proposed hinge curl ..... 153
Table 9-3 Comparison of Day 1 measured and proposed hinge curl..... 154
Table 9-4 Comparison of time-dependent measured and proposed hinge curl before load transfer ..... 155
Table 9-5 Comparison of measured and proposed hinge curl after load transfer..... 156
Table 9-6 Falsework forces (SAP2000)..... 157
Table 9-7 Falsewrok forces (ABAQUS)..... 157
Table 9-8 Comparsion of the net upward load acting on adjacent span ($W_u$) ..... 158

# List of Figures

Figure 1-1 Bridge falsework, Del Paso Park Overhead, Sacramento ..... 159

Figure 1-2 Hinge span in a continuous CIP/PS box girder bridge..... 159

Figure 1-3 In-span hinges of CIP/PS box girder bridges: (a) N170-N5 Connector, Los Angeles; (b) Del Paso Park Overhead (East Bound), Sacramento ..... 160

Figure 1-4 Construction of in-span hinges in CIP/PS box girder bridge..... 160

Figure 1-5 Hinge curl during construction..... 161

Figure 1-6 Hinge curl repair process in N170-N5 Connector, Los Angeles: (a) Discussion between Caltrans engineer and concrete grinder operator; (b) Caltrans engineer while monitoring the grinding operation; (c) Measuring grinding thickness; (d) Deck surface at the hinge after concrete grinding ..... 162

Figure 1-7 Hinge curl repair process in Bradley Overhead, Merced: (a) Chipping concrete cover of top deck reinforcement for long cantilever; (b) Rubble cleanup; (c) Deck surface at the hinge after roughening concrete of the long cantilever and grinding concrete of the short cantilever..... 163

Figure 1-8 Hinge curl repair by loading the short cantilever of an in-span hinge in Del Paso Park Overhead, Sacramento ..... 163

Figure 1-9 Adjustable falsework posts, Del Paso Park Overhead, Sacramento ..... 164

Figure 1-10 Thick concrete cover for top deck reinforcement, Del Paso Park Overhead, Sacramento..... 164

Figure 2-1 Typical longitudinal view of a Bridge with two in-span hinges ..... 165

Figure 2-2 Typical hinge span of an in-span hinge..... 165

Figure 2-3 Typical in-span hinge of CIP/PS bridge..... 165

Figure 2-4 Temporary fill of joint seal assembly blockout void ..... 166

Figure 2-5 Deck grinding at the hinge area using a grinding machine..... 166

Figure 2-6 Deck joint seals after installation: (a) Joint seal assembly; and (b) Bonded joint seal..... 167

Figure 2-7 Typical falsework bent..... 167

Figure 2-8 Falsework posts: (a) Steel posts; and (b) Timber posts..... 168

Figure 2-9 Falsework spanning over: (a) roadway at N170-N5 Connector; and (b) railway at Bradley Overhead ..... 168

Figure 2-10 (a) Skew falsework bents at Del Paso Park OH; (b) Outrigger falsework bent at Wilshire Blvd..... 168

Figure 2-11 Partial falsework removal at: (a) N170-N5 Connector; and (b) Del Paso Park OH..... 169

Figure 2-12 Falsework removal in: (a) hinge span; and (b) adjacent span ..... 169
Figure 2-13 Prestressing process at: (a) Hinge; (b) Abutment ..... 169
Figure 2-14 Stressing sequence at: (a) Hinge 7, Bridge 1; (b) Abutment 9, Bridge 4 .... 170
Figure 2-15 Prestressing operational issues: (a) Stressing hoist transfer; (b) Stressing jack transfer; (c) Hinge reinforcement congestion; (d) Hoist stumble ..... 170
Figure 2-16 Bridge 1 elevation ..... 171
Figure 2-17 Elevation and plan of Frame 2, Bridge 1 ..... 171
Figure 2-18 Typical bent layout in Frame 2, Bridge 1 ..... 172
Figure 2-19 Cross-sectional details of Frame 2, Bridge 1 ..... 172
Figure 2-20 Hinge details, Bridge 1 ..... 173
Figure 2-21 Prestressing tendons profile in Frame 2, Bridge 1 ..... 173
Figure 2-22 Stressing sequence of Frame 2, Bridge 1 ..... 173
Figure 2-23 Bridge 2 elevation ..... 174
Figure 2-24 Elevation and plan of Frame 2, Bridge 2 ..... 174
Figure 2-25 Single column bent in Bridge 2 ..... 175
Figure 2-26 Outrigger bent details, Frame 2, Bridge 2 ..... 175
Figure 2-27 Typical superstructure cross section of Frame 2, Bridge 2 ..... 176
Figure 2-28 Hinge details, Bridge 2 ..... 176
Figure 2-29 Prestressing tendons profile in Frame 2, Bridge 2 ..... 176
Figure 2-30 Stressing sequence of Frame 2, Bridge 2 ..... 177
Figure 2-31 Bridge 3 elevation ..... 177
Figure 2-32 Elevation view of Frame 1, Bridge 3 ..... 178
Figure 2-33 Bent 2 details, Bridge 3 ..... 178
Figure 2-34 Bent 3 details, Bridge 3 ..... 179
Figure 2-35 Bent 4 details, Bridge 3 ..... 179
Figure 2-36 Cross-sectional details of Frame 1, Bridge 3 ..... 180
Figure 2-37 Hinge details, Bridge 3 ..... 180
Figure 2-38 Prestressing tendons profile in Frame 1, Bridge 3 ..... 180
Figure 2-39 Stressing sequence of Frame 1, Bridge 3 ..... 181
Figure 2-40 Elevation view of Bridge 4 ..... 181
Figure 2-41 Elevation and plan views of Frame 2, Bridge 4 ..... 181
Figure 2-42 Typical bent layout in Frame 2, Bridge 4 ..... 182

Figure 2-43 Superstructure cross-sectional details of Frame 2, Bridge 4 ..... 182
Figure 2-44 Hinge details, Bridge 4 ..... 183
Figure 2-45 Prestressing tendons profile in Frame 2, Bridge 4 ..... 183
Figure 2-46 Stressing sequence of Frame 2, Bridge 4 ..... 183
Figure 2-47 Elevation of Bridge 5EB ..... 184
Figure 2-48 Concrete pouring of Closure 1 ..... 184
Figure 2-49 Reinforcement steel and couplers connection between Closure 1 and the Segment B of Frame 3, Bridge 5EB ..... 184
Figure 2-50 Top and bottom views of Closure 1 ..... 185
Figure 2-51 Elevation of Frame 1, Bridge 5EB ..... 185
Figure 2-52 Elevation of Frame 3, Bridge 5EB ..... 185
Figure 2-53 Drop-in span construction views at Closure 1 and 2 ..... 186
Figure 2-54 Drop-in span falsework ..... 186
Figure 2-55 Steel frames holding the drop-in span ..... 186
Figure 2-56 End supports of the drop-in span ..... 187
Figure 2-57 Typical bent layout of Frame 1 and 3, Bridge 5EB ..... 187
Figure 2-58 Superstructure cross-sectional details of Frame 1 and 3, Bridge 5EB ..... 187
Figure 2-59 Hinge and closure details, Bridge 5EB ..... 188
Figure 2-60 Prestressing tendons profile of Frame 1, Bridge 5EB ..... 188
Figure 2-61 Prestressing tendons profile of Frame 3, Bridge 5EB ..... 188
Figure 2-62 Stressing sequence of Frame 1, Bridge 5EB ..... 189
Figure 2-63 Stressing sequence of Frame 3 for Closure 1 and 2, Bridge 5EB ..... 189
Figure 2-64 Elevation of Bridge 5WB ..... 189
Figure 2-65 Elevation and plan views of Frame 3, Bridge 5WB ..... 190
Figure 2-66 Elevation and plan views of Frame 5, Bridge 5WB ..... 190
Figure 2-67 Typical bent layout of Frame 3 and 5, Bridge 5WB ..... 191
Figure 2-68 Superstructure cross-sectional details of Frame 3 and 5, Bridge 5WB ..... 191
Figure 2-69 Hinge details, Bridge 5WB ..... 192
Figure 2-70 Prestressing tendons profile of Frame 5, Bridge 5WB ..... 192
Figure 2-71 Stressing sequence of Frame 5, Bridge 5WB ..... 192
Figure 3-1 Moisture retaining blankets for concrete curing ..... 193
Figure 3-2 Deck surface partial reveal for stations marking during concrete curing ..... 193

Figure 3-3 Digital level used in field measurements (Sprinter 250M) ..... 193

Figure 3-4: (a) Level mounted on the tripod; (b) Dual face leveling rod; (c) Rod bubble level ..... 194

Figure 3-5: (a) Digital level main screen; (b) Digital Thermometer Hygrometer ..... 194

Figure 3-6: (a) Station marking process; (b) Typical station; (c) Typical transverse gridline at the hinge ..... 195

Figure 3-7: (a) Elevation measurment on the adjacent span; (b) Elevation measurment at the hinge; (c) Focusing process and elevation shooting using the measuring trigger key; (d) Elevation recording in the data sheet ..... 196

Figure 3-8 Potential obstacles seen on the bridge deck ..... 197

Figure 3-9 Grid stations of Hinge 3, Bridge 1 ..... 198

Figure 3-10 Grid stations of Hinge 7, Bridge 1 ..... 198

Figure 3-11 Grid stations of Hinge 1, Bridge 2 ..... 199

Figure 3-12 Grid stations of Hinge 2, Bridge 2 ..... 199

Figure 3-13 Grid stations of Hinge, Bridge 3 ..... 200

Figure 3-14 Grid stations of Hinge, Bridge 4 ..... 200

Figure 3-15 Tie-off point in Bridge 4 ..... 201

Figure 3-16 Grid stations of Hinge 1, Bridge 5EB ..... 201

Figure 3-17 Grid stations of Closure 1, Bridge 5EB ..... 202

Figure 3-18 Grid stations of Closure 2, Bridge 5EB ..... 202

Figure 3-19 Grid stations of Hinge 4, Bridge 5WB ..... 203

Figure 3-20 Grid stations of Hinge 2 and Hinge 3, Bridge 5WB ..... 203

Figure 4-1 Immediate deformation at Hinge 3, Bridge 1: (a) Response across the bridge width; (b) Average response ..... 204

Figure 4-2 Immediate deformation at Hinge 7, Bridge 1: (a) Response across the bridge width; (b) Average response ..... 204

Figure 4-3 Immediate deformation at Hinge 1, Bridge 2: (a) Response across the bridge width; (b) Average response ..... 204

Figure 4-4 Immediate deformation at Hinge 2, Bridge 2: (a) Response across the bridge width; (b) Average response ..... 205

Figure 4-5 Immediate deformation at Hinge, Bridge 3: (a) Response across the bridge width; (b) Average response ..... 205

Figure 4-6 Immediate deformation at Hinge, Bridge 4: (a) Response across the bridge width; (b) Average response ..... 205

Figure 4-7 Immediate deformation at Hinge, Bridge 5: (a) Response at C1; (b) Response at C2; (c) Response at H1; (d) Response at H4 ..... 206

Figure 4-8 Time-dependent deformation before load transfer at H3, Bridge 1: (a) L1 response; (b) L2 response; (c) L3 response; (d) Average response ..... 206

Figure 4-9 Time-dependent deformation before load transfer at H7, Bridge 1: (a) L1 response; (b) L2 response; (c) L3 response; (d) Average response ..... 207

Figure 4-10 Time-dependent deformation before load transfer at H1, Bridge 2: (a) L1 response; (b) L2 response; (c) L3 response; (d) Average response ..... 207

Figure 4-11 Time-dependent deformation before load transfer at H2, Bridge 2: (a) L1 response; (b) L2 response; (c) L3 response; (d) Average response ..... 208

Figure 4-12 Self-supporting outrigger bent (Bent 7) after falsework removal ..... 208

Figure 4-13 Time-dependent deformation before load transfer at H, Bridge 3: (a) L1 response; (b) L2 response; (c) Average response ..... 209

Figure 4-14 Time-dependent deformation before load transfer at H, Bridge 4: (a) L1 response; (b) L2 response; (c) Average response ..... 209

Figure 4-15 Time-dependent deformation before load transfer at the P/S hinges, Bridge 5: (a) C1 before lowering the drop-in span; (b) C1 after lowering the drop-in span; (c) C2 before lowering the drop-in span; (d) C2 after lowering the drop-in span; (e) H1; (f) H4 before casting top ledge; (g) H4 after casting top ledge ..... 210

Figure 4-16 Completion of the hinge closure and long cantilever of H1 on Day-68 ..... 211

Figure 4-17 Four 1200mm cubic concrete blocks placed on the short cantilever of H4: (a) Short cantilever view; (b) Hinge view ..... 211

Figure 4-18 Time-dependent deformation after load transfer at H3, Bridge 1: (a) L1 response; (b) L2 response; (c) L3 response; (d) Average response ..... 212

Figure 4-19 Time-dependent deformation after load transfer at H7, Bridge 1: (a) L1 response; (b) L2 response; (c) L3 response; (d) Average response ..... 212

Figure 4-20 Time-dependent deformation after load transfer at H1, Bridge 2: (a) L1 response; (b) L2 response; (c) L3 response; (d) Average response ..... 213

Figure 4-21 Time-dependent deformation after load transfer at H2, Bridge 2: (a) L1 response; (b) L2 response; (c) L3 response; (d) Average response ..... 213

Figure 4-22 Bridge deck grinding at hinge 2 area on Day-197: (a) Hinge 2 view; (b) Adjacent span view ..... 214

Figure 4-23 Partial falsework removal in Frame 2 on Day 148 ..... 214

Figure 4-24 Complete falsework removal in Frame 2 ..... 214

Figure 4-25 Time-dependent deformation after load transfer at H, Bridge 3: (a) L1 response; (b) L2 response; (c) Average response ..... 215

Figure 4-26 Time-dependent deformation after load transfer at H, Bridge 4: (a) L1 response; (b) L2 response; (c) L3 response; (d) Average response ..... 215

Figure 4-27 Time-dependent deformation after load transfer at the P/S hinges, Bridge 5: (a) C1, Bridge 5EB; (b) C2, Bridge 5EB; (c) H1, Bridge 5EB; (d) H4, Bridge 5WB ..... 216

Figure 4-28 Hinge curl history of Bridge 1: (a) Hinge curl at H3; (b) Hinge curl at H7 (LT = load transfer) ..... 216

Figure 4-29 Hinge curl history of Bridge 2 (LT = load transfer): (a) Hinge curl at H1; (b) Hinge curl at H2 ..... 217

Figure 4-30 Hinge curl history at H, Bridge 3 (LT = load transfer) ..... 217

Figure 4-31 Hinge curl history at H, Bridge 4 (LT = load transfer) ..... 217

Figure 4-32 Hinge curl history of Bridge 5 (LT = load transfer): (a) Closure 1, Bridge 5EB; (b) Closure 2, Bridge 5EB; (c) Hinge 1 Bridge 5EB; (d) Hinge 4, Bridge 5WB ..... 218

Figure 4-33 Time-dependent deformation at non-PS hinges, Bridge 5WB: (a) H2; (b) H3 ..... 218

Figure 4-34 Hinge deformation history of non-PS hinges, Bridge 5WB (LT = load transfer): (a) H2; (b) H3 ..... 219

Figure 4-35 Influence of temperature and relative humidity change on deformation behavior: (a) H, Bridge 3; (b) H4, Bridge 5WB ..... 219

Figure 5-1 Parameters used in calculation of short cantilever deflection under dead load ..... 220

Figure 5-2 Prestress tendon path ..... 220

Figure 5-3 MTD 11-34 Deflection factor chart ..... 221

Figure 5-4 Adjustment to theoretical camber ..... 221

Figure 5-5 Short cantilever camber ..... 222

Figure 5-6 Long cantilever camber ..... 222

Figure 5-7 Perspective view of Bridge 1 model ..... 223

Figure 5-8 Perspective view of Bridge 2 model ..... 223

Figure 5-9 Perspective view of Bridge 3 model ..... 224

Figure 5-10 Perspective view of Bridge 4 model ..... 224

Figure 5-11 Perspective view of Bridge 5EB model ..... 224

Figure 5-12 Perspective view of Bridge 5WB model ..... 225

Figure 5-13 Theoretical camber diagram for Bridge 1 ..... 225

Figure 5-14 Theoretical camber diagram for Bridge 2 ..... 225

Figure 5-15 Theoretical camber diagram for Bridge 3 ..... 226
Figure 5-16 Theoretical camber diagram for Bridge 4 ..... 226
Figure 5-17 Theoretical camber diagram for Bridge 5EB ..... 227
Figure 5-18 Theoretical camber diagram for Bridge 5WB ..... 227
Figure 6-1 3-D view of SAP2000 model for Frame 2, Bridge 1 ..... 228
Figure 6-2 3-D view of SAP2000 model for Frame 2, Bridge 2 ..... 228
Figure 6-3 Bent cap modelling ..... 229
Figure 6-4 Modelling of an in-span hinge of a prestressed frame ..... 229
Figure 6-5 Typical tendon layout data in SAP2000 ..... 229
Figure 6-6 Typical pattern of falsework springs in a frame ..... 230
Figure 6-7 SAP2000 parameters for time-dependent properties of concrete ..... 230
Figure 6-8 Time-dependent properties for prestressing steel ..... 230
Figure 6-9 Body constraint at the column-cap beam connection ..... 231
Figure 6-10 Equivalent Fixity Model (Caltrans 2014) ..... 231
Figure 6-11 SAP models for prestressed frames including the long cantilevers : (a) Frame 2, Bridge 5WB; (b) Frame 4, Bridge 5WB ..... 232
Figure 7-1 3D view of a typical ABAQUS model (Frame 2, Bridge 2) ..... 233
Figure 7-2 Perspective view of a typical box-girder cross-section modeled in ABAQUS ..... 233
Figure 7-3 Single and two-column bents with equivalent column sections ..... 234
Figure 7-4 Longitudinal and transverse equivalent prestressing tendons within the superstructure ..... 234
Figure 7-5 A typical pattern of falsework arrangement in FE models ..... 235
Figure 7-6 Typical meshing schemes with mesh sizes: (a) 2.5 ft; (b) 1.67 ft ..... 235
Figure 7-7 Curve fitting for creep coefficient predictions ..... 236
Figure 7-8 Shrinkage strain predictions using different models (ACI 2008) ..... 236
Figure 7-9 ABAQUS models for prestressed frames including the long cantilevers: (a) Frame 2, Bridge 5WB; (b) Frame 4, Bridge 5WB ..... 237
Figure 8-1 Deformed shapes of Frame 2, Bridge 1 (SAP2000): (a) Before stressing; (b) Immediately after stressing ..... 238
Figure 8-2 Deformed shapes of Frame 2, Bridge 2 (SAP2000): (a) Before stressing; (b) Immediately after stressing ..... 238
Figure 8-3 Deformed shapes of Frame 1, Bridge 3 (SAP2000): (a) Before stressing; (b) Immediately after stressing ..... 238

Figure 8-4 Deformed shapes of Frame 2, Bridge 4 (SAP2000): (a) Before stressing; (b) Immediately after stressing ..... 239

Figure 8-5 Deformed shapes of F1EB, Bridge 5 (SAP2000): (a) Before stressing; (b) Immediately after stressing ..... 239

Figure 8-6 Deformed shapes of F3EB (Segment A), Bridge 5 (SAP2000): (a) Before stressing; (b) Immediately after stressing ..... 239

Figure 8-7 Deformed shapes of F3EB (Segment C), Bridge 5 (SAP2000): (a) Before stressing; (b) Immediately after stressing ..... 240

Figure 8-8 Deformed shapes of F5WB, Bridge 5 (SAP2000): (a) Before stressing; (b) Immediately after stressing ..... 240

Figure 8-9 SAP2000 deflections of Bridge 1: (a) at H3; (b) at H7 ..... 241

Figure 8-10 SAP2000 deflections of Bridge 2: (a) at H1; (b) at H2 ..... 241

Figure 8-11 SAP2000 deflections of Bridge 3 at Hinge ..... 241

Figure 8-12 SAP2000 deflections of Bridge 4 at Hinge ..... 242

Figure 8-13 SAP2000 deflections of B5EB: (a) at C1; (b) at C2; (c) at H1 ..... 242

Figure 8-14 SAP2000 deflections of B5WB at H4 ..... 242

Figure 8-15 SAP2000 deflections of prestressed long cantilevers frames in Bridge 5WB: (a) Frame 2 (Day -1); (b) Frame 2 (Day 0); (c) Frame 4 (Day -1); (d) Frame 4 (Day 0) ..... 243

Figure 8-16 Deformed shapes of Frame 2, Bridge 1 (ABAQUS): (a) Before stressing; (b) Immediately after stressing ..... 244

Figure 8-17 Deformed shapes of Frame 2, Bridge 2 (ABAQUS): (a) Before stressing; (b) Immediately after stressing ..... 245

Figure 8-18 Deformed shapes of Frame 1, Bridge 3 (ABAQUS): (a) Before stressing; (b) Immediately after stressing ..... 246

Figure 8-19 Deformed shapes of Frame 2, Bridge 4 (ABAQUS): (a) Before stressing; (b) Immediately after stressing ..... 247

Figure 8-20 Deformed shapes of F1EB, Bridge 5 (ABAQUS): (a) Before stressing; (b) Immediately after stressing ..... 248

Figure 8-21 Deformed shapes of F3EB (Segment A), Bridge 5 (ABAQUS): (a) Before stressing; (b) Immediately after stressing ..... 249

Figure 8-22 Deformed shapes of F3EB (Segment C), Bridge 5 (ABAQUS): (a) Before stressing; (b) Immediately after stressing ..... 250

Figure 8-23 Deformed shapes of F5WB, Bridge 5 (ABAQUS): (a) Before stressing; (b) Immediately after stressing ..... 251

Figure 8-24 ABAQUS deflections of Bridge 1: (a) at H3; (b) at H7 ..... 252

Figure 8-25 ABAQUS deflections of Bridge 2: (a) at H1; (b) at H2 ..... 252
Figure 8-26 ABAQUS deflections of Bridge 3 at Hinge ..... 252
Figure 8-27 ABAQUS deflections of Bridge 4 at Hinge ..... 253
Figure 8-28 ABAQUS deflections of B5EB: (a) at C1; (b) at C2; (c) at H1 ..... 253
Figure 8-29 ABAQUS deflections of B5WB at H4 ..... 253
Figure 8-30 ABAQUS deflections of prestressed long cantilevers frames in Bridge 5WB: (a) Frame 2 (Day -1); (b) Frame 2 (Day 0); (c) Frame 4 (Day -1); (d) Frame 4 (Day 0) ..... 254
Figure 8-31 Measured and calculated deflections of Bridge 1 for H3: (a) Day 0; (b) Day 1; (c) Day 49; (d) Day 92; (e) Day129 ..... 255
Figure 8-32 Measured and calculated deflections of Bridge 1 for H7: (a) Day 0; (b) Day 1; (c) Day 49; (d) Day 92; (e) Day129 ..... 256
Figure 8-33 Measured and calculated deflections of Bridge 2 for H1: (a) Day 0; (b) Day 1; (c) Day 36; (d) Day 97; (e) Day 148; (f) Day 197 ..... 257
Figure 8-34 Measured and calculated deflections of Bridge 2 for H2: (a) Day 0; (b) Day 1; (c) Day 36; (d) Day 97; (e) Day 148; (f) Day 197 ..... 258
Figure 8-35 Concrete grinding work on Frame 2, Bridge 2: (a) Grinding equipment during the operation; (b) Deck surface after grinding half of it ..... 259
Figure 8-36 Measured and calculated deflections of Bridge 3 for H: (a) Day 0; (b) Day 1; (c) Day 22; (d) Day 83 ..... 260
Figure 8-37 Measured and calculated deflections of Bridge 4 for H: (a) Day 0; (b) Day 1; (c) Day 51; (d) Day 99; (e) Day 135; (f) Day 167; (g) Day 170 ..... 261
Figure 8-38 Partial load transfer at H, Bridge 4 ..... 262
Figure 8-39 Measured and calculated deflections of B5EB for H1: (a) Day 0; (b) Day 1; (c) Day 27; (d) Day 68; (e) Day 112; (f) Day 143; (g) Day 184; (h) Day 275 ... 263
Figure 8-40 Measured and calculated deflections of B5EB for C1: (a) Day 0; (b) Day 1; (c) Day 13; (d) Day 45; (e) Day 78; (f) Day 152; (g) Day 239; (h) Day 360 ..... 264
Figure 8-41 Measured and calculated deflections of B5EB for C2: (a) Day 0; (b) Day 1; (c) Day 13; (d) Day 45; (e) Day 78; (f) Day 152; (g) Day 239; (h) Day 360 ..... 265
Figure 8-42 Measured and calculated deflections of B5WB for H4: (a) Day 0; (b) Day 1; (c) Day 30; (d) Day 74; (e) Day 224; (f) Day 254; (g) Day 315; (h) Day 406 ... 266
Figure 8-43 ABAQUS model samples used in the parametric study: (a) with 60-degree angle of skew abutment; (b) with 200 ft radius of horizontal curvature ..... 267
Figure 8-44 Effect of the abutment skew angle on the deformation behavior (group 1): (a) Day 0; (b) Day 30; (c) Day 60 (at Load Transfer); (d) Day 1440 ..... 268

Figure 8-45 Effect of the abutment skew angle on the deformation behavior (group 2): (a) Day 0; (b) Day 30; (c) Day 60 (at Load Transfer); (d) Day 1440 ..... 268

Figure 8-46 Effect of the radius of horizontal curvature on the deformation behavior: (a) Day 0; (b) Day 30; (c) Day 60 (at Load Transfer); (d) Day 1440 ..... 269

Figure 9-1 Typical deformation behavior after stressing..... 270

Figure 9-2 Hinge curl models ..... 270

Figure 9-3 Equivalent nodal loads and DOF's ..... 270

Figure 9-4 Falsework in Bridge 4 ..... 271

Figure 9-5 Deflection factor charts ..... 271

Figure 9-6 Sensitivity of CEB creep model due to change of: (a) Concrete strength ($f_{cm28}$); (b) Relative humidity (RH); (c) Volume-surface ratio (V/S) ..... 272

Figure 9-7 Creep coefficient predictions ..... 273

Figure 9-8 Comparison of measured and calculated hinge curl for H3, Bridge 1 ..... 273

Figure 9-9 Comparison of measured and calculated hinge curl for H7, Bridge 1 ..... 274

Figure 9-10 Comparison of measured and calculated hinge curl for H1, Bridge 2 ..... 274

Figure 9-11 Comparison of measured and calculated hinge curl for H2, Bridge 2 ..... 275

Figure 9-12 Comparison of measured and calculated hinge curl for H, Bridge 3 ..... 275

Figure 9-13 Comparison of measured and calculated hinge curl for H, Bridge 4 ..... 276

Figure 9-14 Comparison of measured and calculated hinge curl for H1, Bridge 5EB ... 276

Figure 9-15 Comparison of measured and calculated hinge curl for C1, Bridge 5WB .. 277

Figure 9-16 Comparison of measured and calculated hinge curl for C2, Bridge 5WB .. 277

Figure 9-17 Comparison of measured and calculated hinge curl for H4, Bridge 5WB .. 278

# Chapter 1 Introduction

## 1.1 Background

Cast-in-place (CIP) post-tensioned concrete (PS) box girder bridges are widely used in highway bridges in California. CIP/PS bridges are typically supported on falsework (Fig. 1-1) during construction until the bridge becomes self-supporting. The falsework functions as a support for the superstructure weight and prestressing loads until superstructure attains the specified concrete strength.

Many of these bridges are long and have a continuous superstructure. Intermediate expansion joints (in-span hinges) are used in the superstructure of long bridges to divide the structure into shorter frames to reduce the stresses in the columns resulting from temperature, creep and shrinkage forces. The hinge span (Fig. 1-2) comprises two cantilevers; short and long. The long cantilever is supported on the short cantilever at the hinge where the two cantilevers are connected as shown in Fig. 1-3. The in-span hinge is an important element that requires special consideration with respect to design, detailing, and construction sequence (Fig. 1-4).

CIP/PS bridges in California have experienced undesirable deflections at in-span-hinges that have led to serviceability issues such as bumps. In-span hinges of prestressed bridges are typically subjected to time-dependent deformation that is referred to as “hinge curl”. Hinge curl consists of an upward deflection of the unloaded short cantilever caused by prestressing forces followed by a downward deflection when it is loaded by the long cantilever.

CIP/PS bridges are normally cambered at in-span hinges to account for final (long term) deflections at these joints and accordingly ensure a smooth road surface between bridge frames for safe and comfortable ride. The final location of hinge is affected by the elastic deflection due to prestressing force and superstructure weight as well as the long term effects due to time-dependent material properties of concrete and prestressing steel.

In general, deflection prediction in prestressed concrete is associated with relative uncertainty, mainly due to concrete creep, and prestress losses. Additional uncertainty may arise in the CIP/PS bridges with in-span hinges due to the presence of the falsework that supports the superstructure during construction stages. Moreover, contractor's schedule and other construction issues affect the construction process and accordingly influence the deformation response of in-span hinges.

In an effort to avoid the adverse effects of hinge curl, the California Department of Transportation (Caltrans) developed a method to estimate the hinge curl through memo to designer (MTD) 11-34 (Caltrans 2012). The memo is designated to address the deformation of in-span hinges in CIP/PS box girder bridges. The overall objective of the memo is to ensure a smooth transition between bridge frames. This is achieved by generating the camber diagram that corresponds to the final deflection profile of bridges. Although this method is being used by bridge designers, significant discrepancy between the estimated and the actual hinge curl has been reported by field engineers. Figure 1-5 shows observed hinge curls in some bridges during construction.

## 1.2 Problem Statement

The method presented in MTD 11-34 does not always lead to accurate estimate of deformations, which could result into mismatch at in-span hinges of bridges. Mismatch of the two sides of an in-span hinge leads to road hazard causing vehicles damage and possible accidents. Hence, hinge curl repair is necessary during construction (Figs. 1-6 to 1-8) to correct the grade differences.

Hinge curl repair may include one or more of the following, loading the short cantilever with massive weights temporarily during construction, jacking the long cantilever using adjustable falsework posts (Fig. 1-9), grinding and chipping of the superstructure concrete at the hinge, and placing polyester concrete overlay. Grinding of concrete generally occurs for the short cantilever while concrete chipping is performed for the long cantilever to roughen the surface for placing an additional concrete layer to even up deck surfaces at the hinge. Bridge plans typically call for an additional concrete cover on the top deck reinforcement (Fig. 1-10) to allow for grinding without interfering with the deck reinforcement. These measures to correct the bridge profile at the hinge results in extra cost and delay, and could excessively reduce the concrete cover on the deck reinforcement making the deck steel susceptible to corrosion.

## 1.3 Previous Research

There are no available reports of past research on any aspects of in-span hinge curl in CIP/PS box girder bridges. The MTD 11-34 is a simple calculation procedure developed by Caltrans for routine design. An earlier version of the document (MTD 11-34, 1994) is used by the Nevada Department of Transportation (NDOT 2008) to estimate

hinge curl for the CIP/PS bridges. Different software packages (Larsa4D, STDS, BD2, SAP2000, ADINA) were used to assist field engineers verify and explain field observations during construction of the Galena Creek Bridge in Northern Nevada (Bond 2012). The superstructure of the bridge is cast-in-place post-tensioned dual cell concrete box girder and has two in-span hinges. These software yielded different results especially, camber results. MIDAS Civil was finally used because it leads to reasonable estimates of field measured deformations. Construction sequence of the Galena Creek Bridge was simulated in MIDAS Civil software, and hinge curl at in-span hinges was predicted from model results. CEP-FIP (1990) was utilized to define the time-dependent material properties of concrete. MIDAS Civil models were more accurate with hinge curl prediction than contractor's models, and thus significant difference between in hinge time-dependent displacements was captured during the field survey.

Over the last few decades numerous studies have been conducted on the concrete creep behavior as well as prestress losses. Different empirical equations have been developed for creep coefficient and prestress losses (ACI 2008 & AASHTO 2012 & PCI 2011). The empirical equations were usually calibrated with test data from small specimens because measured data from full-scale prestressed concrete bridges over long period are very limited.

Few field investigations were conducted on cast-in-place post-tensioned concrete bridges to monitor the variation of mid-span camber and prestress losses with time.

Saiidi et al. (1996) measured the mid-span deflection of a simply supported post-tensioned concrete box girder bridge during the first 30 months. The climatic data (temperature and relative humidity) were also collected since the climate of the bridge

site is characterized with highly variable relative humidity. A variation in the direction of the deflection was observed due to climatic changes. During the last 18 months, the average deflection appeared to have stabilized. The maximum measured deflection was approximately one-half of the predicted value due to the partial fixity provided by the abutments which is normally ignored the routine design calculation.

Saiidi et al. (1998) conducted field and analytical studies on a simply supported post-tensioned concrete box girder bridge over a 2-year period. The measured deflection history of the bridge reflected the variations in prestress force that were caused by climatic changes. The measured deflections showed good agreement with those predicted using a time-dependent design equation. The creep and shrinkage prestress losses predicted using the ACI committee 209 method showed good correlation with the measured losses.

Roschke et al. (1999) monitored time-dependent deflections of a continuous three-span cast-in-place post-tensioned slab skewed bridge with no in-span hinges for 2.5 years. A finite element program, TEXSLAB, was used to predict the deflections including the effects of creep and shrinkage. In general the predicted deflections by the finite element analysis compared well to those measured in field.

Kamatchi et al. (2014) carried out periodic field measurement of camber on a simply supported prestressed box girder bridge located in India for the initial 5 years after construction. The measured cambers at midspan were compared with those obtained using different analytical procedures (ACI 2008). Time-dependent cambers estimated using the CEB MC90-99 model were in closer agreement with field measurements compared to other methods.

In an effort to examine time-dependent behavior of prestressed bridges, a number of studies were conducted on segmentally constructed, cantilever prestressed concrete bridges with intermediate hinges as well as precast prestressed concrete girder bridges.

Witchukreangkrai et al. (2008) presented a study on long-term deflection monitoring of a cantilever prestressed concrete bridge intermediate hinges in Japan. The results of the study showed that the current design practices significantly underestimated the long-term deflections due to the uncertainty in predicting the behavior of creep and shrinkage.

Barr et al. (2010) monitored the camber of five precast prestressed bridge girders during fabrication and service. The cambers were calculated according to different multiplier methods and compared to the measured cambers.. The initial camber was overestimated at release due to the large temperature gradients present during curing. Over time, the measured cambers were in general smaller than the predicted values.

Bazant et al. (2011) conducted a study on deflections of segmental bridges with mid-span hinges. The study showed that excessive long-time deflections due to creep in large-span prestressed, segmental box girders may cause bridge deterioration, excessive vibrations and car passenger discomfort. The study also showed that the creep prediction models of ACI committee 209 (ACI 2008) underestimated the multi-decade creep deflections.

Construction stage analysis is an important tool in understanding the time-dependent behavior of bridges, especially those that undergo different loading stages, such as CIP/PS bridges. Powerful computer programs such as SAP2000 and ABAQUS have the ability to simulate construction sequence as well as the effects of material time-

dependent properties. However, the available literature shows that these features have been used only to a limited extent in the past.

Robertson (2005) conducted field and analytical studies on a segmental prestressed concrete bridge in Hawaii. SAP2000 was used to predict the short term deflections and SFRAME, a time-dependent step-wise finite element analysis program written specifically for analysis of incrementally constructed prestressed concrete bridges, was used to predict long term deflections. The measured short-term deflections were successfully predicted using a linear elastic beam element model in SAP2000. The SFRAME design predictions of long-term deflections differed significantly from the observed deflections. The measured long term deflections were underestimated in some spans and overestimated in others. This was due to the increased creep and shrinkage compared with that anticipated during the design phase, and variability in other material and environmental properties critical to the long-term response.

Hedjazi et al. (2007) studied the creep effects on the time-dependent deflections in segmentally constructed prestressed concrete bridges using ABAQUS software. Three-dimensional models with shell elements were developed for three bridges and the balanced-cantilever construction technique was simulated to verify some proposed equations. Bridge deflections were traced throughout the construction phase and over 30 years after construction. Good agreements between the results of the proposed method and ABAQUS analysis were found.

Bazant et al. (2010) performed an analytical study on excessive deflections of a prestressed box girder segmental bridge with mid-span hinges (Koror-Babeldaob Bridge in Palau). A three dimensional finite element model with solid elements and with

Kelvin-chain-based step-by-step integration in time was developed for the bridge using ABAQUS. The calculated deflections were compared to different predictions. It was concluded that none of the existing creep and shrinkage prediction models are satisfactory as purely predictive tools.

Scheevel et al. (2013) carried out field and analytical studies on a segmental prestressed concrete bridge in Minnesota to study the effect of thermal loading. Frame element model and solid element models were developed using SAP2000 and ABAQUS, respectively. However, construction stages and time-dependent effects were incorporated only in SAP2000. Results for the similar loading conditions were found to correlate fairly well between the two modelling techniques. Also the effect of pier stiffens was investigated analytically and compared to field data. The results showed that modeling the piers using gross moment of inertia predicted satisfactorily the behavior of the bridge superstructure.

### 1.4 Objectives and Scope

The ultimate goal of this research was to develop methods and to generate information from detailed field and analytical studies that will aid Caltrans in estimating the deflection of in-span hinges during and after construction to avoid extra construction cost, repair, and traffic delays. Accurate prediction of hinge curl will also minimize the maintenance work and leads to safer and smoother ride for the traffic over in-span hinges. The goal of the study was achieved through field and analytical studies by investigating the following specific objectives:

1- Examine the actual bridge deformations of five bridges in California in the field during construction.
2- Investigate the correlation between measured and estimated hinge curl based on the current version of the Caltrans document, MTD 11-34
3- Study the deformation behavior of CIP/PS bridges using computer modelling with construction stage analysis including material time-dependent effects. Use simple and detailed modeling using computer programs SAP2000 and ABAQUS, respectively in the modelling part of the study to investigate the deflection of the five bridges and to conduct parametric studies on the effect of skew angle and curvature.
4- Develop a new method for a more accurate estimation of hinge curl and propose a new version of MTD 11-34.

This study was focused on cast-in-place (CIP), bonded post-tensioned concrete, multi-cell box girder bridges with in-span hinges. The bridges had integral bent cap connections with minimal skew and curvature. The effect of skew and curvature was investigated using analytical models to determine the sensitivity of hinge curl to these parameters. The field studies were focused on deformation of short cantilevers, which is the primary source of hinge curl. However, to capture superstructure-bent rotation adjacent to the short cantilever, deflection of the span adjacent to each short cantilever was also investigated. The curl due to differential temperature over the height of the superstructure section was assumed to be negligible compared to the curl due to other effects.

## 1.5 Dissertation Outline

The dissertation is organized in ten chapters. Following the current chapter, Chapter 2 gives an overview on the CIP/PS box girder bridges with in-span hinges and presents the relevant geometrical and design details on the five bridges that were studied in the field. Chapter 3 describes the field measurement process, equipment used for data collection, and the schedule of site visits. Chapter 4 presents the deformations measured in field for the five bridges. The calculation procedure of hinge curl according to Caltrans memo, MTD 11-34 is summarized in Chapter 5. This chapter also includes also comparison between MTD estimated and measured hinge curls and subsequently evaluation of the current hinge curl estimation method. Chapter 6 describes the computer modelling and analysis process of bridges using SAP2000. Chapter 7 presents the finite element modelling and analysis of bridges using ABAQUS. The analytical results from SAP2000 and ABAQUS are presented in Chapter 8, and the correlation between the field measurements and analytical results is discussed. This chapter also presents the parametric studies on the effects of skew and curvature. Chapter 9 details the proposed procedure to estimate hinge curl more accurately than the current method, and summarizes the proposed changes to MTD 11-34. The validation of the proposed method is demonstrated in Chapter 9 as well. The summary of the research, findings from field measurements and analytical studies, in addition to the proposed future research are provided in Chapter 10.

# Chapter 2 Description of the bridges

## 2.1 Introduction

The research team worked closely with Caltrans to identify a group of cast in place (CIP) prestressed concrete box girder bridges with in-span hinges under construction. Five bridges across the State of California were selected to monitor time-dependent deflections of in-span hinges. The sample bridges were selected such that they properly represented the variety of California modern bridges in terms of location, configuration, and geometry. Bridge type and construction schedule were also considered in the selection procedure. Table 2-1 lists general information for the bridges. Three of the bridges are located in southern California, one in central California, and one in northern California.

Geometry, structural configuration with emphasis on in-span hinge properties, construction process, and main design assumptions of the bridges are presented in this chapter.

## 2.2 Bridge type

The sample bridges were selected from cast-in-place, prestressed (CIP/PS) concrete box girder bridge population because this is the most common type of bridges with in-span hinges in the state of California. The bridges are multi-span, continuous structures with at least two frames connected at an in-span hinge as shown in Fig. 2-1. Undesired long-term deflections have been observed in these hinges preventing smooth ride on bridges. Since hinge curl is defined as the summation of time-dependent deflections of short cantilevers under dead load and prestressing force, this study is

focused on deflections of short cantilever and adjacent span to monitor rotation at the support. The adjacent span is the closest full span to the hinge as shown in Fig. 2-1. The span in which the hinge is located typically consists of a short and a long cantilever where the short cantilever (SC) supports the long cantilever (LC) as shown in Fig. 2-2. The sample bridges are composed of different bent types such as single column bents, two-column bents, and outrigger bents. All the columns are reinforced concrete with oblong, circular, or rectangular cross sections. The bridge columns are supported on cast in a drilled hole (CIDH) piles with or without a pile cap.

A total of eight frames with 12 in-span hinges were surveyed to monitor hinge curl behavior. Of the eight frames, seven frames were CIP/PS with ten hinges, and one was CIP/non-PS with two hinges. The non-PS hinges were monitored to compare with PS hinges. Table 2-2 summarizes the hinge information in the five bridges.

### 2.3 In-span hinges

A typical in-span hinge of prestressed box girder bridges normally has two reinforced concrete parts constructed after the completion of prestressing and grouting of hinge span and the adjacent span (Fig. 2-3). The first part is L-shape and comprises a hinge diaphragm at SC side and a seat, and the second part is inverted L-shape comprising a hinge diaphragm at LC side and a top ledge. Hinge diaphragms are connected to the end diaphragms of cantilevers at the construction joint by dowel reinforcement extended from the end diaphragms. For a non-prestressed hinge the first closure pour which is composed of hinge diaphragm of the SC side and the seat, is cast monolithically with the box girder. However the second closure pour is not cast

monolithically with the long cantilever box girder regardless of whether the long cantilever is prestressed or not. Second closure pour is placed after bearings are properly positioned at the hinge centerline, on the hinge seat. The bearing devices used at the hinges of Bridges 1, 2, and 3 are Polytetrafluoroethylene PTFE spherical bearing, and those used in Bridges 4 and 5 are elastomeric pads (Fig. 2-3). Longitudinal cable restrainers are installed at each hinge between the long and short cantilever diaphragms. The restrainers are not anchored until 30 days following the completion of prestressing. The primary purpose of restrainers is to prevent unseating of bridge spans during seismic events, or when it is necessary to limit relative displacement between bridge frames (Caltrans 2008). Hinge restrainers are not shown in Fig. 2-3 for clarity. Deck joint seals such as joint seal assembly and bonded joint seal are installed at in-span hinges to accommodate movements and to provide continuity to the deck slab as shown in Fig. 2-4. The joint seal assembly blockout shown in Fig. 2-3 is filled usually with sand and topped with 3 to 4 inches of concrete or asphalt during construction as shown in Fig. 2-4. This fill is temporary to facilitate deck profilographing and grinding. Measures are taken to prevent intrusion of sand into the joint (Caltrans 1991). If necessary, the deck surface is ground after profilographing to achieve an even and smooth surface on both sides of a hinge. Figure 2-5 shows a deck after grinding. A layer of polyester concrete, if necessary, is placed over the lower surface before grinding to minimize the grinding work and to maintain a minimum remaining concrete cover over the reinforcement. After grinding, the joint seal assembly is installed at the hinge (Fig. 2-6).

## 2.4 Falsework

In this study, falsework refers to a temporary structure used to support the superstructure of cast-in-place box girder bridges during construction. Falsework is composed of steel, timber, or a combination of steel and timber members and connecting elements. Caltrans memo to designers (MTD 11-34) requires the falsework to remain in place to support the hinge span and adjacent spans until load transfer from the long to the short cantilever at the hinge. In addition, MTD 11-34 treats falsework as a rigid structure that would prevent the top of column rotations until the falsework removal. However, falsework flexibility was included in the current study because it could affect the deformation behavior of the bridge.

A conventional falsework system was used for the sample bridges. A typical system was composed of plywood sheets, joists, stringers, top cap, posts, bottom cap, wedges, sand jacks, corbels, and foundation pads as shown in Fig. 2-7. Braces were provided in the longitudinal direction between falsework bents and in the transverse direction in the plane of falsework bents for lateral stability. Falsework systems with different properties such as components material (Fig. 2-8), configuration, and dimension were observed in the sample bridges. In all systems, sand jack, which was a sand-filled container made of wood or steel, was used to release the falsework after it was jammed tightly under the superstructure weight. In this study, falsework release means that that bridge is no longer supported by the falsework.

In some cases, due to constraints imposed by exiting roads, railways, and waterways, the beam and column sizes were larger than those of typical falsework systems to support larger spans extending over the obstacles as shown in Fig. 2-9. In

some other cases falsework bents were skewed, or consisted of outriggers to accommodate traffic beneath the bridge as shown in Fig. 2-10.

In general, falsework remained in place until stressing was completed and cast-in-place concrete of hinges reached the specified strength. Additionally, the removal of falsework supporting a given span did not begin until all required work (excluding concrete above the bridge deck and grouting of prestressing ducts) was completed in that span and in the adjacent spans over a length equal to at least 1/2 of the length of the span where falsework was to be removed (Caltrans 2012). Therefore, partial falsework removal took place in some spans as shown in Fig. 2-11. Load transfer between the long and short cantilevers at the hinge took place when falsework was removed in the hinge span as shown in Fig. 2-12 (a). The condition of unbalanced bridge spans where spans deform freely and are no longer restrained by falsework, would be achieved after complete falsework removal in adjacent spans as shown in Fig. 2-12 (b).

## 2.5 Prestressing

Prestressing tendons are stressed using a high capacity multi-strand jack. The prestressing operation for the bridges was performed at two ends (two-end stressing) in some bridges and at one end (one-end stressing) in others. The number of stressing ends is determined in the design according to the design requirements taking into account friction losses along the frame length among other losses. Two-end stressing is performed non-simultaneously and used to counteract the high friction losses. Figure 2-13 shows the stressing operation at the hinge and at the abutment. Due to the existence of multiple tendons per each box girder, stressing was performed sequentially as shown in

Fig. 2-14. The sequence of stressing was determined such that the distribution of prestressing force ($P_{Jack}$) between girders was not exceeded the ratio of 3:2. According to the number of tendons and the jacking force, stressing of a bridge frame could take a couple of hours when it was stressed at one end and up to a couple of days if it was stressed at both ends. Additionally, other circumstances such as moving the stressing device to the opposite end of the frame and hinge reinforcement congestion extended the stressing duration as shown in Fig. 2-15. All tendon ducts were grouted after stressing to protect tendons against corrosion and to provide a bonded system.

Initial force coefficient, the ratio of jacking force minus instantaneous losses to the jacking force, is typically provided in drawings at the point of no movement of tendon. The force coefficient is one at the jacking location and decreases towards the point of no movement. The point of no movement is a point on the tendon that does not move when the tendon is pulled. For single end stressing, the point of no movement is at the opposite anchorage from stressing. For dual end post tensioning, the location is where the movement in one direction is countered by movement from the other direction and is generally near the middle of the frame (Caltrans 2010).

## 2.6 Prestressing steel

The prestressing strands used in the sample bridges were Grade 270 with an ultimate tensile strength of 270 ksi (1,860 MPa) and a modulus of elasticity of 28,500 ksi (193,000 MPa). The prestressing tendons were 0.6 in (15.24 mm) diameter, low-relaxation, and seven-wire strand (ASTM A416). The specified jacking force was 70% of the specified tendon ultimate strength. A minimum initial concrete compressive

strength, $f'_{ci}$, of 3.5 ksi (25 MPa) was met in the box girder concrete at time of stressing (Caltrans 2010). Table 2-3 lists the design parameters for the prestressed frames such as total jacking force per bridge frame, number of stressing ends, and the instantaneous prestress loss parameters. Friction curvature coefficient, wobble friction coefficient, and the anchor set length are the three parameters causing the instantaneous prestress losses for post-tensioning. The Number of strands is also listed to be used in calculating the tendons area for each frame.

## 2.7 Details of sample bridges

The main design parameters, concrete dimensions of the bridge components, and the prestressing steel details are presented in the following sections. Column heights shown on bridge frame elevations were calculated from the bottom of superstructure to the top of the foundation.

### 2.7.1 Bridge 1: San Luis Rey River Bridge

San Luis Rey River Bridge is located in the San Diego area. The construction started in 2010, and the bridge was opened to traffic in April 2012. The total length of the bridge is approximately 1725 ft (526 m). Bridge 1 consists of three frames extending over nine spans and has two in-span hinges as shown in Fig. 2-16. The field data collection was carried out on the intermediate frame (Frame 2). Frame 2 has a total length of 648 ft (197.5 m) and consists of three spans with two short cantilevers. The surveyed frame has a horizontal curvature with a radius of 1969 ft (600 m) and extends from Hinge 3 to Hinge 7 on Bents 4, 5, 6, and 7. Figure 2-17 shows elevation and plan views of Frame 2. Frame 2 is supported on two-column bents as shown in Fig. 2-18.

The bents are supported on CIDH Type I pile shafts. The specified 28-day compressive strength for columns concrete was 3.6 ksi (25 MPa).

The superstructure of Frame 2 is a continuous, cast-in-place, prestressed, 4-cell concrete box girder. The box girder has a fixed depth while its width changes along the length. Figure 2-19 shows concrete dimensions of typical cross section of Frame 2, and Figure 2-20 shows typical dimensions of Hinge 3 and 7. The frame has longitudinal slope of -2.234% from Hinge 3 towards Hinge 7. The superelevation slope changes with maximum slope of 6% downward towards the west direction.

Superstructure webs of Frame 2 contain 15 ducts for prestressing tendons composed of total 336 strands. The tendons were placed in a parabolic profile shown in Fig. 2-21. The specified initial force at the point of no movement was 0.836 times the jacking force. Design parameters for prestressing are listed in Table 2-3. Two-end stressing was performed for Frame 2 at Hinge 3 and 7 sequentially. Figure 2-22 illustrates the stressing sequence of Frame 2 at Hinge 3. The specified compressive strength for the prestressed concrete in the bridge was 3.6 ksi (25 MPa) at the time of prestressing and 4.5 ksi (31 MPa) at 28 days.

### 2.7.2 Bridge 2: N170-N5 Connector

N170-N5 Connector is located in the Los Angeles area. The connector is spanning from the northbound Hollywood Freeway (SR-170) to the northbound Golden State Freeway (I-5). The construction commenced late 2010, and the bridge was opened to traffic in May 2013. Bridge 2 has a total length of 2352 ft (717 m) and consists of three frames extending over eleven spans with two in-span hinges as shown in Fig. 2-23.

The field data collection was conducted on the intermediate frame (Frame 2). Frame 2 has a total length of 709 ft (216 m) and comprises three spans with two short cantilevers. The surveyed frame is horizontally curved with a radius of 1640 ft (500 m) and extends from Hinge 1 to Hinge 2 on Bents 5, 6, 7, and 8. Figure 2-24 shows elevation and plan view of Frame 2. Bents 5, 6, and 8 are single column bents, and Bent 7 is an outrigger bent. Figures 2-25 and 2-26 show the details of single column bents and outrigger bent, respectively. The bridge is supported on Type II pile shaft foundation. The piles are reinforced concrete and cast in drilled hole (CIDH). The specified 28-day concrete compressive strength for columns is 3.6 ksi (25 MPa).

The superstructure of Frame 2 is a continuous, cast-in-place, 3-cell, prestressed concrete box girder. The box girder has a fixed overall width and depth along its length. Figure 2-27 shows concrete dimensions of typical cross section of Frame 2. Figure 2-28 shows typical dimensions of Hinges 1 and 2. The frame is on a vertical curve starting almost horizontally at Hinge 1 and then continues to Hinge 2 with an average downward longitudinal slope of -1%. The frame has a variable transverse downward slope towards the center of the horizontal curvature with a maximum slope of 7%.

A total of 14 tendons comprised of total 362 strands were used in Frame 2. The tendons were placed in a parabolic profile shown in Fig. 2-29. Design parameters for prestressing are listed in Table 2-3. The specified initial force at point of no movement was 0.781 times the jacking force. Two-end stressing was performed for Frame 2 at Hinge 1 and 2 on several pulls as illustrated in Fig. 2-30. The specified compressive strength for the prestressed concrete in the bridge was 3.6 ksi (25 MPa) at the time of

stressing and 4.0 ksi (28MPa) and 5.0 ksi (35 MPa) for the superstructure and the outrigger bent cap, respectively, at 28 days.

### 2.7.3 Bridge 3: Bradley Overhead

Bradley overhead is located in Merced, California. It is a replacement bridge project with two construction stages. The sample bridge was built in stage 1. The construction began in 2012, and the bridge was opened to traffic in January 2013. The bridge total length is 1161 ft (354 m). Bridge 3 consists of two frames extending over seven spans and has one in-span hinge as shown in Fig. 2-31. The field data collection was conducted on the first frame (Frame 1). Frame 1 has a total length of 489 ft (149 m) and consists of three spans with one short cantilever. The surveyed frame is straight and extends from the seat type Abutment 1 to the hinge on Bents 2, 3, and 4. Figure 2-32 shows elevation view of Frame 1. Bent 2 is a single-column bent, while Bents 3 and 4 are two-column bents in which one of the columns is temporary. The temporary supports are 6.9 ft (2100 mm) diameter columns with CIDH shafts and are to be removed after completing construction stage 2. Figures 2-33 to 2-35 show the details of the bents. The bridge has Type I pile shaft foundation. The piles are reinforced concrete and cast in drilled hole (CIDH). The specified 28-day concrete compressive strength for columns is 4 ksi (28MPa).

The superstructure of Frame 1 is a continuous, cast-in-place, prestressed concrete, 2-cell box girder. The box girder has a fixed overall width and depth along its length. Figure 2-36 shows concrete dimensions of typical cross section of Frame 1, and Figure 2-37 shows typical dimensions of the hinge. Frame 1 is aligned on an average upward

longitudinal slope of 1.2% towards the hinge and has a slope of 2% in the transverse direction towards the overhang.

A total of 9 tendons comprised of 199 strands were used in Frame 1. The tendons were placed in a parabolic profile shown in Fig. 2-38. Design parameters for prestressing are listed in Table 2-3. The specified initial force at point of no movement was 0.908 times the jacking force. Two-end stressing was performed for Frame 1 at Abutment 1 and at the hinge side on several pulls as illustrated in Fig. 2-39. The specified concrete compressive strength for the box girder was 3.6 ksi (25 MPa) at the time of prestressing and 5 ksi (35 MPa) at 28 days.

### 2.7.4 Bridge 4: EB Wilshire Blvd On-Ramp OC

The Wilshire Blvd On-Ramp OC is located in the Los Angeles area. The construction began in 2012, and the bridge was opened to traffic in November 2013. The bridge total length is approximately 1197 ft (365 m) and consists of two frames, Frame 1 that is CIP/RC, and Frame 2 that is CIP/PS. Bridge 4 extends over eight spans and has one in-span hinge as shown in Fig. 2-40. The field data collection was conducted on the second frame (Frame 2). This frame has a total length of 535.8 ft (163.32 m) and consists of three spans with one short cantilever. The surveyed frame is straight and extends from the hinge to the seat type Abutment 9, on Bents 6, 7, and 8. Figure 2-41 shows elevation and plan view of Frame 2. The frame has single-column bents with specified 28-day concrete compressive strength of 5 ksi (35MPa) as shown in Fig. 2-42, and foundations consist of reinforced concrete (RC) pile caps rested on precast pre-stressed (PC/PS) piles with a diameter of 1.2 ft (360 mm).

The superstructure of Frame 2 is a continuous, cast-in-place, prestressed concrete, 3-cell box girder. The box girder of Frame 2 has a fixed depth and variable width along its length. Figure 2-43 shows concrete dimensions of typical cross section of Frame 2, and Figure 2-44 shows typical dimensions of the hinge. This frame lies longitudinally on a vertical curve with starting slope of 4.93% at the hinge and end slope of -6.27% at the abutment. The superstructure of Frame 2 has a variable superelevation with a higher elevation at the deck edge closer to W7 line shown in (Fig. 2-41).

A total of 6 tendons comprised of 205 strands were used in Frame 2. The tendons were placed in a parabolic profile shown in Fig. 2-45. The prestressing design parameters are listed in Table 2-3. One-end stressing was performed for this frame at Abutment 9. The specified initial force at point of no movement was 0.754 times the jacking force. The stressing sequence of Frame 2 is illustrated in Fig 2-46. The specified compressive strength for the prestressed concrete in the bridge was 4.5 ksi (31MPa) at the time of prestressing and 5.0 ksi (35 MPa) at 28 days.

### 2.7.5 Bridge 5: Del Paso Park Overhead

Del Paso Park Overhead “Bridge 5” is a widening bridge project located in Sacramento, California on the interstate 80, Highway (I-80). The project includes two bridges; the east bound bridge (referred to as “5EB” in this document) and the west bound bridge (referred to as “5WB” in this document). The construction began in 2013, and the project was partially opened to traffic in April 2014.

#### 2.7.5.1 Bridge 5EB

The bridge is approximately 1322 ft (403 m) long and consists of three frames: F1, F2, and F3. Frame 1 and 3 are CIP/PS, and Frame 2 is CIP/RC (Fig. 2-47). Bridge 5EB extends over ten spans and has four in-span hinges as shown in Fig. 2-47. The bridge has two in-span hinges are labeled as "closures" (C1 and C2) because they are non-typical hinges as they do not have bottom and top ledges, and two other hinges, which are typical, are labeled Hinge 1 and Hinge 2. The closure is basically a wide reinforced concrete diaphragm constructed with a single concrete casting as shown in Fig. 2-48. Closures 1 and 2 are 3 ft (914 mm) wide and moment connections with dowel bars shown in Fig 2-49. These joints provide full continuity in the superstructure (Fig 2-50).

Only two frames, F1 and F3, were surveyed (Figs. 2-51 and 2-52). Frame 1 comprises three spans with a short cantilever and extends from Abutment 1 to Hinge 1 with total length of 361 ft (110 m) as shown in Fig. 2-51. Frame 3 is 561 ft (171 m) long and consists of three segments (A, B, and C) constructed in two stages as shown in Fig. 2-52. Segments A and C were constructed in the first stage, and the middle segment (B) was constructed in the second stage (Fig. 2-52). Segment B was cast and post-tensioned at higher falsework level and then was lowered to be supported on the other two segments at Closure 1 2 (Fig. 2-53). Segment B was supported by falsework at higher level before lowering to accommodate the light railway travelling underneath, as shown in Fig. 2-54. Before lowering the span, the drop-in span (Segment B) was hanged at Closure 1 and 2 from a steel frame anchored to other segments as shown in Fig. 2-55. The drop-in span was lowered over a weekend and was seated on falsework bents at two

ends. Subsequently, the rest of falsework was removed. Therefore, two falsework bents with large steel posts were provided under each closure as shown in Fig. 2-56 to withstand the span weight. The first segment of Frame 3 (Segment A) is located between Hinge 2 and Closure 1 and supported on Bent 8 and Bent 9. The third segment (Segment C) comprises one span with short cantilever, starts at Closure 2, and ends at seat type Abutment 11. Frame 1 is straight, and Frame 3 is horizontally curved with a radius of 1801 ft (549 m). Bridge 5EB is supported on single-column bents as shown in Fig. 2-57, and its foundations are Type I CIDH pile shafts. The specified 28-day compressive strength for columns concrete is 3.6 ksi (25 MPa).

The superstructure of Frames 1 and 3 is a continuous, cast-in-place, prestressed, 2-cell concrete box girder. The typical box girder cross-section of the bridge is shown in Fig. 2-58. The superstructure has fixed width and depth along the bridge length, except in span 9 where the bridge depth decreases at Bents 9 and 10 towards Closures 1 and 2 to have a minimum depth over the drop-in span length (Segment B). Figure 2-59 shows typical hinge and closure details in the bridge. Frames 1 and 3 have a downward longitudinal slope of 1.1% towards Hinge 1 and Abutment 11, respectively. The superelevation slope is -7% towards the overhang side.

The prestressing design parameters of Frame 1 and the surveyed segments in Frame 3 can be found in Table 2-3. The tendons were placed in a parabolic profile for Frame 1 and 3 as shown in Fig. 2-60 and 2-61, respectively. The specified initial forces at points of no movement were 0.846 times the jacking force for Frame 1 and Segment A of Frame 3, while the respective value was 0.906 for Segment C of Frame 3. The stressing sequence of Frame 1 and 3 is illustrated in Figs 2-62 and 2-63, respectively.

The specified compressive strength for the prestressed concrete in the bridge was 3.6 ksi (25MPa) at the time of stressing and 4.0 ksi (28 MPa) at 28 days.

#### 2.7.5.2 Bridge 5WB

Bridge 5WB is approximately 1342 ft (409 m) long and has three CIP/PS frames and two CIP/RC frames. Bridge 5WB comprises nine spans and has four in-span hinges as shown in Fig. 2-64. Hinge curl and adjacent span deflections were monitored in Frame 3 and 5 at Hinges 2, 3, and 4. Frame 3 is CIP/RC and it is the only non-prestressed frame surveyed in this study. Frame 3 is 169 ft (51.5 m) long and extends between Hinges 2 and 3 to include span 5 and the short cantilevers of both hinges as shown in Fig. 2-65. Frame 5 is CIP/PS with a total length of approximately 318 ft (97 m). It comprises spans 8 and 9, and the short cantilever side of Hinge 4 as shown in Fig. 2-66. Frame 5 starts at Hinge 4 and ends at seat type Abutment 10 (Fig. 2-66). The bridge is horizontally curved, however, the frames are nearly straight as the bridge has a large radius of curvature of 4500 ft (1372 m). The bridge is supported on single-column bents as shown in Fig. 2-67, and the bents are supported on CIDH Type I pile shafts. The specified 28-day compressive strength for columns concrete was 3.6 ksi (25 MPa).

Superstructures of Frames 3 and 5 are continuous and consist of 2-cell box girder cross-section as shown in Fig. 2-68. The superstructure has fixed width and depth throughout the bridge length. Typical hinge details of Bridge 5WB are shown in Fig. 2-69. The specified 28-day compressive strength for the concrete of Frame 3 superstructure was 3.6 ksi (25 MPa). Frames 3 and 5 have a downward longitudinal slope of 1.2%

towards Abutment 10 and Hinge 3, respectively. The superelevation slope is 3% towards the overhang side.

The prestressing design parameters of Frame 5 are listed in Table 2-3. The tendons of Frame 5 were placed in a parabolic path with the profile displayed in Fig. 2-70. Two-end stressing was performed for Frame 5 at Hinge 4 and Abutment 10, and the stressing sequence at both sides is illustrated in Fig. 2-71. The specified initial force at the point of no movement was 0.897 times the jacking force. The specified compressive strength for the prestressed concrete in the bridge was 3.6 ksi (25 MPa) at the time of prestressing and 4.0 ksi (28 MPa) at 28 days.

# Chapter 3 Field Measurements

## 3.1 Introduction

This chapter presents the field measurement process, equipment used for data collection, and the schedule. The primary data collected in the field was vertical deflections of short cantilevers and the adjacent spans. The ambient temperature and relative humidity were also recorded during each data set measurement.

The research team conducted a series of visits to each bridge site for field measurements during construction. The planned preliminary schedule for data collection was Day -1 (the day prior to start of post-tensioning), Day 0 (immediately after post-tensioning), Day 1 (one day after completion of post-tensioning), Day 30 (thirty days after post-tensioning), and approximately one-month intervals afterward. However, the actual schedule deviated from the planned schedule in some cases due to changes in construction schedule, weather and road conditions, and other circumstances.

The first data set was taken after marking stations on the bridge deck. Concrete decks were moist cured continuously for seven days by placing mats or blankets on the deck surface (Caltrans 1991), as shown in Fig. 3-1. However the post-tensioning schedule required the research team to partially uncover the deck in some cases for marking the stations (Fig. 3-2) and placing the cover back when curing was still in progress. The post-tensioning was usually conducted 10 days after casting the top deck slabs. The strength of superstructure concrete was measured at the time of stressing to ensure that it reached at least 70% of the specified 28-day strength. However given the fact that soffits and stems were cast earlier than decks, and from concrete sample test

results, the box girder concrete for all bridges had the specified 28-day compressive strength, f'c, by the time of stressing.

The hinge curl was monitored in five bridges during construction until the opening date of each bridge. The deflection of short cantilevers and their corresponding adjacent spans were measured during different construction stages of each bridge.

### 3.2 Data acquisition instruments

Several alternatives were considered in collecting the deflection data including (a) laser instruments placed off the bridge with markers on the superstructure edge, (b) hand held distance meters used underneath the deck to monitor soffit position relative to fixed stations below the bridges, and (c) a digital level surveying equipment. A fourth option of installing permanent linear variable differential transformers (LVDT) or potentiometers was ruled out without consideration due to interference with construction. Option (a) was not pursued because access to view the side of the bridge was not possible in some cases and in other cases the height of the bridge did not allow for a feasible location to aim at markers on the bridge edge. Furthermore, the superstructure edge was typically covered by formwork. Option (b) was ruled out despite its efficiency and ease of measurement because securing fixed stations under the bridge was no feasible because of changing terrain during construction activities and movement of construction vehicles under the bridge. As a result, option (c) was selected. The vertical deflection of short cantilevers and adjacent spans was measured using Leica Geosystems digital level (Sprinter 250M) with a specified accuracy of 0.039 in (1 mm) (Fig. 3-3). The instrument package included an aluminum tripod (Fig. 3-4a), a dual face aluminum leveling rod (Fig.

3-4b), and a rod bubble level (Fig. 3-4c). The aluminum leveling rod was 16.4 ft (5 m) long and two-sided with four sliding sections that were marked numerically on one side and barcoded on the other side as shown in Fig. 3-4 (b). The barcoded side was used for automated rod readings in this study. The rod bubble level was installed on the numerical side as shown in Fig. 3-4 (c) and was used to ensure that the rod was held plumb during data collection. The digital level had a built-in memory to record measured data, however the data were recorded manually because the volume of data was relatively small and to avoid data loss. The data were read from the level main screen as shown in Fig. 3-5 (a) and then written down in the data sheet of each hinge.

The ambient temperature and relative humidity were recorded using LCD Digital Thermometer Hygrometer shown in Fig. 3-5 (b). The thermometer was placed in shade on the deck surface, and the climatic data were taken during each set of measurement. The time of day when data were collected varied depending on the travel schedule but generally was between 8:00 am and 3:00 pm.

### 3.3 Deflection measurement methodology

Deflections were measured on top of superstructures. A sketch of stations composed of longitudinal and transverse axes were prepared for each hinge. Stations were marked on a grid on the deck surface over the short cantilever of each hinge and its adjacent span. No stations were marked on the overhang area of bridges due to safety considerations and to avoid wearing a harness while working in this zone. Figure 3-6 (a) shows the marking process of a station in Bridge 3 using measurement tape and spray paint, Figure 3-6 (b) shows a typical marked station in Bridge 1, and Figure 3-6c shows a

typical transverse gridline at the hinge. Different colors of spray paint were used, however the research team was asked by Caltrans crew to use white spray paint specifically in Bridge 3 to avoid driver distraction after the bridge is open to traffic in case any station markings are still visible.

The number of longitudinal axes and spacing between them varied among the bridges depending on the bridge width. For each hinge, two transverse gridlines were established on the short cantilever and one line on the adjacent bent centerline. The number of transverse lines in adjacent spans varied among the bridges as discussed later in this chapter. It was first planned to measure the adjacent span deflections at three, quarter point locations. Deflections of adjacent spans in Bridges 2 and 3 were measured according to this plan, but a finer gridline was used in the quarter span adjacent to the short cantilever in other bridges. Additional stations were marked in this zone to closely capture the deformed profile of the adjacent span. Normally the points on the first transverse gridline were marked at a distance of 1 ft (0.305 m) from the edge of the short cantilever as shown in Fig. 3-6 (c). This distance allowed a space for the person holding the rod. Moreover, it minimized the likelihood of these stations being covered by temporary boards placed over the hinge for workers to move between the bridge frames. Elevations at the stations on bridge decks were measured as shown in Fig. 3-7. For each hinge, a data sheet along with a sketch of the stations was developed on which the field data was recorded (Appendix A). In some cases the original stations were not accessible or covered with construction materials and equipment that could not be easily moved. Consequently it was necessary to mark additional auxiliary stations in the vicinity of inaccessible stations. The location of the digital level was important because it should

allow the level to target easily all the available stations. The original planned location of the digital level station was changed in case of any obstacle blocking the view of the rod. Obstacles that blocked the view or covered the stations (Fig. 3-8) were construction tools, concrete blocks, construction materials, trucks, generators, and falsework removal equipment.

Elevation of each station was shot and recorded three times. To do so, the rod was lifted off the station and repositioned before a new reading for the same station was recorded. Subsequently the average reading was used in the data processing. For each data set, the bent close to the hinge was considered as a benchmark, and its elevation was subtracted from all measured elevations to determine the bridge profile on each longitudinal axis. The first measured data set, "Day -1" (before stressing), was used as the reference to calculate the hinge curl and bridge deflections. The immediate hinge curl and deflections of the rest of a bridge were calculated by taking the difference between the bridge profile immediately after stressing (Day 0) and the bridge profile prior to post-tensioning. The time-dependent hinge curl and bridge deflections were calculated by taking the difference between each measured data set at any construction stage and the data on Day -1.

### 3.3.1 Bridge 1

For Bridge 1, the gridlines marked by Caltrans crew were used in field measurements. The gridlines for each hinge consisted of four transverse axes intersecting with three longitudinal axes to form a total of 12 stations as shown in Figs. 3-9 and 3-10. The external longitudinal axes (L1 and L3) were marked at 7.42 ft (2.25 m) from edges to keep a safe distance off the barrier reinforcement. This safe distance was usually kept by placing a wooden barrier parallel to the bridge barrier. The middle longitudinal axis, L2,

was centered between L1 and L3. The spacing between the longitudinal axes changed along the longitudinal profile of Frame 2 according to the bridge width. Four transverse axes, T1 and T2 for Hinge 3, and T7 and T8 for Hinge 7, were marked on the respective short cantilever as shown in Figs. 3-9 and 3-10, respectively, at unequal distances, because other desired stations were not accessible. One transverse axis of stations per each hinge was marked on the adjacent spans. The research team could not mark more stations on the adjacent spans of Hinge 3 and 7 because most stations planned to be marked were covered with construction equipment. Additionally, the time was very limited for the research team to ask for access to these locations as the post-tensioning process was imminent and the first data set had to be collected before post-tensioning.

Deflection and climatic data were collected on Frame 2 in the field for a period of 5 months from Day -1 to the date of opening to traffic. Six visits were made to Bridge 1 for field measurements. One measurement set was taken for each hinge during each visit resulting in 12 data sets for Bridge 1. Table 3-1 summarizes the field measurements schedule for Bridge 1. Data was collected at Hinge 3 and 7 without having a specific order of starting point. In case there were some construction activities at one station, the research team started at another station to avoid interference with construction activities.

### 3.3.2 Bridge 2

A total of 42 stations, 21 stations for each hinge, were marked on Frame 2 of Bridge 2 for field measurements. The stations were located at the intersections of three longitudinal and seven transverse axes as shown in Figs. 3-11 and 3-12. Three longitudinal axes were established on Frame 2, where the external lines, L1 and L3, were

located at 8 ft (2.44 m) from the superstructure edges, and the internal axis, L2, was located 21 ft (6.41 m) from both L1 and L3. Two transverse axes were marked on the short cantilevers of Hinge 1 and 2 at equal distances starting at 1 ft (0.305 m) from the edge of the cantilever. At each hinge, one transverse axis was located on the centerline of the bent close to the hinge and another was located on the centerline of the next bent on the other side of the adjacent span. The transverse axes in the adjacent spans were at quarter points of the span. The level was placed at two locations due to the long adjacent span length (marked by an "x" in Fig. 3.11 and 3.12). Elevations of the stations on T5 were recorded twice from locations 1 and 2, and those on T10 were recorded twice from locations 3 and 4. T5 and T10 were common transverse axes for the two locations. The data collected on the common axes was used to convert the data to the same reference level.

Deflection and climatic data were collected in the field for a period of 8 months from Day -1 to the date of opening to traffic. Fourteen data sets were collected on Frame 2 during seven visits to the bridge site. Seven data sets were obtained per each hinge during different stages of construction. Table 3-2 summarizes the field measurements schedule for Bridge 2.

### 3.3.3 Bridge 3

A grid of 14 points was established on Frame 1 of Bridge 3 for field measurements. The grid was composed of two longitudinal and seven transverse axes as shown in Fig. 3-13. L1 was located at 16 ft (4.88 m) from L2, which was located 1 ft (0.305 m) from the south edge of the superstructure. The first transverse axis (T1) was

located at 2 ft (0.610 m) from the edge of the SC, and the next 2 transverse axes (T2 and T3) were established at even spaces of 14.67 ft (4.47 m) from T1 towards T3. The benchmark axis (T3) was marked on the centerline of Bent 4. Transverse axes T4 to T6 were marked at quarter span and T7 was established on Bent 3.

Deflection and climatic data were obtained 6 times in the field during a period of 4 months from Day -1 to the date of opening to traffic. Two data sets separated by five hours were measured on Day 83 after the load transfer to examine the thermal effect on the hinge curl. Table 3-3 lists the field measurements schedule for Bridge 3. Stations on T1 axis partially faded before the data collection on Day 83 due to the grinding of concrete. However the point elevations were measured and the amount of grinding reported by Caltrans site crew was used in the data processing.

### 3.3.4 Bridge 4

A grid of 30 points was marked on Frame 2 of Bridge 4 for field measurements (Fig. 3-14). Even though the average width of Frame 2 was smaller than its counterparts in Bridges 1 and 2, three longitudinal axes were established. A redundant gridline was useful when points on one longitudinal axis were covered and furthermore gave better understanding of the hinge curl variation in the transverse direction. This was particularly useful because the maximum bridge width was at the hinge. The inner axis L2 was centered between L1 and L3. The first transvers axis, T1, distanced 1 ft (0.305 m) from the edge of the short cantilever into its length, and T2 was at midpoint between T1 and T3, which was located on the centerline of Bent 6. The stations in the first quarter of the adjacent span were marked on a fine grid, but the rest of the span was marked at

quarter points. The fine grid improved the accuracy of the measured deformation of the adjacent span close to the hinge.

Eight sets of deflection and climatic data were collected in the field during a period of 6 months from Day -1 to the date of opening to traffic. Table 3-4 summarizes the field measurements schedule for Bridge 4. The two data sets of Day 167 and Day 170 were obtained after the load transfer but before any concrete grinding at the hinge. The research team ran into some difficulties measuring the elevations in Bridge 4 because of the significant change in the longitudinal alignment of Frame 2, due to its slope change as mentioned in the bridge description in Chapter 2. Wind made rod readings even more difficult particularly when it was necessary to expand the four sections of the rod at the low elevation stations. Furthermore, shooting the elevation of the points lying on T1 was the most challenging where the surveyor assistant had to wear a safety harness while standing near the edge of the short cantilever as shown in Fig. 3-15.

### 3.4 Bridge 5

Since this was a widening project, Bridges 5EB and 5WB had a relative narrow cross-section unlike other bridges. Therefore all the surveyed frames in these two bridges had only one longitudinal axis of stations for each hinge. The longitudinal axis was located 10.25 ft (3.12 m) from the overhang edge. The gridline path coincided with the centerline of the intermediate web of the box-girder. The first transverse axis was set at 1 ft (0.305 m) from the edge of the short cantilevers in all hinges. All the measured hinge curl data were collected before the grinding of concrete at the hinges.

### 3.4.1 Bridge 5EB

A single array of 10 stations was established on Frame 1 of Bridge 5EB for curl monitoring of Hinge 1 as shown in Fig. 3-16. The first transvers axis, T1, was located 1 ft (0.305 m) from the edge of SC, T2 was implemented 8 ft (2.44 m) from T1, and similarly T3 was marked 8 ft (2.44 m) from T2. Transverse axes T7, T8, and T9 were marked at ¼, ½, and ¾ of the adjacent span length, respectively. T4, T5, and T6 divided the first quarter of the adjacent span length into three equal distances at 1/16, 1/8, and 3/16 of the span length, and T10 was located on the centerline of Bent 3.

Deflection and climatic data were collected at Hinge 1 in the field for a period of 10 months from Day -1 to the date of opening to traffic as summarized in Table 3-5. Six data sets out of a total of 11 sets were obtained at Hinge 1 after releasing the falsework and having complete load transfer.

Same station grids were marked on the first and the third segments (A and C) of Frame 3 for Closure 1 and 2 as shown in Figs. 3-17 and 3-18, respectively. Each segment had 8 stations out of which 2 were on the short cantilever, 1 on the centerline of the bent close to the closure, and 5 on the adjacent span and the centerline of the far bent. T1 was located at 1 ft (0.305 m) from the edge of short cantilevers, and T3 was on the bent cap. T2 was at midpoint between T1 and T3. The adjacent spans were marked at quarter points (T5, T6, and T7); and T8 was located on the centerline of Bent 8 and Abutment 11 for Closure 1 and 2, respectively. T4 was marked at 1/8th of the adjacent span length.

Deflection and climatic data were collected on Frame 3 for almost a year from Day -1 to the date of opening to traffic as summarized in Table 3-6. Eighteen data sets were collected at Closure 1 while 17 at Closure 2. The number of readings was lower at

Closure 2 due to a one-day delay in stressing the third segment of Frame 3. The field measurements passed through four phases: before stressing, after stressing, lowering the drop-in span and complete load transfer. The falsework supporting the drop-in span (Segment B) was removed after lowering of Segment B (Third phase). The drop-in span was supported temporarily on steel frames at its ends. Consequently, segments A and C were deemed to be partially loaded at Closures 1 and 2 during the third phase until the complete falsework removal.

### 3.4.2 Bridge 5WB

The gridline for Frame 5 in Bridge 5WB was similar to that of Frame 1 in bridge 5EB for curl monitoring of Hinge 4. A sketch of stations showing the grid dimensions is presented in Fig. 3-19.

Deflection and climatic data were collected for Hinge 4 during a period of 14 months. Dates and construction stages of 16 data sets obtained for Hinge 4 are summarized in Table 3-5.

A total of 11 points were marked on Frame 3 for field measurements as shown in Fig. 3-20. Starting and ending transverse axes (T1 and T11) were at distance of 1 ft (0.305 m) from the edge of the short cantilevers of Hinge 2 and 3, respectively. T5, T6, and T7 were located at quarter points, and T4 and T8 were at $1/8^{th}$ points near Bents 5 and 6, respectively. T2 was at midpoint between T1 and T3 at Hinge 2, and T10 was marked at midpoint between T9 and T11.

The field measurement schedule of Frame 3 is summarized in Table 3-7. Note that, no stressing phase is shown in this table because Frame 3 is a Non/PS frame. The

first two data sets were measured 10 days and 22 days after the deck was cast. The rest of the data were measured after removing the falsework and the complete load transfer from Frames 2 and 4 at Hinges 2 and 3, respectively.

# Chapter 4 Measured Data Analysis and Interpretation

## 4.1 Introduction

The processed measured field data are presented in this chapter. The immediate and time-dependent deformation behavior of prestressed and non-prestressed hinges as well as the effect of temperature and humidity variation on hinge curl is discussed.

The elevation of short cantilevers and the adjacent spans in the sample bridges were measured at the stations described in Chapter 3. Data were collected prior to start of post-tensioning and immediately after completion of post-tensioning, one day and 30 days after post-tensioning, and approximately in one-month intervals afterward until the opening date.

The hinge curl is determined at a hinge centerline. Hinge centerlines were not yet built for elevation measurement because the closure concrete was usually cast several days after the completion of post-tensioning. Therefore, the elevations were extrapolated from those recorded in the vicinity of the centerlines on short cantilevers.

The centerline of the bent close to each hinge was considered as the benchmark. Deflection of short cantilevers and adjacent spans were determined with respect to this benchmark. Time-dependent relative deflections were calculated with respect to the first measured data set (measurement on Day -1).

## 4.2 Immediate deformations

### 4.2.1 Bridge 1

The deflection of short cantilevers and the adjacent spans associated with hinges 3 and 7 in Bridge 1 were measured and plotted in Figs. 4-1 and 4-2, respectively. The

immediate deformation of the adjacent spans of hinges 3 and 7 was recorded at the1/8th and 1/10th points of the span length, respectively. The immediate deflections of short cantilevers measured on different longitudinal gridlines across the bridge width are shown in Figs. 4-1 (a) and 4-2 (a), and the average response is plotted in Figs. 4-1 (b) and 4-2 (b).

It can be seen that the short cantilevers deflected upward immediately after the prestressing of Frame 2, and the adjacent spans deflected downward. Minor difference in hinge curl across the bridge width was observed at Hinge 3 (Fig. 4-1 a). This difference was attributed to the disparity of the post-tensioning forces in the bridge girders due to the tensioning sequence. Recall that the distance between L1 and L3 at the hinge was 41.4 ft (12.6 m). The tensioning sequence varies the elastic shortening losses in the tendons and leads to slightly asymmetrical forces on the bridge section. This difference was not observed at Hinge 7. Hinge 7 was the second stressing end in Frame 2, and accordingly variations in the elastic shortening losses were minimized. Furthermore the distance between L1 and L3 was 30.6 ft (9.3 m) due to the narrower bridge width than that of Hinge 3, which in turn lessened the deflection variation across the bridge width. Hence the post-tensioning forces in the bridge girders were nearly symmetrical.

### 4.2.2 Bridge 2

The immediate deformation of short cantilevers and the adjacent spans associated with hinges 1 and 2 in Frame 2 of Bridge 2 are plotted in Figs. 4-3 and 4-4. Deformations of hinges 1 and 2 were measured with respect to centerlines of Bent 5 and Bent 8, respectively. Displacements were measured on three longitudinal gridlines in the

transverse direction and then averaged. Slight variation in the immediate hinge curl was measured across the bridge width at Hinge 1 while nearly no change was observed at Hinge 2 even though distance between L1 and L3 (Figs. 3-11 and 3-12) was the same for both hinges. The reason as described previously was the different elastic shortening losses due to post-tensioning sequence. This effect was minimized at Hinge 2 since it was the second stressing end.

The first quarter point of the adjacent spans deflected downward, and the second and the third quarter points deflected upward. A downward displacement was recorded at the end of the adjacent span of Hinge 1 (Fig. 4-3 (b)). The main reason was that the end transverse gridline, T7 (Fig. 3-11), was not located exactly on the centerline of Bent 6 due to neglecting the effect of horizontal curvature of the superstructure during the preparation of gridlines sketch. Additionally, the bending of the bent cap and the axial shortening of the column contributed to the downward deflection. Note that the nearly flat profile in Fig. 4-3 between the origin and the first quarter span station in the adjacent span does not represent the true profile. It is believed that deflection between the bent and the quarter point was larger than that of the quarter point and that the actual profile was smooth. The upward deflection measured at the end of the adjacent span of Hinge 2 was due to immediate deflection of Bent 7 after completion of post-tensioning. Bent 7 was a post-tensioned outrigger bent (Fig. 2-26) and was prestressed simultaneously with Frame 2.

### 4.2.3 Bridge 3

The immediate deflection of the short cantilever and the adjacent span corresponding to the single hinge of Bridge 3 is shown in Fig. 4-5. The relative deformation was measured with respect to the centerline of Bent 4. The measurements on the longitudinal gridlines L1 and L2 (Fig. 3-13) were comparable because the hinge was at the second stressing end, and consequently the effect of different elastic shortening was minimal (Fig. 4-5 (a)).

Upward immediate hinge movement was observed due to the post-tensioning of the short cantilever. The adjacent span displaced downward at the first quarter point while it displaced upward at the mid-span and at the third quarter point. A small relative upward displacement was observed in Bent 3 (Fig. 4-5) due to axial shortening in columns of Bent 4 under the post-tensioning force.

### 4.2.4 Bridge 4

The immediate displacements of the short cantilever and the adjacent span corresponding to the single hinge in Bridge 4 measured on longitudinal gridlines L1, L2, and L3 (Fig. 3-14) and the average response are shown in Fig. 4-6. As mentioned in Chapter 3, more stations were added within the first quarter of the adjacent span to obtain a smoother and more precise profile for the deformation in the vicinity of the short cantilever. The general deformation pattern was nearly similar to that in the previous bridges. Unlike previous bridges, the upward deflection of the adjacent span at the middle point was higher than the hinge curl due to the relatively short cantilever length. In addition, Bridge 4 had a one-end stressing from Abutment 9 that caused more post-

tensioning friction losses at the hinge than that of the adjacent span. The variation in the displacement values across the bridge width was due to the post-tensioning sequence as discussed previously.

### 4.2.5 Bridge 5

The immediate deformed shapes of short cantilevers and the adjacent spans corresponding to the prestressed hinges in Bridge 5 are presented in Fig. 4-7. The deformation behavior of these hinges had identical pattern and was comparable to those of other bridges. Small downward displacements were measured in the 1/8th span adjacent to short cantilevers of C1, C2, and H4, and no displacement was recorded at the corresponding point of H1 (Fig. 4-7 (c)). The bent adjacent to H1 (Bent 4) had a skewed column at an angle of 40.5° measured from the bent centerline unlike adjacent bents of C1, C2, and H4 which had non-skewed columns. This reduced the bent cap rotation and consequently the deflection of adjacent span in the vicinity of the bent. The effect of column skew was not pronounced on the deflection of the cantilever as much as of the adjacent span due to the difference in deformation response between cantilever beams and fixed ended beams. The maximum measured upward displacement of adjacent spans was recorded at the mid-span.

## 4.3 Time-dependent deformation

As discussed in Chapter 3, the field measurements passed through different construction stages until the opening date. Time-dependent measured deflections were studied in two main phases: 1) before load transfer and 2) after load transfer. These two phases are discussed in the following sections.

### 4.3.1 Phase 1- before load transfer

This phase of construction starts after completion of post-tensioning and ends immediately prior to the start of load transfer from the long cantilever to the short cantilever at a hinge. Casting the top ledge of a hinge is not necessarily considered as load transfer since the long cantilever still is supported on falsework until the concrete reaches the specified strength.

#### 4.3.1.1 Bridge 1

The measured time-dependent displacements before load transfer are presented in Figs. 4-8 and 4-9 for hinges 3 and 7, respectively. The plots also include the immediate deformation measured after the stressing (Day 0) as a benchmark. Displacements were measured on longitudinal gridlines L1 to L3 presented in Figs. 3-9 and 3-10. The deformation behavior at both hinges showed similar trend across the bridge width. The upward deflection of short cantilever increased at Day 1 and Day 49 and the downward displacements of the adjacent spans increased due to creep of concrete.

#### 4.3.1.2 Bridge 2

Figures 4-10 and 4-11 show the time-dependent deformation behavior of Bridge 2 before load transfer for Hinges 1 and 2, respectively. Displacements were measured on longitudinal gridlines L1 to L3 presented in Figs. 3-11 and 3-12. The average upward deflections of the short cantilevers of both hinges increased from Day 0 to Day 36. However, the average deflection of the short cantilever of Hinge 1 decreased from Day 36 to Day 97 while that of Hinge 2 remained nearly unchanged over that period as shown

in Figs. 4-10 (d) and 4-11 (d). The reason for the change in the trend was the additional weight of hinge seats, which were cast between Day 36 and Day 97.

The overall deformation behavior of the adjacent span of Hinge 1 was consistent along L1, L2, and L3. In all cases the deflection at the mid-span increased with time. However the deflections varied slightly among the gridlines due to the effect of the post-tensioning sequence as described previously. The average downward displacement of the first quarter point of adjacent spans of both hinges increased until Day 36. The deflections of this point varied across the bridge width in H1 on Day 97. The average displacement was upward at this location. Unlike H1, nearly no additional deflection was recorded at the quarter point in Hinge 2 after Day 36.

Relative upward displacement at Bent 7 did not change significantly from Day 0 to Day 1. However the direction of measured displacement at Bent 7 was switched at Day 36, and a significant downward displacement was recorded (Fig. 4-11). The measured displacement increased at Day 97 in the same direction. The considerable displacement in the opposite direction was due to the partial falsework removal on Day 2 in vicinity of Bent 7, which was an outrigger bent (Fig. 4-12).

#### 4.3.1.3 Bridge 3

The measured time-dependent deformation before load transfer for the short cantilever and the adjacent span of the "hinge" in Bridge 3 is depicted in Fig. 4-13. Overall, the longitudinal gridlines L1 and L2 (Fig. 3-13) had nearly same displacement profile. No deformation change was observed between Day 0 and Day 1 in the short cantilever and the adjacent span. The average response in Day 22 showed additional

upward hinge curl and additional downward displacement at the first quarter points of the adjacent span, while the rest of the span had insignificant deformation change.

#### 4.3.1.4 Bridge 4

The time-dependent relative displacements for the “hinge” in Bridge 4 before load transfer are shown in Fig. 4-14. The deformation response was consistent along the longitudinal gridlines across the bridge width. The deflection of the short cantilever increased from Day 1 to Day 135 at different rates. The adjacent span had an increasing downward displacement at the first quarter span station. The mid-span upward displacement increased slowly until Day 99 and then decreased slightly at Day 135. This insignificant displacement reduction was attributed to the time-dependent losses in the post-tensioning forces due to steel relaxation, concrete creep, and shrinkage.

#### 4.3.1.5 Bridge 5

The time-dependent displacements before load transfer for the investigated prestressed hinges in Bridge 5 are presented in Fig. 4-15. The deformation response had a similar trend for the four hinges. The plots show that the deflection of short cantilevers generally increased over the time as long as they were not restrained by casting the top ledge of the hinge or by placing additional weight on the cantilevers.

The deformation of adjacent spans in the first quarter point near the hinge gradually increased downward. The response at the second and third quarter points showed an upward growing displacement over the time.

Deformation response before load transfer was divided into two stages for C1 and C2 curves due to a change in the loading condition. The first stage started after stressing

and extended until lowering the drop-in span and removing the falsework underneath on Day 45. The second stage extended from Day 45 until the complete falsework removal under the short cantilevers and the adjacent spans on Day 175. During the first stage, the short cantilever deflection increased until Day 44 and in the second stage, starting Day 78 until Day 152, the trend was reversed. The reason was the partial load transferred sometime between Day 44 and Day 78 due to the lowering of the drop-in span as described in Chapter 2. The load transfer was incomplete since the falsework was still up and supporting the short cantilevers and adjacent spans of C1 and C2. While the cantilevers of C1 and C2 continued to move down gradually in the second stage, the adjacent spans camber kept growing at the mid-span.

Hinge 1 cantilever had an increasing deflection until Day 27, and then this trend changed by having less deflection on Day 68. The deformation trend of the adjacent span near the cantilever was similar to that of the cantilever but in the opposite direction. The adjacent span had a growing camber at the mid-span until Day 68 (Fig. 4-15 (e)). The reduction of deflections in the short cantilever and the adjacent span was because of additional weight applied by casting the RC slab deck of the long cantilever and the top ledge of the hinge (Fig. 4-16).

The deformation response of Hinge 4 before load transfer underwent two stages, one was before casting the top ledge of the hinge closure as presented in Fig. 4-15 (f), and the second was after the completion of the hinge closure as shown in Fig. 4-15 (g). During the first stage, the cantilever deflection increased and the adjacent span near the hinge moved downward, while the rest of the span camber remained nearly unchanged after the initial displacement.

The top ledge was cast few days before Day 97. In the second stage, the cantilever deflection remained nearly unchanged on Day 97 due to concrete blocks placed on the short cantilever as shown in Fig. 4-17. The downward deflection increased further due to the applied weight on Day 138. Subsequent data sets collected on Day 182, Day 212, and Day 224 showed an upward deflection due to concrete blocks removal, however the cantilever did not fully recover the downward deflection. The adjacent span deformation did not substantially change, however it had minor fluctuations over time.

### 4.3.2 Phase 2 - After load transfer

This phase starts after falsework removal in which the load is transferred from long cantilever to the short cantilever. The field measurements in this phase were continued until or shortly before the bridge opening dates. The majority of long-term deflections occur in the first four years of this phase due the effects of creep and shrinkage.

#### 4.3.2.1 Bridge 1

Deformation of hinges 3 and 7 after the load transfer are plotted in Figs. 4-18 and 4-19, respectively. The deformation profile measured in the last data collection before load transfer was also superimposed as a reference and labeled as “Before LT.” The short cantilever deflected downward at both hinges after load transfer. Relative displacement magnitudes varied slightly across the bridge width at both cantilevers. The reason was an uneven load distribution transferred from the long cantilevers because of the horizontal curvature of Frame 2 and variable prestress losses within the girders. The

average response of the cantilever showed slight reduction in the upward deflection at Hinge 1 and no significant change in Hinge 2 between Day 92 and Day 129.

#### 4.3.2.2 Bridge 2

Figures 4-20 and 4-21 show the time-dependent deformation response after load transfer for bridge 2 at Hinge 1 and 2, respectively. Day 97 represents the last data measured before load transfer. Some stations were inaccessible due to various obstacles (Fig. 3-8) during Day 148, therefore new stations were marked as close as possible to the original stations. Measured elevations at inaccessible stations were then calculated based on data collected at the auxiliary stations and other available stations. Data were not collected on gridlines L1 and L2 at hinge 2 on Day 197 because of the grinding of concrete deck surface. All stations on these gridlines had been removed due to concrete grinding. The entire deck surface of frame 2 was ground on Day 197 to correct the grades as shown in Fig. 4-22. Therefore the data were recorded only on L3 for hinge 2.

The grinding thickness at Hinge 1 was shallower than that of Hinge 2. Some stations were removed due to grinding and consequently elevations were interpolated during the data processing. The average deformation response measured on Day 148 at Hinge 1 (Fig. 4-20 (d)) showed a drop of 1.38 in (35 mm) in the short cantilever deflection, and the adjacent span had a jump of 0.553 in (14 mm) in the camber at mid-span. This was due to the partial falsework removal (Fig. 4-23) on Day 148 before the complete removal prior to Day 197 (Fig. 4-24). The falsework was removed under the hinged span but remained in the adjacent span of Hinge 1. The average deflections of the cantilever and the adjacent span of Hinge 1 were reversed on Day 197 with respect to

Day 148 as shown in Fig 4-20 (d). This behavior was not observed in the cantilever and the adjacent span of Hinge 2. The cantilever of Hinge 2 did not deflect significantly between the two data sets after load transfer, while the adjacent span underwent some additional downward deflection on Day 197 due to creep of concrete.

#### 4.3.2.3 Bridge 3

The deformation behavior of the cantilever and the adjacent span of Frame 1 in Bridge 3 after load transfer is shown in Fig. 4-25. The data set measured on Day 83 represents the response after load transfer and data set measured on Day 22 (marked as "Before LT") represents the last measurement before load transfer. Falsework was removed in two stages to eventually transfer the load completely on Day 65. The upward deflection of the cantilever decreased due to load transfer while the adjacent span deflected downward under its self-weight. The adjacent span deformation profile near the hinge remained almost unchanged after load transfer. The deformation behavior showed nearly comparable deflections across the bridge width as seen in Figs. 4-25 (a) and (b).

#### 4.3.2.4 Bridge 4

Deformation profiles of Bridge 4 after load transfer across the bridge width and the average responses are plotted in Fig. 4-26. Two data sets were collected after falsework removal on Day 167 and Day 170. Downward relative deflections were measured on the adjacent span on Day 167 with respect to Day 135, before load transfer. Additional downward deformations were recorded in the adjacent span on Day 170 due to creep of concrete. The average deformation behavior of the short cantilever showed an

increased downward deflection from Day 135 to Day 167. The average cantilever profile remained nearly unchanged on Day 170 compared to Day 167 as shown in Fig. 4-26 (d).

#### 4.3.2.5 Bridge 5

Time-dependent deflections for cantilevers and adjacent spans of the P/S hinges in Bridge 5 are plotted in Fig. 4-27. Unlike previous bridges, the camber of adjacent span increased over time after load transfer due to dominating effect of prestressing force. Few data sets showed a small reduction in the camber due to the unbalanced spans effect after falsework removal as well as prestressing losses. The short cantilevers continued to deflect downward after the load transfer.

## 4.4 Hinge curl history

The variation of measured hinge curls with time at the centerline of hinges is discussed in this section. The hinge curls at centerline were extrapolated from the measured deflections as discussed previously in this chapter.

### 4.4.1 Bridge 1

The hinge curl histories for Hinge 3 and Hinge 7 in Bridge 1 are shown in Fig. 4-28. The average immediate (elastic) hinge curls along with time-dependent curls before and after the load transfer are shown in this figure. The dashed line indicates the time of load transfer. Immediate hinge curl is defined as that measured on Day 0, which is immediately after completion of post-tensioning at both ends. The stressing of Frame 2 in bridge 1 took nearly 3 days. The immediate hinge curl measured at Hinge 3 was smaller than that of Hinge 7 due to the shorter cantilever of Hinge 3. The hinge curls increased by

approximately 32% at both hinges on Day 1. The increase was approximately 45% on Day 49.

Load was transferred from the long cantilevers to the short cantilevers at Day 85 and Day 70 for hinges 3 and 7, respectively. The first data collected after load transfer was on Day 92, and showed a downward displacement of 0.355 in (9 mm) and 0.738 in (19 mm) at hinges 3 and hinge 7, respectively. The deflection due to the load transfer is a function of short cantilever length and the load magnitude transferred at a hinge. The average measured hinge curl at Hinge 3 decreased by 0.100 in (3 mm) from Day 92 to Day 129, however the curl at Hinge 7 remained approximately unchanged after Day 92.

### 4.4.2 Bridge 2

The immediate and time-dependent hinge curls measured at Hinges 1 and 2 in Frame 2 of Bridge 2 are presented in Fig. 4-29. The magnitude of measured immediate hinge curl was comparable at the two hinges due to similarities in dimensions, lengths, and prestressing force between the two short cantilevers and adjacent spans. The stressing of Frame 2 and the outrigger bent (Bent 7) was completed in three days. Curls measured at Hinges 1 and 2 on Day 1 increased by approximately 18% compared to Day 0 and increased by 26% and 45%, respectively, on Day 36. The larger increase at Hinge 2 was due to the downward deformation of the outrigger bent (B7) resulted by the partial falsework removal on Day 2. The measured deflections on Day 97 were slightly lower at both hinges due to additional weight of hinge seats that had been cast between data collection on Day 36 and Day 97. The hinge curl on Day 148 at Hinge 1 significantly dropped (Fig. 4-29 (a)) due to the partial falsework removal. The falsework under the

hinge 1 span was removed, but falsework under the adjacent span remained in place. The upward hinge curl was restored again on Day 197 after the complete falsework removal, but with a reduction of 0.708 in (18 mm) from the last measurement before load transfer on Day 97. The curl measured in Hinge 2 on Day 148 decreased due to the load transfer. Data measured after 49 days on Day 197 showed insignificant change in Hinge 2 curl as shown in Fig. 4-29 (b).

### 4.4.3 Bridge 3

The hinge curl behavior in Frame 1 of Bridge 3 is shown in Fig. 4-30. The stressing of Frame 1 was completed in two days. The measured data indicated an immediate upward movement on Day 0 but nearly no additional curl on Day 1 unlike other hinges. The data measured on Day 22 showed approximately 20% increase in hinge curl. The load was transferred, and falsework was removed completely on Day 65. Only one data set was measured after load transfer on Day 83 and it showed a drop of 55% in the hinge curl.

### 4.4.4 Bridge 4

The measured hinge curl response for Bridge 4 is plotted in Fig. 4-31. Day 0 hinge curl in Bridge 4 was smaller than that of other bridges due to the shorter cantilever in this bridge. Hinge curl increased by approximately 20%, 49%, 145%, and 181% on Day 1, Day 51, Day 99, and Day 135, respectively. The load was transferred on Day 165, and another data set was collected on Day 167. This measurement showed that the hinge curl decreased by 33% after load transfer. The measured curl on Day 170 showed

approximately no change from Day 167. The location of the hinge at the last measurement was 0.394 in (10 mm) higher than its initial location at Day -1.

### 4.4.5 Bridge 5

Figure 4-32 shows hinge curl histories for investigated P/S hinges in Bridge 5. Hinge 1 and Hinge 4 were in Frame 1 of Bridge 5EB and Frame 5 of Bridge 5WB, respectively. The immediate curl in these hinges was comparable because of similarities in prestressing force and the cantilever length. The measured curls in hinges C1 and C2 on Day 0 were comparable and both were smaller than those of hinges 1 and 4 due to the relatively shorter cantilevers. The measured hinge curls on Day 1 increased by 32%, 62%, 68%, and 135% at H4, H1, C1 and C2, respectively, compared to Day 0. The curls in hinges C1 and C2 increased respectively by 79% and 185% on Day 13 and by factors of 220% and 260% on Day 44.

The load was transferred partially on Day 45 and fully on Day 175 at C1 and C2. Figure 4-32 (a) and (b) shows a reduction in hinge curls due to load transfer. After the load was transferred completely, the hinge curl at C1 and C2 remained approximately unchanged over the time.

The curl in H1 increased by about 86% on Day 27 as shown in Fig. 4-32 (c) and decreased on Day 68 due to the long cantilever weight (Fig. 4-16). After load transfer on Day 100, H1 curl decreased gradually from 0.248 in (6 mm) on Day 68 to 0.104 in (3 mm) on Day 275. The hinge curl at H4 increased continuously from Day 0 to Day 74 on which the measured curl was 2.67 times the immediate hinge curl (Fig. 4-32 (d)). A reduction was observed in H4 curl on Day 97 and additional reduction was observed on

Day 138 as shown in Fig. 4-32 (c). This reduction was due to the weight of the long cantilever in addition to placing concrete blocks on the short cantilever (Fig. 4-17). The curl at H4 increased again from Day 138 to Day 212 after the concrete blocks were removed. The curl on Day 224 was 0.039 in (1 mm) less than that of Day 212 which was negligible. The load was completely transferred on Day 240, and the hinge curl decreased gradually afterwards due to creep of concrete. On the last measurement on Day 406, the curl in H4 decreased to 31% of the maximum measured hinge curl before load transfer. The hinge position on the last day was 0.194 in (5 mm) higher than its original position before stressing on Day -1.

### 4.5 Deformation behavior of non-PS hinges

Deformation response of the non-PS hinges in Bridge 5 was investigated during field measurements. The two hinges that were studied, H2 and H3, are in frame 3 in Bridge 5WB as described in Chapter 2. Time-dependent deflections of short cantilevers and the common adjacent span are shown in Figs. 4-33 (a) and (b) for Hinges 2 and 3, respectively. Although Hinges 2 and 3 have a common adjacent span, two separate plots are presented in Fig. 4-33. Each plot shows the deformation behavior with respect to the bent near the respective hinge. Since Frame 3 is not post-tensioned, Day 0 represents the first day after the superstructure completion. The first data set on F3 was collected 10 days after casting the deck slab and was used as the reference data. Therefore, the first deformation behavior curves shown on the plots were labeled Day 22 which were measured 12 days after Day 10. The measured displacements on Day 22 were very small on the short cantilevers and the adjacent span for both hinges. This response was

expected since there were no additional forces applied to the frame and because the falsework still supported the frame.

The Day 53 data indicated a slight downward deflection in the short cantilevers and a significant deflection in the adjacent span at the middle. That behavior was a result of the falsework removal and load transfer. The deflections for the cantilevers and adjacent span increased slightly over the time until Day 205, when the last data set was collected.

Figures 4-34 (a) and (b) show the hinge curl histories at hinges 2 and 3, respectively. It can be seen that non- PS hinge curls were negligible before load transfer. The hinge moved downward about 30 days after the completion of the superstructure due to load transfer at both hinges and removal of the falsework. The downward hinge curls increased continuously with time due to creep of concrete.

### 4.6 Temperature and relative humidity effect

The ambient temperature and relative humidity were recorded during each data set measurement and are listed in Tables 4-1 to 4-8. The effect of temperature and relative humidity variation on deformation of short cantilevers and adjacent spans was investigated. The influence of the weather change was examined by measuring the bridge elevations for the same stations of a hinge two times. The two collected data sets were separated by less than 24 hours to capture the extreme values of temperature and relative humidity during the day. The study was conducted two times at two different hinges, one in Bridge 3 and the other in Bridge 5WB. The collected data represented two different loading stages, after load transfer in Bridge 3 and before load transfer in Bridge 5WB.

Figure 4-35 (a) shows the deflection of Bridge 3 at the hinge, and Fig. 4-35 (b) shows the deflection at Hinge 4 in Bridge 5WB.

The two data sets collected for Bridge 3 were after load transfer when there was no falsework. They were collected on Day 83 and separated by 5 hours to ensure measuring deformation at the maximum and minimum temperature and relative humidity in that day. The temperature and relative humidity collected in the morning were respectively 1°C and 70% while they were 10°C and 34% at noon.

The data on Bridge 5WB was collected twice, 22 hours apart in two consecutive days, Day 73 and Day 74. The recorded temperature and relative humidity on Day 73 were respectively 30°C and 25% whereas 21°C and 36% were recorded on Day 74.

It can be concluded from Fig. 4-35 that the change in temperature and relative humidity during the day did not influence the deformation behavior of the short cantilever and the adjacent span significantly. Hinge curl decreased by approximately 13% at both hinges due to the temperature increase. The adjacent span deflection decreased by about 23% at the middle with the temperature increase at Bridge 3 as seen in Fig. 4-35 (a). The camber of the adjacent span of Hinge 4 increased by about 15% at the middle due to the temperature rise as shown in Fig. 4-35 (b).

## 4.7 Summary of field measurement findings

All the short cantilevers and adjacent spans exhibited similar deformation trends immediately after stressing and over time. Deflection values varied among bridges depending on the design parameters of each bridge such as prestressing force and length of the short cantilever and adjacent span. Deflection of the short cantilever varied across

the bridge width insignificantly at the first stressing end while no deflection difference in the transverse direction was observed at the second stressing end.

The downward deflection of adjacent spans in the vicinity of the bent adjacent to the short cantilever revealed that the bent cap rotates after stressing and consequently increases the upward deflection of the cantilever. This demonstrates that the bent flexibility affects hinge curl and should be taken into account.

The immediate hinge curl increases over time with variable rates before load transfer. Placing extra weights, and casting hinge diaphragms and top ledges restrained upward deflection of the short cantilever and, in some cases, led to downward displacement. Hinge curl behavior after load transfer changed somehow among hinges, and was mainly dependent on the load and span length ratios between bridge spans.

Non-prestressed hinges showed almost no deflection in the cantilever and adjacent span before load transfer. After the load transfer deflections were observed in the cantilever and adjacent span according to the load value and spans length. Variation of environmental conditions such as temperature and relative humidity during the day did not affect significantly the deflection values of the cantilever and adjacent span before and after load transfer.

# Chapter 5 Comparison of Measured and MTD 11-34 Hinge Curls

## 5.1 Introduction

The procedure to estimate hinge curl developed by Caltrans has been published in Memo to Designers (MTD) 11-34 (Caltrans, 2012). This procedure along with the predicted hinge curls for the five bridges that were the subject of field measurements are presented in this chapter. Based on the correlation between the measured and calculated data, the method in MTD 11-34 is evaluated and modifications are proposed to improve correlation.

## 5.2 MTD 11-34 Method

MTD 11-34 addresses the deformation behavior of in-span hinges for cast-in-place prestressed concrete box girder bridges. The deformation behavior, hinge curl or camber, consists of the upward deflection of the unloaded short cantilever due to stressing, as well as the downward deflection of the short cantilever after it is loaded by the long cantilever. The final location of the hinge is influenced by the time over which the short cantilever is left unloaded after stressing. This time period is usually between 30 and 180 days, but is not known exactly at time of bridge design as it depends on the actual construction schedule. Therefore a table of time-dependent camber values is typically provided as part of the contract plans.

The MTD provides a method to predict the hinge curl and the associated camber values that are listed on contract plans. The procedure assumes that falsework remains in the adjacent spans until load is transferred from the long cantilever to the short cantilever. MTD 11-34 accounts for long term effects on hinge curl due to concrete creep and

shrinkage through time-dependent deflection factors. It also accounts for the joint rotation at top of columns resulted from span deflections after (and not before) complete falsework removal. This is referred to as unbalanced span effect and is estimated by utilizing the Caltrans bridge analysis and design software (CTBridge) or other similar software. Deflection is considered to be positive when it is downward. Camber is positive when it is upward. It is assumed in MTD 11-34 that joint rotation prior to falsework removal is negligible because it is restrained by the falsework.

### 5.2.1 Method of calculation

The key steps of hinge curl calculation method in the MTD 11-34 are presented in this section.

Step 1- Determine the deflection of the short cantilever at the centerline of a hinge due to dead load (Fig. 5-1):

$$\Delta_{DL} = \underbrace{\frac{w.L_1^{\,3}}{24EI}(4L_3 - L_1)}_{(a)} + \underbrace{\frac{P.L_2^{\,2}}{6EI}(3L_3 - L_2)}_{(b)} \qquad (5.1)$$

Where

(a) = Deflection of short cantilever due to its self-weight

(b) = Deflection of short cantilever due to diaphragm weight at hinge closure at the end of the short cantilever

w = Uniform self-weight of the prismatic section of the short cantilever

P = Weight of the portion of the hinge diaphragm that fills the voids of the prismatic section in the short cantilever side

$L_1$ = Length of short cantilever measured from the face of the hinge diaphragm to the face of the support

$L_2$ = Length of short cantilever measured from the face of support to the centroid of the short cantilever hinge diaphragm

$L_3$ = Length of short cantilever measured from the face of support to the centerline of the hinge

E = Concrete modulus of elasticity calculated based on $f'_c$

I = Average moment of inertia of short cantilever span

In Eq. 5.1 it is assumed that rotation at the cantilever to pier connection is negligible because the falsework is assumed to prevent any deformation.

Step 2- Determine the deflection of the short cantilever at centerline of a hinge due to prestressing force (Fig. 5-2):

$$\Delta_{PS} = \frac{-P_j . FC . L_1}{12EI} . [e_1(8L_3 - 3L_1) + e_2(4L_3 - 3L_1)] \qquad (5.2)$$

Where

$P_j$ = Design jacking force

FC = Average initial force coefficient at the time of stressing in the short cantilever (unitless)

$e_1$ = Eccentricity at centerline of the bent. An eccentricity above the centerline is positive.

$e_2$ = Eccentricity at anchorage in the hinge diaphragm. An eccentricity above the centerline is positive.

Here again pier-superstructure rotation is neglected due to presence of the falsework.

Step 3- Determine the deflection of the short cantilever at the centerline of a hinge due to the load transferred from the long cantilever:

$$\Delta_{\text{reaction}} = \frac{\text{T.}\,L_3{}^3}{3EI} \qquad (5.3)$$

Where

T = Load transferred from long cantilever due to its self-weight and prestressing only. "T" includes the weight of the cast-in-place hinge diaphragms and ledges. The transferred load is determined from the longitudinal model analysis of the bridge as the shear demand at the face of the short cantilever hinge diaphragm.

Step 4- Calculate the immediate hinge curl after the completion of post tensioning:

$$\Delta_{\text{Curl}} = \Delta_{\text{DL}} + \Delta_{\text{PS}} \qquad (5.4)$$

Step 5- Calculate Displacement Adjustment for Short Cantilever (SC) using the following equations.

Adjustment SC is the profile adjustment required for the short cantilever at the hinge. The adjustment can take both positive and negative values and is calculated as follows for different load transfer time:

$$\text{Day 0 value} = 3.00\Delta_{\text{curl}} + 3.00\Delta_{\text{reaction}}$$

$$\text{Day 30 value} = 3.00\Delta_{\text{curl}} + 2.60\Delta_{\text{reaction}}$$

$$\text{Day 60 value} = 3.00\Delta_{\text{curl}} + 2.20\Delta_{\text{reaction}}$$

$$\text{Day 90 value} = 3.00\Delta_{\text{curl}} + 1.80\Delta_{\text{reaction}}$$

$$\text{Day 120 value} = 3.00\Delta_{\text{curl}} + 1.60\Delta_{\text{reaction}}$$

$$\text{Day 180 value} = 3.00\Delta_{\text{curl}} + 1.55\Delta_{\text{reaction}}$$

$$\text{Day 240 vlaue} = 3.00\Delta_{\text{curl}} + 1.50\Delta_{\text{reaction}}$$

$$\text{Day 360 vlaue} = 3.00\Delta_{\text{curl}} + 1.40\Delta_{\text{reaction}}$$

$$\text{Day 720 value} = 3.00\Delta_{\text{curl}} + 1.25\Delta_{\text{reaction}}$$

$$\text{Day 1440 value} = 3.00\Delta_{\text{curl}} + 1.00\Delta_{\text{reaction}}$$

If the difference between Adjustment "SC" values of Day 0 and Day 720 is less than or equal to 0.5 inch (12.7 mm), it is reasonable to assume that hinge curl effects are negligible, and a time-dependent camber table is not to be used. Hence, an equal camber obtained from the theoretical camber is implemented at the hinge for both short and long cantilevers. The theoretical camber is the profile corresponding to the long term bridge deflection when load transfer is assumed to take place on Day 0, and it is determined using CTBridge as discussed in the next two sections. Note that MTD assumes there will be no additional time-dependent deflection at the hinge after four years of stressing.

Step 6- Calculate Adjustment Displacement for Long Cantilever (LC) using the following equations.

Adjustment LC is the profile adjustment required for the long cantilever at the hinge and can take both positive and negative values. Adjustment LC is calculated as follows for different load transfer time:

$$\text{Day 0 value} = 2.00\Delta_{\text{curl}} + 3.00\Delta_{\text{reaction}}$$

$$\text{Day 30 value} = 1.60\Delta_{\text{curl}} + 2.60\Delta_{\text{reaction}}$$

$$\text{Day 60 value} = 1.20\Delta_{\text{curl}} + 2.20\Delta_{\text{reaction}}$$

$$\text{Day 90 value} = 0.80\Delta_{\text{curl}} + 1.80\Delta_{\text{reaction}}$$

$$\text{Day 120 value} = 0.60\Delta_{\text{curl}} + 1.60\Delta_{\text{reaction}}$$

$$\text{Day 180 value} = 0.55\Delta_{\text{curl}} + 1.55\Delta_{\text{reaction}}$$

$$\text{Day 240 value} = 0.50\Delta_{\text{curl}} + 1.50\Delta_{\text{reaction}}$$

$$\text{Day 360 value} = 0.40\Delta_{\text{curl}} + 1.40\Delta_{\text{reaction}}$$

$$\text{Day 720 value} = 0.25\Delta_{\text{curl}} + 1.25\Delta_{\text{reaction}}$$

$$\text{Day 1440 value} = 0.00\Delta_{\text{curl}} + 1.00\Delta_{\text{reaction}}$$

The deflection factors used in the Adjustment "SC" and Adjustment "LC" equations are derived from the curve shown in Fig. 5-3. This curve represents the time-dependent deflection in a cast-in-place prestressed concrete element with respect to immediate deflection. For example, the total deflection including the long term effects of creep and shrinkage is three times the immediate elastic deflection over a four-year period. The curve starts at a value of 1.00 representing the immediate elastic deflection for a given load at Day 0, which is considered the day in which the post-tensioning of short cantilever is completed.

Adjustments SC and LC utilize the deflection factors in the graph (Fig. 5-3) based on the long term location of the hinge.

For example, the Day 30 value for Adjustment SC is $2.60\Delta_{reaction} + 3.00\ \Delta_{curl}$. The maximum deflection factor of 3.00 is applied to $\Delta_{curl}$ assuming that the short cantilever is loaded by its self-weight and prestressed immediately after it is cured sufficiently. The term of $2.60\Delta_{reaction}$ represents the notion that 30 days has elapsed since prestressing the short cantilever. The deflection factor at Day 30 is 1.40 (Fig. 5-3) meaning that the component of the deflection factor representing creep and shrinkage in the amount of 0.40 (1.40-1.00) of long-term deflection has already occurred in the short cantilever.

Thus, the transfer load component, $\Delta_{reaction}$, will only be subjected to the remaining deflection factor of 2.60 (3.00-0.40).

The Adjustment "LC" for Day 30 is $2.60\Delta_{reaction} + 1.60\ \Delta_{curl}$. Adjustment "LC" signifies the amount of camber for the long cantilever to match the location of the short cantilever when the load is transferred. The factor of 1.60, applied to $\Delta_{curl}$, represents the notion that at 30 days, the short cantilever has already undergone $1.40\Delta_{curl}$ of deflection, and the remainder is $(3.00\text{-}1.40)\Delta_{curl}$. The $2.60\Delta_{reaction}$ signifies that the transfer load component, $\Delta_{reaction}$, will only be subjected to the remaining deflection factor of 2.60 (3.00-0.40).

### 5.2.2 Development of camber diagram

Development of the camber diagram involves incorporating the Adjustment "SC" and Adjustment "LC" values calculated previously with the theoretical camber of the hinge span as shown in Fig. 5-4. Once the Adjustments values are added to the theoretical camber of the span, the new values are referred to as Camber "SC" and Camber "LC", respectively. The values of Camber "SC" and Camber "LC" are those implemented in field to ensure a smooth ride over in-span hinges after 4 years and are different than Adjustment "SC" and Adjustment "LC".

Figure 5-4 shows Adjustment "SC", Adjustment "LC", and the theoretical camber of the span with the hinge. Points 1, 2, and 3 represent the adjustment required to the theoretical camber at the hinge to obtain final camber values of Camber "SC" and Camber "LC". It can be seen in Fig. 5-4 that neither Adjustment "SC" nor Adjustment "LC" is required at point 1 if the load is transferred immediately on Day 0. Cambers LC

and SC are provided at the edges of the long and short cantilevers as represented by points 2 and 3, respectively (Fig. 5-4). These adjustments are intended to match the elevation of points 2 and 3 sometime after completion of post-tensioning. The load is usually transferred from the long cantilever to the shot cantilever from 30 to 180 days after prestressing the short cantilever. Time-dependent camber values are tabulated in plans to help contractor adjust the falsework before casting the superstructure depending on the scheduled time of load transfer. Usually camber values are provided for up to 720 days with 30-day intervals.

Steps 7 to 9 are required to develop a time-dependent camber diagram.

Step 7- Obtain the theoretical camber of the long cantilever at quarter span points of the long cantilever from CTBridge. The camber values are designated as $LC_{0.25}$, $LC_{0.50}$, $LC_{0.75}$, $LC_{1.00}$, and SC and are respectively the unadjusted camber at the first, second, and third quarter points on the long cantilever, unadjusted camber at the edge of the long cantilever, and unadjusted camber at the edge of the short cantilever. When obtaining the theoretical camber from CTBridge, the unadjusted camber value at the edge of the short cantilever, SC, is equal to its corresponding value at the edge of the long cantilever, $LC_{1.00}$ if the short cantilever is on the right side of the span. When the short cantilever is on the left side of the span, SC is equal to $LC_{0.00}$. The theoretical camber values include a deflection factor of 3.0 to account for time-dependent increases.

Step 8- Adjust short cantilever camber for time-dependent correction.

The effect of bridge deflection after load transfer is incorporated in this step to obtain Camber “SC”. Generally, unbalanced spans resulting from complete removal of falsework will generate deflections that differ from the Adjustment “SC” values due to

the rotation of superstructure-pier joint. Therefore, one can estimate the deflection due to joint rotation, $\delta_{SC}$, by calculating the difference between the theoretical camber determined by CTBridge and Adjustment "SC" at Day 0 as shown in Fig. 5-5. $\delta_{SC}$ is calculated as follows:

$\delta_{SC}$ = Theoretical SC (Step 7) – Adjustment SC at Day 0 (Step 5)

Time-dependent values of Camber "SC" are calculated by an algebraic sum of $\delta_{SC}$ and Adjustment "SC" associated with the time of load transfer.

Step 9- Adjust long cantilever camber for time-dependent correction at $LC_{1.00}$ (hinge) as shown in Fig. 5-6. $\delta_{LC1.00}$ is the deflection at the edge of the long cantilever due to joint rotation after falsework removal in the span with the hinge and adjacent spans, and is calculated as:

$\delta_{LC1.00}$ = $LC_{1.00}$ (Step 7) – Adjustment "LC" at Day 0 (Step 6)

Camber "LC" is calculated similarly to Camber "SC" by the algebraic sum of $\delta_{LC1.00}$ and Adjustment "LC" associated with the time of load transfer.

At other locations along the long cantilever, adjustment "LC" is linearly interpolated. For example, at the 3/4 L point, Adjustment "LC" is factored by 3/4 as follows:

$\delta_{LC0.75}$ = $LC_{0.75}$ (Step 7) – Adjustment "LC" at Day 0 (Step 6)*3/4

The camber values are calculated by an algebraic sum of $\delta_{LC0.75}$ and Adjustment $LC_{0.75}$.

Note that if the hinge span configuration is reversed, in which the short cantilever is on the left, the factor applied to Adjustment "LC" at the 3/4 L point would be 1/4 instead of ¾ (Fig. 5-6).

### 5.2.3 CTBridge analysis

CTBridge is a computer program specifically designed to aid the analysis and design of typical California highway bridges. CTBridge allows for description of bridge geometry, reinforcement, and loads in terms familiar to bridge engineers. This information is used by CTBridge to construct a numerical model that is subsequently solved using finite element methodology. The program is equipped with a graphical user interface that allows viewing of the numerical model. The program utilizes both US and SI units, and its results are obtainable through viewing and printing the tabular reports or the graphical details.

Three-dimensional spline models were generated for Bridges 1 to 5 as shown in Figs. 5-7 to 5-12. The models were built by defining cross section geometries, material properties, span lengths, and bents configuration. The horizontal and vertical alignment features were used to define horizontal curves and longitudinal slopes, respectively. Prestressing tendons were lumped into a single tendon whose path was located at the centroid of the tendons. A prestressing tendon path was defined for each frame. Prestress design parameters, such as jacking force, anchor set, coefficient of friction, wobble coefficient, and the number of stressing ends were also defined for each bridge frame. Column connections to bent caps and foundations were considered to be rigid. Gross moment of inertia was used for all bridge components except for temporary columns that were pinned at the top in Bridge 3. Since the program does not have the capability of assigning different types of connection to the columns of a bent, a significantly reduced moment of inertia was assigned to the temporary columns in Bridge 3 to simulate their top pinned connection by eliminating their flexural stiffness. A roller boundary condition

was assigned to hinges, and a fixed boundary condition was used at moment connections C1 and C2 in Bridge 5EB (Chapter 2, Section 2.7.5.1). The seat-type abutment in Bridge 5EB was modeled with a roller support. Skewed abutments (Abutment 1 in Bridge 5WB) were defined in the program by the angle of skew.

The goals of CTBridge analysis in this study were to obtain the theoretical camber of the bridges (Figs 5-13 to 5-18), to calculate the average initial force coefficient at the time of stressing in the short cantilever (FC), and to determine the shear demand at the face of the short cantilever end diaphragm. The theoretical camber was particularly determined at the PS hinges to generate the final camber according to steps 7, 8, and 9. The calculated camber inherently includes a long-term deflection factor of 3.0 which is multiplied by the unfactored displacements due to dead load and prestressing force. The calculated FC was used in Eq. 5.2, and the shear demand was used in Eq. 5.3.

## 5.3 Comparison of MTD estimated and measured hinge curls

Hinge curls for the sample bridges were calculated using MTD 11-34 and compared to those measured in the field. MTD 11-34 procedure aims mainly to estimate the final camber corresponding to the final hinge location. However, the immediate and time-dependent hinge curls can also be calculated using the MTD. These curls were used to compare with the measured immediate and time-dependent hinge curls.

### 5.3.1 Immediate hinge curl

The immediate hinge curl occurs right after the completion of stressing of the short cantilever and is calculated according to MTD 11-34 using equation 5.4. The

calculated immediate hinge curls are compared in this section to those measured on Day 0.

Table 5-1 and 5-2 summarize the predicted deflections of the short cantilevers under dead load and prestressing load, respectively. These values were used in immediate hinge curl calculations based on MTD 11-34. Table 5-3 compares the estimated and measured immediate hinge curl for the ten hinges. Since bridges 1, 2, and 3 had two-end stressing, the measured hinge curls listed in Table 5-4 for those bridges were obtained by dividing the original measured hinge curls by a deflection factor of 1.30. This deflection factor accounts for the creep that occurs during the post-tensioning process, which was assumed to be an average of one day under total prestressing force. The stressing operation took between two to three days to be completed. The deflection factor was calculated using the creep model of CEB/FIP code 90-99 for concrete structures (ACI 209.2R, 2008). Deflection factor chart of MTD 11-34 was not used due to the reasons that are discussed later in this chapter and Chapter 9. The correlation between the measured and calculated results is discussed at the end of this chapter.

### 5.3.2 Time-dependent hinge curl

Time-dependent hinge curl is any hinge deformation after Day 0 where the long term effects such as creep and shrinkage are present due to the elapsed time after the initial loading. Therefore, Day 1 is considered when the first time-dependent hinge curl takes place. Time-dependent curls are discussed for the two stages of before and after load transfer. The correlation between the measured and calculated results is discussed at the end of this chapter.

#### 5.3.2.1 Before load transfer

Since the adjacent spans are still supported on falsework before load transfer, MTD procedure assumes that joint rotations at the superstructure pier connection and deflections due to this rotation are negligible. Hence deflection factors derived from MTD time chart are simply multiplied by the immediate hinge curl to estimate the time-dependent hinge curl at any time before load transfer. Table 5-4 summarizes the comparison of hinge curls at Day 1, and Table 5-5 summarizes the time-dependent hinge curl comparison for different times before load transfer. The measured hinge curl values listed in Table 5-4 for bridges 1, 2, and 3 are those measured on Day 0, which technically represents Day 1, due to the duration taken to complete stressing. Comparisons between the calculated and measured hinge curls before load transfer are discussed in Section 5.4.

#### 5.3.2.2 After load transfer

The Caltrans memo deals with this stage through developing the camber diagram based on the bridge long-term deformation (deformations at and after 4 years). Therefore the maximum applicable deflection factors are applied to the elastic deflections as described earlier in this chapter. However, the hinge curl at any time after load transfer is estimated by applying the appropriate deflection factor associated with the time at which the deflection is calculated. For example, the short cantilever deflection due to load transfer ($\Delta_{reaction}$) immediately after load transfer can be found by considering only the deflection component with no factors applied. In other words a factor of 1.00 is multiplied by $\Delta_{reaction}$. If $\Delta_{reaction}$ is to be determined 30 days after the load transfer, deflection factor at time of load transfer is subtracted from deflection factor at 30 days

after load transfer to obtain the additional net deflection factor for $\Delta_{reaction}$. The net deflection factor accounts for the increasing $\Delta_{reaction}$ resulted in those 30 days only, since the short cantilever has already undergone a certain amount of deflection due to creep and shrinkage until the load transfer. $\Delta_{curl}$ is adjusted by a deflection factor that accounts for the elapsed time since stressing until the time at which the deflection after load transfer is calculated.

Although the effect of joint rotation resulting from falsework removal ($\delta_{SC}$, step 8) inherently includes a factor of 3.00, it was treated in a similar manner as the $\Delta_{curl}$ effect by dividing $\delta_{SC}$ by 3.00, then to multiply the result by the same deflection factor that is applicable to $\Delta_{curl}$. This approach was taken to ensure consistency with MTD 11-34 procedure, in which the same amount of $\delta_{SC}$ value is applied to Camber "SC" equations (step 8), regardless of the elapsed time between the initial condition and load transfer. The reason for this approach was to be able to compare the measured hinge curl in early days after the load transfer with values implicit in the MTD 11-34 approach. Note that this method is not explicitly used by MTD 11-34 since the main objective is to find the final hinge location and not the intermediate hinge curls.

The calculated loads transferred from long cantilevers and deflections of short cantilevers due to load transfer are listed in Tale 5-6. Adjustment "SC" was calculated for different times based on Step 5 of MTD, and the results were listed in Table 5-7. Although the difference between Adjustment "SC" at Day 0 and Day 720 was less than 0.5 in (12.7 mm) for all hinges, the hinge curl was calculated to better understand the correlation between measured and estimated hinge curl.

The theoretical camber values at the hinges obtained from CTBridge, SC, and deflections due to joint rotation, $\delta_{SC}$, are listed in Table 5-8. Long cantilever camber was not considered in the comparison since no deflections were measured on the long cantilevers in this study. Comparison between the calculated and measured hinge curls after load transfer is summarized in Table 5-9 and is evaluated in the following section.

### 5.4 Evaluation of MTD 11-34

The curls measured in the ten hinges were substantially different from those estimated using the current design equations. Hinge curls listed in Tables 5-3, 5-4, and 5-5 showed that MTD 11-34 considerably underestimated the hinge curls. It can be seen in Table 5-3 shows that the estimated immediate curls were 37% to 83% smaller than the measured curls, with the average of differences and the standard deviation being -62% and 15%, respectively. If results of Closure 1 and 2, which are not typical hinges, are excluded, the average difference and standard deviation become -68% and 11%, respectively.

Percent differences were 61% to 87% in Day 1 (Table 5-4) with all the calculated results underestimating the hinge curls with an average of 74%.

The time at which subsequent measurements were taken prior to load transfer varied (Table 5-5). But the trend in the correlation is the same as that of the immediate and Day 1 curls with the underestimation ranging from 48% to 87%. The average difference and the standard deviation were -70% and 9%. The average percent difference and standard deviation remained nearly the same when the closures were excluded (Tables 5-4 and 5-5).

The measured deflections of the adjacent spans have clearly revealed the main sources of the discrepancy between the measured and estimated curls. The measured deformation plots presented in Chapter 4 in all the five bridges consistently showed that there was always significant rotation at the superstructure-pier connection near the hinge despite the presence of the falsework. The current MTD document recognizes that the connection will undergo rotations only due to the unbalanced spans effect after falsework removal. The downward displacements measured in adjacent spans close to the hinges demonstrated that end of the cantilever is partially fixed rather than fully fixed as assumed in the MTD procedure. The rotation at the support of the short cantilever led to hinge curls that exceed the assumed values (Akl et al. 2013)

The measured and estimated hinge curls after load transfer are listed in Table 5-9. The estimated hinge curl and percent difference with the measured curl were not calculated for Day 148 at H1 in Bridge 2 because the falsework was only partially removed as mentioned in Chapter 4. Most of the estimated hinge curls after load transfer were still lower, and few were higher, than the measured data for the five bridges (Table 5-9). Although this disagreement could highly depend on the accuracy of immediate hinge curl prediction, another factor also contributed to the difference. The MTD time-dependent correction factors assume a linear relationship for the first 90 days after stressing, whereas in reality the relationship is nonlinear.

The accuracy of deflection factors is particularly important in the first three months after stressing when most of the creep deformation occurs. This is the time window during which there is a high probability for the load transfer. Accurate estimation of time-dependent hinge curl before load transfer can minimize the necessary

corrective actions in the field to control hinge curl such as placing weights on short cantilevers or grinding of concrete at the hinge.

Although long cantilevers were not surveyed in this study because they are supposed not to deflect before load transfer, the camber at the edge of the long cantilever is an important factor in addressing the adverse effects of hinge curl during construction. The short cantilever of in-span hinges tends to deflect upward after post-tensioning until the load transfer and therefore the location of the long cantilever at the hinge should match the short cantilever at the load transfer. As described earlier in this chapter the deflection due to joint rotation, $\delta_{LC1.00}$, is the difference between Adjustment "LC" at Day 0 and the theoretical camber, $LC_{1.00}$. In the current MTD method, Adjustment "LC" at Day 0 is calculated assuming that the immediate hinge curl already occurred and should not be included in the analysis. As a result, only the time-dependent $\Delta_{curl}$ is considered using a factor of 2.00, whereas $LC_{1.00}$ obtained from CTBridge inherently includes $3\Delta_{curl}$ since the short and long cantilevers move simultaneously at the hinge. Hence the difference between Adjustment "LC" at Day 0 and $LC_{1.00}$ does not represent the deflection due to joint rotation after load transfer, $\delta_{LC1.00}$. This issue was corrected in the proposed hinge curl calculation method described in Chapter 9.

Time-dependent correction made in step 8 is believed to be another source of inaccuracy in the estimated curls. There are two issues in how the deflection due to joint rotation, $\delta_{SC}$, is incorporated in camber calculations. The first is applying the same time-dependent correction factor (automatically applied) to ($\delta_{SC}$) in Camber "SC" regardless of the elapsed time. The second is treating this deflection component ($\delta_{SC}$) as it exists since Day 0 that is already tripled.

Deflection due to joint rotation ($\delta_{SC}$) is the deflection that occurs under the spans weight and prestressing forces after complete falsework removal. Hence falsework removal should be considered as a new loading stage, where a certain amount of creep deformation has already occurred. Therefore the increase in deflection after falsework removal should be treated differently to consider the elapsed time before load transfer.

# Chapter 6 Analytical Studies with Stick Models

## 6.1 Introduction

The five bridges were analyzed using the structural analysis program, SAP2000, version 15.0.1 (CSI 2011) under gravity and PT forces. Finite element method using beam elements (stick or spine model) was utilized to develop bridge numerical models. Out of total 11 SAP2000 models, 10 were for the PS hinges and one was for the non-PS hinges in Bridge 5WB.

The main objective of the analyses presented in this chapter was to determine the deformation of the short cantilevers and their adjacent span using a relatively simple model. Additional analytical studies were conducted using the simple model for Frames 2 and 4 in Bridge 5WB to determine the deformation of the long cantilever in that bridge. More detailed analytical modeling using finite element is presented in Ch. 7. The analytical results from this chapter and Ch. 7 are compared with field measurements in Ch. 8.

## 6.2 Geometry of the analytical models

The deformation of the bridges was studied in the longitudinal direction. Only the parts of the bridge between hinges or between hinges and abutments were modeled. A two-dimensional model (Figure 6-1) was sufficient for the analysis of all bridges except Bridge 2. The longitudinal slope, superelevation, horizontal curvature, and vertical curvature were not included in the analytical models. A three-dimensional model had to be developed for Bridge 2 to include the behavior of the post-tensioned outrigger bent (Bent 7) in the analysis (Fig. 6-2).

### 6.2.1 Superstructures and bents

Frame elements with equivalent cross-section properties were used to model the superstructures and bents. Superstructures were modeled with frame elements located at the center of gravity of the box-girder section. Based on a series of sensitivity analyses, it was found that deformations of the superstructure can be captured sufficiently using approximately 70-in (1778-mm) long elements. The bent caps were modelled with a frame element divided into two equal segments in the longitudinal direction of the bridge at the location of the column (segments 1 and 2 in Fig. 6-3). The equivalent properties of the bent cap in the transverse direction were assigned to the cross-sections properties of the frame segments. Long cantilevers of in-span hinges were not modeled and instead the load from the long cantilever to the short cantilever was applied to the center line of each hinge. The hinge diaphragm and the seat were idealized using two frame elements with equivalent properties as shown in Fig 6-4.

The feature of general frame sections in SAP2000 was used to define cross-section properties of the superstructures. The superstructures were assumed to be uncracked due to the post-tensioning force, and therefore the gross moment of inertia was used. Shear deformation in superstructures was assumed to be negligible. The box girders in each span were modelled using a prismatic element with average cross-section properties, neglecting variable superstructure width in Bridge 1 and Bridge 4.

The specified column cross section areas were used in the analytical models for circular and rectangular sections, but general frame sections with equivalent cross-section properties were used for oblong columns. Two-column bents were modeled using a single column with section properties that were twice those of single columns. The

calculated hinge curls before falsework removal (load transfer) were insensitive to whether gross or cracked column moment of inertia was used, but was sensitive afterward. However it was decided to use gross moment of inertia for all deformation analyses because for non-seismic analysis of concrete bridge columns typically the gross moment of inertia is used (Caltrans 2014).

### 6.2.2 Tendons

Prestressing tendons can be modeled in the program either using equivalent prestressing loads or be included as structural elements. The second approach was selected in this study because this approach enables to include the long-term prestressing losses automatically based on the time-dependent properties of tendon material (CSI 2011). The feature of tendon objects in SAP2000 was used to model the prestressing steel. An equivalent parabolic tendon profile along each bridge frame was defined. The equivalent tendon profile was assumed to be at the center of gravity of actual tendons because all deflections are calculated based on the resultant prestressing force applied to the center of gravity of the prestressing stands (Nawy 2009). Tendon eccentricities were calculated with respect to the center of gravity of the box girder and then plugged in the tendon layout input data table as shown in Fig. 6-5. The maximum tendon discretization length was set to 60 in (1524 mm) based on a series of sensitivity analyses. The total area of prestressing tendons was calculated based on the plans. Other properties such as torsional constant, moment of inertia, and shear area were automatically calculated by the program based on the equivalent tendon area.

### 6.2.3 Falsework

Bridge falsework is a temporary structure with several components made of different materials. Because of the nature of the falsework structure, different types of connections including wooden wedges, sand boxes, and others to support the superstructure are used. The estimation of falsework stiffness is complex and is highly dependent on connections with properties that are not well defined. It was decided in this study to model the falsework-bridge interaction in the analyses using equivalent springs. The stiffness of springs was a combination of the falsework stiffness and the effect of its support settlement.

The falsework stiffness increases over time due to closure of potential gaps between the different components (Carden et al. 2006), consolidation of supporting sand jacks (Sanders and Ashford 2008), creep deformation in timber components, and potential change in the soil properties. Additionally the potential crushing in the wood fibers of timber components of falsework increases the uncertainty and complexity of falsework stiffness calculation (Caltrans 2012). It was assumed in this study that falsework reached its maximum stiffness before post-tensioning because the majority of aforementioned changes occurred before prestressing. The lateral stiffness of falsework was not considered in numerical models.

Falsework was modeled with series of compression-only springs. Zero-length Gap-Link elements in SAP2000 with no initial gap was used. The falsework supporting each span was modeled with three Gap-Link elements at the quarter points of the span length as shown in Fig. 6-6. An equivalent compressive stiffness of 1500 kip/in (263 kN/mm) was specified for each spring. This stiffness was primarily determined to

achieve a good correlation with the measured deflections in the cantilever as well as the adjacent span. In addition, due to the accumulated crushing in timber components (Caltrans 2012), the falsework was believed to deflect approximately 0.5 in (13 mm) under the wet concrete weight before stressing. An additional Gap-Link element was assumed at the1/8$^{th}$ point of the adjacent span length close to the short cantilever (Fig. 6-6). This spring was added to closely match the measured hinge curl particularly before load transfer, where the adjacent span was observed to engage the falsework the most in this zone. A single gap-link was also provided at the tip of the short cantilever to prevent downward deflection before stressing. Another single Gap-Link with a very high stiffness was provided at the hinge centerline to model the falsework supporting the long cantilever.

### 6.3 Material properties

Elastic material with time-dependent properties was assigned to the superstructures and the columns. Time-dependent material properties included the modulus of elasticity, creep and shrinkage of concrete, and prestressing steel relaxation.

#### 6.3.1 Concrete

Isotropic normal weight concrete material was used in the numerical models. The behavior of concrete was defined using the modulus of elasticity, Poisson's ratio, coefficient of thermal expansion, and shear modulus. The modulus of elasticity was calculated as $E_c = 33{,}000\, K_1\, w_c 1.5\, \sqrt{f'_c}\ (ksi)$ (AASHTO 2012). $K_1$ is the correction factor for source of aggregate and was taken as 1.00. $w_c$ is the unit weight of concrete and was considered as 0.145 k/ft$^3$ (22.78 kN/m$^3$). A concrete Poisson's ratio of 0.2, a

coefficient of thermal expansion of 5.5E-06 /°F (9.9E-06 /°C), and a shear modulus of 1692 ksi (1.17E-06 GPa) were assigned to the concrete material.

### 6.3.2 Prestressing steel

Prestressing tendons were modeled with uniaxial material properties. A416Gr270 was used as specified in the prestressing drawings. The yield strength, ultimate strength, and the modulus of elasticity were 245 ksi (1690 MPa), 270 ksi (1860 MPa), and 28500 ksi (193 GPa), respectively. The unit weight was assumed to be 490 lb/ft$^3$ (77 kN/m$^3$).

### 6.3.3 Time-dependent properties

The time-dependent properties of concrete and prestressing steel were defined based on CEB-FIP model (CEB-FIP 1990). This model was selected since it is currently then the only available model supported by the program.

The time-dependent properties for concrete are generated internally in SAP2000 based on five parameters: cement type coefficient, relative humidity percentage, notional size, shrinkage coefficient, and shrinkage start age (Fig. 6-7).

A cement type coefficient is used to determine the concrete modulus of elasticity. For example, this coefficient is 0.25 for normal and rapid hardening cement and 0.38 for slow hardening cement (ACI 2008). It was assumed that normal or rapid hardening cement was used in the sample bridges and consequently a coefficient of 0.25 was assigned.

The percentage of relative humidity was the first parameter used for creep calculations. Although the measured relative humidity percentage varied over the field

measurements course, an average relative humidity of 50% was used for all bridge models.

Notional size (h) was the second parameter required for creep calculations and was calculated as $h = 2\,A_c/\,u\,(in)$ (CEB-FIP 1990). In this equation $A_c$ is the cross-section area of the component (in-sq), and $u$ is the perimeter of the component in contact with atmosphere (in).

Two parameters were needed to calculate concrete shrinkage: the shrinkage coefficient ($\beta_{SC}$) and the shrinkage start age. $\beta_{SC}$ is defined based on the cement type. For example $\beta_{SC}$ is 4 and 5 respectively for cement type of slow hardening and normal or rapid hardening. In this study $\beta_{SC}$ was assumed to be 5 for all bridge models. Since concrete decks were moist cured continuously for seven days (Chapter 3), the shrinkage start age was assumed to be 7 days.

The time-dependent relaxation of the prestressing steel is defined by one parameter in the program. This parameter is called CEB-FIP Class (Fig. 6-8) and defined based on CEB-FIP model (CEB-FIP 1990). Class 1 is used for normal relaxation strands and Class 2 is used for improved relaxation strands. Class 2 was selected for this study since the prestressing strands were low relaxation.

### 6.4 Boundary Conditions and constraints

Abutments were modelled as roller supports, and column foundations were modelled as fixed supports. The in-span hinges were modelled as free joints with 3 degrees of freedom in 2-D analyses.

Constrained rotational degrees of freedom around the out of plane axis (Y-axis) were defined for the frame element connecting the column to the superstructure, using the body constraints feature. This was to simulate the rigid zone in the column-cap beam connections (Fig. 6-9).

The columns were modeled using clear heights in all bridges regardless of the type of foundation. Note that the equivalent fixity model shown in Fig. 6-10 is only used for seismic analysis and is not applicable to bridge analysis under service loads. In other words, the depth of fixity ($d_f$) was assumed to be zero in the analytical models.

## 6.5 Loading

The CIP-PS box girder bridges typically undergo different construction stages as mentioned previously. Therefore, separate load cases were defined and then combined at different stages to capture construction phases.

### 6.5.1 Load cases

Different load patterns, dead load (DL), prestressing force (PS), and the load transferred from long cantilevers (T), were defined in the analytical models. Self-weight of bridge components was computed automatically by the program but the hinge diaphragm weight was defined manually as concentrated loads. These loads were added to DL.

The total jacking force was applied to the prestressing steel using the tendon load feature in SAP2000. The stressing sequence was not taken into account because the prestressing tendons were lumped into an equivalent tendon. Nonetheless, the elastic shortening losses were automatically calculated by the program, and the immediate losses

due to friction and anchorage set were computed based on user-defined curvature coefficient, wobble coefficient, and anchorage set slip. Other losses such as creep, shrinkage, and steel relaxation were set to zero as they were automatically calculated by the program based on the time-dependent material properties.

The transfer load from the long cantilever was defined as a point load at the hinge centerline. The load magnitude was taken equal to the shear demand at the face of the short cantilever obtained from CTBridge as discussed in Chapter 5.

### 6.5.2 Construction stages

Static staged construction analysis was performed to model the different construction stages. The time-dependent effects were included in the analyses by specifying the duration of each stage. The actual age of the bridge columns at the beginning of the analysis was defined according to the construction schedule. The construction stages were defined by adding or removing a portion of the structure and applying loads at a specific stage. The number of loading stages was defined in such a way that the deflections could be obtained according to the field measurements schedule. Moreover, additional stages were defined to simulate the uncaptured stages such as upon and few years after falsework removal and load transfer. Eventually the final hinge location was calculated by defining a 4-year stage.

## 6.6 Analytical model of the long cantilever frame

Beam-stick models were developed for prestressed Frames 2 and 4 in Bridge 5WB as shown in Fig. 6-11. These frames were not described in detail in Chapter 2 since they were not surveyed. The purpose of this study was to analytically investigate the

deformation behavior of the prestressed long cantilever of in-span hinges to possibly address the discrepancy in elevations between non prestressed short cantilevers and prestressed long cantilevers that was observed at some of hinges in Bridge 5. Several sources contributed to this discrepancy such as post-tensioning and construction errors. Due to the slope of the tendon profile at the stressing end (hinge) in the long cantilever (Fig. 6-11), the jacking force at the anchorage zone has a vertical downward force component. Consequently a downward displacement occurred near the edge and increased the discrepancy in elevations between the long and short cantilevers at the hinge. Therefore it was prudent to analytically estimate the deflection of the edge of the long cantilever due the post-tensioning and long term effects.

Similar assumptions were made in modelling the prestressed long cantilever frames. Falsework supporting the long cantilever was modeled using four Gap-Link elements located at the edge of the cantilever and the quarter points of the span length. The falsework in adjacent spans was modeled with three Gap-Link elements at the quarter points. Compression stiffness of 1000 kip/in (175 kN/mm) was assigned to the gap-link elements so that the mid-span deflections of the cantilevers do not exceed the accumulated displacement of 0.5 in (13 mm) due to the potential crushing in falsework components before stressing (Caltrans 2012).

Time-dependent properties of concrete and tendons were included in the staged construction analysis. The total number of loading stages was smaller than that of the short cantilevers because there was no load transfer stage in the analysis of the long cantilever frames.

In the numerical models it was assumed that the falsework was remained in place for one year after stressing. This assumption was made to calculate the long term displacements in addition to immediate deflections.

### 6.7 Summary

Deformation analyses of the five bridges with time-dependent effects were conducted using a relatively simple model with line elements. Two-dimensional analytical models were developed for the majority of bridges and simplifying assumptions were made. The interaction between falsework and the superstructure was included. The results of the numerical analyses and their correlation with field measurements are discussed in details in Chapter 8 (section 8.2).

# Chapter 7 Finite Element Analysis of Bridges

## 7.1 Introduction

A series of 3-D finite element analysis (FEA) was conducted in this study using ABAQUS software developed by Dassault Systèmes Simulia Corp. (Simulia 2014). The main objective of this analysis was to develop elaborate numerical models to capture the deformation behavior across the bridge width, and the effect of other geometrical changes on hinge curl as discussed in the parametric studies in Chapter 8.

The geometry of bridge components, material properties, elements types, mesh configurations, boundary conditions, interaction among various bridge components, loads, analysis steps, and other assumptions made in the numerical modeling are discussed in this chapter.

## 7.2 Finite element modeling of bridge frames with short cantilevers

Three-dimensional finite element models were developed for the frames with short cantilevers in each bridge. Complete ABAQUS environment (ABAQUS/CAE) was utilized to create the models, the general purpose finite element analyzer (ABAQUS/Standard) was used to analyze the models, and ABAQUS/viewer was used to post-process the output database and to generate visual results.

### 7.2.1 Geometry

A total of nine 3D models of the frames that included short cantilevers were developed to investigate the deformation behavior of in-span hinges. Eight models contained prestressed hinges, and one model contained non-PS hinges. Due to relatively small longitudinal and transverse slopes and their negligible effects on hinge

deformations, the frames were modeled with no slope. Moreover, the horizontally curved bridges were modelled as straight bridges because the radius of horizontal curve was relatively large (greater than 1640 ft (500 m)). Figure 7-1 shows a typical 3D view of Frame 2 of Bridge 2 with three spans and two short cantilevers. The longitudinal, transverse, and vertical directions of the bridge model is along the Z-axis, X-axis, and Y-axis, respectively.

#### 7.2.1.1 Superstructure and bents

3D solid elements with solid homogenous section properties were used to create the superstructures and bents. Each span was created separately, and then all spans were combined in the assembly module. The soffit and web flares near the bents were neglected in FE models. Therefore the thickness of box-girder webs and the soffit slab was assumed to be constant throughout the span length as shown in Fig. 7-2. The geometry of the multi-cell box girder cross-sections was simplified by removing the interior fillets and approximating the exterior rounded corners by right angle corners. Columns with oblong cross-sections were idealized using equivalent rectangular columns of the same moment of inertia, and similarly circular columns were converted to equivalent square columns. Figure 7-3 shows 3D views of single and two-column bents with equivalent rectangular and square columns, respectively. These simplifications were made to produce a high quality mesh without complex models.

#### 7.2.1.2 Prestressing tendons

The prestressing tendons were modelled using 3D wire shapes with truss section properties. Tendons within a web of a box girder or a bent cap were lumped into one

equivalent tendon with a combined cross sectional area (Fig. 7-4). Equivalent tendons in a box girder had identical longitudinal profile matching the center of gravity of the prestressing force.

#### 7.2.1.3 Falsework

It was reasonable and sufficiently accurate to model the falsework by a series of compression only vertical truss elements. 3D wire shapes in ABAQUS with truss section properties were used to model the falsework. A similar pattern to what implemented in SAP2000 models (Chapter 6) was used to distribute the falsework elements in the longitudinal direction regardless of the actual falsework configuration (Fig. 7-5). Three falsework bents at quarter points were modelled in adjacent spans and an additional bent was modelled at $1/8^{th}$ point only in the span closest to the hinge. Similar to the SAP models, falsework elements were modeled such that the combined vertical stiffness at each bent was 1500 kip/in (263 kN/mm) in adjacent spans.

Although falsework heights varied among bridges and even within a bridge, an average height of 41 ft (12 m) was assigned to all falsework elements to simplify the calculation of equivalent vertical stiffness. Falsework elements were placed on the centerline of box girder webs to avoid stress concentration on the bridge soffit slab. Accordingly the number of falsework elements varied in the transverse direction based on the bridge width and number of girders. Each falsework bent modeled in ABAQUS consisted of multiple posts (3 to 5 posts) and the cross-section properties of these posts were adjusted to produce the combined axial stiffness of 1500 kip/in (263 kN/mm).

Finite element models included two falsework bents supporting the short cantilevers (Fig. 7-5). One bent was located exactly at the edge of the short cantilever, and the other was placed at the hinge centerline to support the short cantilever self-weight and to carry the load transferred form the long cantilever, respectively. A high combined axial stiffness was assigned to the latter to represent the equivalent falsework stiffness of the long cantilever.

### 7.2.2 Elements and meshing

Two types of elements were used to construct the FE models. 8-node, reduced integration solid elements (C3D8R) were utilized to model concrete, and 2-node, linear truss elements (T3D2) were used to model prestressing tendons and falsework.

A series of sensitivity analyses were conducted to optimize the mesh size based on stress and deformation responses. A satisfactory approximate global mesh size of 2.5 ft (0.76 m) was selected for FE models of bridges 1, 2, and 3, and a mesh size of 1.67 ft (0.51 m) was used for bridges 4 and 5 models as shown in Fig. 7-6. The same mesh size was assigned to different components of any given bridge model to ensure continuity. The superstructure deflections were not sensitive to the mesh size of falsework elements. Therefore, single elements were used to model the falsework.

### 7.2.3 Material models

All materials used in FEA were linear, elastic, and isotropic. The time-dependent deformation of the bridges was simulated in the FE models by utilizing time-dependent concrete properties.

#### 7.2.3.1 Concrete

Superstructures were assumed to be crack free and remain elastic due to the prestressing effect. Columns were also assumed to remain elastic under service loads, and hence the gross moment of inertia was used.

The behavior of concrete was modeled with five main properties: density, the modulus of elasticity, Poisson's ratio, creep, and shrinkage. A mass density of $2.248 \times 10^{-7}$ kip/in$^3$ ($2.402 \times 10^{-12}$ kN/mm$^3$) was specified for concrete to account for the self-weight of concrete components. The elastic behavior of concrete was modeled by specifying the Young's modulus and Poisson's ratio. The concrete Poisson's ratio was assumed to be 0.2, and the modulus of elasticity was calculated according to $E_c = 33{,}000\ K_1\ w_c 1.5\ \sqrt{f'_c}\ (ksi)$ (AASHTO 2012). $f'_c$ is the specified compressive strength of concrete (ksi) at 28 days. $K_1$ is the correction factor for source of aggregate and was taken as 1.00. $w_c$ is the unit weight of concrete and was considered as 0.145 kcf.

Creep is a time-dependent property of concrete and is linearly proportional to the concrete compressive stress when the stress is less than $0.5f'_c$ (Gilbert 2011). At higher stress levels, concrete creep increases at a faster rate and becomes nonlinear with respect to the stress. The calculated compressive stress in concrete was less than $0.5\,f'_c$, and consequently it was reasonable to assume linear creep relationship with respect to the stress. Two creep laws are available in ABAQUS, the hyperbolic-sine law and the power-law. The hyperbolic-sine law varies exponentially with stress at high stress levels and becomes the power-law at low stress levels. Therefore the hyperbolic-sine law is normally used in regions of high stress, such as around a crack tip, where creep strain rates frequently depend exponentially on stress. The power-law is generally simpler and

has two forms, strain-hardening and time-hardening creep laws. The time-hardening version of the power-law creep model is recommended in cases when the stress state remains essentially constant, while the strain-hardening law should be used when the stress state varies during analysis (Simulia 2014). Since the stresses in the five bridges were small and changed slightly within the elastic range, the time hardening form of the power law model was used for modelling the creep.

The time-hardening creep law is expressed as

$$\dot{\varepsilon}^{cr} = \mathrm{A}\tilde{q}^{n}t^{m} \qquad (7.1)$$

Where

$\dot{\varepsilon}^{cr}$ = the uniaxial creep strain rate

$\tilde{q}$ = is the uniaxial stress

$t$ = is creep time

A, $n$, $and\ m$ = constants and calibrated based on CEB MC90-99 creep model (ACI 2008) utilizing curve fitting procedure (Fig. 7-7). To generate the ABAQUS-Creep curve, creep coefficients were calculated as follows:

The creep strain expression was determined by integrating Eq. 7.1 with respect to time and expressed as:

$$\bar{\varepsilon}^{cr}(\mathrm{t}) = \mathrm{A}\tilde{q}^{n}\frac{t^{m+1}}{m+1} \qquad (7.2)$$

Creep coefficient is the ratio of the creep strain to the initial strain. Hence, the creep strain at any time can also be expressed as a function of the corresponding creep coefficient as the following (Gilbert 2011):

$$\bar{\varepsilon}^{cr}(\mathrm{t}) = \frac{\sigma.\phi(\mathrm{t},\mathrm{t}_0)}{E} \qquad (7.3)$$

Where,

$\sigma$ = the initial stress

$\phi(\mathrm{t},\mathrm{t}_0)$ = the creep coefficient at any time t due to a load applied at age $t_0$

$E$ = the initial Young's modulus

Equations 7.2 and 7.3 were set equal to each other. The parameters were varied to determine creep coefficients that best match those obtained from CEB-creep model. By definition the uniaxial stress, $\tilde{q}$, is equal to the initial stress, $\sigma$. Therefore the stress order, n, was set equal to 1 to match with the CEB-creep model. The values of A, n, and m were determined to be $2.45\text{x}10^{-5}$, 1, and -0.8, respectively in FE analyses.

Concrete shrinkage causes a time-dependent strain in an unloaded and unrestrained specimen at constant temperature (Gilbert 2011). The strain occurs over several years after casting and generally increases with time but at a decreasing rate. Fig. 7-8 shows shrinkage strain plots according to different codes. Each curve can be idealized by a bilinear relationship between the shrinkage strain and time, in which the intersection of the two branches typically occurs at around 60 days.

The shrinkage effect on the hinge curl was investigated using SAP2000 models and found to be insignificant before load transfer. Falsework removal and load transfer stages normally occurred not sooner than 60 days from the completion of prestressing at the hinge due to hinge construction and to allow time for hardened concrete to achieve the specified strength. Therefore it was reasonable for this study to assume the effective strain rate of concrete shrinkage was the slope of the second branch of the idealized

relationship. The shrinkage strain rate used in the FEA was calculated based on CEB MC90-99 model (ACI 2008) and it was $4.5x10^{-7}$. A negative sign was specified to this value since the material model was designated for swelling deformation.

#### 7.2.3.2 Prestressing steel

A Young's modulus of 28000 ksi (193 MPa) and Poisson's ratio of 0.3 were assigned to the prestressing steel. A mass density of $7.345x10^{-7}$ kip/in$^3$ ($7.849x10^{-12}$ kN/mm$^3$) was specified to account for the self-weight of the prestressing tendons within the superstructure. A coefficient of thermal expansion of $6.5x10^{-6}$ per degree Fahrenheit ($1.17x10^{-5}$ per degree Celsius) was used to enable generating the prestressing forces by applying temperature loadings.

#### 7.2.3.3 Falsework

As discussed previously, the estimation of falsework stiffness is complex and is highly dependent on connections with properties that are not well defined. Consequently, an equivalent linear elastic stiffness with compression-only members was used to model the falsework. Although falsework elements were made of steel or timber, the falsework elements in FEA were assumed to be made of equivalent steel members. Typical steel Young's modulus of 29000 ksi (200 GPa) and Poisson's ratio of 0.3 were specified, and the weight of the elements was neglected.

### 7.2.4 Boundary conditions and constraints

Boundary conditions were utilized to model the supports, and constraints were used to model the interaction between bridge components. Column foundations were

assumed to be fixed, abutments were modeled as roller supports, and falsework elements were assumed to be pinned at the base.

Tie constraint in ABAQUS is normally used to fully join together two parts of a model, and was used to simulate the continuity between different components of a bridge such as bent caps to box girders and columns to bent caps.

Multi-point constraints in ABAQUS (MPC) are used to constrain the degrees of freedom of "slave" nodes to those of a "control" node. MPC of beam type were applied to girder ends of a frame at the hinges or abutments to simulate the anchorage zones. The Beam MPC ensured compatibility of deformation between tendons and girders at the anchorage zones.

Embedded region constraint in ABAQUS was used to model bonded prestressing system that represented the actual PT system in the five bridges. Tie constraints were used to simulate the superstructure-falsework interaction in the FE models. The compression-only behavior of falsework elements was modeled in the material properties.

### 7.2.5 Loads

Different loads including dead loads and prestressing forces were applied to the FE models. Loading conditions varied depending on the load type and time of application. Loading conditions such as self-weight of the bridge components, load transfer from long cantilevers, and post-tensioning forces, were applied separately to the FE model and combined in the analyses using an appropriate loading sequence.

The self-weight of bridge components was calculated by the program based on defined material density in the material property module and the gravity acceleration in the load module. The self-weight was applied as a uniformly distributed load on the bridge components. The load transferred from the long cantilever was modeled with multiple vertical point loads applied across the bridge width on the hinge seat.

The post-tensioning forces were simulated using uniform temperature loading, and were applied simultaneously with no stressing sequence. Different temperatures were specified along the tendon length to generate equivalent initial jacking stresses after instantaneous losses due to friction, elastic shortening, and anchorage set. The initial stressing forces were obtained from SAP2000 analysis verified using the CTBrige analysis results.

### 7.2.6 Analysis and loading steps

The finite element analyses involved two types of analysis, static analysis and visco analysis. Several loading steps comprising the static and visco analyses were defined in each model to simulate the construction sequence. Static steps were used to model instantaneous elastic response, and visco steps were used to simulate the time-dependent response due to creep and shrinkage. Loading steps were defined such that elastic deformation followed by creep deformation can be captured for each loading condition during the bridge construction and the following four years.

The sequence of loading was defined in each model based on the actual schedule of construction and data collection. The typical loading sequence defined at the hinges included five static steps and three visco steps. The sequential static loading steps were

the bridge self-weight, post-tensioning, casting the hinge seats, load transferred from the long cantilevers, and falsework removal. Falsework removal was modeled by simply inactivating the falsework supports.

The visco steps were used to model the time-dependent response over the time elapsed between two static steps or following a static step over four years of service. Therefore the three typical visco steps were defined after the post-tensioning, after casting the hinge seat, and after complete falsework removal. Additional loading steps were used because of other circumstances during construction such as partial falsework removal and load transfer at different times within the same bridge at different hinges.

### 7.3 Finite element modeling of the long cantilever frame

A finite element analysis was conducted to study the behavior of long cantilevers. As discussed previously in Chapter 6, the purpose of this study was to analytically investigate potential displacements at the edge of the long cantilever after the stressing using a detailed model.

Two FE models were developed for Frame 2 and Frame 4 located in Bridge 5WB (Fig. 7-9). Construction stages were simulated using three steps. The falsework was assumed to support the bridge throughout the analysis. Two of the loading steps were static steps to account for the self-weight and post-tensioning, and one was visco step to account for the long term effects after one year. Other assumptions used in FEA of these frames were similar to those discussed previously.

# Chapter 8 Comparison of Measured and Calculated Results and Parametric Studies

## 8.1 Introduction

In this chapter the results of bridge analyses using SAP2000 and ABAQUS are presented and compared with the field data. The purpose of this comparison was to assess the appropriateness of relatively simple models of SAP2000 and the elaborate FE models of ABAQUS in estimating the hinge curl in the five bridges. This chapter also presents the results of parametric studies of bridges using ABAQUS to investigate the sensitivity of calculated hinge curl to skew angle and horizontal curvature, features that were absent in the five surveyed bridges.

## 8.2 SAP2000 analysis results

Figures 8-1 to 8-8 show the deformed shapes of the bridges in two stages, before stressing, and immediately after stressing. The vertical deformations are exaggerated for clarity. The deformation trends were similar in all the five bridges. The deformations in the short cantilevers were minimal before stressing, but were upward (hinge curl) and in the axial direction after stressing. Adjacent spans deflected downward before stressing under their self-weight due to the flexibility of falsework. After stressing, the downward deflection was partially offset due to the prestressing as can be seen in Fig. 8-1. The prestressing force also increased the downward deflection in the adjacent span on the side of the short cantilever due to the rotation of beam-column connection.

The calculated immediate and time-dependent deflections of the short cantilevers and the adjacent spans after stressing using SAP2000 are plotted in Figs 8-9 to 8-14. The

deflections are reported at nine points across the frames. One point was at the hinge centerline, two other points on the short cantilever, one on the bent centerline near the hinge, four across the adjacent span length, and the last one on the centerline of the far bent. The first point on the short cantilever was located at its edge (prior to hinge closure), and the second point was located at the mid-point of the short cantilever length. The four points on the adjacent span length were at the location of falsework springs, at 1/8, 1/4, 1/2, and 3/4 of the span length. The immediate bridge deflections after prestressing and the time-dependent deflections were calculated with respect to the deformed shape right before stressing. SAP2000 results were plotted for five stages, immediately after stressing (Day 0), one day after stressing (Day 1), the day before casting the hinge top ledge (The day of casting the closure concrete in C1 and C2), immediately after load transfer, and at 4 years from completion of prestressing (Day 1440).

The deflection plots in Figs 8-9 to 8-14 showed an increasing deflection of the short cantilever over time until the day of casting the top ledge for hinges or the closure concrete for C1 and C2. Time-dependent deflections of adjacent spans before load transfer nearly remained unchanged in bridges 1, 2, 3, and 4 as shown in Figs. 8-9 to 8-12. However, upward deflections in adjacent spans of B5EB and B5WB slightly increased over time before load transfer as shown in Figs. 8-13 and 8-14. The $1/8^{th}$ points of the adjacent spans length deflected downward immediately after stressing (Day 0) and remained nearly unchanged over time until load transfer.

At load transfer, all short cantilevers deflected downward immediately due to the long cantilever reaction as expected. Some adjacent spans deflected downward after

complete falsework removal while other adjacent spans remained unchanged. For example the adjacent span in Bridge 3 immediately deflected downward at load transfer (Day 64) as shown in Fig. 8-11, while the deflection of the adjacent span in Bridge 4 remained unchanged at load transfer (Day 167) as shown in Fig. 8-12. This was attributed to the unbalanced spans effect after falsework removal, where deflections of the bridge spans could vary among bridges according to the span length and other design parameters such as prestressing force and superstructure cross-section dimensions. The downward displacement at the far bent of the adjacent span of H2 in Bridge 2 was due to the deflection of the outrigger bent (Bent 7) after falsework removal (Fig. 8-10 b).

After load transfer, deflections continued to increase due to concrete creep and shrinkage. Deflections of short cantilevers and adjacent spans did not have a consistent trend as can be seen in Figs. 8-9 to 8-14 due to the variation of span length ratio and other design parameters among bridge spans.

The prestressed long cantilevers frames of in-span hinges exhibited consistent deformation behavior as shown in Fig. 8-15. A downward displacement of 0.20 in (5 mm) was obtained at the edge of the cantilever immediately after stressing in SAP models. . This displacement did not change over a one-year period that included the long term effects in concrete and prestressing steel.

### 8.3 ABAQUS analysis results

Figures 8-16 to 8-23 show the calculated deformed shape of the bridges before and immediately after stressing using ABAQUS. The prestressed frames of the five bridges exhibited similar deformation response. The part of the spans adjacent to the

hinges all deflected downward after stressing and confirmed that the pier-superstructure connections rotated. Note in Fig. 8-17 b that the outrigger bent deflected slightly upward due to the post-tensioning effect.

ABAQUS analysis results for immediate and time-dependent deflections of the short cantilevers and adjacent spans are presented in Figs 8-24 to 8-29. These deflection curves were calculated at the centerline of the box girder on the top deck surface. The deflection at the centerline of the box girders was equal to average deflections across the bridge width since the prestressing forces were equal in all girders of a bridge model.

Deflections for each hinge and closure in the longitudinal direction were calculated and reported at nine locations described previously. In general, the deflections obtained from finite element analyses showed similar trend to those calculated from stick model analysis immediately after stressing and afterward. Typically, the short cantilevers deflected upward, the points located at the $1/8^{th}$ of the adjacent span length deflected downward, and the rest of the adjacent span length deflected upward immediately after stressing. After load transfer and similar to SAP results, no consistent trend was captured among the hinges in the deflection of short cantilevers and adjacent spans due to the variation in the design proportions among the bridge spans.

Figure 8-30 shows the deformation response of the long cantilevers in Frame 2 and Frame 4 of Bridge 5EB. The trend in ABAQUS results was the same as that in SAP2000 results. That is an immediate downward displacement of 0.20 in (5 mm) occurred at the edge of the cantilevers after stressing and the displacement did not change over a one-year period.

### 8.4 Correlation between analytical results and field data

The calculated and measured deflections are plotted in Figs. 8-31 to 8-34, 8-36, 8-37, and 8-39 to 8-42. The calculated deflections were plotted at the nine locations described previously, and the measured deflections were plotted at the field measurement stations. Deflections were compared at different times during construction until opening the bridges to traffic. Some of the intermediate measured data were not included in the comparison at each hinge because the trend in the correlation between the measured and calculated data was sufficiently captured by other data. Because in Bridges 1, 2, and 3 double-end stressing was applied in the field, the "Day 0" measured data already included some creep deformation, which was absent in the calculated data. To account for this effect, the measured Day 0 data were divided by 1.3 before comparing them with the calculated data. This factor accounts for 30% additional deflection due to creep which was calculated according to CEB MC90-99 creep model (ACI 2008).

Deflection profiles of Bridge 1 at H3 and H7 showed a near perfect agreement between the measured and calculated deflections as shown in Figs. 8-31 and 8-32. This agreement was observed on all days along the short cantilever and the first 1/8 of the adjacent span length. A prefect agreement was also observed between the SAP and ABAQUS deflection profiles along the short cantilevers and the adjacent spans of these hinges.

The measured and calculated deflections of Bridge 2 at H1 and H2 were in reasonable agreement particularly before load transfer (Figs. 8-33 and 8-34). After load transfer (Day 165 and Day 135 for H1 and H2, respectively), the calculated responses deviated from the measured deflections. This could be attributed to concrete grinding

performed around Day 197 for the entire deck surface of Frame 2 to adjust the longitudinal profile (Fig 8-35). The difference between the SAP and ABAQUS deflection profiles of adjacent span of H2 was due to different deflections of the outrigger bent (Bent 7) in the two models (Fig. 8-34 (e) and (f)). After load transfer, Bent 7 in SAP2000 experienced larger downward deflection than that of ABAQUS model due to the different approach used in modeling the superstructure of Frame 2. In SAP2000 stick model, the superstructure reaction was transferred as a point load applied to the cap beam, while the reaction was distributed in the 3D FE model. This imposed higher instantaneous deformation on the outrigger bent and accordingly higher time-dependent deflections in the stick model.

The measured, SAP, and ABAQUS deflections of Bridge 3 at H were in perfect agreement as shown in Fig. 8-36. The minor difference shown in Fig. 8-36 (d) between the measured and ABAQUS deflections in the adjacent span is considered insignificant compared to the span length.

The measured and calculated deflection profiles of Bridge 4 at H indicated good agreement before load transfer on Day 167 as shown in Fig. 8-37 (a) to (e). The calculated deflections deviated from the measured data, particularly in the adjacent span, after load transfer due to the procedure and schedule of falsework removal (Fig. 8-37 (f) and (g)). Falsework was partially removed on Days 167 and 170, and one falsework bent was still up supporting the long cantilever. Therefore, the load was not completely transferred to the short cantilever (Fig 8-38). The falsework was completely removed in SAP and ABAQUS models at one step. Therefore the calculated deflections of short cantilever and the adjacent span were smaller than the measured data (Fig. 8-37 f and g).

The calculated and measured deflections of Bridge 5EB at H1 were in good agreement as shown in Fig. 8-39. However, the calculated deflections were not close to the measured data in the adjacent span before load transfer on Day 100 as shown in Fig. 8-39 (a) to (d). The correlation between the measured and calculated deflections of Bridge 5EB at C1 and C2 was acceptable as shown in Fig. 8-40 and Fig. 8-41 except for the deflections of the short cantilever after the load transfer on Day 175 (Fig. 8-40 (g) and (h)). These differences are believed to be a result of the partial load transfer that occurred on Day 45 due to the partial falsework removal discussed in previous chapters. Although this partial load transfer was simulated in the computer models, the effect was not captured perhaps because of the simplifications made in falsework modelling.

The measured and calculated deflections of Bridge 5WB at H4 had a good agreement throughout the field measurement course as shown in Fig. 8-42.

In general, the correlation between the measured and calculated results was satisfactory. Furthermore, the calculated hinge curls from SAP and ABAQUS were close indicating that the stick model might be sufficient for calculating hinge curls. The differences between the measured and those calculated using SAP and ABAQUS could be attributed to several sources including:

1- Possible differences between the specified and actual geometry, e.g., dimensions and post-tensioning duct profiles.
2- The assumption of uncracked section properties and excluding steel reinforcing bars in the numerical models.
3- Possible difference between the specified and actual concrete properties and prestressing losses.

4- Temporary construction loads, including trucks and concrete blocks that were sometime present during field measurements and could not be removed and were not simulated in computer models.

### 8.5 Effect of geometry of bridges on the hinge curl

The skew angle and the horizontal curvature in the five bridges that were studied in the field were insignificant. To determine the potential effects of these features on the hinge curl, a parametric study was carried out by varying the abutment skew angle and the horizontal curvature of bridges. The hinges were assumed to have zero skew. The study was conducted using the finite element approach to allow for elaborate three-dimensional modeling that is necessary to capture the skew and curvature of the bridge. ABAQUS models were developed for bridge frames with different skew angle of abutments and radius of horizontal curvature as shown in Fig 8-43. Both short-term and long-term curls were studied. The bridge cross-section dimensions used in the parametric study were similar to those of Bridge 5. However an overhang was modeled at each edge to make the cross section of the model symmetric. The prestressing steel was designed such that the service load stresses in the superstructure did not exceed the AASHTO stress limits. It was assumed that the load was transferred 60 days after stressing. Deflection curves were plotted in Figs. 8-44 to 8-46 for the intermediate girder. The deflections were calculated at eight points in the longitudinal direction. The location of these points was similar to those described earlier in this chapter, but the point on the edge of the short cantilever was excluded.

### 8.5.1 Effect of skew angle of abutment

Two groups of ABAQUS models were developed, one with two-span bridge frame (group 1) and another with one-span frame (group 2). Although hinge curl was expected to be insensitive to the abutment skew angle in frames with multiple spans, group 1 was studied to confirm this assumption. Therefore group 1 included only two models, one with no-skew abutment and the other was with a 60-degree skew abutment. The span length was 170 ft (52 m) in both spans, and the short cantilever was 30 ft (9 m) long. Group 2 consisted of four models, one with no-skew abutment and three with abutment skew angles of 20, 40, and 60 degrees. A short cantilever length of 30 ft (9 m) and an adjacent span length of 170 ft (52 m) were also used in the parametric study of this group.

Figures 8-44 and 8-45 show the sensitivity of deflections to the abutment skew angle for group 1 and 2, respectively. It can be seen that deflections in neither group were sensitive to skew angles before load transfer. After load transfer, the short cantilever deflections of group 1 remained unchanged with changing the skew angle from zero to 60 degrees. Mid-span deflections of the adjacent span of the model with 60-degree skewed abutment were slightly higher than those with non-skewed abutment on the day of load transfer and after four years (Figs. 8-44 (c) and (d)).

On the day of load transfer and over a period of four years, the hinge curl and mid-span deflections of the adjacent spans of group 2 slightly changed with changing the skew angle (Fig. 8-45). On the day of load transfer, the hinge curl of the model with a 60-degree skewed abutment was only 0.05 in (1.27 mm) lower than that of with no skew angle, and was 0.1 in (2.54) lower after four years.

### 8.5.2 Effect of horizontal curvature

Two of the five bridges included in the field study on bridges with horizontally curved alignment. The radius of horizontal curve radius was 1969 ft (600 m) for Bridge 1 and 1640 ft (500 m) for Bridge 2. According to the National Cooperative Highway Research Program a radius of 800 ft (244 m) or higher is considered to be large and might be neglected NCHRP 2008. The effect of the horizontal curvature on hinge curl was investigated utilizing ABAQUS models for four, one-span frames with a cantilever. One model was straight and used as a bench mark, and the other three models were horizontally curved with radius of 200 ft (61 m), 500 ft (152 m), and 800 ft (244 m). The length of the short cantilever was assumed to be 30 ft (9 m) and that of the adjacent span was assumed to be 88 ft (27 m).

The deflections of the bench mark and horizontally curved ABAQUS models are plotted in Fig. 8-46. The graphs indicate that the deflections were not sensitive to the radius of the horizontal curvature before load transfer even for the very low radius of 200 ft (61 m). The load transfer and the 4-year hinge curls for the curved frames were slightly higher than those of the straight frame with a maximum deflection difference of less than 0.05 in (1 mm) (Fig. 8-46 (c) and (d)). The corresponding deflections of the adjacent span were also insensitive to change in the radius after load transfer.

# Chapter 9 Proposed Method for Hinge Curl Estimation

## 9.1 Introduction

This chapter presents a new proposed method to estimate hinge curl for prestressed box girder bridges during and after construction. The draft new version of MTD prepared using the current MTD format and a numerical example are presented in App. B. Comparisons between the measured hinge curls and those calculated using the current version of MTD 11-34, SAP2000, ABAQUS, and the proposed method are presented to evaluate the accuracy of the proposed method.

## 9.2 Proposed method to estimate hinge curl

As discussed in Chapter 5, the current Caltrans method described in MTD 11-34 to estimate hinge curl leads to results that can be significantly different than those encountered in the field. To improve hinge curl estimates, a new method is proposed in this Chapter. The proposed method is divided into two parts with the first part for immediate and the second part for time-dependent hinge curl estimation.

### 9.2.1 Immediate hinge curl

The measured data showed that the assumed fixed support for the short cantilever in the current Caltrans method led to underestimation of the immediate hinge curl. The logic behind assuming a fixed support is the presence of falsework in the span adjacent to the hinge. The falsework in the current method is assumed to restrain downward deflection of the adjacent span and rotation at the end of the span. Figure 9-1 shows a typical exaggerated deformed shape for a bridge frame after stressing. The rotation of the pier-superstructure connection near the hinge was found to induce additional curl at the

hinge. This joint rotation is due to different sources. The flexibility of the superstructure-bent connection supporting short cantilevers is due to the flexibility of: (a) the columns, (b) the span adjacent to the short cantilever, and (c) the falsework supporting the adjacent span. The influence of other bents and spans is negligible. Figure 9-2 illustrates the difference between boundary conditions assumed by MTD and those of the proposed model for estimating the immediate hinge curl. The rotational spring presented in the proposed model accounts for the connection flexibility. The procedure proposed in this section was developed to estimate the immediate hinge curl taking into account the flexibility of the short cantilever support.

The proposed equation to estimate the deflection of the short cantilever immediately after stressing is as follows:

$$\Delta_{\text{curl}} = \Delta_{\text{DL}} + \Delta_{\text{PS}} + \Delta_{\text{flexible}} \qquad (9.1)$$

$\Delta_{\text{DL}}$ and $\Delta_{\text{PS}}$ are obtained according to the current MTD equations presented in Chapter 5, and $\Delta_{\text{flexible}}$ is determined using the procedure described in the following section.

#### 9.2.1.1 Hinge curl due to flexibility of the short cantilever support

To account for support flexibility, a simple model of the frame was considered. Figure 9-3 shows a sketch of the pier and the adjacent span. The short cantilever is assumed to be on the left side of the pier. The cantilever is not shown in the figure for simplicity, but the equivalent forces are shown. The term “column” or “columns” is used in subsequent description to represent combined properties of all the vertical elements in pier. The base of the columns and the right support of the adjacent span are assumed to

be fixed, and the column axial deformation is neglected. Therefore, the system has only two degrees of freedom (DOF). The falsework is modeled by a series of compression-only springs. Due to the flexibility of posts, connections, and other filler materials, the falsework typically deforms under vertical and post-tensioning forces.

The force-displacement relationship of the frame can be written as follows:

$$\begin{Bmatrix} M \\ F \end{Bmatrix} = \begin{bmatrix} K_{11} & K_{12} \\ K_{21} & K_{22} \end{bmatrix} \begin{Bmatrix} \theta_{spring} \\ \Delta_{HZ} \end{Bmatrix} \quad (9.2)$$

The following equations are expanded from Eq. (9.2):

$$M = K_{11}\theta_{spring} + K_{12}\Delta_{HZ} \quad (9.3)$$

$$F = K_{21}\theta_{spring} + K_{22}\Delta_{HZ} \quad (9.4)$$

By substituting $\Delta_{HZ}$ from (9.4) in (9.3) and solving for $\theta_{spring}$:

$$\theta_{spring} = \frac{K_{22}M - K_{12}F}{K_{11}K_{22} - {K_{12}}^2} \quad (9.5)$$

Where

F = the average post-tensioning force in the short cantilever after instantaneous losses, and is calculated as follows:

$$F = P_j * FC \quad (9.9)$$

Where

$P_j$ = Design jacking force

FC = Average initial force modification factor at the time of stressing in the short cantilever to account for the instantaneous prestress losses

M = the unbalanced moment acting at the short cantilever support and calculated as follows:

$$M = M_{SC} - M_{adjacent} \quad (9.6)$$

Where

$M_{SC}$ = the moment acting at the short cantilever support due to post-tensioning and self-weight

$M_{adjacent}$ = the fixed end moment at the left end of the adjacent span due to span weight, prestress force, and falsework reactions. These moments are calculated as follows:

$$M_{SC} = Fe_1 - w\left(L_1 + \frac{C}{2}\right)^2/2 - P\left(L_2 + \frac{C}{2}\right) \quad (9.7)$$

Where

w = Uniform self-weight of the prismatic segment of the short cantilever (Fig. 5-1)

P = Weight of the hinge diaphragm excluding the part accounted for in w (Fig. 5-1)

$e_1$ = PT eccentricity at centerline of the bent. An eccentricity above the centerline is positive (Fig. 5-2)

$L_1$ = Length of short cantilever measured from the inner face of the hinge diaphragm to the face of the support (Fig. 5-1)

$L_2$ = Length of short cantilever measured from the face of support to the centroid of the short cantilever end diaphragm (Fig. 5-1)

C = Column width in the bridge longitudinal direction

$$M_{adjacent} = \frac{W_u(L_4)^2}{12} * Z \quad (9.8)$$

Where

$W_u$ = the equivalent falsework upward reaction on the adjacent span, assumed to be 5 k/ft (73 kN/m) for typical falsework (Fig. 9-4 and Fig. 2-8). This reaction was obtained by matching the measured and calculated curls in the five bridges. More details are provided in Sec. 9.3.2.

$L_4$ = center to center adjacent span length

Z = factor to account for the end support condition in the adjacent span away from the hinge, 1 for moment connection and 1.5 for simple support.

The elements of the stiffness matrix (Eq. 9-2) are calculated as follows:

$$K_{11} = K_{\text{rotation}}(\text{Adjacent span}) + K_{\text{rotation}}(\text{Column}) \tag{9.10}$$

$$K_{12} = K_{21} = -K_{\text{lateral}}(\text{Column}) \tag{9.11}$$

$$K_{22} = K_{\text{axial}}(\text{Adjacent span}) + \frac{2K_{\text{lateral}}}{H}(\text{Column}) \tag{9.12}$$

Where

$$K_{\text{rotation}}(\text{Adjacent span}) = \left(\frac{KEI_{\text{adjacent}}}{L_4}\right) \tag{9.13}$$

$$K_{\text{rotation}}(\text{Column}) = \left(\frac{4EI_{\text{column}}}{H}\right) \tag{9.14}$$

$$K_{\text{axial}}(\text{Adjacent span}) = \left(\frac{EA_{\text{adjacent}}}{L_4}\right) \tag{9.15}$$

$$K_{lateral}(Column) = \left(\frac{6EI_{column}}{H^2}\right) \quad (9.16)$$

Where

K = Coefficient to account for the end support condition in the adjacent span away from the hinge, 4 for moment connection and 3 for simple support

H = Clear column height

$I_{adjacent}$ = Average moment of inertia of the adjacent span

$I_{column}$ = Column gross moment of inertia

$A_{adjacent}$ = Average cross-section area for the adjacent span

E = Modulus of elasticity of concrete in the adjacent span and the adjacent column

The hinge curl due to the support rotation is calculated as follows:

$$\Delta_{flexible} = -\theta_{spring} * \left(L_3 + \frac{C}{2}\right) \quad (9.17)$$

Where

The negative sign indicates an upward deflection (curl)

L3 = Length of short cantilever from the face of support to the centerline of the hinge (Fig. 5-1)

Using the proposed method, the net upward load acting on the adjacent span before load transfer, $W_u$, was calibrated for each hinge such that the calculated hinge curl matched the measured data immediately after stressing, and then an intensity of 5 k/ft (73 kN/m) was proposed uniformly. To do so, Eq. 9.2 was used utilizing the short cantilever moment, $M_{SC,}$ to calculate the rotation angle and the horizontal displacement. That means the effect of the adjacent span (span weight, prestress force, falsework reaction) was ignored to determine the maximum hinge curl due to the support rotation, $\Delta_{Flexible}$.

The total hinge curl immediately after stressing was obtained by adding the calculated $\Delta_{flexible}$ to the other components of hinge curl (Eq. 9-1). As expected, the magnitudes of these total curls were higher than those measured because at this stage the falsework resistance in the adjacent span was completely neglected. Because superstructure axial DOF is uncoupled from rotation, the falsework resistance affects only the moment. Therefore, the support rotation of the cantilever and $M_{SC}$ had to be reduced to account for the falsework. The proposed procedure was utilized again to back calculate the moment, $M_{Actual}$, that is required to produce the actual rotation angle at the support due to flexibility, $\theta_{spring\ (Actual)}$. The actual hinge curl due to support flexibility, $\Delta_{flexible\ (Actual)}$, was derived from field measurements by subtracting $\Delta_{curl\text{-}MTD}$ from the measured curl immediately after stressing. Then $\theta_{spring\ (Actual)}$ was calculated by dividing $\Delta_{Flexible\ (Actual)}$ by the length of the short cantilever. The calculated $M_{Actual}$ was subtracted from $M_{SC}$, to determine the contribution of the adjacent span ($M_{adjacent\ (Actual)}$) to the moment developed at the support immediately after stressing. The moment $M_{adjacent\ (Actual)}$ was assumed to be a fixed end reaction caused by the net upward load acting on the adjacent span, $W_u$, due to the span weight, prestress force, and falsework forces. Consequently, $W_u$ was calculated for the hinges in the five bridges. The back calculated upward load in the adjacent spans ranged from 3.55 k/ft (52 kN/m) to 6.08 k/ft (89 kN/m) with an average value of 5 k/ft (73 kN/m), which was used in the proposed method.

### 9.2.2 Time-dependent hinge curl

As discussed in Chapter 5 Section 5.4, the method to determine time-dependent hinge curls before and after load transfer in the current MTD 11-34 document should be

refined by adjusting the time-dependent coefficients of the adjustment and camber calculations for both cantilevers of an in-span hinge. The current MTD method states that when the difference between the calculated Adjustment "SC" in Day 0 and Day 720 is less than 0.5 in (13 mm), time-dependent hinge curls should no longer be calculated and shown on plans. The current MTD method usually underestimates time-dependent hinge curls, and hence applying this threshold may not be appropriate. Therefore it is recommended to calculate time-dependent hinge curls and provide camber table in all cases without any threshold.

#### 9.2.2.1 Before load transfer

Time-dependent deflections before load transfer are sensitive to immediate deflections and the time-dependent deflection factors. In MTD, it is assumed that long term deflections due to concrete creep and shrinkage occur in four years and are three times the immediate deflections. Since the longest period of field measurements in the present study was approximately one year, the long-term deflection factor of 3.0 could not be evaluated based on the field data. As a result the validity of this factor was investigated utilizing SAP2000 analysis. In SAP2000 models, the boundary conditions had to remain unchanged during 4 years and therefore falsework removal was excluded in these analyses. According to SAP2000 analyses, the long-term deflection factor varied from 2.40 to 2.70 due to concrete creep alone. Including shrinkage properties in the analyses enhanced the correlation between calculated and the measured deflections after load transfer. Therefore a total deflection factor of 3.0 was found to be reasonable to model the long term effect of concrete creep and shrinkage.

It was found that the current MTD deflection factors for shorter periods, particularly in the first three months, needed to be refined because of the issues discussed in Chapter 5 (Section 5.4). A different deflection factor chart was suggested in this study using the CEB MC90-99 creep model (ACI 2008). The CEB creep model was developed by Muller and Hilsdorf 1990 and revised in 1999. The CEB creep model is based on a comprehensive design code for concrete structures produced jointly by the Euro-International Committee for Concrete (CEB) and International Federation for Prestressing (FIP) (CEB-FIP 1990). Eurocode 2 (EC 2) for concrete structures is heavily based on the CEB Model Code. The CEB MC90-99 model is closely related to the CEB MC90 model; however, it has been adjusted to take into account the particular characteristics of high-strength concretes. The CEB creep model is valid for normal weight concrete with an average compressive strength of 2.9 ksi (20 MPa) to 13 ksi (90MPa) that is exposed to a mean relative humidity of 40 to 100 %. The CEB model accounts for some parameters such as age of concrete at loading ($t_0$), concrete mean compressive strength at 28 days ($f_{cm28}$), relative humidity (RH), volume-surface ratio (V/S), and cement type ($\alpha$). The age of concrete at loading ($t_0$) was assumed to be 28 days in all bridges since all reported values of the concrete compressive strength at stressing showed that superstructures reached the specified 28-day concrete compressive strength. Cement type was assumed to be normal hardening in creep calculations and accordingly the effect of cement type $\alpha$ was taken equal to 0. Figure 9-5 shows the current and the CEB deflection factor charts, and Table 9-1 lists the corresponding deflection factors. Figure 9-6 shows the factors for different concrete strengths, relative humidities, and volume- surface ratios. The difference in deflection factors due to

changing these parameters was insignificant particularly in the first three months where most of the creep deformation occurs. As a result, representative values of 4 ksi (28 mpa), 50%, 10 were selected for the concrete strength, relative humidity, and volume-surface ratio, respectively to be used in the deflection factor chart.

The estimate of creep coefficients using CEB MC90-99 was also compared to those obtained using ACI 209R model (ACI 2008) and AASHTO creep model (AASHTO 2012) (Fig. 9-7). Standard conditions were considered in computing the creep coefficients using ACI 209. The comparison shows that ACI 209 produced higher creep coefficients and AASHTO provided lower predictions compared to CEB MC90-99. Generally, creep and shrinkage can vary over a wide range and, without specific physical tests or prior experience with materials, the use of the empirical methods cannot be expected to yield results with errors less than ±50 percent (AASHTO 2012). CEB creep model had the best agreement with the current (MTD) deflection factor chart as shown in Fig. 9-5 but with a better representation of the nonlinear relationship between the time and deflection. Moreover, the CEB creep model has been recommended by different sources in the literature (Meyerson, 2001 & ACI 2008 & Kamatchi 2014).

#### 9.2.2.2 After load transfer

Due to the inconsistency found in the current MTD between Adjustment "LC" at Day 0 and the theoretical camber, the calculated long cantilever camber, Camber "LC", needs further refinement to reduce problems during construction. Therefore $\Delta_{curl}$ in Adjustment "LC" (Day 0) should take a factor of 3.00 instead of 2.00 to be consistent

with the theoretical camber obtained from CTBridge, and produce a value that represents the deflection due to joint rotation after load transfer, $\delta_{LC}$.

Other adjustments are proposed to address the two issues (Chapter 5, Sec. 5.4) that were identified in incorporating the deflection due to joint rotation after load transfer, $\delta$ (obtained based on CTBridge results), in the camber calculations of step 8 and 9. It is recommended to first remove the long term effects and determine the elastic component of that deflection by dividing ($\delta$) by 3.00. Then apply an appropriate deflection factor to the elastic deflection due to joint rotation ($\delta/3$) when adding this component to Adjustment "SC" and "LC" in the camber calculations. The appropriate deflection factor is recommended to be the same deflection factor given to the deflection due to load transfer ($\Delta_{reaction}$). For example, to calculate the camber of the short cantilever if load is transferred on Day 60, the equation should be as follows:

Since, Adjustment "SC" for Day 60 = $1.98\Delta_{reaction} + 3.00\Delta_{curl}$

Then, Camber "SC", Day 60 = Adjustment "SC" + 1.98 * ($\delta_{SC}/3$)

The deflection factor of 1.98 was calculated according to the CEB deflection factor chart.

In the proposed method it is assumed that the far end of the adjacent span is fixed. However when the far bent is an outrigger, it is recommended to include the deflection of the outrigger cap beam in the hinge curl calculation. The hinge curl is adjusted by adding the additional curl calculated as follows:

$$\Delta_{additional} = \frac{\Delta_{outrigger}}{L_4}\left(L_3 + \frac{C}{2}\right) \qquad (9.18)$$

Where

$\Delta_{outrigger}$ = Camber value of the outrigger beam at the center of bridge. Other parameters were defined previously.

### 9.3 Verification of the proposed method

To evaluate the accuracy of the proposed method to estimate hinge curl, the calculated curls were compared to the measured data as well as those calculated using MTD method presented in Chapter 5. Additionally, the proposed value for the net upward load acting on the adjacent span ($W_u$) utilized in Eq. 9.8, was verified by the analytical results from SAP2000 and ABAQUS.

#### 9.3.1 Measured and calculated hinge curls

Table 9-2 lists the calculated immediate hinge curls using the proposed equation and the percent differences with those measured in field. The proposed equation underestimated the hinge curl by 4% to 28% for some hinges, while it overestimated curls by 1% to 13% in other hinges. The proposed equation overestimated the immediate curl by 95% and 114% for the closure 1 and 2, respectively. The overestimation percent for the closures were high because the curls at these locations were small, and therefore the effect of any difference between the calculated and measured deflections is significant in terms of percentage. The absolute difference between the measured and calculated deflections for the closures was approximately 0.1 (3 mm). The average percent difference and standard deviation were calculated including and excluding the closures. The average percent differences between the calculated hinge curls and measured data are 14 and -8 including and excluding closures, respectively. The corresponding average

differences using MTD were -62 and -68 as listed in Table 5-3. The standard deviations of the percent differences are 47 and 14 including and excluding closures, respectively. The corresponding values using MTD were 15 and 10 as presented previously in Table 5-3.

The difference between standard deviations associated with the proposed method and MTD was high when closures were included but became much lower when excluding the closures. The standard deviation excluding closures was considered more realistic to represent the correlation between the proposed method and the field data in this aspect.

Table 9-3 lists the measured and calculated hinge curls on Day 1 and comparison between the data. The hinge curls were calculated based on the proposed method once using the current deflection factor chart (MTD) and then using the suggested chart (CEB). It is clear from the percent differences that using the CEB chart led to better predictions over the current chart.

Table 9-4 lists measured and calculated time-dependent hinge curls before load transfer and the percent differences. Here again the data indicate that the CEB factors enhanced the calculated time-dependent hinge curls.

The measured time-dependent hinge curls and those calculated according to the proposed method after load transfer are listed in Table 9-5. The proposed method overestimated the curls for some hinges and underestimated for others. A scatter in the percent differences within the same hinge can also be observed at some hinges for example in Hinge 4, Bridge 5WB. In general, the calculated curls within a short time after load transfer do not sufficiently indicate the accuracy of the calculation method.

This is because of the sources of error that were mentioned in Chapter 8 as well as other variables during construction that are difficult to capture in the calculation and may affect the hinge curl temporarily. In addition, the hinge curl within that period range is not as crucial as the hinge curl before load transfer and the final hinge curl.

Figures 9-8 to 9-17 show the plots of measured and calculated hinge curls using the current MTD 11-34, SAP2000, ABAQUS, and the proposed method. The load transfer stage is shown on the graphs with a vertical broken line. As discussed previously, hinge curls were measured prior to start of post-tensioning until the opening of the bridges to traffic, which varied from 83 to 406 days after stressing. However hinge curls were calculated for up to four years.

Overall, MTD underestimated the hinge curls. In contrast, correlation between the measured hinge curls and those calculated using the proposed method and the numerical models was reasonably close. Some differences were observed between the measured and calculated hinge curls using the proposed method in Hinge 1 of Bridge 2 and Hinge 4 of Bridge 5WB plotted in Figs. 9-10 and 9-17, respectively. This was due to the partial falsework removal in Bridge 2, and temporarily loading the short cantilever of Hinge 4 in Bridge 5WB during construction to adjust the elevations on the both sides of the hinge. These effects were not included in the proposed method because they are unusual. However including these effects in the FE analyses, good correlation between measured curls and FE results was observed (Fig. 9-10). The correlation between the measured and the calculated curl using the proposed method was somewhat restored in Hinge 4 (Fig. 9-17) after removing the temporary weight in the field. The hinge curl started to increase again around Day 138 before load transfer. The measured and

calculated hinge curls for Closures 1 and 2 were significantly different particularly after load transfer as shown in Figs. 9-15 and 9-16, respectively. This was due to the early partial load transfer (Chapter 4) that was not included in the calculations.

The graphs plotted in Figs. 9-8 to 9-17 show substantial differences between the hinge curls estimated by the current MTD and those measured or calculated by other methods. After load transfer the difference became less pronounced at some hinges as shown in Figs. 9-8, 9-10, and 9-17. Overall, the proposed method substantially improved the accuracy of hinge curl estimation over the current method (MTD 11-34).

### 9.3.2 Falsework forces

As discussed previously, the interaction between the falsework and the adjacent span was idealized with an upward uniform distributed load ($W_u$) of 5k/ft (73 kN/m). The falsework force was calibrated to achieve a reasonable match between the measured and calculated hinge curls. The results of SAP and ABAUQS analyses were also used to verify the empirical falsework force. The falsework forces obtained from SAP2000 and ABAQUS analyses are listed in Table 9-6 and 9-7, respectively. $F_{1/8}$, denotes the forces in the falsework bent modelled at $1/8^{th}$ of the adjacent span length. $F_{1/4}$, $F_{1/2}$, and $F_{3/4}$ denote the forces in the falsework bents modelled at quarter points of the adjacent span. Good agreement was found between SAP2000 and ABAQUS results.

Table 9-8 lists the empirical falsework forces after stressing and calculated forces using SAP2000 and ABAQUS. $W_{u\,(SAP)}$ and $W_{u\,(ABAQUS)}$ were calculated for each hinge by dividing the total corresponding falsework forces ($F_{1/8}$, $F_{1/4}$, $F_{1/2}$, and $F_{3/4}$) by the adjacent span length. The average of empirical falsework forces are 5.6 kip/ft (82 kN/m)

and 4.99 kip/ft (73 kN/m) respectively including and excluding the closures. It can be seen that the results from SAP2000 and ABAQUS that the recommended $W_u$ of 5.0 kip/ft (73 kN/m) is reasonable. $W_{u\,(SAP)}$ and $W_{u\,(ABAQUS)}$ were approximately 14% and 25%, respectively lower than the proposed load $W_{u\,(Empirical)}$. Although ABAQUS models were more elaborate than SAP models, better agreement was obtained between $W_{u\,(Empirical)}$ and $W_{u\,(SAP)}$. This is only true for the average values, but for individual hinge, ABAQUS results were generally in better agreement with the empirical forces.

### 9.4 Proposed changes to MTD 11-34

The proposed method for hinge curl calculation showed good agreement with the measured data and can overcome the shortcomings of the current Caltrans methodology. Consequently it is recommended to supersede the current MTD 11-34. Appendix B presents the draft new version of MTD and a numerical example. The key proposed changes and adjustments to the current MTD 11-34 document (Caltrans 2012) are as follows:

- Include the additional hinge curl due to the flexibility of the short cantilever support, $\Delta_{flexible}$, in the equation for immediate hinge curl $\Delta_{curl}$.
- Remove the threshold of 0.5 in difference between Adjustment "SC" of Day 0 and Day 720 (Step 5 of MTD 11-34) and include time-dependent cambers for all cases.
- Replace the current deflection factor chart with the CEB chart and update the procedure accordingly.

- Change the deflection factor of $\Delta_{curl}$ from 2.00 to 3.00 in Adjustment "LC" at Day 0.
- Apply an appropriate time-dependent deflection factor to the deflection due to joint rotation after load transfer, $\delta$, for both short and long cantilevers based on the elapsed time before load transfer.
- In case an outrigger bent supports the far end of the adjacent span, the deflection of the bent cap should be incorporated in the hinge curl calculation.
- According to the analytical results for the long cantilever frames of in-span hinges, an upward camber of 0.2" (5 mm) may be provided at the edge of the long cantilever in addition to the calculated camber value at $LC_{1.00}$. This recommendation is to be incorporated in construction details.

# Chapter 10 Summary and Conclusions

## 10.1 Summary

This document is focused on the prediction of time-dependent deflection of in-span hinges in cast-in-place (CIP), post-tensioned concrete (PS), box girder bridges. This type of bridges tends to develop hinge deflections that are different than those estimated using the current design method described in the Caltrans memo to designer (MTD) 11-34, "Hinge Curl" (Caltrans 2012). The upward movement of the short cantilever due post-tensioning is referred to as "hinge curl". Extra construction cost and delay, and serviceability problems arise because of mismatch of the superstructure on the two sides of the bridge. The main objective of the study was to quantify the differences, identify the causes, and develop methods to improve hinge curl estimation in CIP/PS box girder bridges.

The study consisted of six parts: (1) field measurement of hinge movements in five bridges, (2) analysis of data and comparison with the estimated movements using the current method, (3) analytical studies of the five bridges using relative simple models utilizing software package SAP2000, (4) analytical studies of the five bridges using detailed finite element models utilizing ABAQUS, (5) analytical parametric studies of the effect of superstructure skew and horizontal curvature on the hinge curl, and (6) development of a new, practical method to improve on estimation of hinge curl.

In part 1, five bridges in the state of California were identified for field measurements. A total of eight bridge frames were surveyed during construction; seven were CIP/PS with ten hinges and one was CIP/non-PS with two hinges. Deflections of

superstructures were measured and monitored using electronic surveying equipment on the top deck surface. A grid of stations was marked on the top deck surface of the short cantilever and its adjacent span at each hinge. Elevations were measured before stressing, immediately after stressing, and periodically afterward during construction until bridges were opened to traffic. Temperature and relative humidity data were collected during each field visit. Other information about bridge properties were reported by Caltrans and were used in the bridge analyses. The field data were collected over 3 to 14 months depending on the bridge and construction schedule.

The data were analyzed in part 2 and deflections were plotted and studied for the surveyed cantilevers and adjacent spans. Hinge curls were calculated according to the latest version of Caltrans MTD 11-34. To apply the Caltrans method, computer models were developed for the five bridges using CTBridge software (CTBridge 2012) and results were utilized in deflection calculations. The MTD estimated curls were compared to those measured in field and accordingly the prediction accuracy of the memo was evaluated. Substantial differences between the field data and estimated hinge curls were noted. The assumption about the boundary conditions and other issues in the current Caltrans procedure were determined to be the primary sources of differences between the estimated and actual hinge curls.

Analytical modelling was used in this study for further investigation of the deformation behavior of the bridges. Two analytical modelling approaches were investigated; stick model using SAP2000 (part 3 of the study) and finite element model using ABAQUS (part 4 of the study). The purpose of using SAP2000 was to investigate analytically the deformation behavior of CIP/PS bridges using relatively simple models.

Because SAP2000 model did not capture the three-dimensional cross-section properties as well as other geometrical changes, the more sophisticated program ABAQUS was used to capture the deformation behavior across the bridge width, and the effect of skew abutment and horizontal curvature on hinge curl. Computer models of the surveyed bridge frames were developed on the two computer programs with some simplifying assumptions. Time-dependent material properties were defined and construction-stage analysis was implemented in both programs to capture the time-dependent deformation response. Bridge deflections were plotted for different times and compared to the actual response from field measurements. Deflections were also calculated using the computer programs for up to four years after stressing. It is commonly assumed that after four years all the time-dependent deformations reach their final values.

In part 5, parametric study was conducted utilizing the finite element approach on ABAQUS to investigate the effect of horizontal curvature alignment of bridges and skew angle of abutments on hinge curl. None of the bridges that were surveyed in the field had significant skew or curvature. The purpose of the study in part 5 was to determine if additional factors should be incorporated in hinge curl calculation due to skew and curvature.

To improve the accuracy of hinge curl estimation a new method was proposed in part 6 and incorporated in a new document with the MTD 11-34 format. A new step-by-step numerical example was included in the document. The new method addresses the effect of substructure flexibility on hinge curl and incorporates time-dependent deflection factors in a consistent manner. Additionally, refinements and adjustments were proposed for improving the time-dependent hinge curl prediction. Hinge curls were calculated

according to the proposed method and compared to field measurements and analytical results from SAP2000 and ABAQUS to validate the new procedure.

## 10.2 Observations

This section presents the observations from the field measurements and the analytical studies of the five bridges

1- Despite variation in bridge geometry and prestress forces, all bridges exhibited similar deformation patterns at the hinge and in the span adjacent to the short cantilever.

2- The measured instantaneous hinge curls are considerably higher than those calculated according to the MTD 11-34 document. The ratio of instantaneous measured to calculated hinge curls ranged from 1.6 to 5.8 for the surveyed prestressed hinges.

3- The significant rotation that was observed at the short cantilever to pier cap connection was the reason for the higher actual hinge curls.

4- The deflection factor chart utilized in MTD 11-34 for estimating the long term effects due to creep and shrinkage led to time-dependent hinge curls that were lower than those measured in field.

5- The current method for calculating the long cantilever camber correction, Adjustment “LC”, at Day 0 was found to be inconsistent with the theoretical camber obtained from CTBridge analysis. The resulting difference between these two terms does not represent the deflection due to joint rotation after

falsework removal, $\delta_{LC}$, and causes errors in the calculated time-dependent camber for the long cantilever.

6- Hinge curls appeared to be somewhat insensitive to variation of temperature and relative humidity within the same day. It is impractical to include hinge curl variation due to temperature and relative humidity in design equations due to the fact that the environmental conditions are variable and cannot be predicted at the time of design.

7- Measured deflections at non prestressed hinges confirmed that hinge curl is unique to prestressed bridges.

8- Construction sequence implemented by utilizing staged construction analysis in SAP2000 or by performing multi-step analysis in ABAQUS, estimated the actual deformation response of the surveyed bridges well.

9- SAP2000 analysis results showed that time-dependent variation of the concrete modulus of elasticity and relaxation of the prestressing steel have negligible effect on hinge curl.

10- The power-law creep model with time-hardening version in the ABAQUS library was the most suitable material model to simulate concrete creep effects on hinge curl.

11- Ignoring shrinkage effect in SAP2000 and ABAQUS analyses led to inaccurate estimation of hinge curl. Concrete shrinkage affected significantly the long-term deflections of bridges after falsework removal but had minimal effects on deflections before falsework removal.

12- Based on the results of computer analysis for Bridge 2, deflection of the outrigger bent located at the far end of the adjacent span of in-span hinges has to be accounted for because it affects hinge curl after falsework removal.

13- Within practical ranges, neither the horizontal curvature nor skew angle of the bridge affected the hinge curl before load transfer. After load transfer there were some minor differences as the skew angle and curvature changed.

14- The proposed equation significantly improves the immediate hinge curl prediction. The ratio of instantaneous measured to estimated hinge curls dropped considerably using the proposed equation and ranged from 0.5 to 1.4 for the surveyed prestressed hinges.

15- The proposed adjustments to the time-dependent deflection factor chart and camber equations of MTD 11-34 improved substantially the prediction of time-dependent deflections of in-span hinges.

## 10.3 Conclusions

It should be recognized that exact prediction of in-span hinge deflections is not possible due to uncertainties in material properties of concrete, prestress losses, falsework configuration and deformation, and other factors such as construction tolerances. Nonetheless, efforts were made in this research to develop a rational method to estimate hinge curl with reasonable accuracy leading to less corrective measures in the field. Based on the field survey of superstructure deformation at the hinge and the adjacent span in five bridges and analytical studies, the following are the main conclusions of this research:

1- The assumed fixed connection of the short cantilever support leads to the underestimation of the immediate hinge curl.
2- Post-tensioning of continuous superstructures causes rotation at pier locations even at the presence of falsework.
3- The time-dependent deflection factors and the deflection due to joint rotation after falsework removal in the current MTD method need to be revised.
4- A stick model analysis using SAP2000 leads to results that are in good agreement with those obtained from the detailed three-dimensional finite element model using ABAQUS for straight bridges.
5- Effect of concrete shrinkage should be taken into account in computer modelling of hinge curl.
6- Influence of curvature and skew angle on hinge curl is negligible.
7- Considering the flexibility of the short cantilever support, and the proposed adjustments for equation of time-dependent deflections, lead to reasonably accurate hinge curl estimates.

# References


1. AASHTO. *AASHTO LRFD Bridge Design Specifications (6th Edition).* Washington, DC: American Association of State Highway and Transportation Officials, 2012.
2. ACI. Guide for Modeling and Calculating Shrinkage and Creep in Hardened Concrete (ACI 209.2R-08). Farmington Hills, MI: American Concrete Institute, 2008.
3. Akl, A., M. Saiidi, and A. Vosooghi. "Field Studies of Post-Tensioned Bridge Hinge Curl." PCI Convention and National Bridge Conference. Grapevine, Texas, 2013. 11pp.
4. Barr, P., and F. and Angomas. "Differences between Calculated and Measured Long-Term Deflections in a Prestressed Concrete Girder Bridge." ASCE Journal of Performance of Constructed Facilities, 2010: 603-609.
5. Bažant, Z., M. Hubler, and Q. Yu. "Pervasiveness of Excessive Segmental Bridge Deflections: Wake-Up Call for Creep." ACI Structural Journal, 2011: 766-774.
6. Bažant, Z., Q. Yu, G. Li, G. Klein, and V. KRístek. "Excessive Deflections of Record-Span Prestressed Box Girder." ACI Concrete International, 2010: 44-52.
7. Bond, H. "Construction Challenges of the GALENA CREEK BRIDGE." May 16, 2012. http://www.goodengineers.com/invitation/Invitation/seminars/HBond_PTG_Galena_16may2012Midasoft_v2%20%282%29.pdf.
8. Caltrans. Bridge Deck Construction Manual. Sacramento, CA: California Department of Transportation, 1991.
9. Caltrans. Bridge Design Practice Manual. Sacramento, CA: California Department of Transportation, 2014.

10. Caltrans. Bridge Design Specifications. Sacramento, CA: California Department of Transportation, 2000.
11. Caltrans. Construction Manual. Sacramento, CA: California Department of Transportation, 2013.
12. Caltrans. Falsework Manual (Revision No. 36). Sacramento, CA: California Department of Transportation, 2012.
13. Caltrans. Memo to Designers 11-3: Designer's Checklist for Prestressing in Post-tensioned Concrete Box Girders. Sacramento, CA: California Department of Transportation, 2010.
14. Caltrans. Memo To Designers 11-31: Curved Post-Tensioned Bridges. Sacramento, CA: California Department of Transportation, 2010.
15. Caltrans. Memo To Designers 11-34: Hinge Curl. Sacramento, CA: California Department of Transportation, 2012.
16. Caltrans. Memo To Designers 11-34: Hinge Curl. Sacramento, CA: California Department of Transportation, 1994.
17. Caltrans. Memo To Designers 20-3: Restrainers at Support Joints. Sacramento, CA: California Department of Transportation, 2008.
18. Caltrans. Prestress Manual. Sacramento, CA: California Department of Transportation, 2005.
19. Carden, L., A. Itani, and G. Pekcan. Recommendations for the Design of Beams and Posts in Bridge Falsework. Reno, NV: University of Nevada Reno, CCEER Report No. 05-11, 2006.

20. CEB-FIP. Model Code for Concrete Structures. Lausanne, Switzerland: Comité Euro International du Beton, 1990.
21. CSI. "Structural Analysis Program (Software and Reference Manual)." SAP2000 15.0.1. Computers and Structures, Inc. (CSI), 2011.
22. CTBridge. "Caltrans Bridge Analysis and Design." CTBridge 1.5.6. California Department of Transportation, 2012.
23. Gilbert, R., and G. Ranzi. Time-Dependent Behaviour of Concrete Structures. New York, NY: Spon Press, 2011.
24. Hedjazi, S., A. Rahai, and K. Sennah. "Evaluation of creep effects on the time-dependent deflections and stresses in prestressed concrete bridges." Bridge Structures, 2007: 119-132.
25. Hinkle, S. Investigation of time-dependent deflection in long span, high strength, prestressed concrete bridge beams. Blacksburg, VA: M.Sc. thesis, Virginia Polytechnic Institute and State University, 2006.
26. Juirnarongrit, T., and S. Ashford. Effect of Pile Diameter on the Modulus of Sub-Grade Reaction. La Jolla, CA: University of California, San Diego, 2005.
27. Kamatchi, P., et al. "Long-Term Prestress Loss and Camber of Box-Girder Bridge." ACI Structural Journal, 2014: 1-10.
28. Meyerson, R. Compressive Creep of Prestressed Concrete Mixtures with and without Mineral Admixtures. Blacksburg, VA: M.Sc. thesis, Virginia Polytechnic Institute and State University, 2001.
29. Nawy, E. Prestressed Concrete: A Fundamental Approach. Upper Saddle River, NJ: Pearson Higher EDucation, 2009.

30. NCHRP. Development of Design Specifications and Commentary for Horizontally Curved Concrete Box-Girder Bridges. Washington, DC: Transportation Research Board, Report 620, 2008.
31. NDOT. Structures Manual. Carson City: Nevada Department of Transportation, 2008.
32. PCI. PCI Design Handbook (7th Edition). Chicago, IL: Precast and Prestressed Concrete Institute, 2011.
33. Robertson, I. "Prediction of vertical deflections for a long-span prestressed concrete bridge structure." Engineering Structures, 2005: 1820-1827.
34. Roschke, P., K. Pruski, and N. Sripadanna. "Time-Dependent Behavior of Post-Tensioned Slab Bridge." ACI Structural Journal, 1999: 400-408.
35. Saiidi, M., E. Hutchens, and D. Gardella. "Bridge Prestress Losses in Dry Climate." ASCE Journal of Bridge Engineering, 1998: 111-116.
36. Saiidi, M., J. Shields, D. O'Connor, and E. Hutchens. "Variation of Prestress Force in a Prestressed Concrete Bridge During the First 30 Months." PCI Journal, 1996: 66-72.
37. Sanders, P., and S. Ashford. Load Capacity, Failure Mode and Design Criteria Investigation of Sand Jacks. La Jolla, CA: University of California, San Diego, SSRP-05/06, 2008.
38. Scheevel, C., K. Morris, and A. Schultz. Wakota Bridge Thermal Monitoring Program. St. Paul, MN: Minnesota Department of Transportation, MN/RC 2013-11, 2013.
39. Simulia. "Finite Element Program (Software and Documentation)." Abaqus 6.14. Dassault Systèmes Simulia Corp., 2014.

40. Witchukreangkrai, E., K. Tsuchida, T. Maeda, and Y. Watanabe. "Long-term deflection monitoring of a cantilever prestressed concrete bridge with intermediate hinges over 25 years." CONCREEP 8 conference. Ise-Shima, Japan, 2008. 639-645.

Table 2-1 Summary of bridges

| Bridge Label | Bridge Name | Bridge No. | Location |
|---|---|---|---|
| 1 | **San Luis Rey River Bridge** | 57-1208R | San Diego |
| 2 | **N170-I5 Connector** | 53-2976 | Los Angeles |
| 3 | **Bradley Overhead** | 39-0044 | Merced |
| 4 | **EB Wilshire Blvd On-Ramp OC** | 53-3021S | Los Angeles |
| 5EB | **Del Paso Park Overhead** | 24-0193R | Sacramento |
| 5WB | **Del Paso Park Overhead** | 24-0193L | Sacramento |

Table 2-2 Summary of hinges

| Bridge | Frame number | Frame type | Hinge label |
|---|---|---|---|
| 1 | Frame 2 “F2” | CIP/PS | Hinge 3 “H3” |
| | | | Hinge 7 “H7” |
| 2 | Frame 2 “F2” | CIP/PS | Hinge 1 “H1” |
| | | | Hinge 2 “H2” |
| 3 | Frame 1 “F1” | CIP/PS | Hinge “H” |
| 4 | Frame 2 “F2” | CIP/PS | Hinge “H” |
| 5EB | Frame 1 “F1” | CIP/PS | Hinge 1 “H1” |
| | Frame 3 “F3” | CIP/PS | Closure 1 “C1” |
| | | | Closure 2 “C2” |
| 5WB | Frame 3 “F3” | CIP/RC | Hinge 2 “H2” |
| | | | Hinge 3 “H3” |
| | Frame 5 “F5” | CIP/PS | Hinge 4 “H4” |

Table 2-3 Prestressing design parameters

| Bridge | Frame | Pjack | | Friction curvature coefficient “μ” | Friction wobble coefficient “K” | | Anchor set | |
|---|---|---|---|---|---|---|---|---|
| | | Kip | KN | | /ft | /m | in | mm |
| 1 | F2 | 14754 | 65,630 | 0.20 | 0.0002 | 0.00066 | 0.375 | 10 |
| 2 | F2 | 15910 | 70,771 | 0.20 | 0.0002 | 0.00066 | 0.375 | 10 |
| 3 | F1 | 8745 | 38,900 | 0.20 | 0 | 0 | 0.375 | 10 |
| 4 | F2 | 9000 | 40,034 | 0.15 | 0.0002 | 0.00066 | 0.375 | 10 |
| 5EB | F1 | 3600 | 16,014 | 0.15 | 0.0002 | 0.00066 | 0.375 | 10 |
| | F3 (A) | 5800 | 25,800 | 0.15 | 0.0002 | 0.00066 | 0.375 | 10 |
| | F3 (C) | 4400 | 19,572 | 0.15 | 0.0002 | 0.00066 | 0.375 | 10 |
| 5WB | F5 | 4800 | 21,352 | 0.15 | 0.0002 | 0.00066 | 0.375 | 10 |

Table 3-1 Field measurements schedule for Bridge 1

| Bridge name | San Luis Rey River Bridge |
|---|---|
| Bridge number | 1 |
| Hinge Label | H3 & H7 |
| Before stressing | "Day -1"<br>Monday-10/31/11 |
| After stressing | "Day 0"<br>Wednesday-11/2/11 |
| | "Day 1"<br>Thursday-11/3/11 |
| After pouring the hinge closure | "Day 49"<br>Wednesday-12/21/11 |
| After load transfer and falsework removal | "Day 92"<br>Wednesday-2/1/12 |
| | "Day 129"<br>Wednesday-3/7/12 |
| Opening date | April, 2012 |

Table 3-2 Field measurements schedule for Bridge 2

| Bridge name | N170-N5 Connector |
|---|---|
| Bridge number | 2 |
| Hinge Label | H1 & H2 |
| Before stressing | "Day -1"<br>Friday-9/21/12 |
| After stressing | "Day 0"<br>Thursday - 10/4/12 |
| | "Day 1"<br>Friday-10/5/12 |
| | "Day 36"<br>Thursday-11/9/12 |
| After pouring the hinge seat (bottom ledge) | "Day 97"<br>Wednesday-1/9/13 |
| After load transfer and falsework removal | "Day 149"<br>Friday-3/1/13 |
| | "Day 197"<br>Friday-4/19/13 |
| Opening date | May, 2013 |

Table 3-3 Field measurements schedule for Bridge 3

| Bridge name | Bradley Overhead |
|---|---|
| Bridge number | 3 |
| Hinge Label | H |
| Before stressing | "Day -1"<br>Friday-10/19/12 |
| After stressing | "Day 0"<br>Wednesday-10/24/12 |
| | "Day 1"<br>Thursday-10/25/12 |
| After pouring the hinge closure | "Day 22"<br>Thursday-11/15/12 |
| After load transfer and falsework removal | "Day 83"<br>Tuesday-1/15/13<br>Two data sets<br>(8:00 am & 1:00 pm) |
| Opening date | January, 2013 |

Table 3-4 Field measurements schedule for Bridge 4

| Bridge name | EB Wilshire Blvd On-Ramp OC |
|---|---|
| Bridge number | 4 |
| Hinge Label | H |
| Before stressing | "Day -1"<br>Monday – 5/6/13 |
| After stressing | "Day 0"<br>Wednesday - 5/8/12 |
| | "Day 1"<br>Thursday - 5/9/12 |
| | "Day 51"<br>Friday - 6/28/13 |
| | "Day 99"<br>Thursday - 8/15/13 |
| After pouring the hinge seat (bottom ledge) | "Day 135"<br>Friday - 9/20/13 |
| After load transfer and falsework removal | "Day 167"<br>Friday - 10/22/13 |
| | "Day 170"<br>Monday - 10/25/13 |
| Opening date | November, 2013 |

Table 3-5 Field measurements schedule for Hinge 1 and Hinge 4, Bridge 5

| Bridge name | Del Paso Park Overhead "East Bound" | Del Paso Park Overhead "West Bound" |
|---|---|---|
| Bridge number | 5EB | 5WB |
| Hinge Label | H1 | H4 |
| Before stressing | "Day -1" Wednesday-6/5/13 | "Day -1" Friday-3/22/13 |
| After stressing | "Day 0" Wednesday-6/12/13 | "Day 0" Wednesday-4/3/13 |
| | "Day 1" Thursday-6/13/13 | "Day 1" Thursday-4/4/13 |
| | | "Day 30" Friday-5/3/13 |
| | | "Day 64" Wednesday-6/5/13 |
| After pouring the hinge seat (bottom ledge) | "Day 27" Tuesday-7/9/13 | "Day 73" Wednesday-6/12/13 |
| | | "Day 74" Thursday-6/13/13 |
| After pouring the top ledge | "Day 68" Friday 8/9/13 | "Day 97" Tuesday-7/9/13 |
| | | "Day 138" Friday-8/9/13 |
| | | "Day 182" Wednesday-10/2/13 |
| | | "Day 212" Friday-11/1/13 |
| | | "Day 224" Wednesday-11/13/13 |
| After load transfer and falsework removal | "Day 112" Wednesday-10/2/13 | "Day 254" Friday-12/13/13 |
| | "Day 143" Friday-11/1/13 | "Day 315" Wednesday-2/12/14 |
| | "Day 155" Wednesday-11/13/13 | "Day 345" Friday-3/14/14 |
| | "Day 184" Friday-12/13/13 | "Day 406" Wednesday-5/14/14 |
| | "Day 245" Wednesday-2/12/14 | |
| | "Day 275" Friday-3/14/14 | |
| Opening date | April, 2014 | June, 2014 |

Table 3-6 Field measurements schedule for Closure 1 and 2, Bridge 5EB

| Bridge name | Del Paso Park Overhead "East Bound" | |
|---|---|---|
| Bridge number | 5EB | |
| Hinge Label | C1 | C2 |
| Before stressing | "Day -1" Friday-3/15/13 | "Day -1" Tuesday-3/19/13 |
| After stressing | "Day 0" Wednesday-3/20/13 | "Day 0" Thursday-3/21/13 |
| | "Day 1" Thursday-3/21/13 | "Day 1" Friday-3/22/13 |
| | "Day 2" Friday-3/22/13 | "Day 12" Tuesday-4/2/13 |
| | "Day 13" Tuesday-4/2/13 | "Day 13" Wednesday-4/3/13 |
| | "Day 14" Wednesday-4/3/13 | "Day 43" Friday-5/3/13 |
| | "Day 44" Friday-5/3/13 | |
| After lowering the drop-in span and the closure concrete placement | "Day 77" Thursday-6/5/13 | "Day 76" Thursday-6/5/13 |
| | "Day 84" Thursday-6/12/13 | "Day 83" Thursday-6/12/13 |
| | "Day 85" Friday-6/13/13 | "Day 84" Friday-6/13/13 |
| | "Day 111" Tuesday-7/9/13 | "Day 110" Tuesday-7/9/13 |
| | "Day 152" Monday-8/19/13 | "Day 151" Monday-8/19/13 |
| After load transfer and falsework removal | "Day 196" Wednesday-10/2/13 | "Day 195" Wednesday-10/2/13 |
| | "Day 227" Friday 11/1/13 | "Day 226" Friday 11/1/13 |
| | "Day 239" Wednesday-11/13/13 | "Day 238" Wednesday-11/13/13 |
| | "Day 269" Friday-12/13/13 | "Day 268" Friday - 12/13/13 |
| | "Day 330" Wednesday-2/12/14 | "Day 329" Wednesday-2/12/14 |
| | "Day 360" Friday-3/14/14 | "Day 359" Friday-3/14/14 |
| Opening date | April, 2014 | |

Table 3-7 Field measurements schedule for Hinge 2 and 3, Bridge 5WB

| | |
|---|---|
| Bridge name | Del Paso Park Overhead "East Bound" |
| Bridge number | 5WB |
| Hinge Label | H2 & H3 |
| After casting the deck | "Day 10", Reference<br>Friday – 11/1/13 |
| | "Day 22"<br>Wednesday - 11/13/13 |
| After load transfer and falsework removal | "Day 53"<br>Friday - 12/13/13 |
| | "Day 114"<br>Wednesday - 2/12/14 |
| | "Day 144"<br>Friday - 3/14/14 |
| | "Day 205"<br>Wednesday - 5/14/14 |
| Opening date | June, 2014 |

Table 4-1 Temperature and relative humidity data recorded for Bridge 1

| | San Luis Rey River Bridge | | | | | |
|---|---|---|---|---|---|---|
| | Bridge 1 | | | | | |
| | Hinge 3 | | | Hinge 7 | | |
| | Time | Temp.(°F) | RH% | Time | Temp.(°F) | RH% |
| Day -1 | 10:50 am | 74 | 35 | 10:20 am | 70 | 37 |
| Day 0 | 3:00 pm | 87 | 10 | 2:20 pm | 85 | 11 |
| Day 1 | 7:30 am | 49 | 43 | 6:50 am | 50 | 36 |
| Day 49 | 1:45 pm | 72 | 35 | 2:20 pm | 67 | 44 |
| Day 92 | 2:20 pm | 72 | 48 | 2:40 pm | 72 | 48 |
| Day 129 | 2:00 pm | 69 | 25 | 2:35 pm | 66 | 25 |

Table 4-2 Temperature and relative humidity data recorded for Bridge 2

| | N170-I5 Connector | | | | | |
|---|---|---|---|---|---|---|
| | Bridge 2 | | | | | |
| | Hinge 1 | | | Hinge 2 | | |
| | Time | Temp.(°F) | RH% | Time | Temp.(°F) | RH% |
| Day -1 | 9:10 am | 88 | 48 | 10:20 am | 90 | 41 |
| Day 0 | 12:50 pm | 82 | 37 | 2:10 pm | 84 | 32 |
| Day 1 | 9:25 am | 70 | 65 | 10:15 am | 71 | 63 |
| Day 36 | 9:40 am | 75 | 31 | 10:50 am | 73 | 25 |
| Day 97 | 12:10 pm | 73 | 25 | 12:50 pm | 74 | 25 |
| Day 148 | 11:50 am | 84 | 21 | 12:40 pm | 88 | 20 |
| Day 197 | 12:15 pm | 88 | 20 | 2:15 pm | 89 | 20 |

Table 4-3 Temperature and relative humidity data recorded for Bridge 3

| | Bradley Overhead | | |
|---|---|---|---|
| | Bridge 3 | | |
| | Hinge | | |
| | Time | Temp.(°F) | RH% |
| Day -1 | 9:20 am | 70 | 72 |
| Day 0 | 9:40 am | 55 | 67 |
| Day 1 | 9:30 am | 61 | 62 |
| Day 22 | 12:25 am | 76 | 28 |
| Day 83 (morning) | 8:25 am | 34 | 70 |
| Day 83 (noon) | 1:15 pm | 50 | 34 |

Table 4-4 Temperature and relative humidity data recorded for Bridge 4

| | EB Wilshire Blvd On-Ramp OC | | |
|---|---|---|---|
| | Bridge 4 | | |
| | Hinge | | |
| | Time | Temp.(°F) | RH% |
| Day -1 | 1:15 pm | 77 | 39 |
| Day 0 | 2:15 pm | 81 | 29 |
| Day 1 | 12:30 pm | 76 | 43 |
| Day 51 | 12:50 pm | 98 | 32 |
| Day 99 | 10:10 am | 82 | 45 |
| Day 135 | 10:15 am | 70 | 74 |
| Day 167 | 10:40 am | 66 | 65 |
| Day 170 | 11:00 am | 71 | 51 |

Table 4-5 Temperature and relative humidity data recorded at Hinge 1, Bridge 5EB

| | Del Paso Park Overhead | | |
|---|---|---|---|
| | Bridge 5EB | | |
| | Hinge 1 | | |
| | Time | Temp.(°F) | RH% |
| Day -1 | 12:00 pm | 85 | 26 |
| Day 0 | 1:45 pm | 90 | 21 |
| Day 1 | 8:30 am | 66 | 39 |
| Day 27 | 10:25 pm | 84 | 24 |
| Day 68 | 11:50 am | 86 | 23 |
| Day 112 | 9:35 am | 65 | 35 |
| Day 143 | 11:45 am | 69 | 32 |
| Day 155 | 11:30 am | 71 | 27 |
| Day 184 | 11:55 am | 54 | 35 |
| Day 245 | 11:20 am | 64 | 58 |
| Day 275 | 11:10 am | 69 | 41 |

Table 4-6 Temperature and relative humidity data recorded at Closure 1 and Closure 2, Bridge 5EB

| | Del Paso Park Overhead | | | | | |
|---|---|---|---|---|---|---|
| | Bridge 5EB | | | | | |
| | Closure 1 | | | Closure 2 | | |
| | Time | Temp.(°F) | RH% | Time | Temp.(°F) | RH% |
| Day -1 | 12:10 pm | 75 | 42 | 1:10 pm | 83 | 31 |
| Day 0 | 3:45 pm | 69 | 64 | 3:40 pm | 69 | 30 |
| Day 1 | 3:00 pm | 66 | 37 | 8:50 am | 48 | 37 |
| Day 13 | 11:30 am | 72 | 47 | 12:00 pm | 76 | 40 |
| Day 44 | 1100 am | 86 | 22 | 11:30 am | 87 | 21 |
| Day 78 | 10:50 am | 73 | 42 | 11:20 am | 78 | 36 |
| Day 86 | 11:05 am | 80 | 28 | 11:25 am | 85 | 26 |
| Day 111 | 10:45 am | 89 | 22 | 11:05 am | 90 | 21 |
| Day 152 | 11:20 am | 92 | 26 | 11:50 am | 94 | 24 |
| Day 196 | 9:50 am | 66 | 33 | 10:15 am | 68 | 31 |
| Day 227 | 12:00 pm | 70 | 29 | 12:20 pm | 69 | 30 |
| Day 239 | 11:50 am | 72 | 27 | 12:05 pm | 72 | 27 |
| Day 269 | 12:10 pm | 53 | 36 | 12:40 pm | 55 | 33 |
| Day 330 | 11:45 am | 67 | 54 | 12:00 pm | 68 | 53 |
| Day 360 | 11:30 am | 72 | 35 | 11:45 am | 73 | 34 |

Table 4-7 Temperature and relative humidity data recorded at Hinge 4, Bridge 5WB

| | Del Paso Park Overhead | | |
|---|---|---|---|
| | Bridge 5WB | | |
| | Hinge 4 | | |
| | Time | Temp.(°F) | RH% |
| Day -1 | 9:10 am | 51 | 34 |
| Day 0 | 3:30 pm | 81 | 33 |
| Day 1 | 9:00 am | 55 | 95 |
| Day 30 | 12:00 pm | 92 | 19 |
| Day 64 | 12:45 pm | 89 | 25 |
| Day 73 | 10:40 am | 86 | 25 |
| Day 74 | 9:20 am | 70 | 36 |
| Day 97 | 11:35 am | 91 | 20 |
| Day 138 | 10:35 am | 89 | 30 |
| Day 182 | 9:15 am | 64 | 37 |
| Day 212 | 10:45 am | 63 | 39 |
| Day 224 | 10:30 am | 67 | 32 |
| Day 254 | 10:45 am | 50 | 38 |
| Day 315 | 12:50 pm | 68 | 49 |
| Day 345 | 10:25 am | 63 | 47 |
| Day 406 | 10:30 am | 82 | 24 |

Table 4-8 Temperature and relative humidity data recorded at Hinge 2 and Hinge 3, Bridge 5WB

| | Del Paso Park Overhead | | |
|---|---|---|---|
| | Bridge 5WB | | |
| | Hinge 2 & Hinge 3 | | |
| | Time | Temp.(°F) | RH% |
| Day 10 | 10:45 am | 64 | 38 |
| Day 22 | 11:05 am | 72 | 28 |
| Day 53 | 11:15 am | 52 | 36 |
| Day 114 | 12:20 pm | 68 | 50 |
| Day 144 | 10:45 am | 64 | 48 |
| Day 205 | 11:00 am | 83 | 23 |

Table 5-1 Deflection of the short cantilevers due to dead load

| | | B1 | | B2 | | B3 | B4 | B5EB | | | B5WB |
|---|---|---|---|---|---|---|---|---|---|---|---|
| | | H3 | H7 | H1 | H2 | H | H | H1 | C1 | C2 | H4 |
| $A_{SC}$ | $ft^2$ | 128 | 106 | 129.3 | 129.3 | 72 | 81 | 47.68 | 40.51 | 40.51 | 47.68 |
| | $m^2$ | 11.89 | 9.85 | 12.01 | 12.01 | 6.69 | 7.53 | 4.43 | 3.76 | 3.76 | 4.43 |
| w | k/in | 1.6 | 1.325 | 1.616 | 1.616 | 0.9 | 1.013 | 0.596 | 0.506 | 0.506 | 0.596 |
| | KN/m | 277.2 | 229.5 | 279.9 | 279.9 | 155.9 | 175.5 | 103.2 | 87.6 | 87.6 | 103.2 |
| $L_1$ | in | 246.5 | 316.1 | 279.4 | 262.7 | 334.7 | 231 | 180 | 144 | 144 | 198 |
| | m | 6.261 | 8.029 | 7.096 | 6.673 | 8.501 | 5.867 | 4.572 | 3.657 | 3.657 | 5.029 |
| $L_2$ | in | 230 | 299.6 | 264.7 | 248 | 319.9 | 222 | 168 | 132 | 132 | 186 |
| | m | 5.842 | 7.609 | 6.723 | 6.299 | 8.125 | 5.638 | 4.267 | 3.352 | 3.352 | 4.724 |
| $L_3$ | in | 300.6 | 370.3 | 358.2 | 341.4 | 391.7 | 267 | 216 | 162 | 162 | 240 |
| | m | 7.635 | 9.406 | 9.098 | 8.672 | 9.949 | 6.782 | 5.486 | 4.115 | 4.115 | 6.096 |
| E | Ksi | 4060 | 4060 | 3863 | 3863 | 4317 | 4287 | 3834 | 4287 | 4287 | 3834 |
| | Gpa | 28 | 28 | 26.6 | 26.6 | 29.7 | 29.7 | 26.4 | 29.5 | 29.5 | 26.4 |
| $I_{SC}$ | $*10^7$ ($in^4$) | 2.59 | 2.06 | 3.64 | 3.64 | 1.49 | 1.41 | 0.62 | 0.44 | 0.44 | 0.62 |
| | $*10^{12}$ mm | 10.77 | 8.57 | 15.14 | 15.14 | 6.19 | 5.87 | 2.58 | 1.83 | 1.83 | 2.58 |
| $t_{diaphragm}$ | ft | 2.75 | 2.75 | 2.46 | 2.46 | 2.46 | 1.5 | 2 | 2 | 2 | 2 |
| | m | 0.838 | 0.838 | 0.749 | 0.749 | 0.749 | 0.457 | 0.609 | 0.609 | 0.609 | 0.609 |
| $A_{void}$ | $ft^2$ | 247 | 181 | 165 | 165 | 121 | 140 | 60 | 54 | 54 | 60 |
| | $m^2$ | 23 | 16.8 | 15.3 | 15.3 | 11.2 | 13 | 5.6 | 5 | 5 | 5.6 |
| P | kips | 102 | 85 | 61 | 61 | 45 | 32 | 18 | 16 | 16 | 18 |
| | KN | 454 | 378 | 271 | 271 | 200 | 142 | 80 | 71 | 71 | 80 |
| **$\Delta_{DL}$** | **in** | **0.015** | **0.037** | **0.016** | **0.013** | **0.037** | **0.001** | **0.006** | **0.003** | **0.003** | **0.009** |
| | **mm** | **0.381** | **0.94** | **0.406** | **0.33** | **0.94** | **0.025** | **0.152** | **0.076** | **0.076** | **0.229** |

Table 5-2 Deflection of the short cantilevers due to prestressing force

| | | B1 | | B2 | | B3 | B4 | B5EB | | | B5WB |
|---|---|---|---|---|---|---|---|---|---|---|---|
| | | H3 | H7 | H1 | H2 | H | H | H1 | C1 | C2 | H4 |
| $P_J$ | $*10^3$ kips | 14.77 | 14.77 | 15.91 | 15.91 | 8.745 | 9 | 3.6 | 5.8 | 4.4 | 4.8 |
| | $*10^3$ KN | 65.70 | 65.70 | 70.77 | 70.77 | 38.90 | 40.00 | 16.00 | 25.80 | 19.57 | 21.35 |
| FC | | 0.86 | 0.87 | 0.86 | 0.86 | 0.9 | 0.754 | 0.85 | 0.846 | 0.906 | 0.9 |
| $e_1$ | in | 30 | 30 | 33 | 33 | 33 | 29 | 29 | 30 | 30 | 29 |
| | mm | 762 | 762 | 838 | 838 | 838 | 737 | 737 | 762 | 762 | 737 |
| $e_2$ | in | 0 | 0 | -7 | -7 | 13 | 15 | 0 | 7 | 12 | 0 |
| | mm | 0 | 0 | -178 | -178 | 330 | 381 | 0 | 178 | 305 | 0 |
| **$\Delta_{PS}$*** | **in** | **-0.124** | **-0.244** | **-0.142** | **-0.128** | **-0.265** | **-0.103** | **-0.066** | **-0.085** | **-0.072** | **-0.115** |
| | **mm** | **-3.15** | **-6.20** | **-3.61** | **-3.25** | **-6.73** | **-2.62** | **-1.68** | **-2.16** | **-1.83** | **-2.92** |

The negative sign represents the deflection in the upward direction.

Table 5-3 Comparison of estimated and measured immediate hinge curl

| | | $\Delta_{Actual-0}$ | | $\Delta_{MTD-0}$ | | % Difference |
|---|---|---|---|---|---|---|
| | | in | mm | in | mm | |
| Bridge 1 | H3 | -0.426 | 10.82 | -0.110 | 2.79 | -74 |
| | H7 | -0.634 | 16.10 | -0.208 | 5.28 | -67 |
| Bridge 2 | H1 | -0.705 | 17.91 | -0.128 | 3.25 | -82 |
| | H2 | -0.671 | 17.04 | -0.116 | 2.95 | -83 |
| Bridge 3 | H | -0.614 | 15.60 | -0.228 | 5.79 | -63 |
| Bridge 4 | H | -0.204 | 5.18 | -0.093 | 2.36 | -54 |
| Bridge 5EB | H1 | -0.185 | 4.70 | -0.066 | 1.68 | -64 |
| | C1 | -0.132 | 3.35 | -0.083 | 2.11 | -37 |
| | C2 | -0.116 | 2.95 | -0.069 | 1.75 | -41 |
| Bridge 5WB | H4 | -0.233 | 5.92 | -0.106 | 2.69 | -54 |
| Average % Difference | | | | | | -62 |
| Standard deviation | | | | | | 15 |
| Average % Difference (Excluding C1 and C2) | | | | | | -68 |
| Standard deviation (Excluding C1 and C2) | | | | | | 11 |

Table 5-4 Comparison of estimated and measured hinge curl on Day 1

| | | $\Delta_{Actual-1}$ | | $\Delta_{MTD-1}$ | | % Difference |
|---|---|---|---|---|---|---|
| | | in | mm | in | mm | |
| Bridge 1 | H3 | -0.554 | 14.07 | -0.111 | 2.82 | -80 |
| | H7 | -0.824 | 20.93 | -0.211 | 5.36 | -74 |
| Bridge 2 | H1 | -0.917 | 23.29 | -0.130 | 3.30 | -86 |
| | H2 | -0.872 | 22.15 | -0.118 | 3.00 | -87 |
| Bridge 3 | H | -0.798 | 20.27 | -0.231 | 5.87 | -71 |
| Bridge 4 | H | -0.242 | 6.15 | -0.094 | 2.39 | -61 |
| Bridge 5EB | H1 | -0.299 | 7.59 | -0.067 | 1.70 | -78 |
| | C1 | -0.221 | 5.61 | -0.084 | 2.13 | -62 |
| | C2 | -0.273 | 6.93 | -0.070 | 1.78 | -74 |
| Bridge 5WB | H4 | -0.306 | 7.77 | -0.107 | 2.72 | -65 |
| Average % Difference | | | | | | -74 |
| Standard deviation | | | | | | 9 |
| Average % Difference (Excluding C1 and C2) | | | | | | -75 |
| Standard deviation (Excluding C1 and C2) | | | | | | 9 |

Table 5-5 Comparison of estimated and measured time-dependent hinge curl before load transfer

| | | | $\Delta_{Actual}$ | | $\Delta_{MTD}$ | | % Difference |
|---|---|---|---|---|---|---|---|
| | | Day | in | mm | in | mm | |
| Bridge 1 | H3 | 49 | -0.818 | -20.78 | -0.183 | -4.65 | -78 |
| | H7 | 49 | -1.200 | -30.48 | -0.345 | -8.76 | -71 |
| Bridge 2 | H1 | 36 | -1.152 | -29.26 | -0.189 | -4.80 | -84 |
| | | 97 | -0.990 | -25.15 | -0.288 | -7.32 | -71 |
| | H2 | 36 | -1.274 | -32.36 | -0.172 | -4.37 | -87 |
| | | 97 | -1.211 | -30.76 | -0.261 | -6.63 | -78 |
| Bridge 3 | H | 22 | -0.954 | -24.23 | -0.294 | -7.47 | -69 |
| Bridge 4 | H | 51 | -0.303 | -7.70 | -0.156 | -3.96 | -48 |
| | | 99 | -0.500 | -12.70 | -0.210 | -5.33 | -58 |
| | | 135 | -0.572 | -14.53 | -0.224 | -5.69 | -61 |
| Bridge 5EB | H1 | 27 | -0.343 | -8.71 | -0.090 | -2.29 | -74 |
| | C1 | 13 | -0.248 | -6.30 | -0.097 | -2.46 | -61 |
| | | 43 | -0.421 | -10.69 | -0.130 | -3.30 | -69 |
| | C2 | 13 | -0.331 | -8.41 | -0.081 | -2.06 | -76 |
| | | 43 | -0.419 | -10.64 | -0.108 | -2.74 | -74 |
| Bridge 5WB | H4 | 30 | -0.433 | -11.00 | -0.148 | -3.76 | -66 |
| | | 64 | -0.512 | -13.00 | -0.197 | -5.00 | -61 |
| | | 74 | -0.618 | -15.0 | -0.211 | -5.36 | -66 |
| Average % Difference | | | | | | | -70 |
| Standard deviation | | | | | | | 9 |
| Average % Difference (Excluding C1 and C2) | | | | | | | -69 |
| Standard deviation (Excluding C1 and C2) | | | | | | | 10 |

Table 5-6 Deflection of the short cantilevers due to load transfer

| | | B1 | | B2 | | B3 | B4 | B5EB | | | B5WB |
|---|---|---|---|---|---|---|---|---|---|---|---|
| | | H3 | H7 | H1 | H2 | H | H | H1 | C1 | C2 | H4 |
| T | kips | 1626 | 1233 | 1780 | 1719 | 860 | 780 | 355 | 460 | 435 | 430 |
| | $*10^3$ KN | 7233 | 5485 | 7918 | 7645 | 3826 | 3470 | 1579 | 2046 | 1935 | 1913 |
| **$\Delta_{reaction}$** | **in** | **0.140** | **0.249** | **0.194** | **0.162** | **0.265** | **0.082** | **0.050** | **0.034** | **0.033** | **0.083** |
| | **mm** | **3.56** | **6.32** | **4.93** | **4.11** | **6.73** | **2.08** | **1.27** | **0.86** | **0.84** | **2.11** |

Table 5-7 Calculated Adjustment "SC" for different times

| | | B1 | | B2 | | B3 | B4 | B5EB | | | B5WB |
|---|---|---|---|---|---|---|---|---|---|---|---|
| Adjustment "SC" | | H3 | H7 | H1 | H2 | H | H | H1 | C1 | C2 | H4 |
| Day 0 | in | 0.09 | 0.12 | 0.20 | 0.14 | 0.11 | -0.03 | -0.05 | -0.15 | -0.11 | -0.07 |
| | mm | 2.29 | 3.05 | 5.08 | 3.56 | 2.79 | -0.76 | -1.27 | -3.81 | -2.79 | -1.78 |
| Day 30 | in | 0.03 | 0.02 | 0.12 | 0.07 | 0.01 | -0.07 | -0.07 | -0.16 | -0.12 | -0.10 |
| | mm | 0.76 | 0.51 | 3.05 | 1.78 | 0.25 | -1.78 | -1.78 | -4.06 | -3.05 | -2.54 |
| Day 60 | in | -0.02 | -0.08 | 0.04 | 0.01 | -0.10 | -0.10 | -0.09 | -0.17 | -0.14 | -0.14 |
| | mm | -0.51 | -2.03 | 1.02 | 0.25 | -2.54 | -2.54 | -2.29 | -4.32 | -3.56 | -3.56 |
| Day 90 | in | -0.08 | -0.18 | -0.04 | -0.06 | -0.21 | -0.13 | -0.11 | -0.19 | -0.15 | -0.17 |
| | mm | -2.03 | -4.57 | -1.02 | -1.52 | -5.33 | -3.30 | -2.79 | -4.83 | -3.81 | -4.32 |
| Day 120 | in | -0.11 | -0.23 | -0.07 | -0.09 | -0.26 | -0.15 | -0.12 | -0.19 | -0.16 | -0.19 |
| | mm | -2.79 | -5.84 | -1.78 | -2.29 | -6.60 | -3.81 | -3.05 | -4.83 | -4.06 | -4.83 |
| Day 180 | in | -0.11 | -0.24 | -0.08 | -0.10 | -0.27 | -0.15 | -0.12 | -0.20 | -0.16 | -0.19 |
| | mm | -2.79 | -6.10 | -2.03 | -2.54 | -6.86 | -3.81 | -3.05 | -5.08 | -4.06 | -4.83 |
| Day 240 | in | -0.12 | -0.25 | -0.09 | -0.11 | -0.29 | -0.16 | -0.12 | -0.20 | -0.16 | -0.19 |
| | mm | -3.05 | -6.35 | -2.29 | -2.79 | -7.37 | -4.06 | -3.05 | -5.08 | -4.06 | -4.83 |
| Day 360 | in | -0.13 | -0.28 | -0.11 | -0.12 | -0.31 | -0.16 | -0.13 | -0.20 | -0.16 | -0.20 |
| | mm | -3.30 | -7.11 | -2.79 | -3.05 | -7.87 | -4.06 | -3.30 | -5.08 | -4.06 | -5.08 |
| Day 720 | in | -0.16 | -0.31 | -0.14 | -0.15 | -0.35 | -0.18 | -0.14 | -0.21 | -0.17 | -0.22 |
| | mm | -4.06 | -7.87 | -3.56 | -3.81 | -8.89 | -4.57 | -3.56 | -5.33 | -4.32 | -5.59 |
| Day 1440 | in | -0.19 | -0.38 | -0.19 | -0.19 | -0.42 | -0.20 | -0.15 | -0.22 | -0.18 | -0.24 |
| | mm | -4.83 | -9.65 | -4.83 | -4.83 | -10.7 | -5.08 | -3.81 | -5.59 | -4.57 | -6.10 |
| Diff. between Day 0 & Day 720 | in | 0.25 | 0.43 | 0.34 | 0.29 | 0.46 | 0.15 | 0.09 | 0.06 | 0.06 | 0.15 |
| | mm | 6.35 | 10.92 | 8.64 | 7.37 | 11.68 | 3.81 | 2.29 | 1.52 | 1.52 | 3.81 |

Table 5-8 Theoretical camber at hinges and deflections due to joint rotation

| | | B1 | | B2 | | B3 | B4 | B5EB | | | B5WB |
|---|---|---|---|---|---|---|---|---|---|---|---|
| | | H3 | H7 | H1 | H2 | H | H | H1 | C1 | C2 | H4 |
| SC | in | -0.37 | 0.05 | -0.51 | -0.30 | 0.24 | -0.01 | 0.08 | 0.25 | 0.51 | -0.23 |
| | mm | -9.4 | 1.3 | -13 | 7.6 | 6.1 | -0.3 | 2 | 6.4 | 13 | -5.9 |
| $\delta_{SC}$ | in | -0.46 | -0.07 | -0.71 | -0.44 | 0.12 | 0.02 | 0.13 | 0.39 | 0.62 | -0.16 |
| | mm | -11.7 | -1.8 | -18 | -11.2 | 3 | 0.5 | 3.3 | 10 | 15.8 | -4.1 |

Table 5-9 Hinge curl comparison after load transfer

| | | | $\Delta_{Actual}$ | | Top Ledge cast | LT | $\Delta_{MTD}$ | | % Diff. |
|---|---|---|---|---|---|---|---|---|---|
| | | Day | in | mm | @Day | @Day | in | mm | |
| Bridge 1 | H3 | 92 | -0.464 | -11.79 | 45 | 85 | -0.419 | -10.6 | -10 |
| | | 129 | -0.360 | -9.14 | | | -0.453 | -11.5 | 26 |
| | H7 | 92 | -0.461 | -11.71 | 45 | 70 | -0.194 | -4.9 | -58 |
| | | 129 | -0.490 | -12.45 | | | -0.189 | -4.8 | -62 |
| Bridge 2 | H1 | 148 | 0.391 | 9.93 | 105 | 165 | NA | NA | NA |
| | | 197 | -0.282 | -7.16 | | | -0.696 | -17.7 | 147 |
| | H2 | 148 | -0.484 | -12.29 | 105 | 135 | -0.472 | -12 | -3 |
| | | 197 | -0.438 | -11.13 | | | -0.476 | -12.1 | 9 |
| Bridge 3 | H | 83 | -0.460 | -11.68 | 20 | 65 | -0.065 | -1.7 | -86 |
| Bridge 4 | H | 167 | -0.381 | -9.68 | 150 | 165 | -0.127 | -3.2 | -67 |
| | | 170 | -0.394 | -10.01 | | | -0.127 | -3.2 | -68 |
| Bridge 5EB | H1 | 112 | -0.197 | -5.00 | 65 | 100 | -0.003 | -0.1 | -99 |
| | | 143 | -0.205 | -5.21 | | | -0.001 | 0 | -100 |
| | | 155 | -0.197 | -5.00 | | | -0.001 | 0 | -100 |
| | | 184 | -0.181 | -4.60 | | | -0.001 | 0 | -100 |
| | | 245 | -0.124 | -3.15 | | | 0.001 | 0 | -101 |
| | | 275 | -0.104 | -2.64 | | | 0.001 | 0 | -101 |
| | C1 | 196 | -0.007 | -0.18 | 45 | 175 | 0.151 | 3.8 | -2260 |
| | | 227 | -0.038 | -0.97 | | | 0.154 | 3.9 | -505 |
| | | 239 | -0.060 | -1.52 | | | 0.154 | 3.9 | -357 |
| | | 269 | -0.022 | -0.56 | | | 0.156 | 4 | -810 |
| | | 330 | 0.006 | 0.15 | | | 0.161 | 4.1 | 2583 |
| | | 360 | 0.026 | 0.66 | | | 0.163 | 9.5 | 527 |
| | C2 | 195 | -0.185 | -4.70 | 45 | 175 | 0.374 | 9.6 | -302 |
| | | 227 | -0.179 | -4.55 | | | 0.379 | 9.7 | -312 |
| | | 238 | -0.192 | -4.88 | | | 0.380 | 9.8 | -298 |
| | | 268 | -0.143 | -3.63 | | | 0.384 | 9.8 | -369 |
| | | 329 | -0.083 | -2.11 | | | 0.394 | 10 | -575 |
| | | 359 | -0.118 | -3.00 | | | 0.397 | 10.1 | -437 |
| Bridge 5WB | H4 | 254 | -0.426 | -10.82 | 90 | 240 | -0.313 | -8 | -27 |
| | | 315 | -0.273 | -6.93 | | | -0.317 | -8.1 | 16 |
| | | 345 | -0.275 | -6.99 | | | -0.319 | -8.1 | 16 |
| | | 406 | -0.194 | -4.93 | | | -0.322 | -8.2 | 66 |

Table 9-1 Deflection factor values for the current and proposed methods

| Time (Days) | Current (MTD) | Proposed (CEB) |
|---|---|---|
| 0 | 1.00 | 1.00 |
| 1 | 1.01 | 1.30 |
| 3 | 1.04 | 1.42 |
| 10 | 1.13 | 1.60 |
| 30 | 1.40 | 1.83 |
| 60 | 1.80 | 2.02 |
| 90 | 2.20 | 2.14 |
| 120 | 2.40 | 2.23 |
| 180 | 2.45 | 2.37 |
| 240 | 2.50 | 2.47 |
| 360 | 2.60 | 2.62 |
| 720 | 2.75 | 2.86 |
| 1440 | 3.00 | 3.06 |

Table 9-2 Comparison of immediate (Day 0) measured and proposed hinge curl

| | | $\Delta_{Actual-0}$ | | $\Delta_P$ | | % Difference |
|---|---|---|---|---|---|---|
| | | in | mm | in | mm | |
| Bridge 1 | H3 | -0.426 | -11 | -0.423 | -11 | 1 |
| | H7 | -0.634 | -16 | -0.702 | -18 | 13 |
| Bridge 2 | H1 | -0.705 | -18 | -0.521 | -13 | -25 |
| | H2 | -0.671 | -17 | -0.523 | -13 | -21 |
| Bridge 3 | H | -0.614 | -16 | -0.629 | -16 | 4 |
| Bridge 4 | H | -0.204 | -5 | -0.209 | -5 | 2 |
| Bridge 5EB | H1 | -0.185 | -5 | -0.133 | -3 | -28 |
| | C1 | -0.132 | -3 | -0.257 | -7 | 95 |
| | C2 | -0.116 | -3 | -0.249 | -6 | 114 |
| Bridge 5WB | H4 | -0.233 | -6 | -0.224 | -6 | -4 |
| Average % Difference | | | | | | 14 |
| Standard deviation | | | | | | 47 |
| Average % Difference (Excluding C1 and C2) | | | | | | -8 |
| Standard deviation (Excluding C1 and C2) | | | | | | 14 |

$\Delta_P$: Calculated hinge curl using the proposed method

Table 9-3 Comparison of Day 1 measured and proposed hinge curl

| | | $\Delta_{Actual-1}$ | | $\Delta^*_{P\ (MTD)}$ | | % Diff. | $\Delta^*_{P\ (CEB)}$ | | % Diff. |
|---|---|---|---|---|---|---|---|---|---|
| | | in | mm | in | mm | | in | mm | |
| Bridge 1 | H3 | -0.554 | -14 | -0.429 | -11 | -23 | -0.550 | -14 | -1 |
| | H7 | -0.824 | -21 | -0.711 | -18 | -14 | -0.913 | -23 | -11 |
| Bridge 2 | H1 | -0.917 | -23 | -0.527 | -13 | -42 | -0.677 | -17 | -26 |
| | H2 | -0.872 | -22 | -0.530 | -13 | -39 | -0.680 | -17 | -22 |
| Bridge 3 | H | -0.798 | -20 | -0.638 | -16 | -20 | -0.818 | -21 | 3 |
| Bridge 4 | H | -0.242 | -6 | -0.212 | -5 | -13 | -0.272 | -7 | 12 |
| Bridge 5EB | H1 | -0.299 | -8 | -0.134 | -3 | -55 | -0.172 | -4 | -42 |
| | C1 | -0.221 | -6 | -0.260 | -7 | 18 | -0.334 | -8 | 51 |
| | C2 | -0.273 | -7 | -0.252 | -6 | -8 | -0.323 | -8 | 18 |
| Bridge 5WB | H4 | -0.306 | -8 | -0.227 | -6 | -26 | -0.292 | -7 | -5 |
| Average % Difference | | | | | | -22 | | | 0 |
| Standard deviation | | | | | | 19 | | | 25 |
| Average % Difference (Excluding C1 and C2) | | | | | | -29 | | | -9 |
| Standard deviation (Excluding C1 and C2) | | | | | | 14 | | | 18 |

*: Includes time factor

$\Delta^*_{P\ (MTD)}$: Proposed hinge curl utilizing the current deflection factor chart

$\Delta^*_{P\ (CEB)}$: Proposed hinge curl utilizing the proposed deflection factor chart

Table 9-4 Comparison of time-dependent measured and proposed hinge curl before load transfer

| | | | $\Delta_{Actual\text{-}TD}$ | | $\Delta^*_{P\ (MTD)}$ | | % Diff. | $\Delta^*_{P\ (CEB)}$ | | % Diff. |
|---|---|---|---|---|---|---|---|---|---|---|
| Bridge | Hinge | Day | in | mm | in | mm | | in | mm | |
| Bridge 1 | H3 | 49 | -0.818 | -21 | -0.702 | -18 | -14 | -0.821 | -21 | 0 |
| | H7 | 49 | -1.200 | -31 | -1.165 | -30 | -3 | -1.362 | -35 | 13 |
| Bridge 2 | H1 | 36 | -1.152 | -30 | -0.771 | -20 | -33 | -0.968 | -25 | -16 |
| | | 97 | -0.990 | -25 | -1.172 | -30 | 18 | -1.114 | -28 | 13 |
| | H2 | 36 | -1.274 | -32 | -0.774 | -20 | -39 | -0.972 | -25 | -24 |
| | | 97 | -1.211 | -31 | -1.176 | -30 | -3 | -1.119 | -28 | -8 |
| Bridge 3 | H | 22 | -0.954 | -24 | -0.812 | -21 | -15 | -1.102 | -28 | 15 |
| Bridge 4 | H | 51 | -0.303 | -8 | -0.351 | -9 | 16 | -0.407 | -10 | 34 |
| | | 99 | -0.500 | -13 | -0.472 | -12 | -6 | -0.449 | -11 | -10 |
| | | 135 | -0.572 | -15 | -0.504 | -13 | -12 | -0.470 | -12 | -18 |
| Bridge 5EB | H1 | 27 | -0.343 | -9 | -0.180 | -5 | -47 | -0.237 | -6 | -31 |
| | C1 | 13 | -0.248 | -6 | -0.301 | -8 | 21 | -0.421 | -11 | 70 |
| | | 43 | -0.421 | -11 | -0.403 | -10 | -4 | -0.491 | -12 | 17 |
| | C2 | 13 | -0.331 | -8 | -0.291 | -7 | -12 | -0.408 | -10 | 23 |
| | | 43 | -0.419 | -11 | -0.390 | -10 | -7 | -0.475 | -12 | 13 |
| Bridge 5WB | H4 | 30 | -0.433 | -11 | -0.314 | -8 | -27 | -0.408 | -10 | -6 |
| | | 64 | -0.512 | -13 | -0.417 | -11 | -19 | -0.453 | -12 | -12 |
| | | 74 | -0.618 | -15 | -0.446 | -11 | -28 | -0.462 | -12 | -25 |
| Average % Difference | | | | | | | -12 | | | 3 |
| Standard deviation | | | | | | | 18 | | | 24 |
| Average % Difference (Excluding C1 and C2) | | | | | | | -15 | | | -5 |
| Standard deviation (Excluding C1 and C2) | | | | | | | 18 | | | 18 |

$\Delta_{Actual\text{-}TD}$: Measured time-dependent hinge curls before load transfer
$\Delta^*_{P\ (MTD)}$: Proposed hinge curl utilizing the current deflection factor chart
$\Delta^*_{P\ (CEB)}$: Proposed hinge curl utilizing the proposed deflection factor chart

Table 9-5 Comparison of measured and proposed hinge curl after load transfer

| | | | $\Delta_{Actual}$ | | Top Ledge cast | LT | $\Delta_{P-LT}$ | | % Diff. |
|---|---|---|---|---|---|---|---|---|---|
| | | Day | in | mm | @Day | @Day | in | mm | |
| Bridge 1 | H3 | 92 | -0.464 | -12 | 45 | 85 | -0.600 | 15 | 29 |
| | | 129 | -0.360 | -9 | | | -0.613 | 16 | 70 |
| | H7 | 92 | -0.461 | -12 | 45 | 70 | -0.725 | 18 | 57 |
| | | 129 | -0.490 | -13 | | | -0.723 | 18 | 47 |
| Bridge 2 | H1 | 148 | 0.391 | 10 | 105 | 165 | -0.861 | 22 | 320 |
| | | 197 | -0.282 | -7 | | | -0.878 | 22 | 211 |
| | H2 | 148 | -0.484 | -12 | 105 | 135 | -0.975 | 25 | 101 |
| | | 197 | -0.438 | -11 | | | -0.985 | 25 | 125 |
| Bridge 3 | H | 83 | -0.460 | -12 | 20 | 65 | -0.570 | 14 | 24 |
| Bridge 4 | H | 167 | -0.381 | -10 | 150 | 165 | -0.278 | 7 | -27 |
| | | 170 | -0.394 | -10 | | | -0.278 | 7 | -29 |
| Bridge 5EB | H1 | 112 | -0.197 | -5 | 65 | 100 | -0.129 | 3 | -35 |
| | | 143 | -0.205 | -5 | | | -0.127 | 3 | -38 |
| | | 155 | -0.197 | -5 | | | -0.126 | 3 | -36 |
| | | 184 | -0.181 | -5 | | | -0.125 | 3 | -31 |
| | | 245 | -0.124 | -3 | | | -0.122 | 3 | -2 |
| | | 275 | -0.104 | -3 | | | -0.121 | 3 | 16 |
| | C1 | 196 | -0.007 | 0 | 45 | 175 | -0.265 | 7 | >>100 |
| | | 227 | -0.038 | -1 | | | -0.261 | 7 | >>100 |
| | | 239 | -0.060 | -2 | | | -0.259 | 7 | >>100 |
| | | 269 | -0.022 | -1 | | | -0.256 | 7 | >>100 |
| | | 330 | 0.006 | 0 | | | -0.249 | 6 | >>100 |
| | | 360 | 0.026 | 1 | | | -0.247 | 6 | >>100 |
| | C2 | 195 | -0.185 | -5 | 45 | 175 | -0.161 | 4 | -13 |
| | | 227 | -0.179 | -5 | | | -0.152 | 4 | -15 |
| | | 238 | -0.192 | -5 | | | -0.149 | 4 | -22 |
| | | 268 | -0.143 | -4 | | | -0.142 | 4 | -1 |
| | | 329 | -0.083 | -2 | | | -0.128 | 3 | 55 |
| | | 359 | -0.118 | -3 | | | -0.123 | 3 | 5 |
| Bridge 5WB | H4 | 254 | -0.426 | -11 | 90 | 240 | -0.406 | 10 | -5 |
| | | 315 | -0.273 | -7 | | | -0.412 | 10 | 51 |
| | | 345 | -0.275 | -7 | | | -0.414 | 11 | 51 |
| | | 406 | -0.194 | -5 | | | -0.419 | 11 | 116 |

$\Delta_{P-LT}$: Calculated hinge curls after load transfer according to the proposed method

Table 9-6 Falsework forces (SAP2000)

| | | $F_{1/8}$ | | $F_{1/4}$ | | $F_{1/2}$ | | $F_{3/4}$ | |
|---|---|---|---|---|---|---|---|---|---|
| | | kip | kN | kip | kN | kip | kN | kip | kN |
| Bridge 1 | H3 | 413 | 1837 | 417 | 1855 | 242 | 1076 | 87 | 387 |
| | H7 | 392 | 1744 | 368 | 1637 | 161 | 716 | 45 | 200 |
| Bridge 2 | H1 | 518 | 2304 | 546 | 2429 | 392 | 1744 | 246 | 1094 |
| | H2 | 495 | 2202 | 506 | 2251 | 338 | 1503 | 261 | 1161 |
| Bridge 3 | H | 258 | 1148 | 300 | 1334 | 240 | 1068 | 125 | 556 |
| Bridge 4 | H | 219 | 974 | 200 | 890 | 93 | 414 | 56 | 249 |
| Bridge 5EB | H1 | 60 | 267 | 18 | 80 | 0 | 0 | 0 | 0 |
| | C1 | 189 | 841 | 90 | 400 | 0 | 0 | 0 | 0 |
| | C2 | 86 | 383 | 75 | 334 | 0 | 0 | 0 | 0 |
| Bridge 5WB | H4 | 189 | 841 | 120 | 534 | 0 | 0 | 0 | 0 |

Table 9-7 Falsewrok forces (ABAQUS)

| | | $F_{1/8}$ | | $F_{1/4}$ | | $F_{1/2}$ | | $F_{3/4}$ | |
|---|---|---|---|---|---|---|---|---|---|
| | | kip | kN | kip | kN | kip | kN | kip | kN |
| Bridge 1 | H3 | 442 | 1966 | 382 | 1699 | 157 | 698 | 0 | 0 |
| | H7 | 335 | 1490 | 263 | 1170 | 119 | 529 | 88 | 391 |
| Bridge 2 | H1 | 426 | 1895 | 395 | 1757 | 294 | 1308 | 385 | 1713 |
| | H2 | 510 | 2269 | 491 | 2184 | 224 | 996 | 0 | 0 |
| Bridge 3 | H | 245 | 1090 | 276 | 1228 | 204 | 907 | 95 | 423 |
| Bridge 4 | H | 221 | 983 | 192 | 854 | 75 | 334 | 42 | 187 |
| Bridge 5EB | H1 | 108 | 480 | 59 | 262 | 0 | 0 | 0 | 0 |
| | C1 | 183 | 814 | 34 | 151 | 0 | 0 | 0 | 0 |
| | C2 | 90 | 400 | 72 | 320 | 0 | 0 | 0 | 0 |
| Bridge 5WB | H4 | 181 | 805 | 72 | 320 | 0 | 0 | 0 | 0 |

Table 9-8 Comparsion of the net upward load acting on adjacent span ($W_u$)

| | | $L_{Adjacent}$ | | $W_{u\ (Empirical)}$ | | $W_{u\ (SAP)}$ | | $W_{u\ (ABAQUS)}$ | |
|---|---|---|---|---|---|---|---|---|---|
| | | ft | m | Kip/ft | kN/m | Kip/ft | kN/m | Kip/ft | kN/m |
| Bridge 1 | H3 | 195 | 60 | 4.27 | 62 | 5.94 | 87 | 5.03 | 73 |
| | H7 | 195 | 60 | 4.65 | 68 | 4.95 | 72 | 4.13 | 60 |
| Bridge 2 | H1 | 222 | 68 | 5.87 | 86 | 7.66 | 112 | 6.76 | 99 |
| | H2 | 210 | 64 | 6.08 | 89 | 7.61 | 111 | 5.83 | 85 |
| Bridge 3 | H | 151 | 46 | 4.80 | 70 | 6.11 | 89 | 5.43 | 79 |
| Bridge 4 | H | 171 | 52 | 4.20 | 61 | 3.32 | 48 | 3.10 | 45 |
| Bridge 5EB | H1 | 121 | 37 | 3.55 | 52 | 0.64 | 9 | 1.39 | 20 |
| | C1 | 154 | 47 | 11.05 | 161 | 1.81 | 26 | 1.41 | 21 |
| | C2 | 88 | 27 | 6.75 | 99 | 1.91 | 28 | 1.85 | 27 |
| Bridge 5WB | H4 | 154 | 47 | 4.78 | 70 | 2.06 | 30 | 1.64 | 24 |
| Average | | | | 5.60 | 82 | 4.20 | 61 | 3.66 | 53 |
| Standard deviation | | | | 2 | 30 | 2.4 | 36 | 1.9 | 28 |
| Average (Excluding C1 and C2) | | | | 4.99 | 73 | 4.46 | 65 | 3.86 | 56 |
| Standard deviation (Excluding C1 and C2) | | | | 1 | 12 | 2.4 | 35 | 1.9 | 27 |

Figure 1-1 Bridge falsework, Del Paso Park Overhead, Sacramento

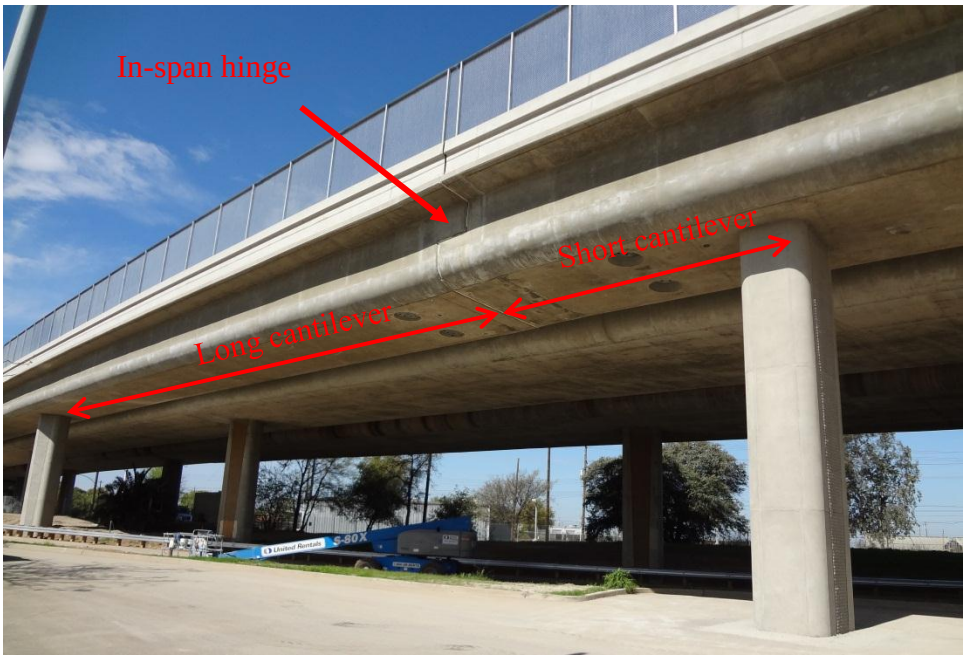


Figure 1-2 Hinge span in a continuous CIP/PS box girder bridge


(a) (b)

Figure 1-3 In-span hinges of CIP/PS box girder bridges: (a) N170-N5 Connector, Los Angeles; (b) Del Paso Park Overhead (East Bound), Sacramento

Figure 1-4 Construction of in-span hinges in CIP/PS box girder bridge

Figure 1-5 Hinge curl during construction


(a) (b)

(c) (d)

Figure 1-6 Hinge curl repair process in N170-N5 Connector, Los Angeles: (a) Discussion between Caltrans engineer and concrete grinder operator; (b) Caltrans engineer while monitoring the grinding operation; (c) Measuring grinding thickness; (d) Deck surface at the hinge after concrete grinding

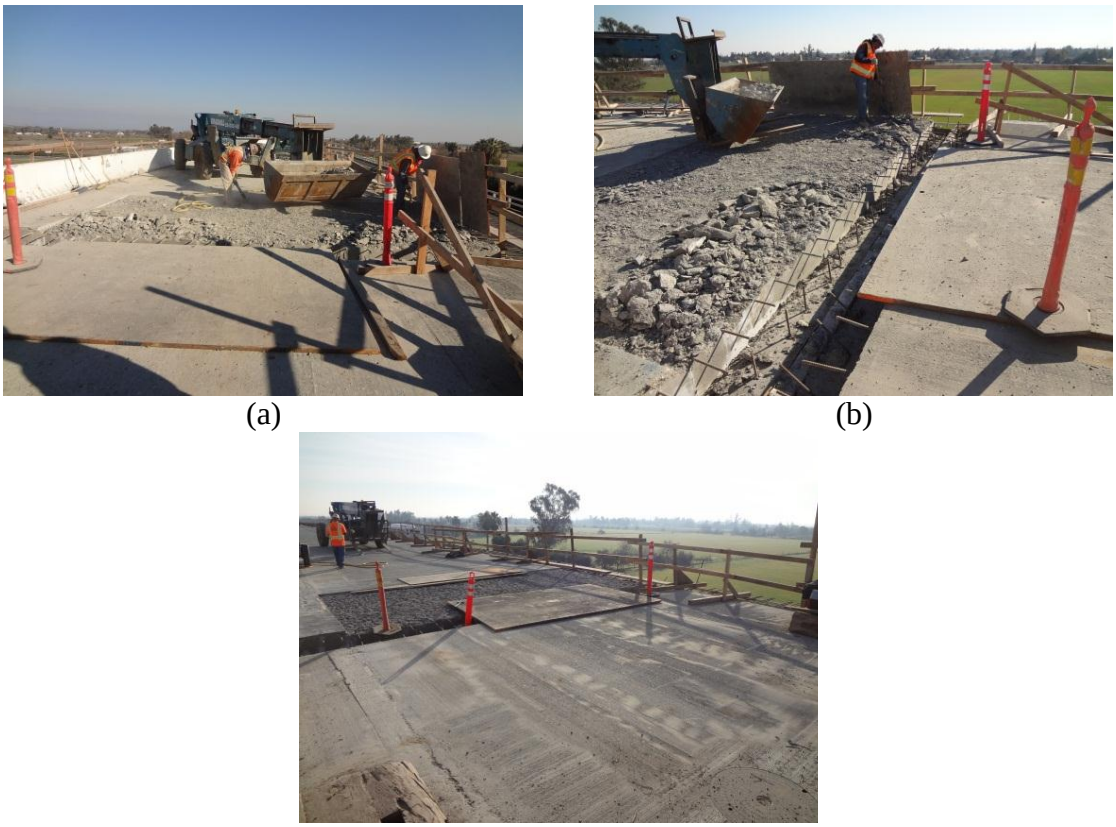

(a) (b)

(c)

Figure 1-7 Hinge curl repair process in Bradley Overhead, Merced: (a) Chipping concrete cover of top deck reinforcement for long cantilever; (b) Rubble cleanup; (c) Deck surface at the hinge after roughening concrete of the long cantilever and grinding concrete of the short cantilever

Figure 1-8 Hinge curl repair by loading the short cantilever of an in-span hinge in Del Paso Park Overhead, Sacramento


Figure 1-9 Adjustable falsework posts, Del Paso Park Overhead, Sacramento


Figure 1-10 Thick concrete cover for top deck reinforcement, Del Paso Park Overhead, Sacramento

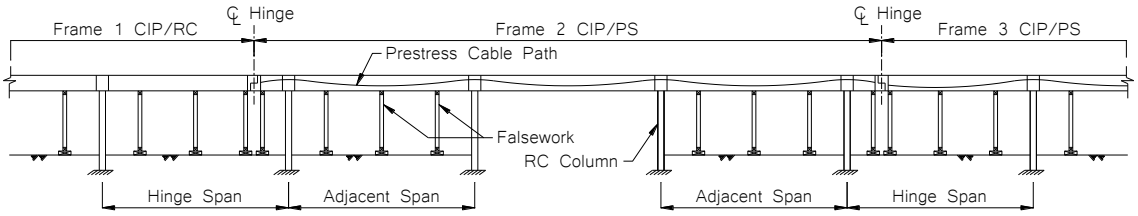


Figure 2-1 Typical longitudinal view of a Bridge with two in-span hinges

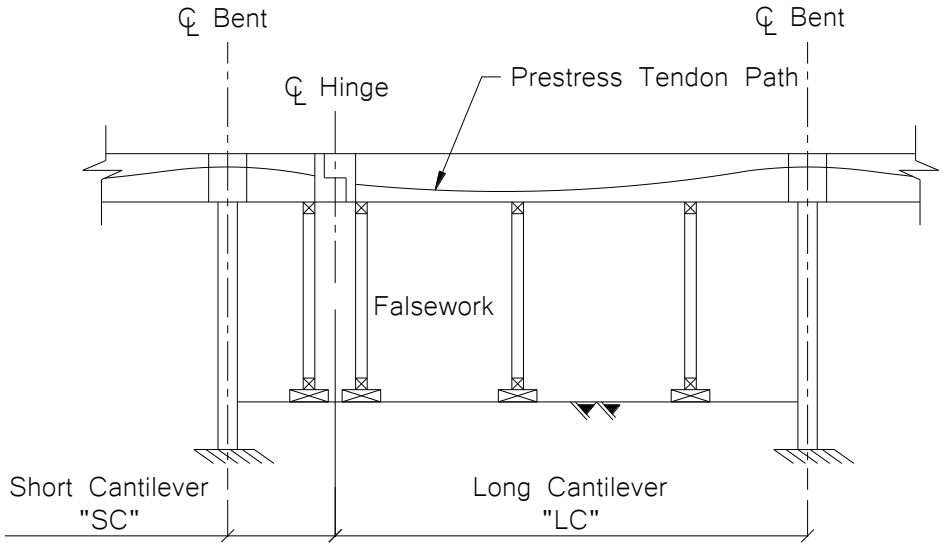


Figure 2-2 Typical hinge span of an in-span hinge

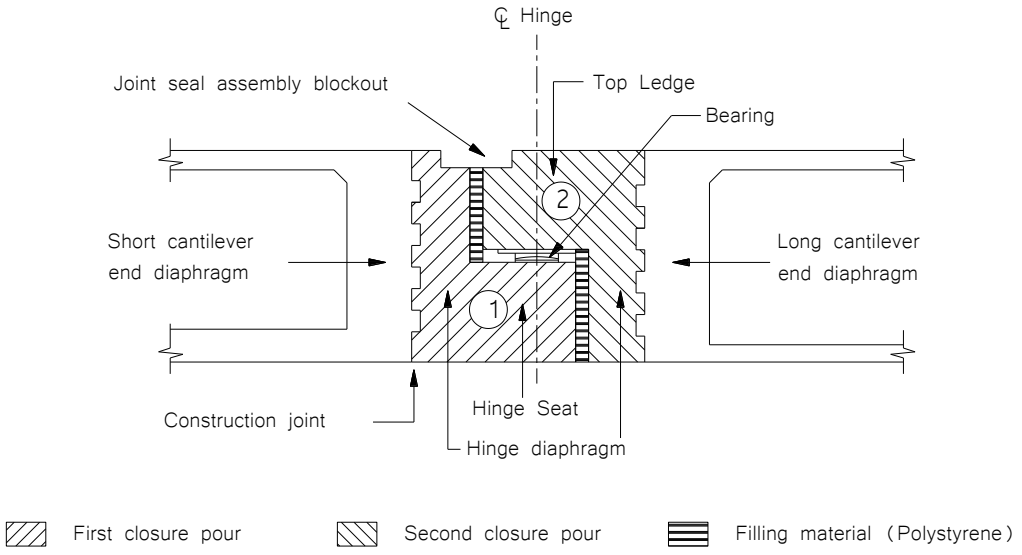


Figure 2-3 Typical in-span hinge of CIP/PS bridge

Figure 2-4 Temporary fill of joint seal assembly blockout void

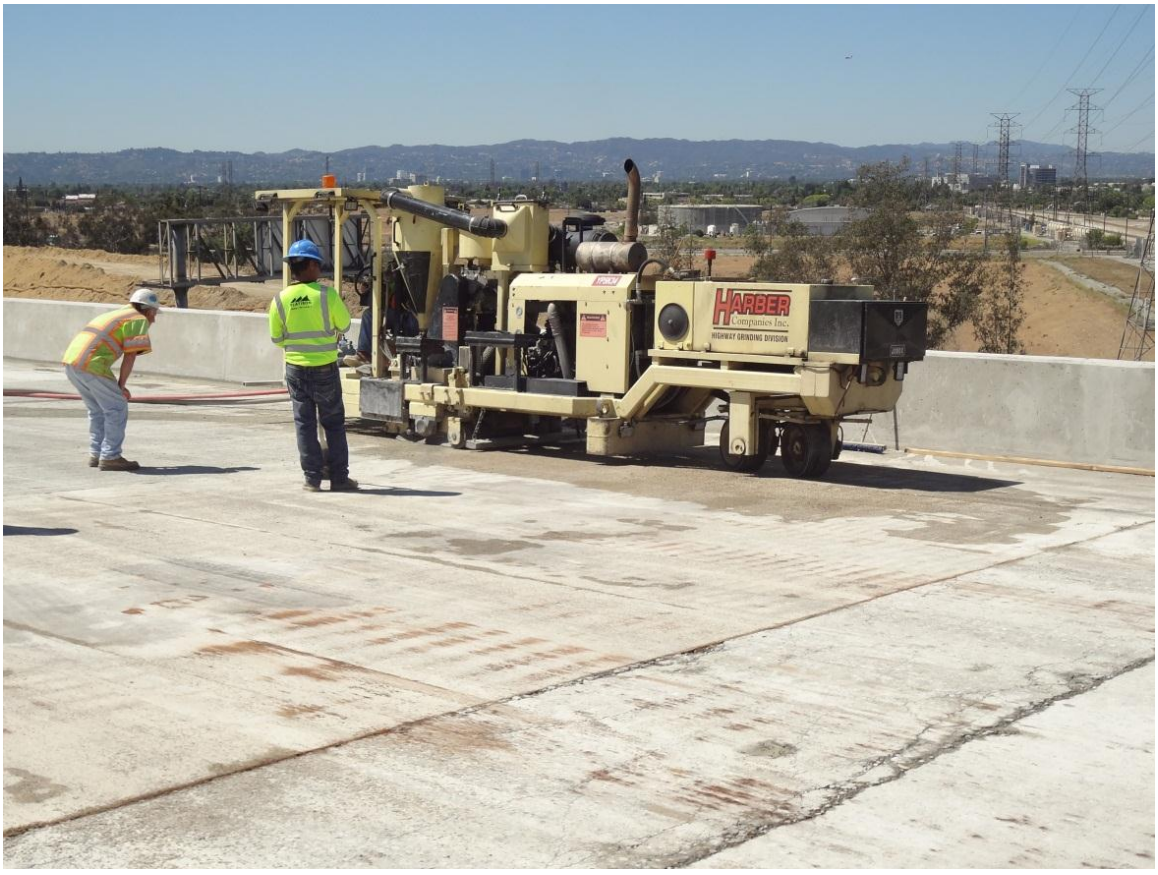


Figure 2-5 Deck grinding at the hinge area using a grinding machine

(a) (b)

Figure 2-6 Deck joint seals after installation: (a) Joint seal assembly; and (b) Bonded joint seal

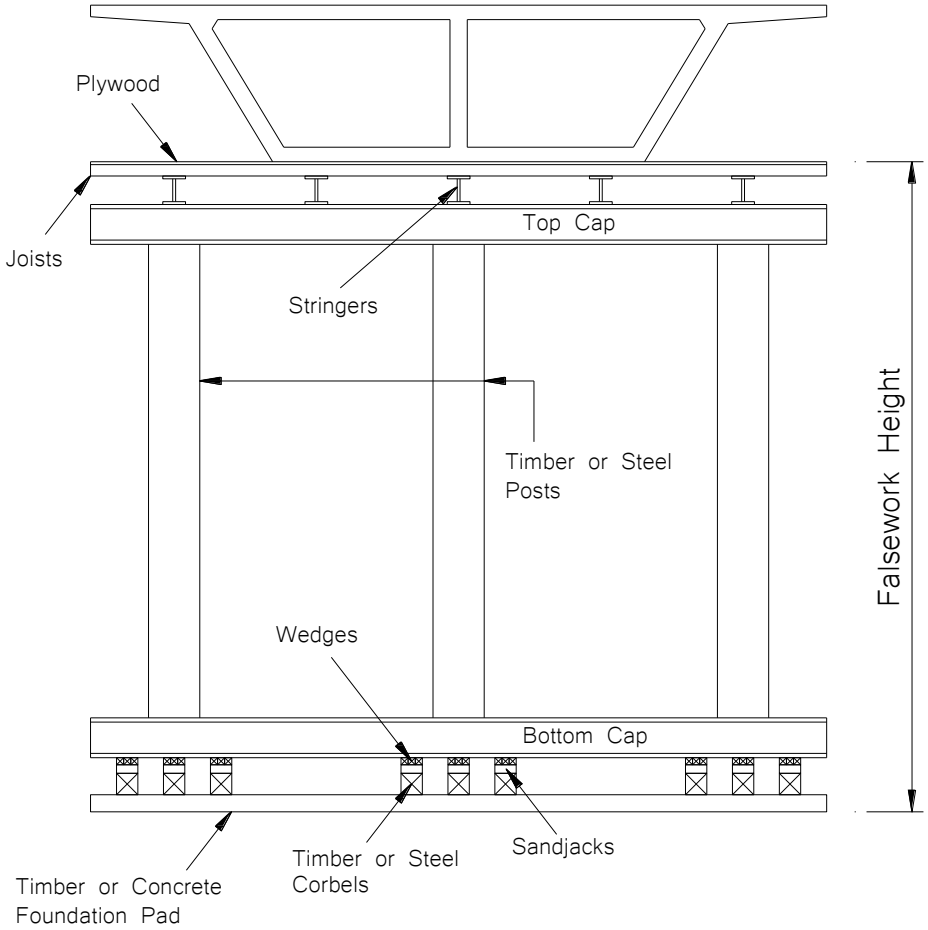


Figure 2-7 Typical falsework bent

(a)

(b)

Figure 2-8 Falsework posts: (a) Steel posts; and (b) Timber posts

(a)

(b)

Figure 2-9 Falsework spanning over: (a) roadway at N170-N5 Connector; and (b) railway at Bradley Overhead

(a)


(b)

Figure 2-10 (a) Skew falsework bents at Del Paso Park OH; (b) Outrigger falsework bent at Wilshire Blvd


(a) (b)

Figure 2-11 Partial falsework removal at: (a) N170-N5 Connector; and (b) Del Paso Park OH


(a) (b)

Figure 2-12 Falsework removal in: (a) hinge span; and (b) adjacent span

(a) (b)

Figure 2-13 Prestressing process at: (a) Hinge; (b) Abutment

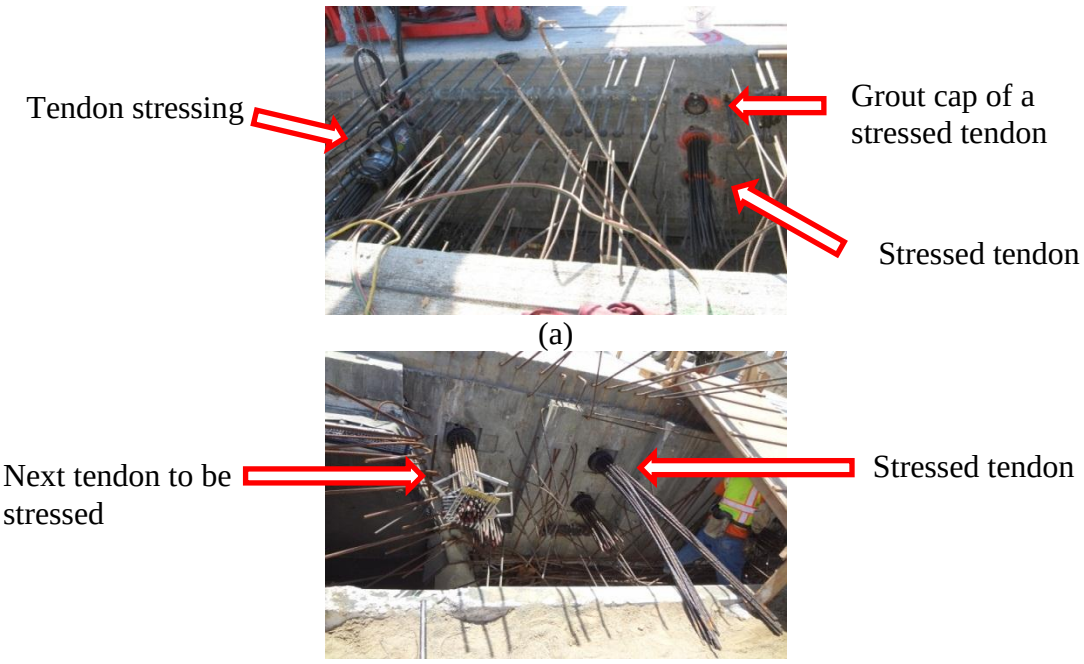


Figure 2-14 Stressing sequence at: (a) Hinge 7, Bridge 1; (b) Abutment 9, Bridge 4


Figure 2-15 Prestressing operational issues: (a) Stressing hoist transfer; (b) Stressing jack transfer; (c) Hinge reinforcement congestion; (d) Hoist stumble

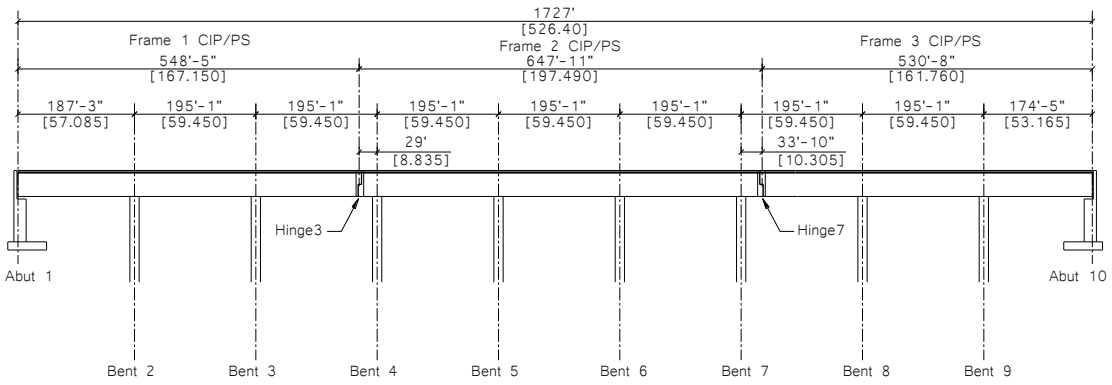


Figure 2-16 Bridge 1 elevation

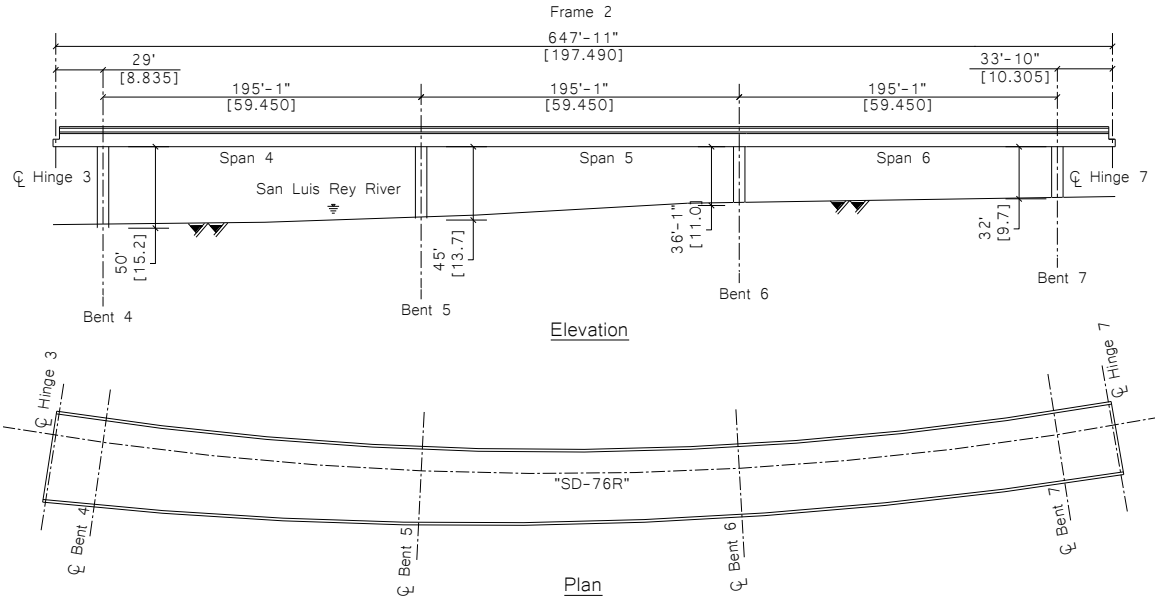


Figure 2-17 Elevation and plan of Frame 2, Bridge 1

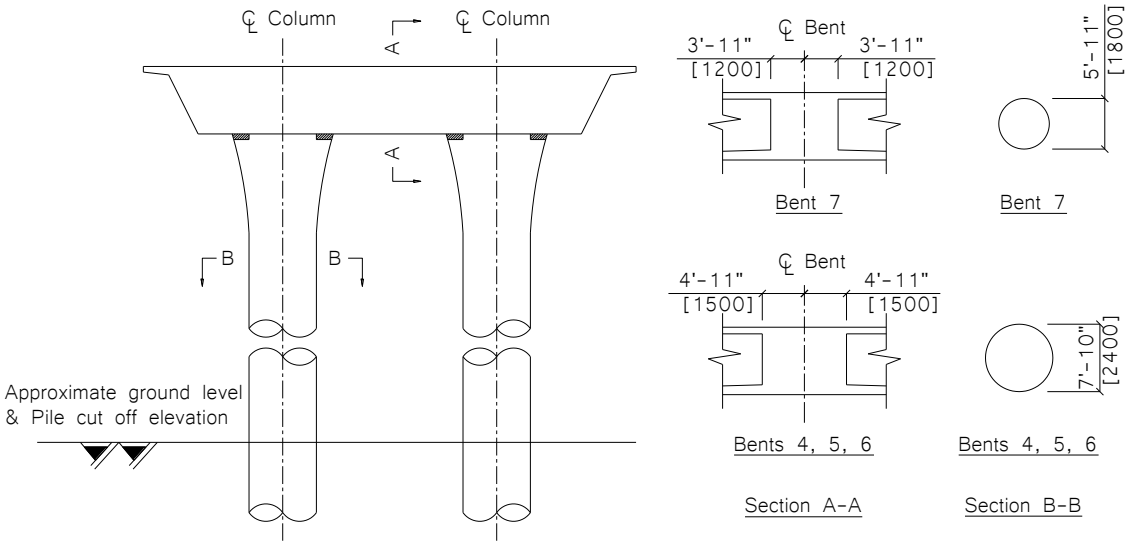


Figure 2-18 Typical bent layout in Frame 2, Bridge 1

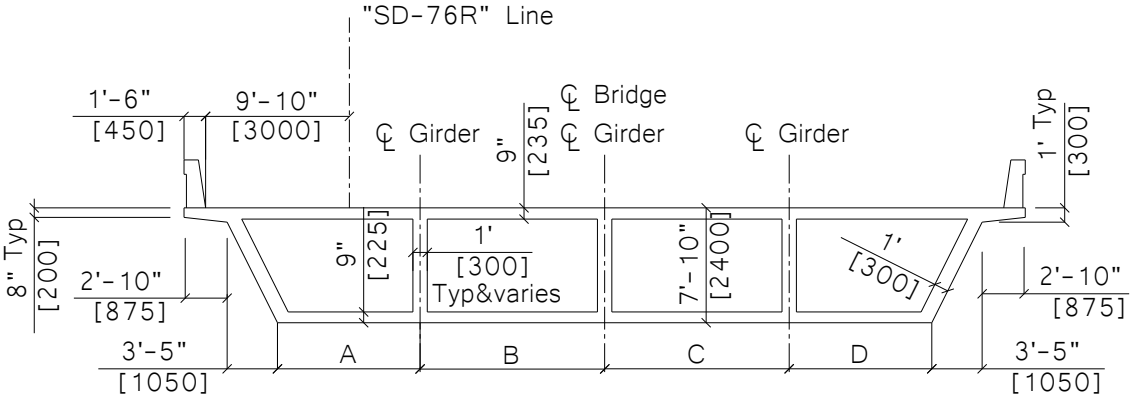


| Location | A | | B | | C | | D | |
|---|---|---|---|---|---|---|---|---|
| ℄ Hinge 3 | 9'-10" | 3000 | 12'-10" | 3900 | 12'-10" | 3900 | 9'-10" | 3000 |
| ℄ Bent 4 | 9'-10" | 2990 | 12'-8" | 3860 | 12'-8" | 3860 | 9'-7" | 2930 |
| ℄ Bent 5 | 9'-1" | 2760 | 11'-9" | 3585 | 11'-9" | 3585 | 8'-7" | 2610 |
| ℄ Bent 6 | 8'-2" | 2495 | 10'-11" | 3315 | 10'-11" | 3315 | 7'-8" | 2340 |
| ℄ Bent 7 | 7'-2" | 2180 | 9'-11" | 3030 | 9'-12" | 3045 | 6'-11" | 2115 |
| ℄ Hinge 7 | 6'-11" | 2100 | 9'-10" | 3000 | 9'-10" | 3000 | 6'-11" | 2100 |

Figure 2-19 Cross-sectional details of Frame 2, Bridge 1

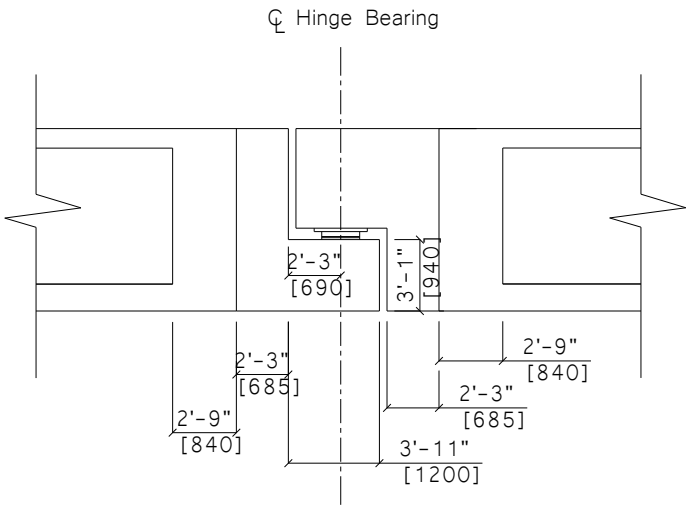


Figure 2-20 Hinge details, Bridge 1

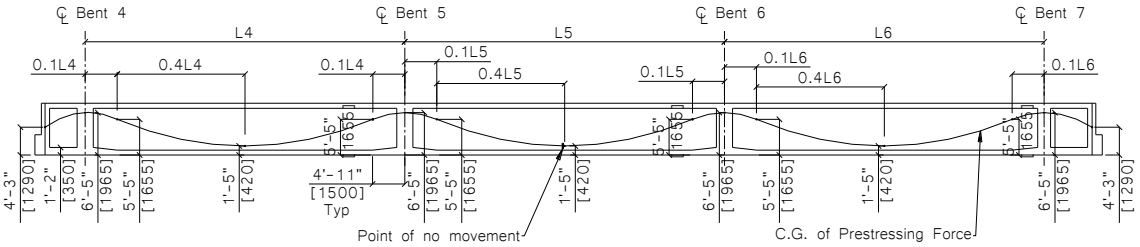


Figure 2-21 Prestressing tendons profile in Frame 2, Bridge 1

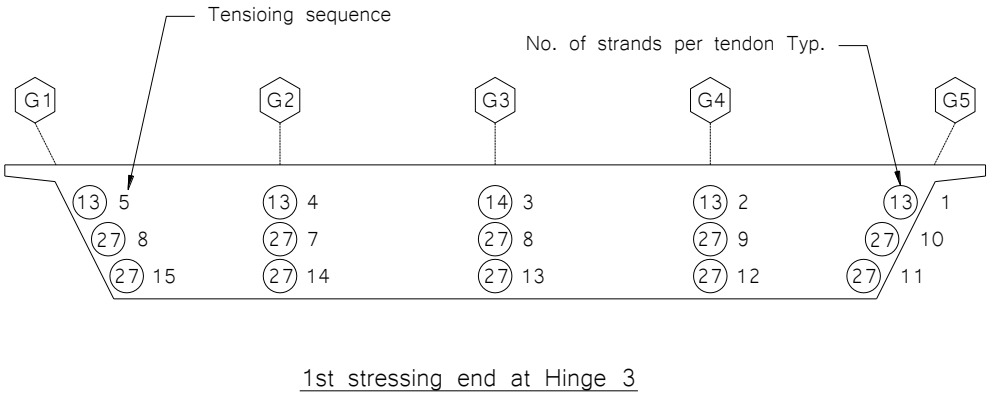


Figure 2-22 Stressing sequence of Frame 2, Bridge 1

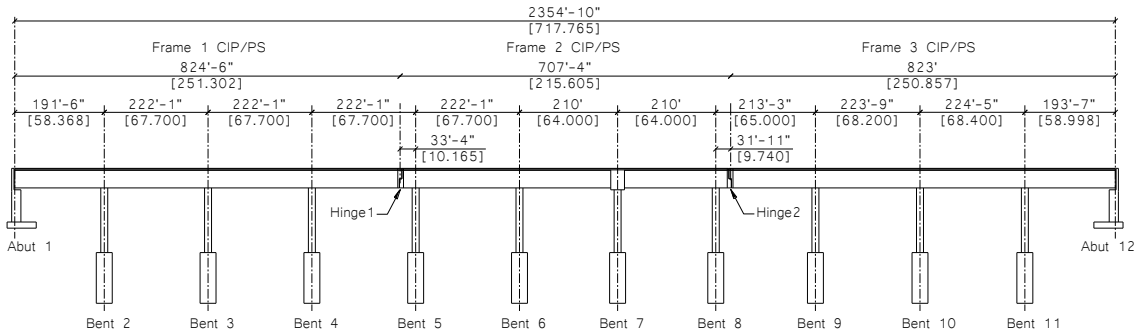


Figure 2-23 Bridge 2 elevation

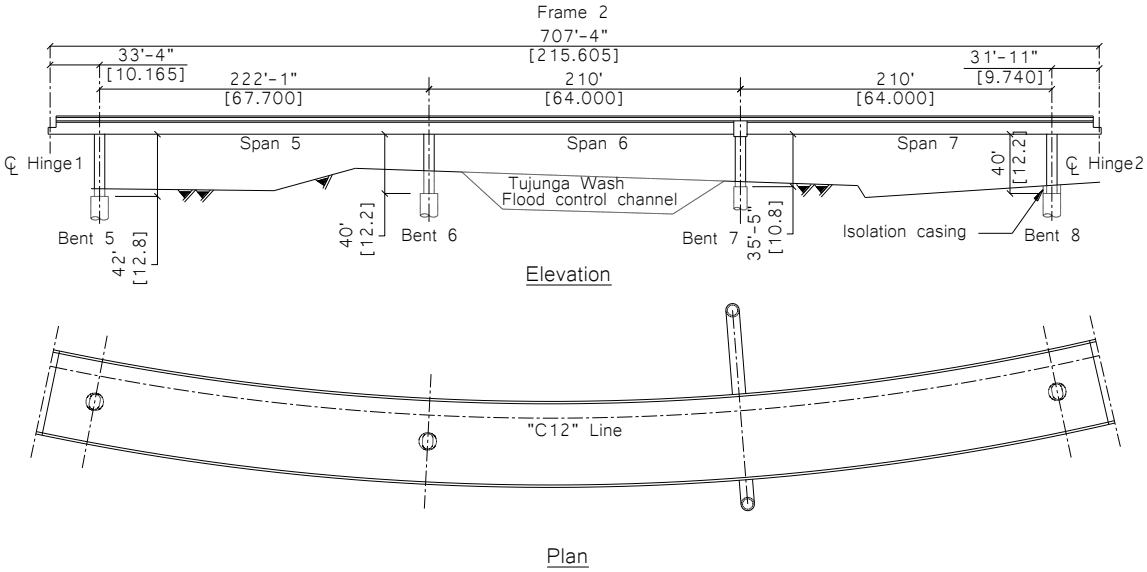


Figure 2-24 Elevation and plan of Frame 2, Bridge 2

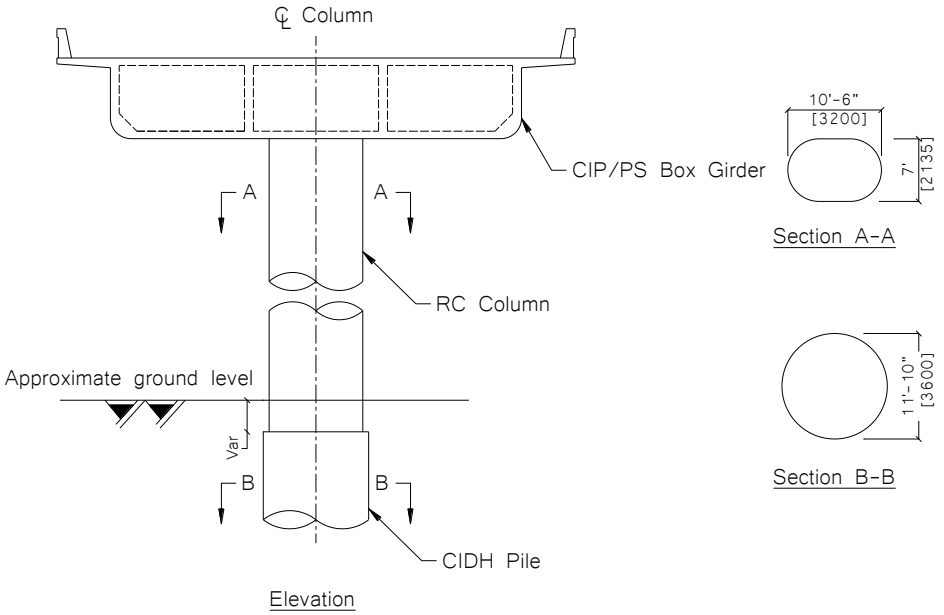


Figure 2-25 Single column bent in Bridge 2

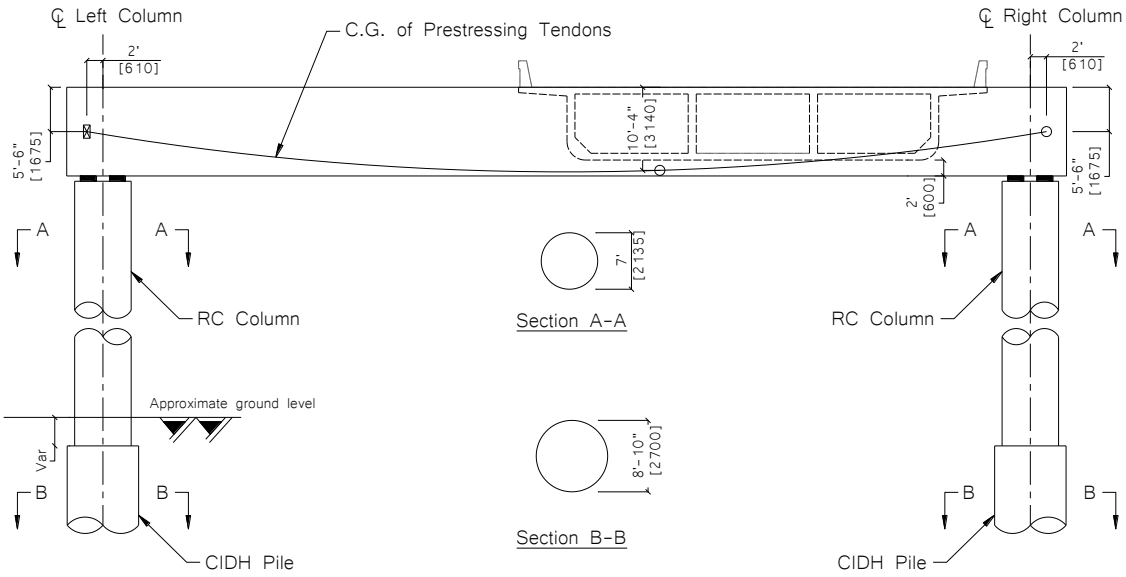


Figure 2-26 Outrigger bent details, Frame 2, Bridge 2

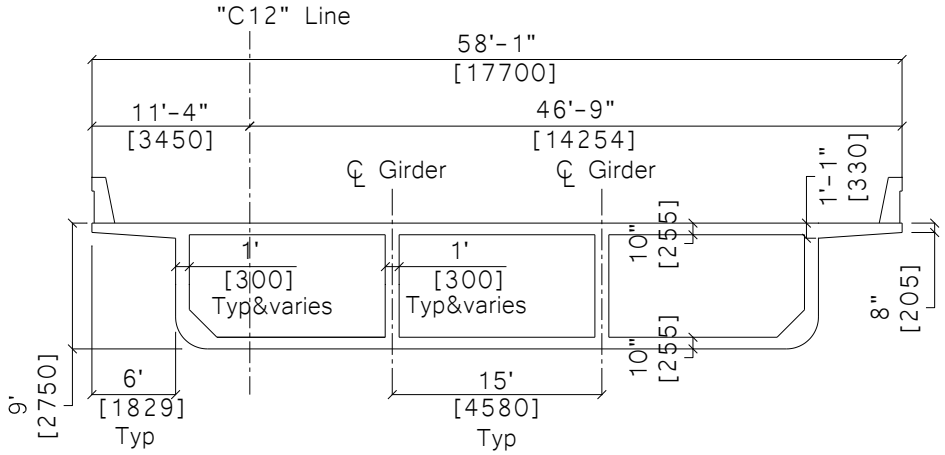


Figure 2-27 Typical superstructure cross section of Frame 2, Bridge 2

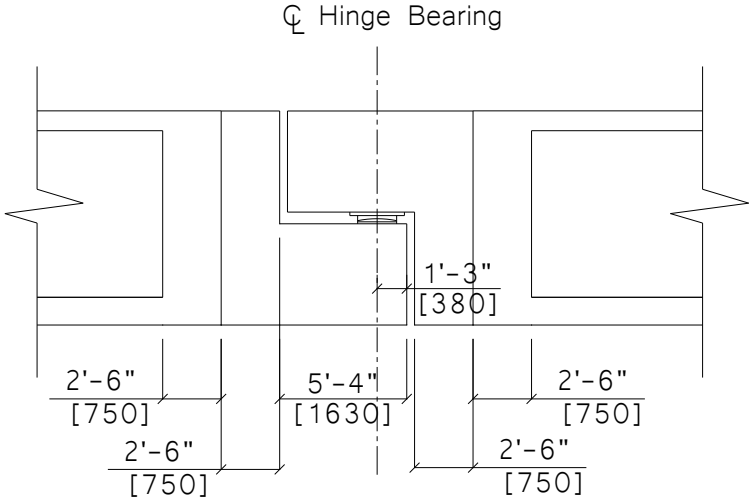


Figure 2-28 Hinge details, Bridge 2

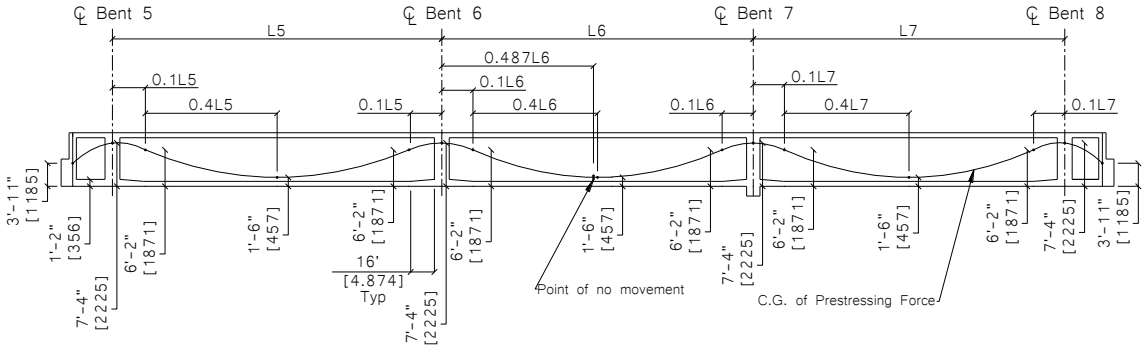


Figure 2-29 Prestressing tendons profile in Frame 2, Bridge 2

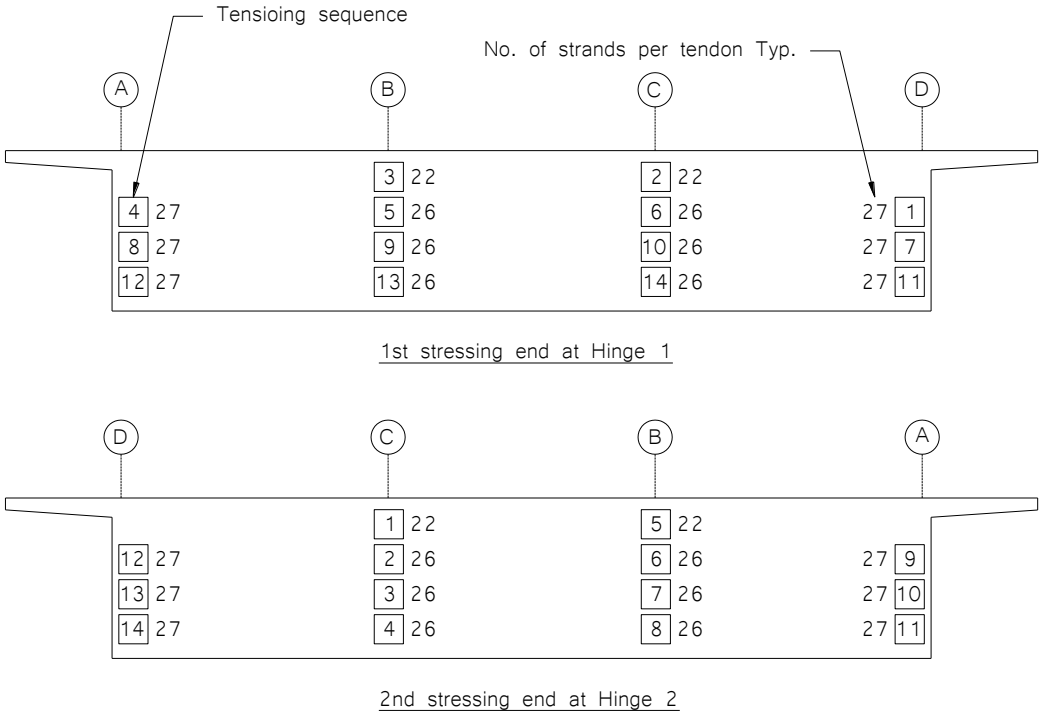


Figure 2-30 Stressing sequence of Frame 2, Bridge 2

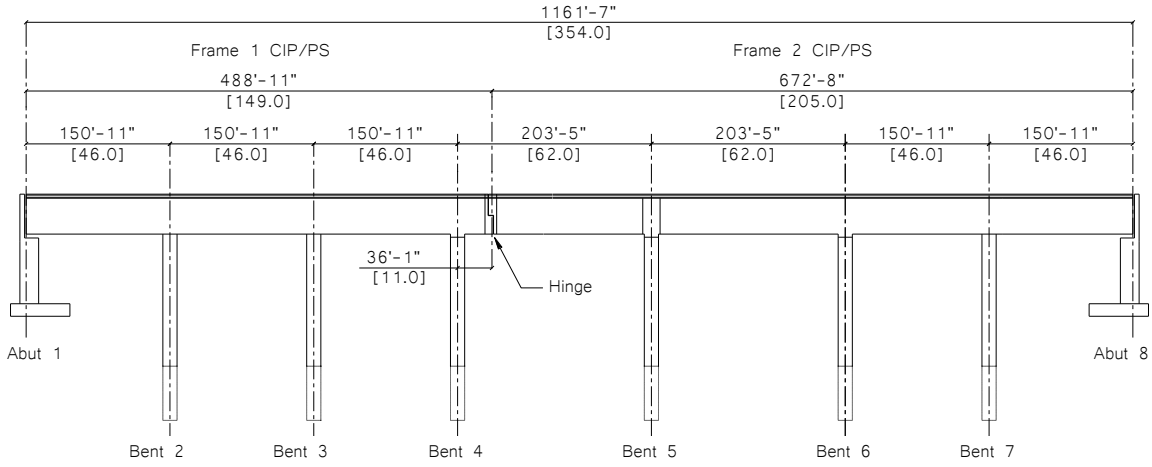


Figure 2-31 Bridge 3 elevation

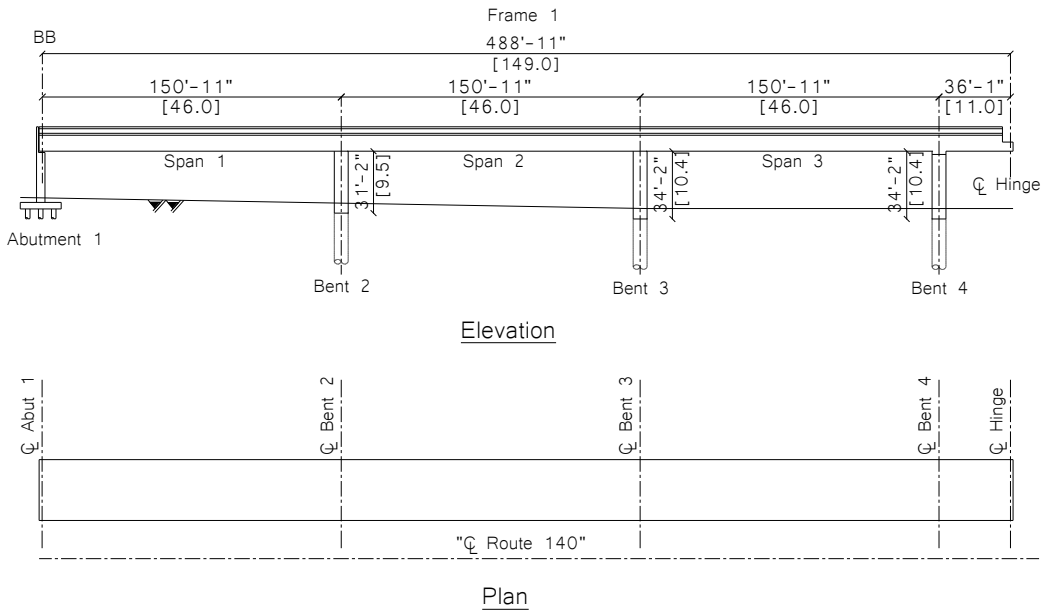


Figure 2-32 Elevation view of Frame 1, Bridge 3

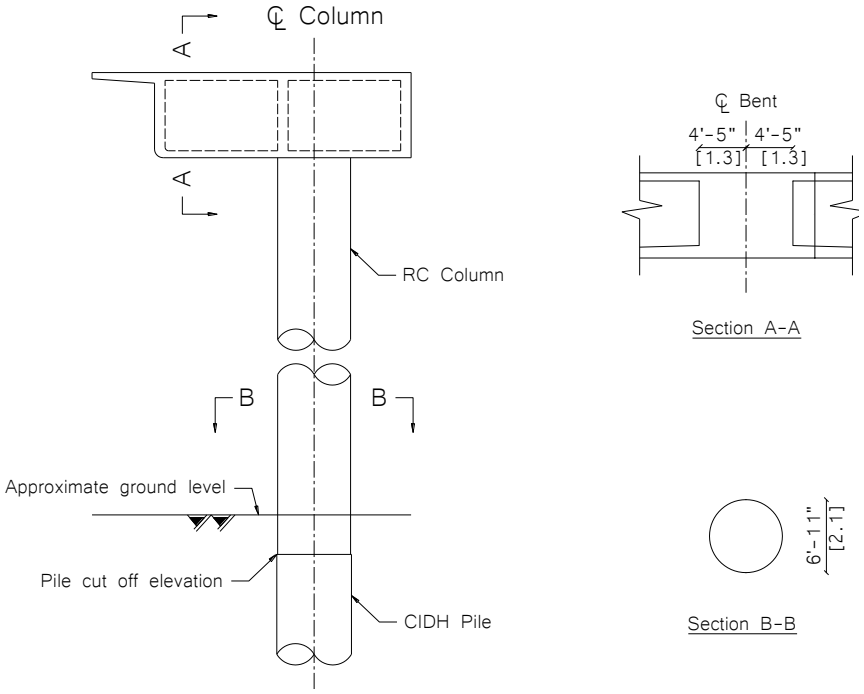


Figure 2-33 Bent 2 details, Bridge 3

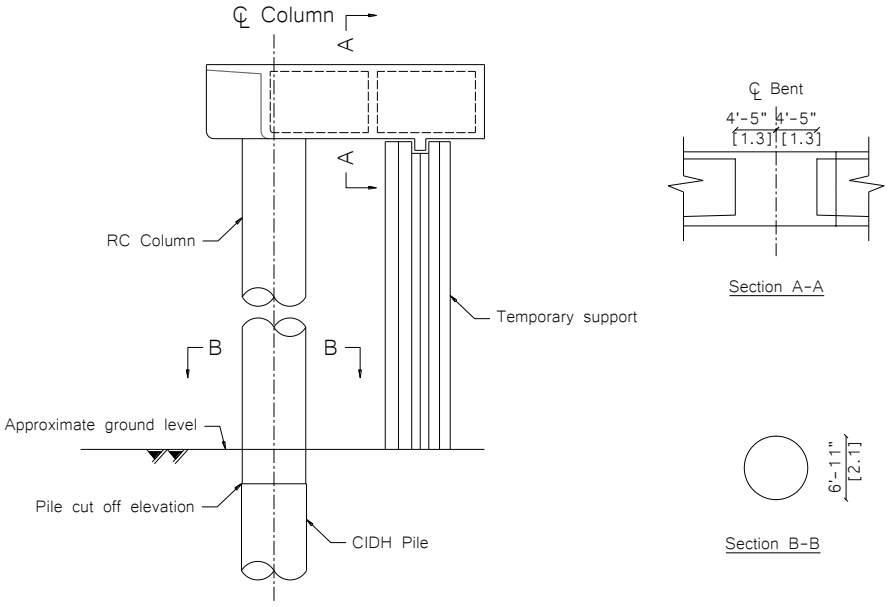


Figure 2-34 Bent 3 details, Bridge 3

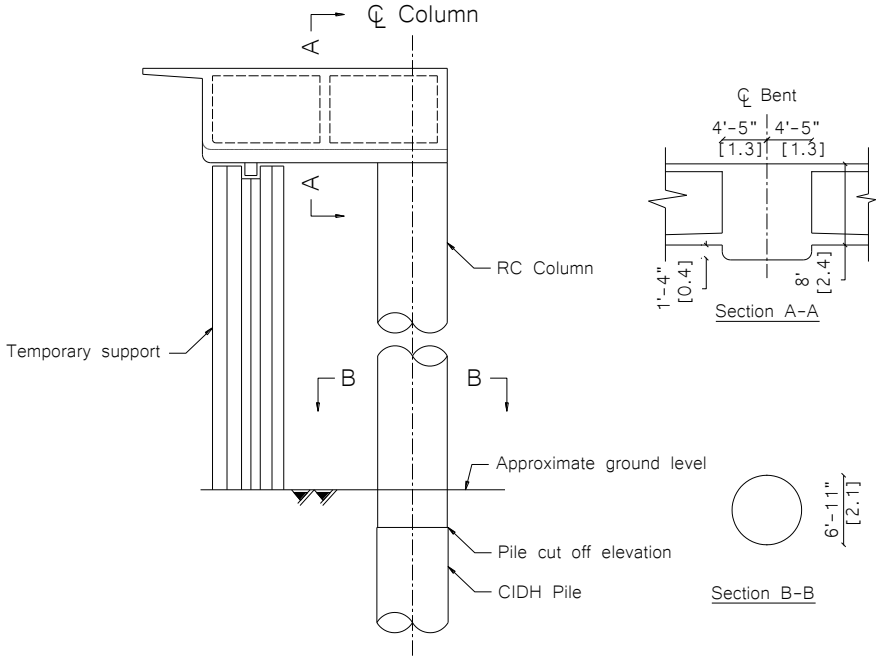


Figure 2-35 Bent 4 details, Bridge 3

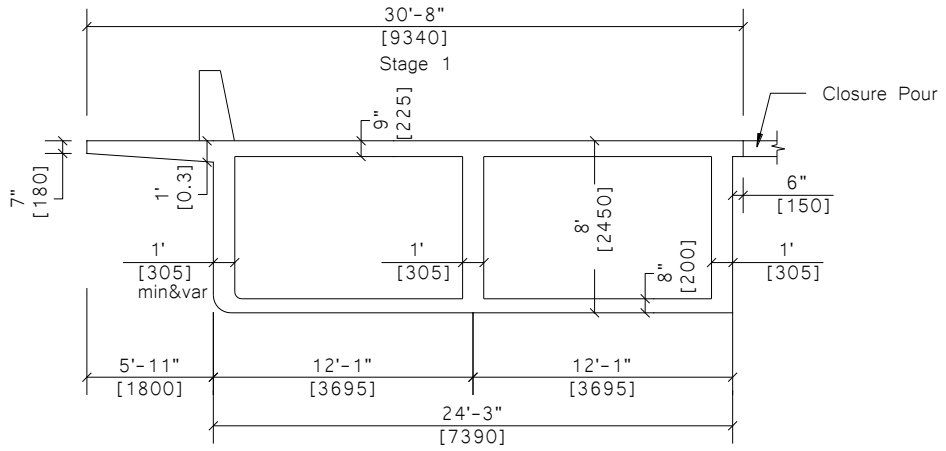


Figure 2-36 Cross-sectional details of Frame 1, Bridge 3

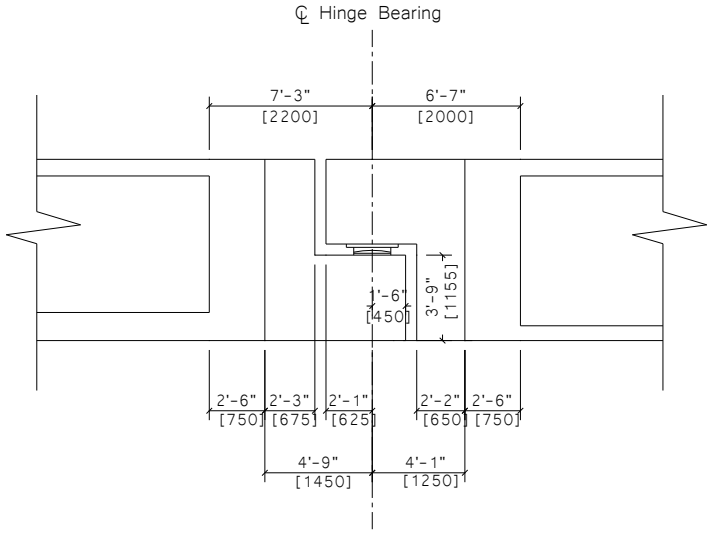


Figure 2-37 Hinge details, Bridge 3

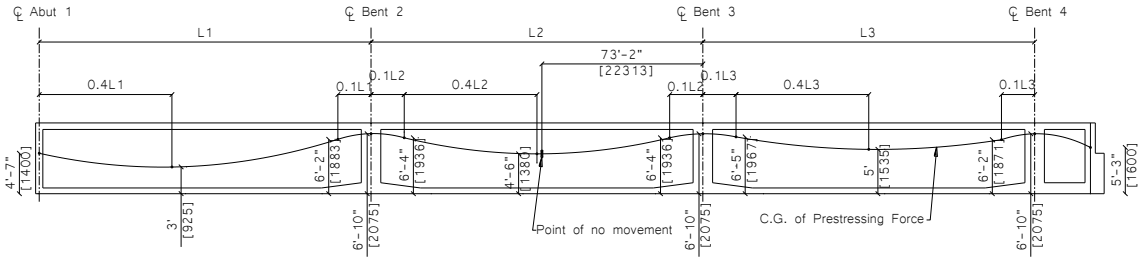


Figure 2-38 Prestressing tendons profile in Frame 1, Bridge 3

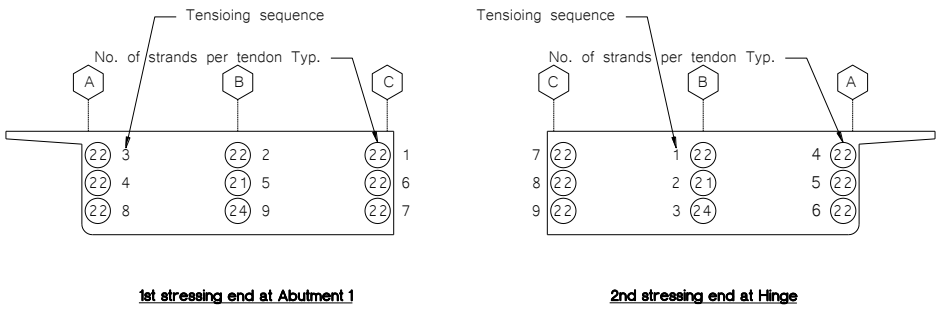


Figure 2-39 Stressing sequence of Frame 1, Bridge 3

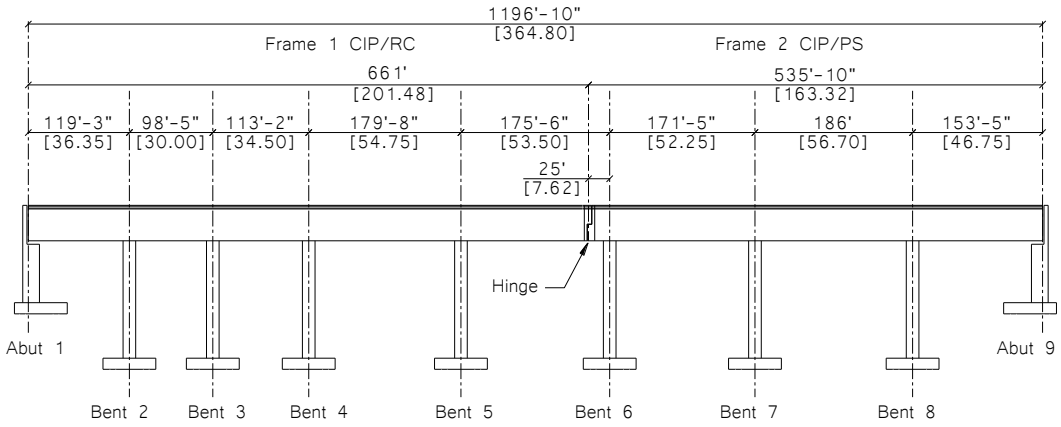


Figure 2-40 Elevation view of Bridge 4

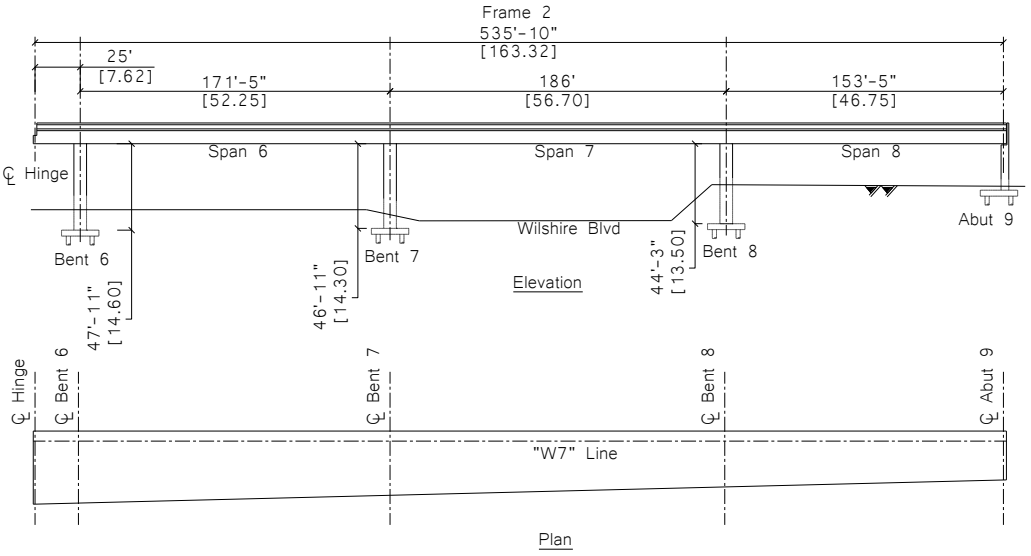


Figure 2-41 Elevation and plan views of Frame 2, Bridge 4

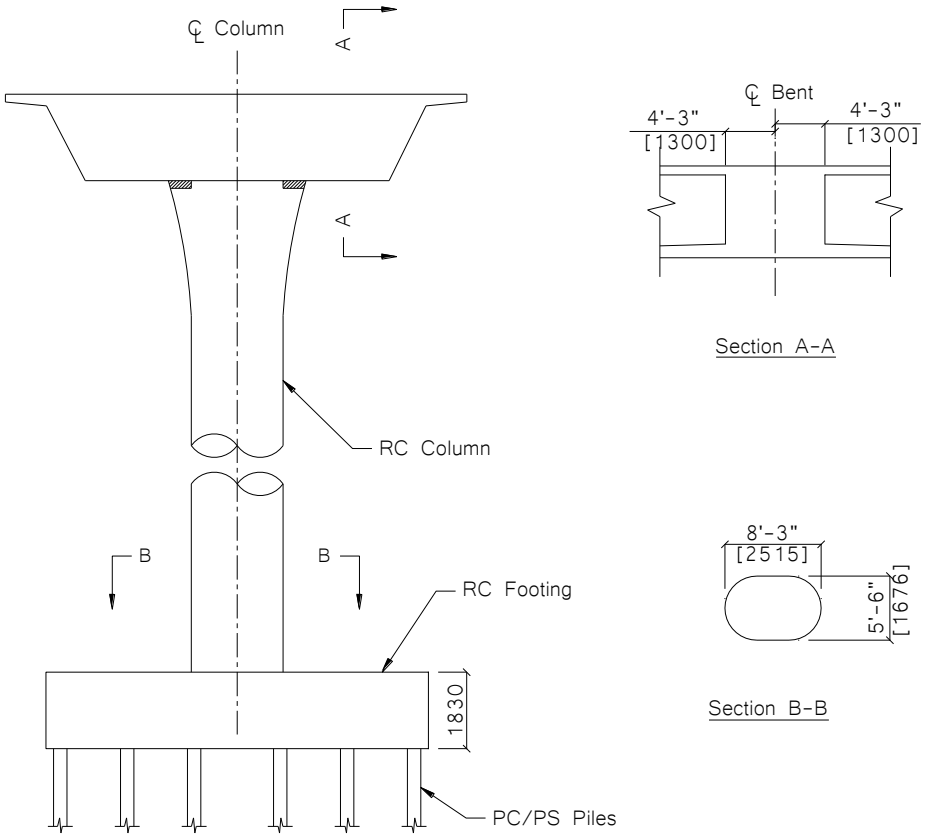


Figure 2-42 Typical bent layout in Frame 2, Bridge 4

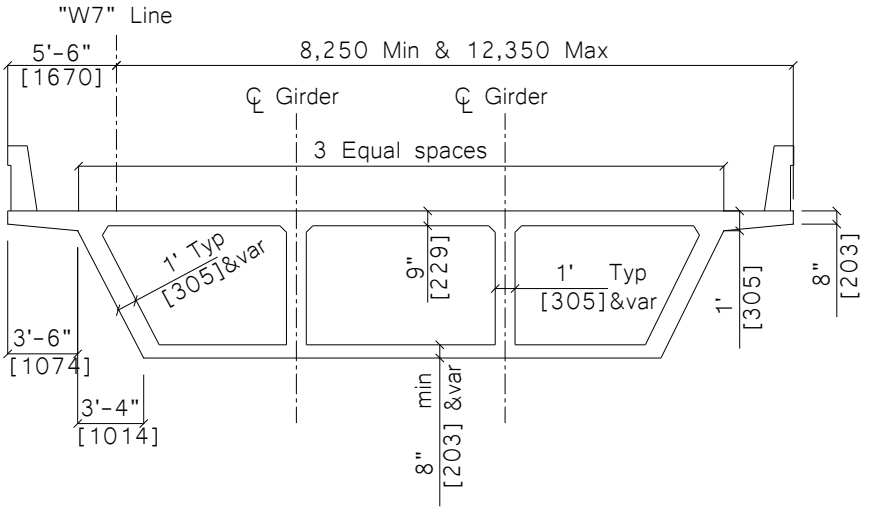


Figure 2-43 Superstructure cross-sectional details of Frame 2, Bridge 4

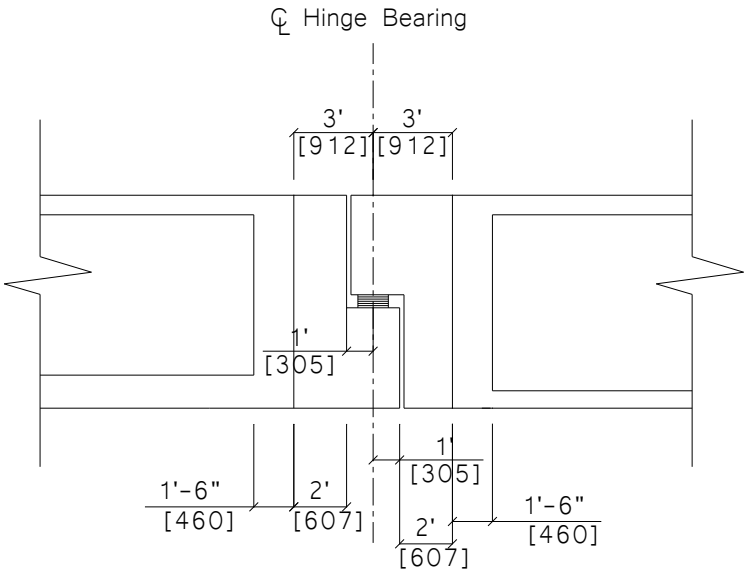


Figure 2-44 Hinge details, Bridge 4

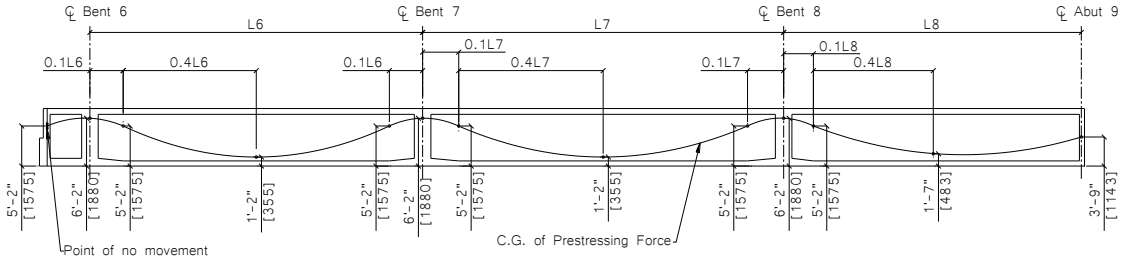


Figure 2-45 Prestressing tendons profile in Frame 2, Bridge 4

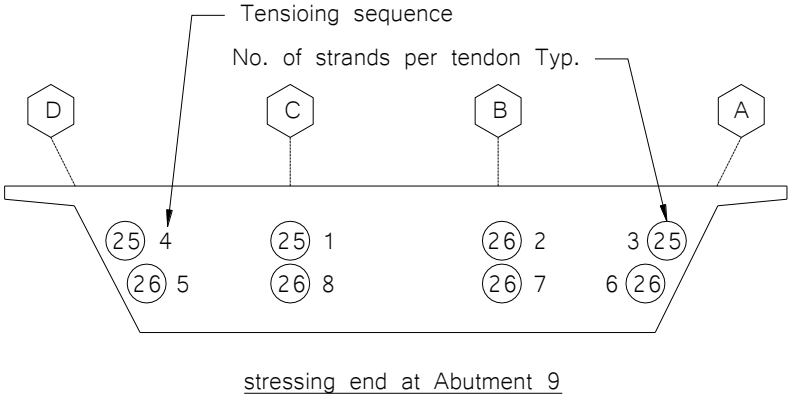


Figure 2-46 Stressing sequence of Frame 2, Bridge 4

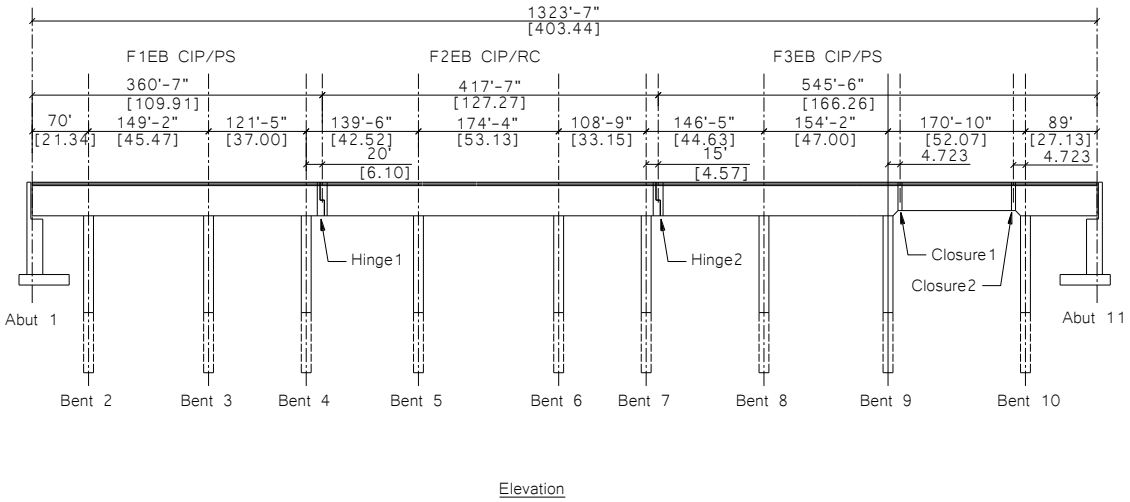


Elevation

Figure 2-47 Elevation of Bridge 5EB

Figure 2-48 Concrete pouring of Closure 1

Figure 2-49 Reinforcement steel and couplers connection between Closure 1 and the Segment B of Frame 3, Bridge 5EB

Figure 2-50 Top and bottom views of Closure 1

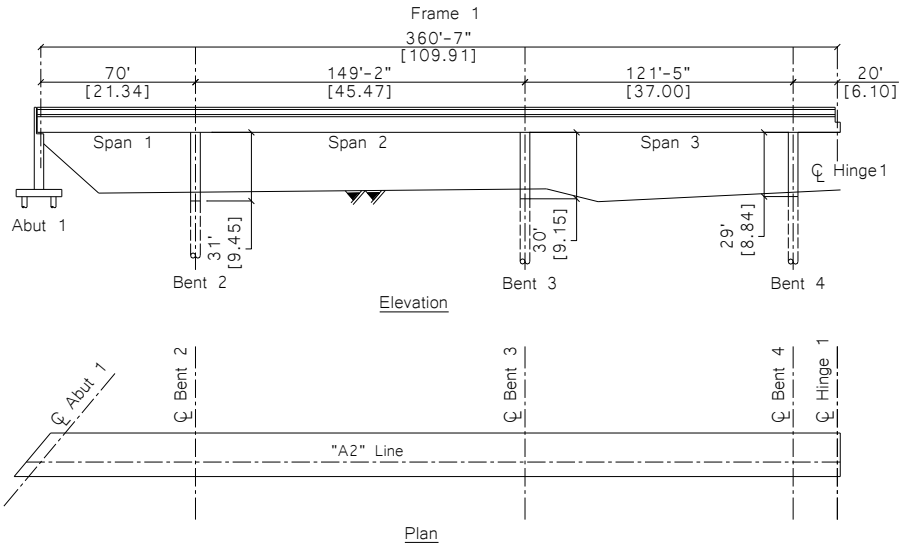


Figure 2-51 Elevation of Frame 1, Bridge 5EB

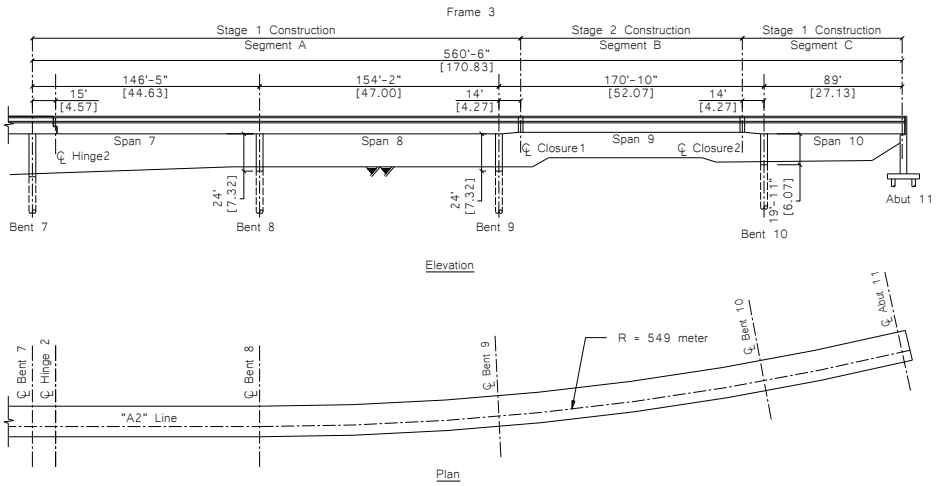


Figure 2-52 Elevation of Frame 3, Bridge 5EB


Figure 2-53 Drop-in span construction views at Closure 1 and 2


Figure 2-54 Drop-in span falsework


Figure 2-55 Steel frames holding the drop-in span


Figure 2-56 End supports of the drop-in span

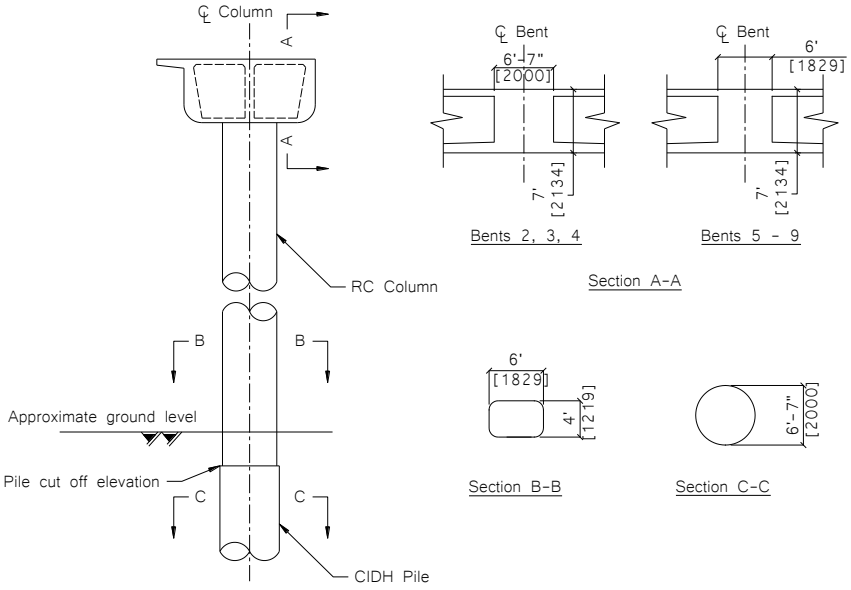


Figure 2-57 Typical bent layout of Frame 1 and 3, Bridge 5EB

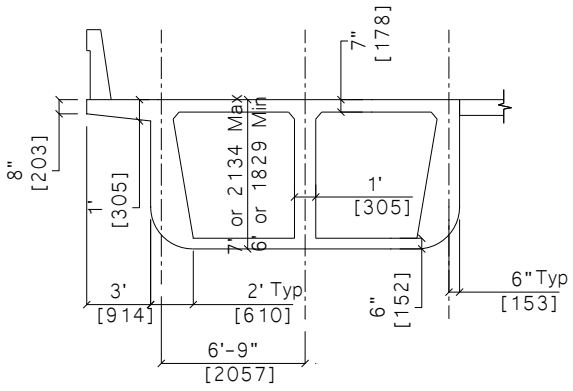


Figure 2-58 Superstructure cross-sectional details of Frame 1 and 3, Bridge 5EB

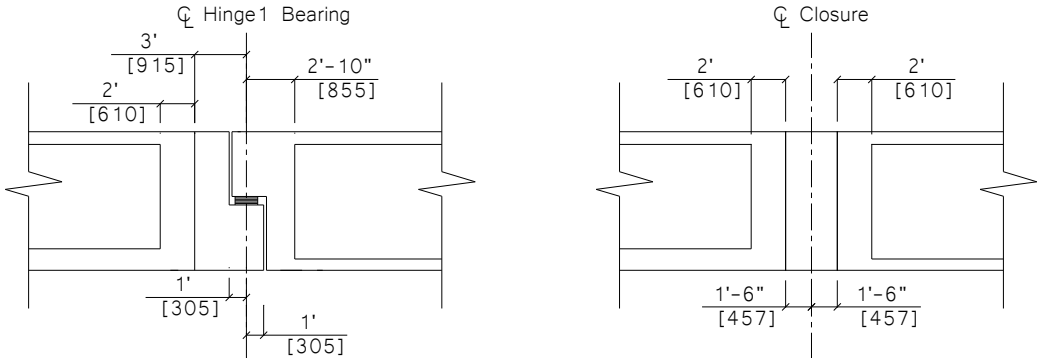


Figure 2-59 Hinge and closure details, Bridge 5EB

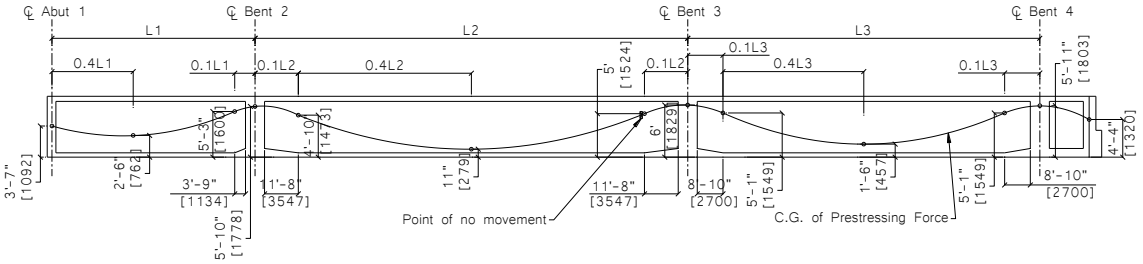


Figure 2-60 Prestressing tendons profile of Frame 1, Bridge 5EB

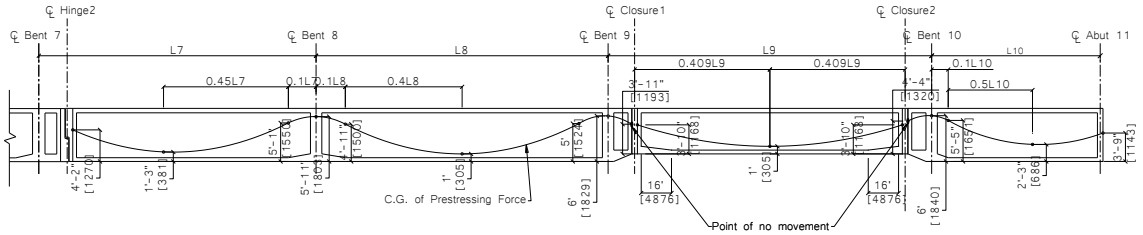


Figure 2-61 Prestressing tendons profile of Frame 3, Bridge 5EB

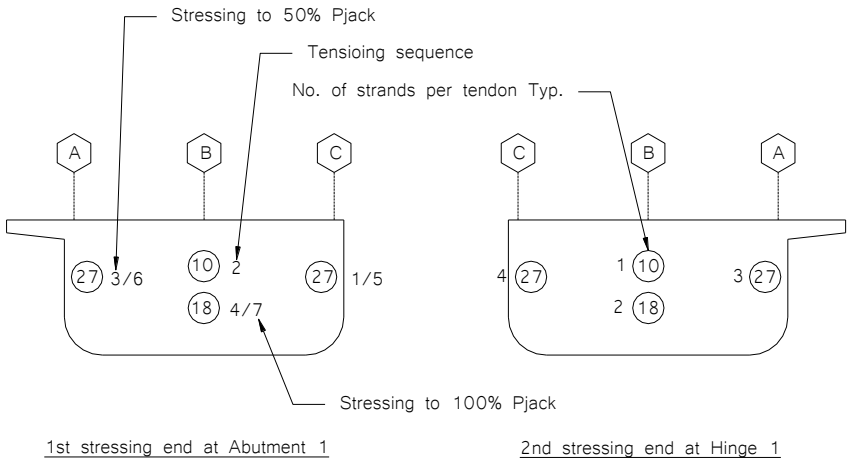


Figure 2-62 Stressing sequence of Frame 1, Bridge 5EB

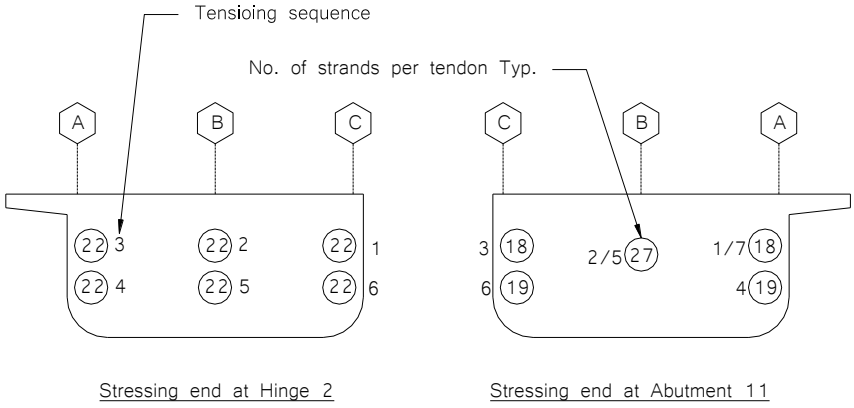


Figure 2-63 Stressing sequence of Frame 3 for Closure 1 and 2, Bridge 5EB

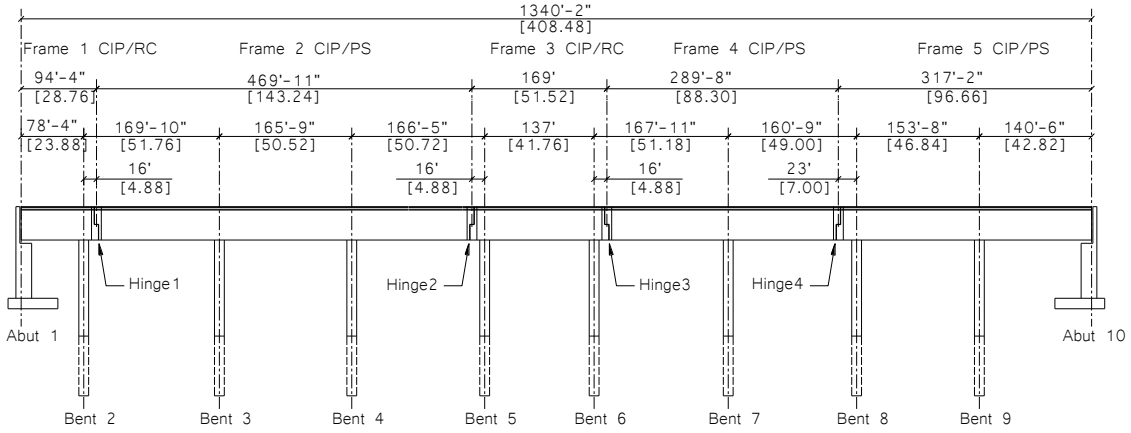


Figure 2-64 Elevation of Bridge 5WB

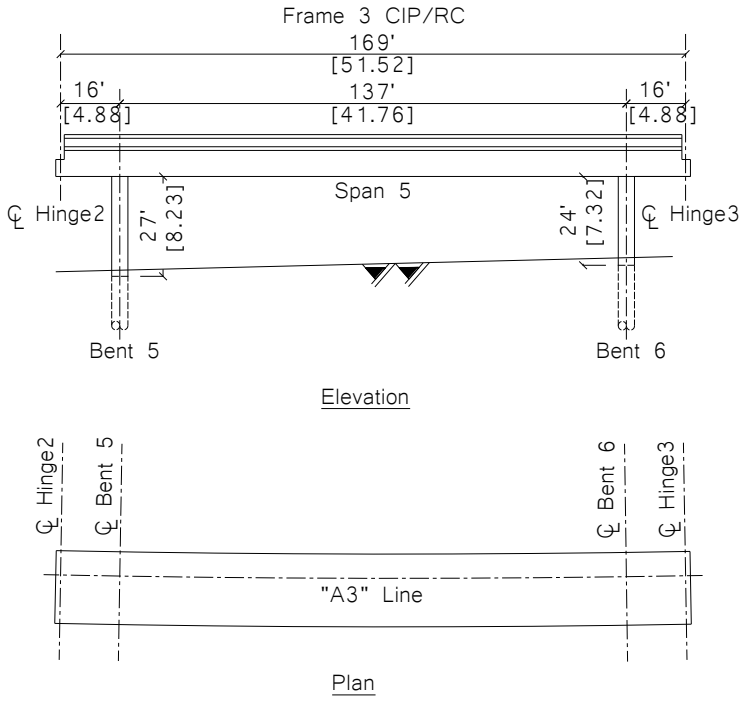


Figure 2-65 Elevation and plan views of Frame 3, Bridge 5WB

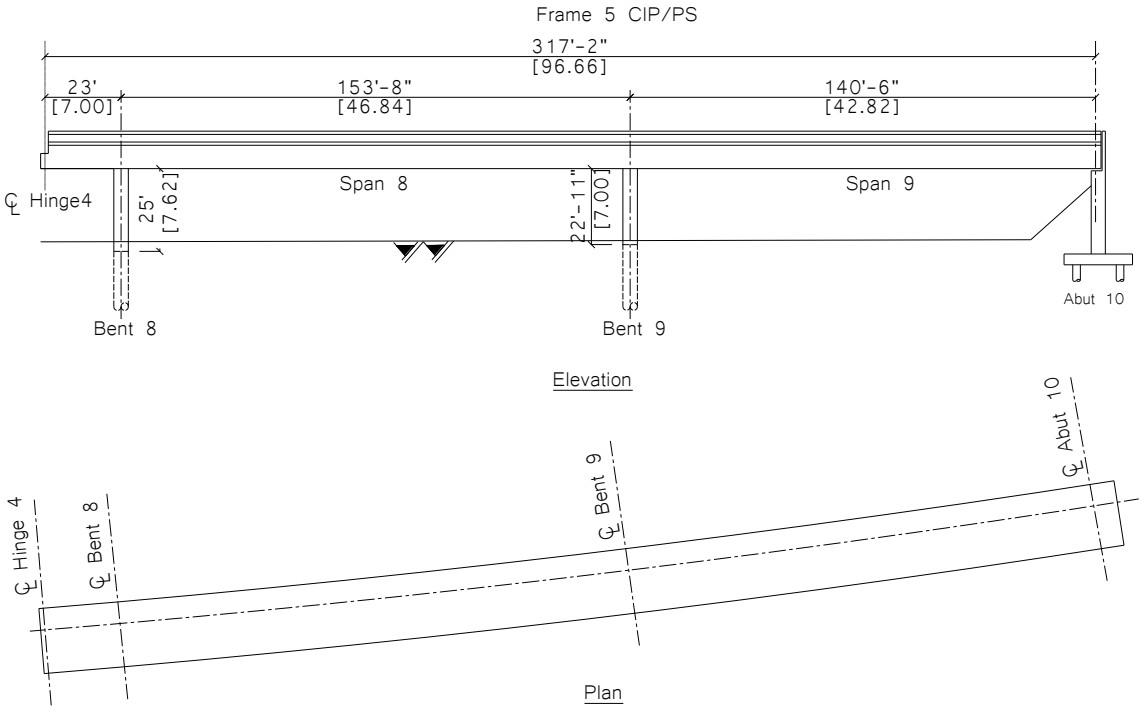


Figure 2-66 Elevation and plan views of Frame 5, Bridge 5WB

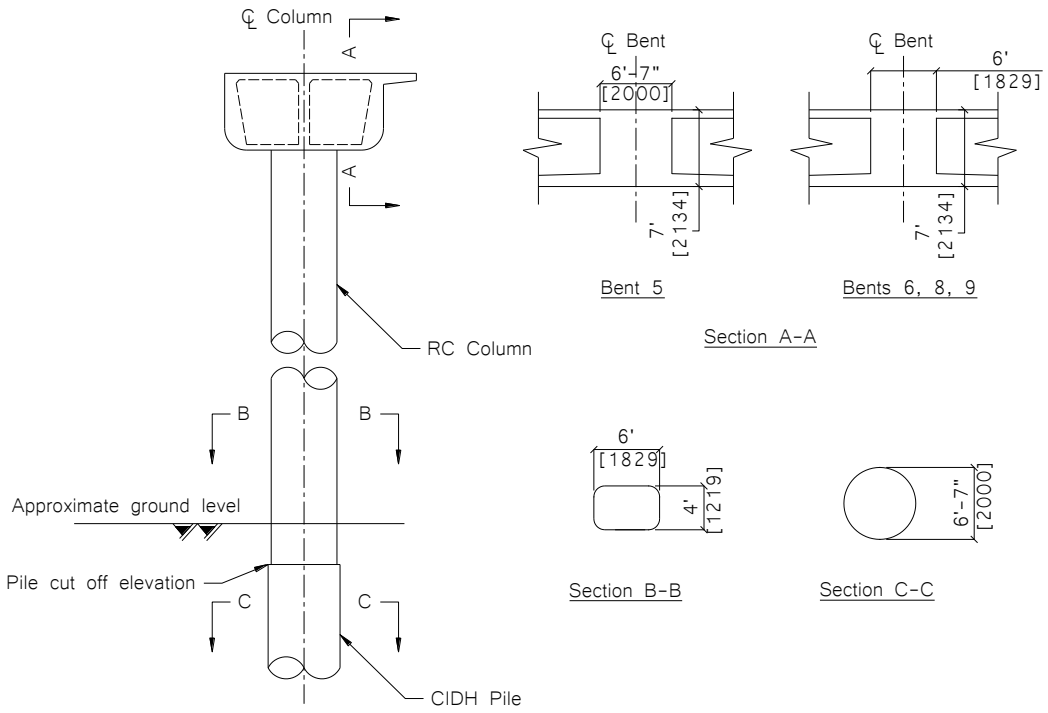


Figure 2-67 Typical bent layout of Frame 3 and 5, Bridge 5WB

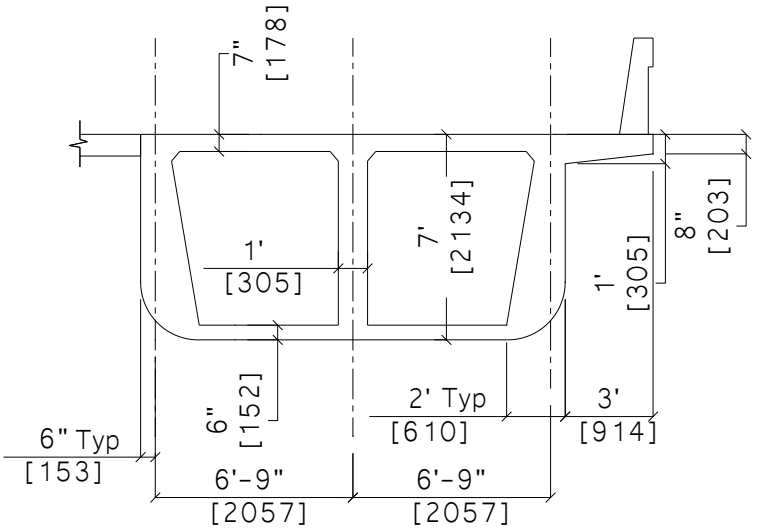


Figure 2-68 Superstructure cross-sectional details of Frame 3 and 5, Bridge 5WB

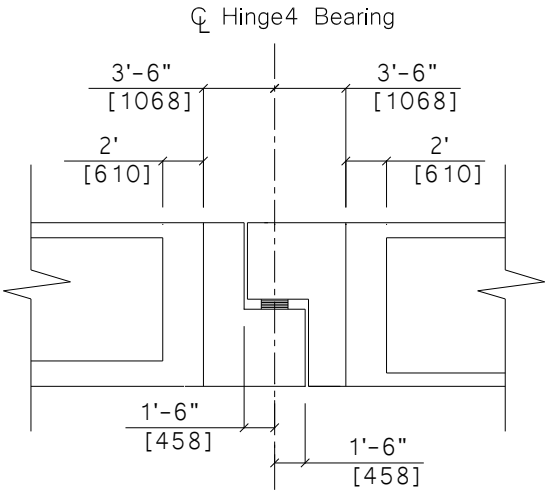


Figure 2-69 Hinge details, Bridge 5WB

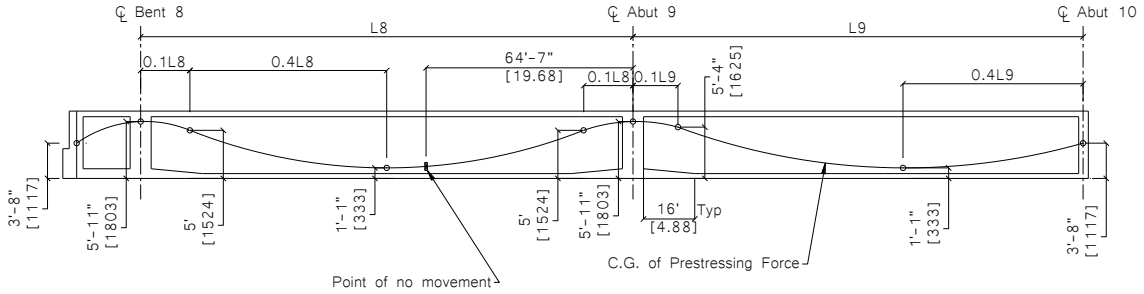


Figure 2-70 Prestressing tendons profile of Frame 5, Bridge 5WB

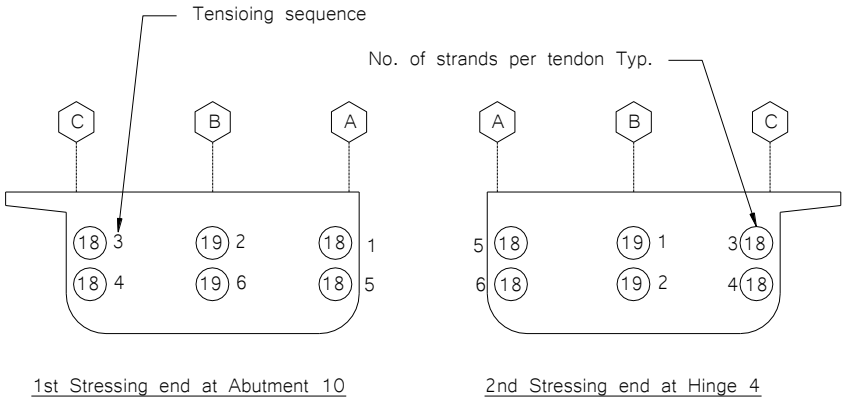


Figure 2-71 Stressing sequence of Frame 5, Bridge 5WB


Figure 3-1 Moisture retaining blankets for concrete curing


Figure 3-2 Deck surface partial reveal for stations marking during concrete curing


Figure 3-3 Digital level used in field measurements (Sprinter 250M)

(a)

(b)

(c)

Figure 3-4: (a) Level mounted on the tripod; (b) Dual face leveling rod; (c) Rod bubble level


(a)


(b)

Figure 3-5: (a) Digital level main screen; (b) Digital Thermometer Hygrometer

(a)

(b)

(c)

Figure 3-6: (a) Station marking process; (b) Typical station; (c) Typical transverse gridline at the hinge

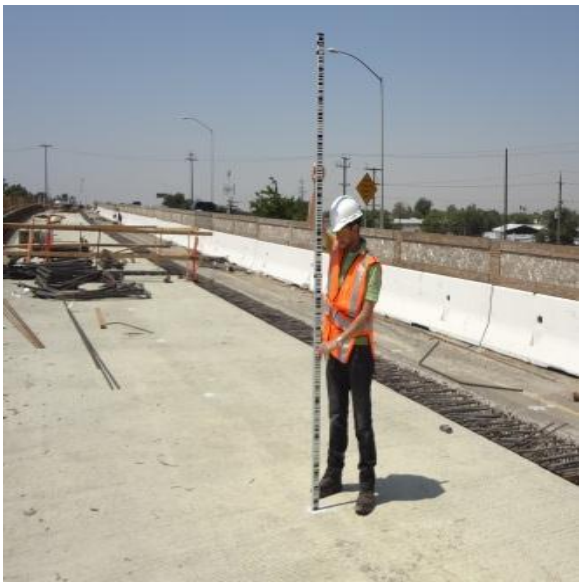

(a)

(b)

(c)

(d)

Figure 3-7: (a) Elevation measurment on the adjacent span; (b) Elevation measurment at the hinge; (c) Focusing process and elevation shooting using the measuring trigger key; (d) Elevation recording in the data sheet

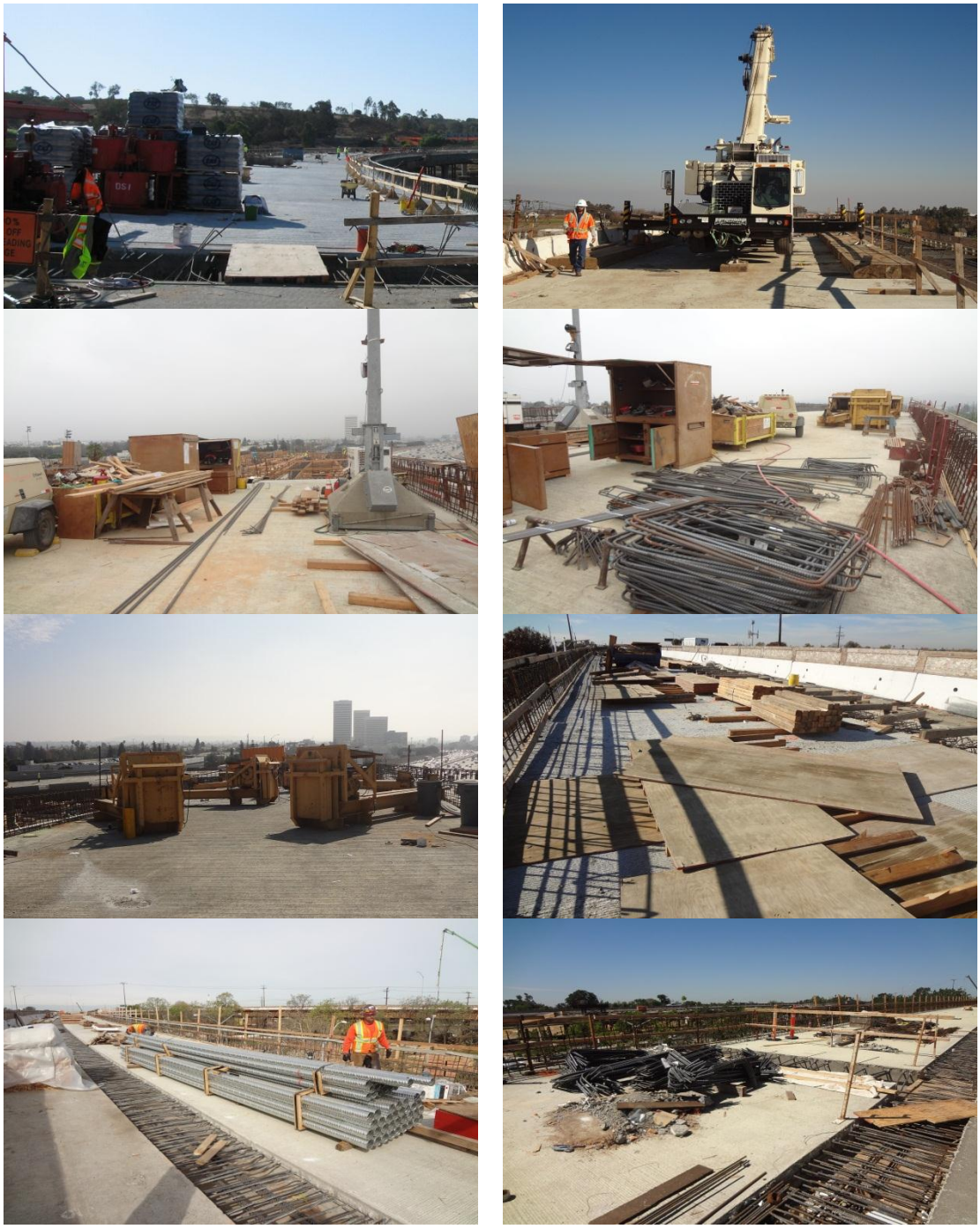

Figure 3-8 Potential obstacles seen on the bridge deck

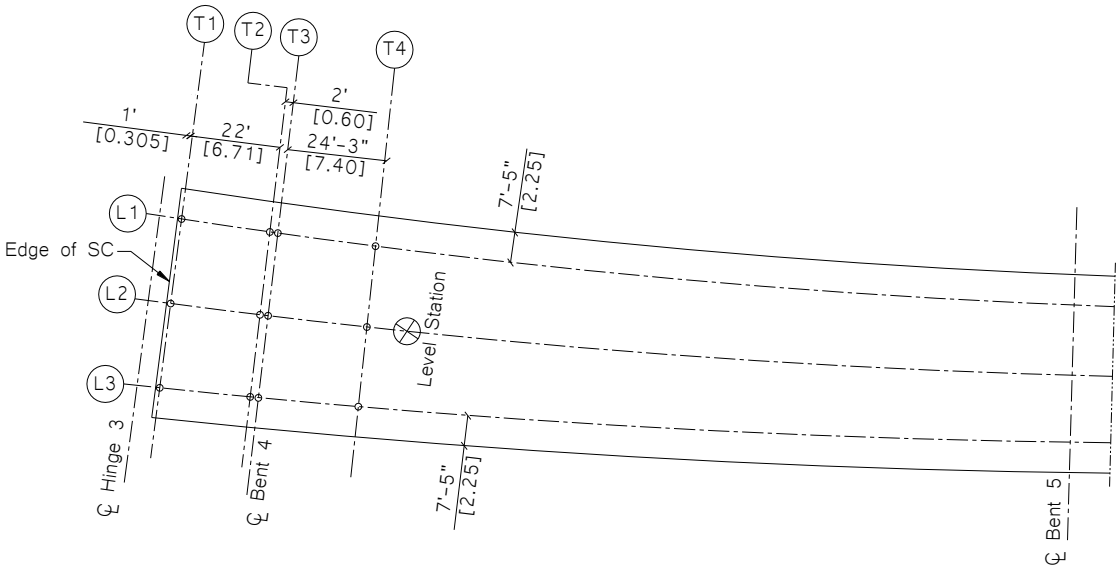


Figure 3-9 Grid stations of Hinge 3, Bridge 1

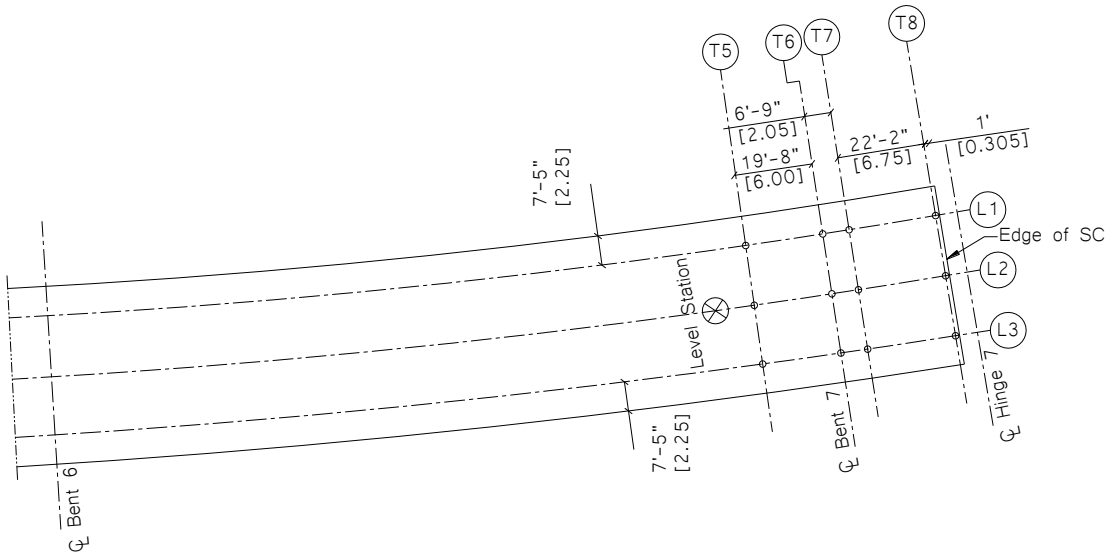


Figure 3-10 Grid stations of Hinge 7, Bridge 1

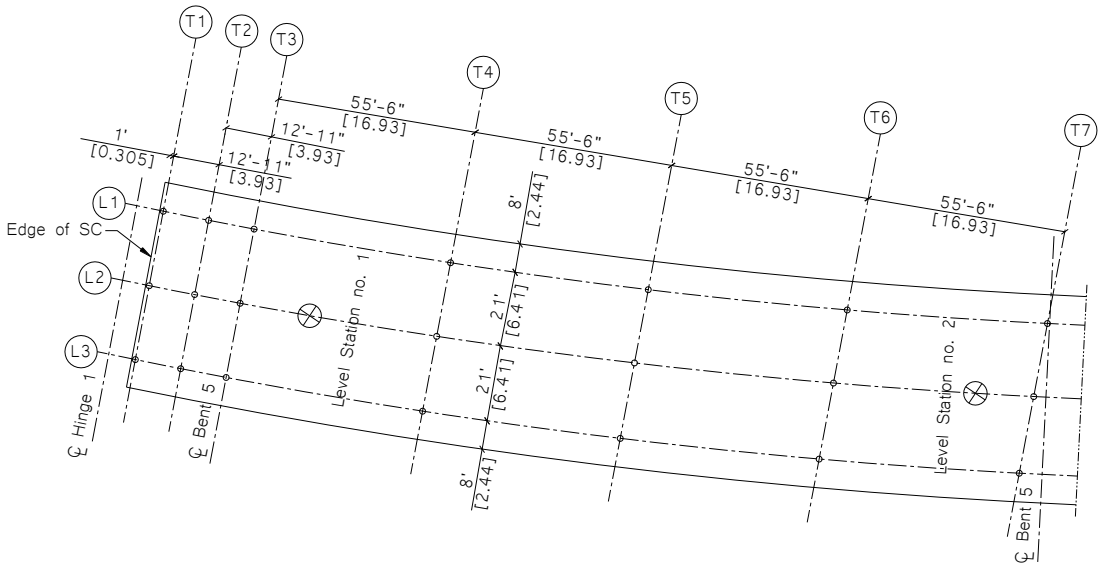


Figure 3-11 Grid stations of Hinge 1, Bridge 2

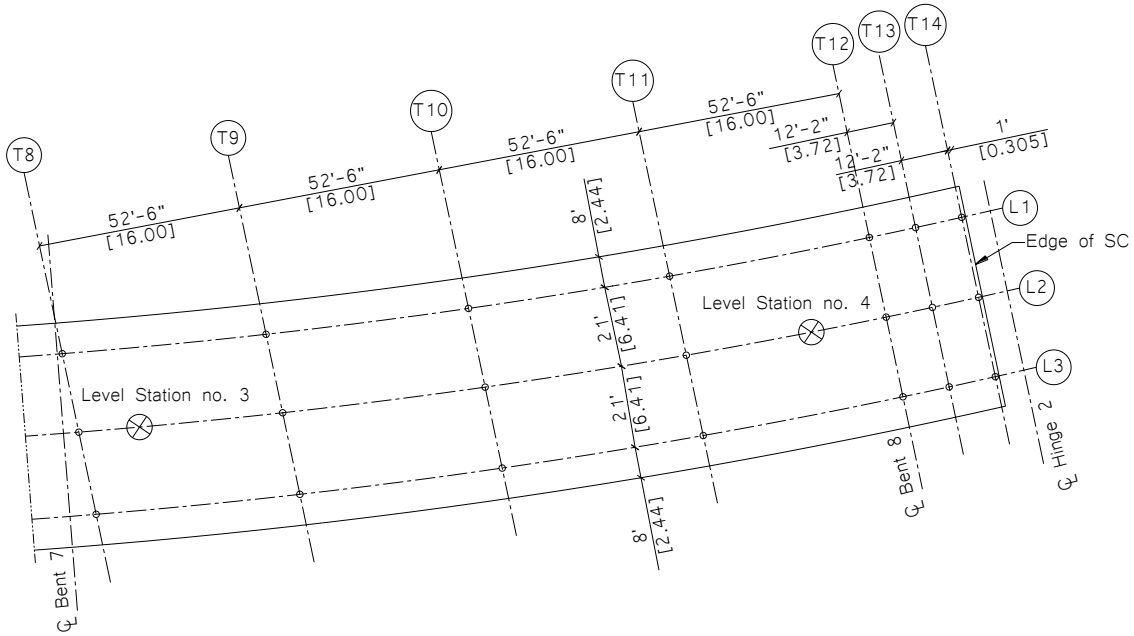


Figure 3-12 Grid stations of Hinge 2, Bridge 2

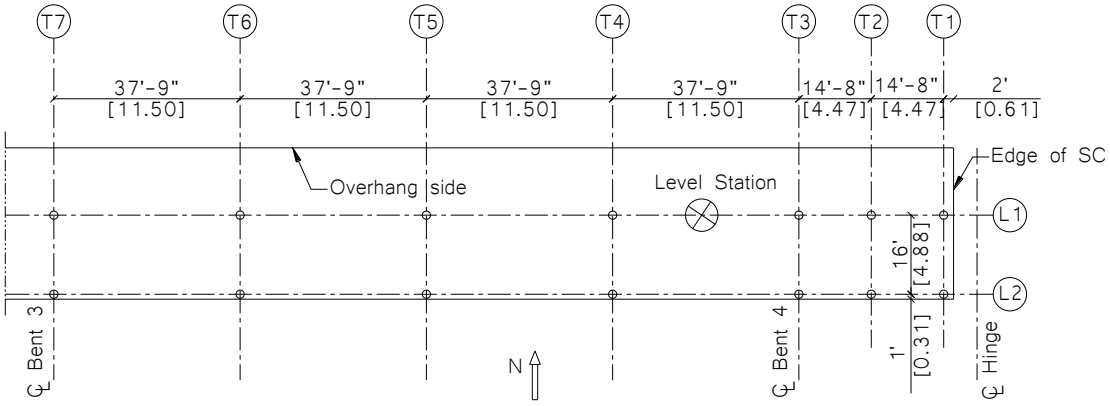


Figure 3-13 Grid stations of Hinge, Bridge 3

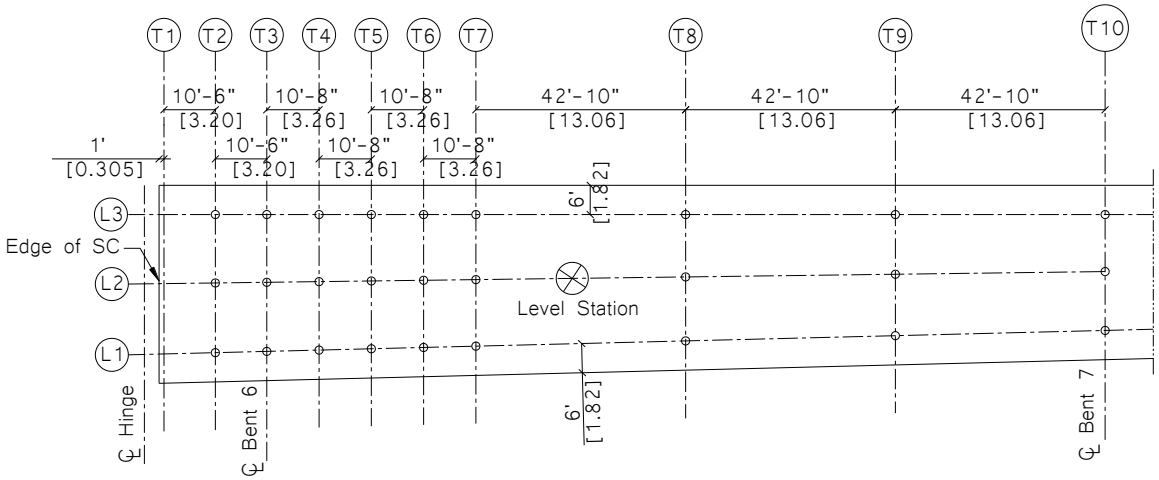


Figure 3-14 Grid stations of Hinge, Bridge 4


Figure 3-15 Tie-off point in Bridge 4

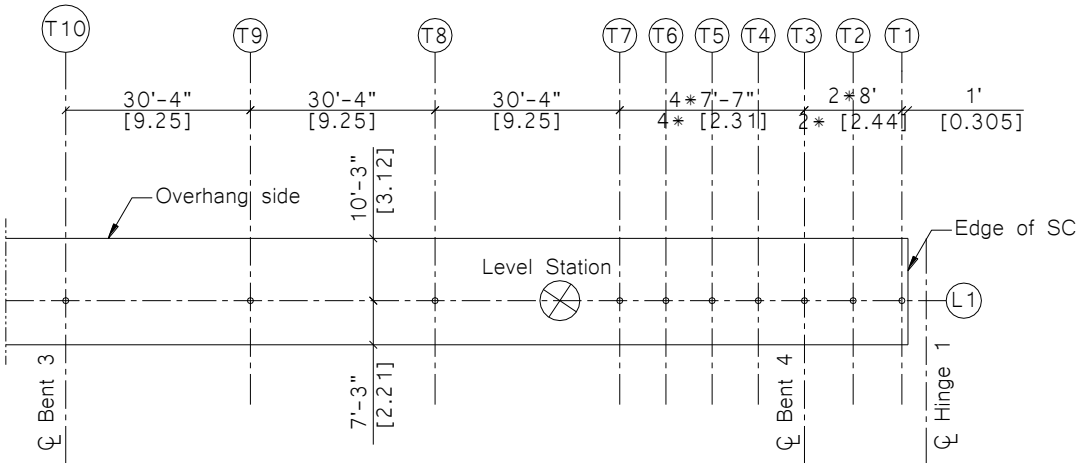


Figure 3-16 Grid stations of Hinge 1, Bridge 5EB

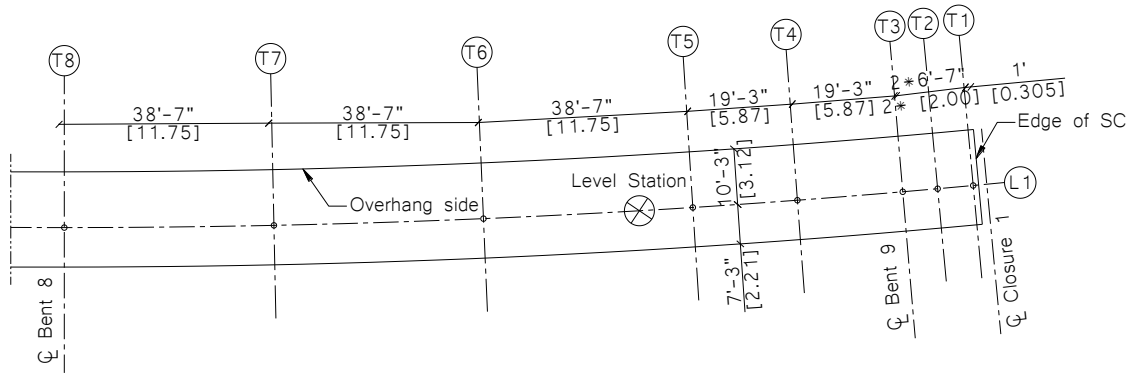


Figure 3-17 Grid stations of Closure 1, Bridge 5EB

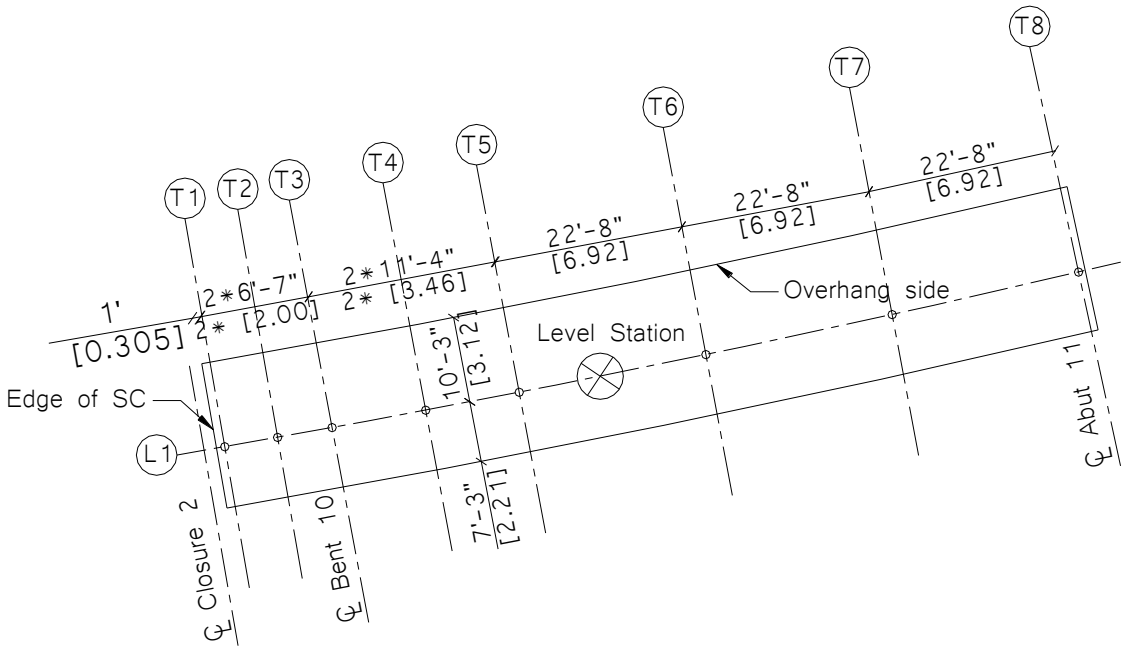


Figure 3-18 Grid stations of Closure 2, Bridge 5EB

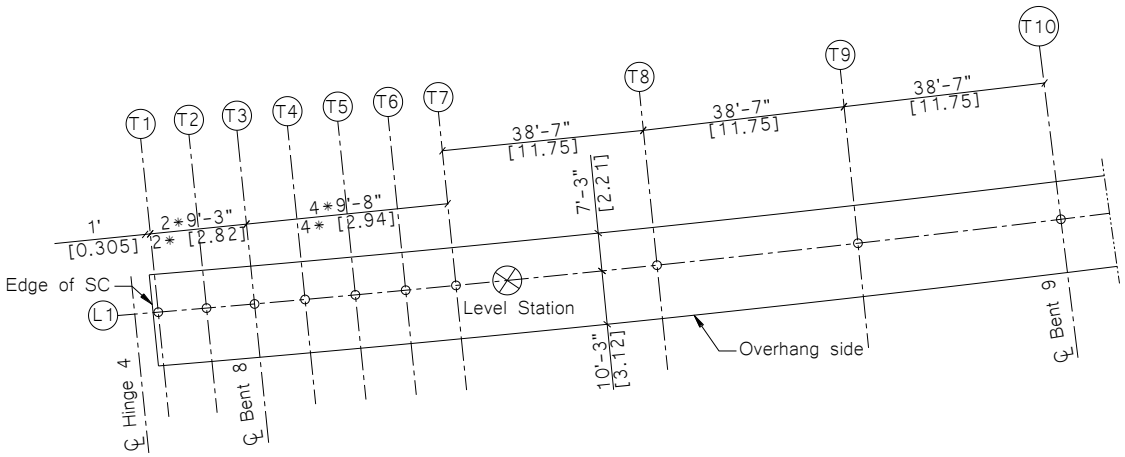


Figure 3-19 Grid stations of Hinge 4, Bridge 5WB

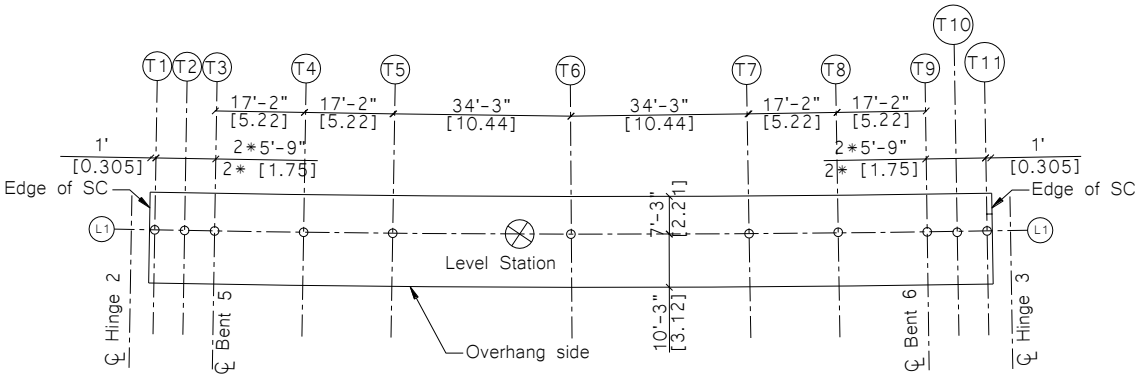


Figure 3-20 Grid stations of Hinge 2 and Hinge 3, Bridge 5WB

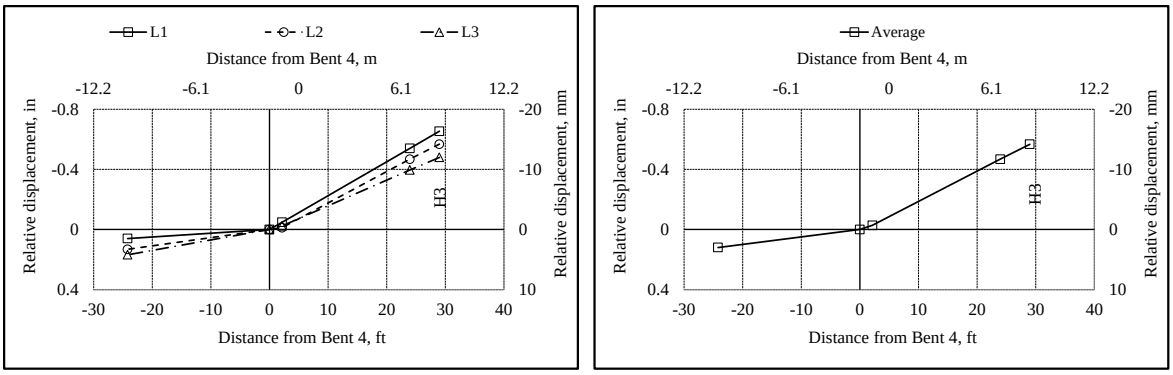


(a) (b)

Figure 4-1 Immediate deformation at Hinge 3, Bridge 1: (a) Response across the bridge width; (b) Average response

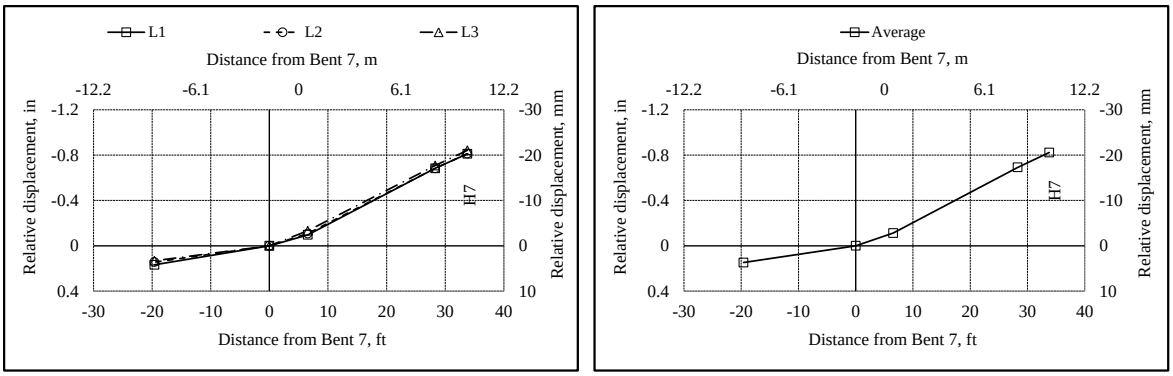


(a) (b)

Figure 4-2 Immediate deformation at Hinge 7, Bridge 1: (a) Response across the bridge width; (b) Average response

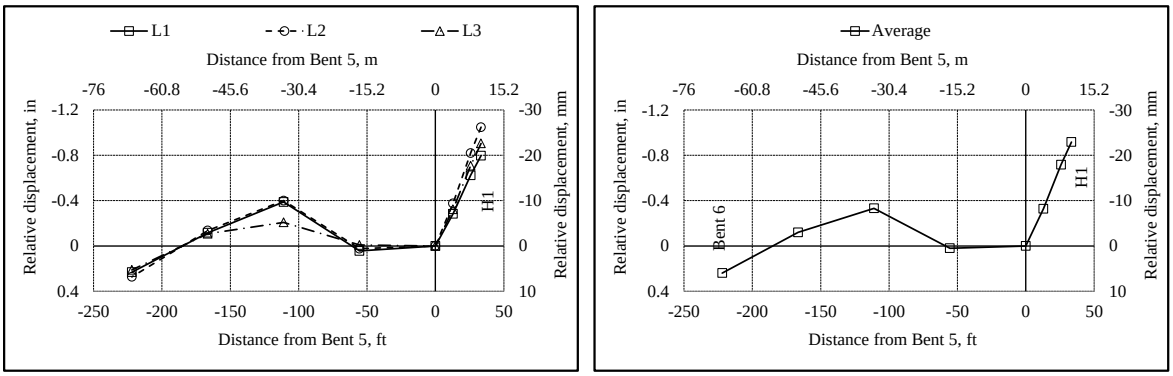


(a) (b)

Figure 4-3 Immediate deformation at Hinge 1, Bridge 2: (a) Response across the bridge width; (b) Average response

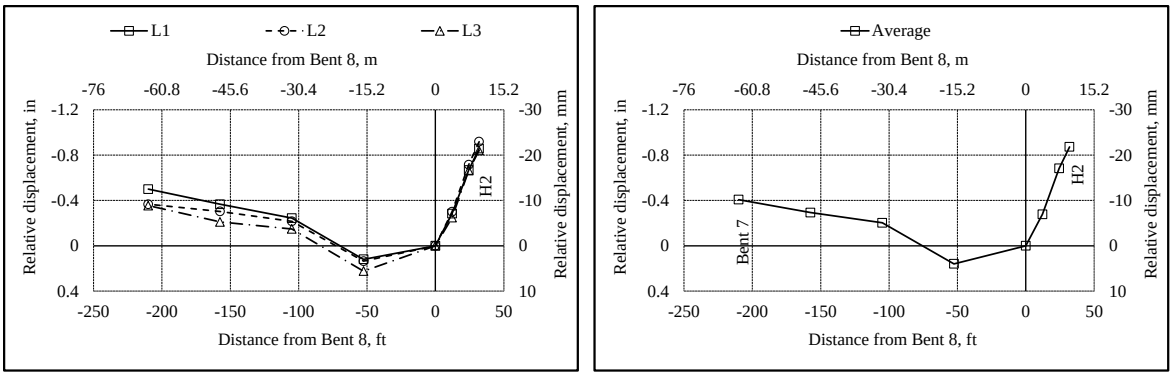


(a) (b)

Figure 4-4 Immediate deformation at Hinge 2, Bridge 2: (a) Response across the bridge width; (b) Average response

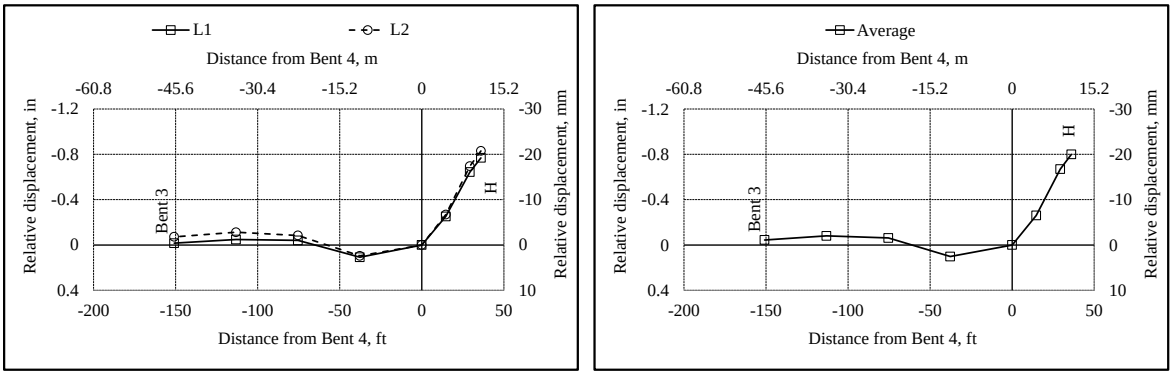


(a) (b)

Figure 4-5 Immediate deformation at Hinge, Bridge 3: (a) Response across the bridge width; (b) Average response

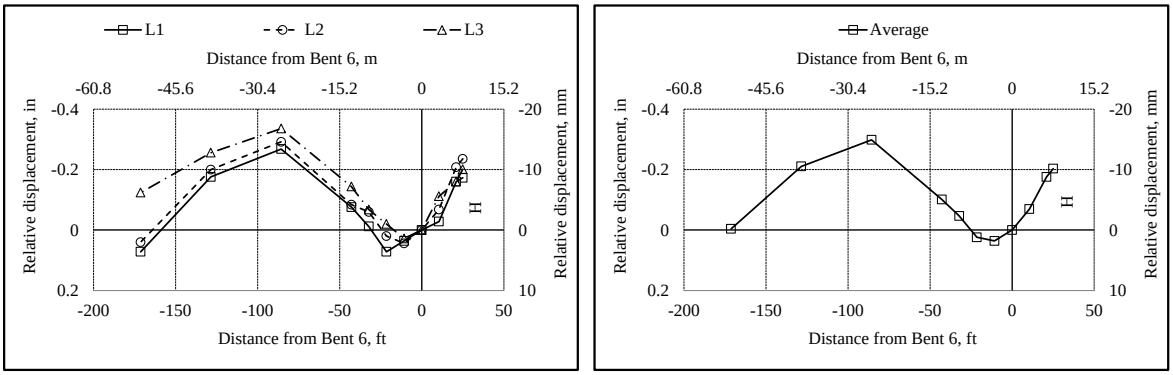


(a) (b)

Figure 4-6 Immediate deformation at Hinge, Bridge 4: (a) Response across the bridge width; (b) Average response

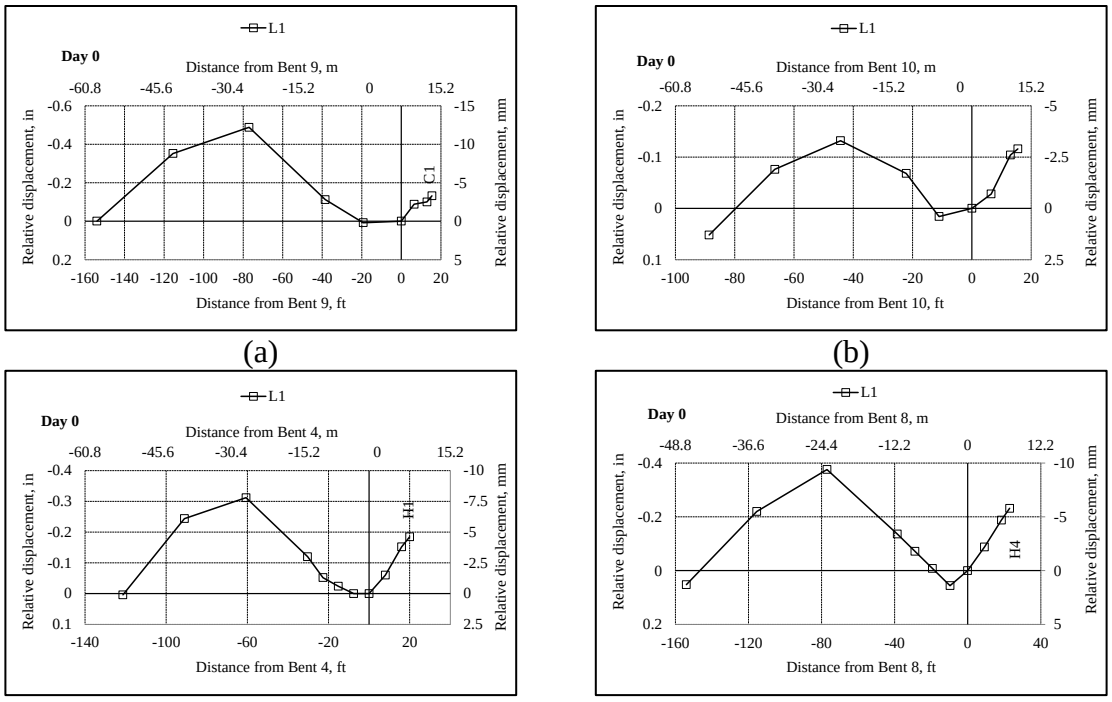


Figure 4-7 Immediate deformation at Hinge, Bridge 5: (a) Response at C1; (b) Response at C2; (c) Response at H1; (d) Response at H4

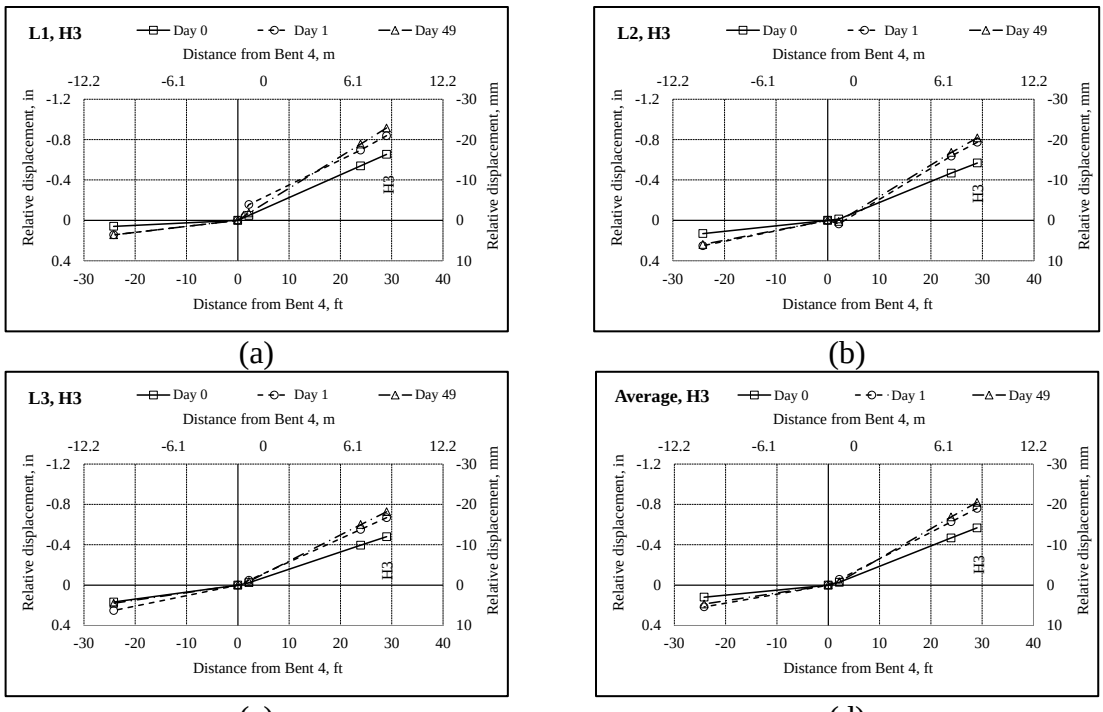


Figure 4-8 Time-dependent deformation before load transfer at H3, Bridge 1: (a) L1 response; (b) L2 response; (c) L3 response; (d) Average response

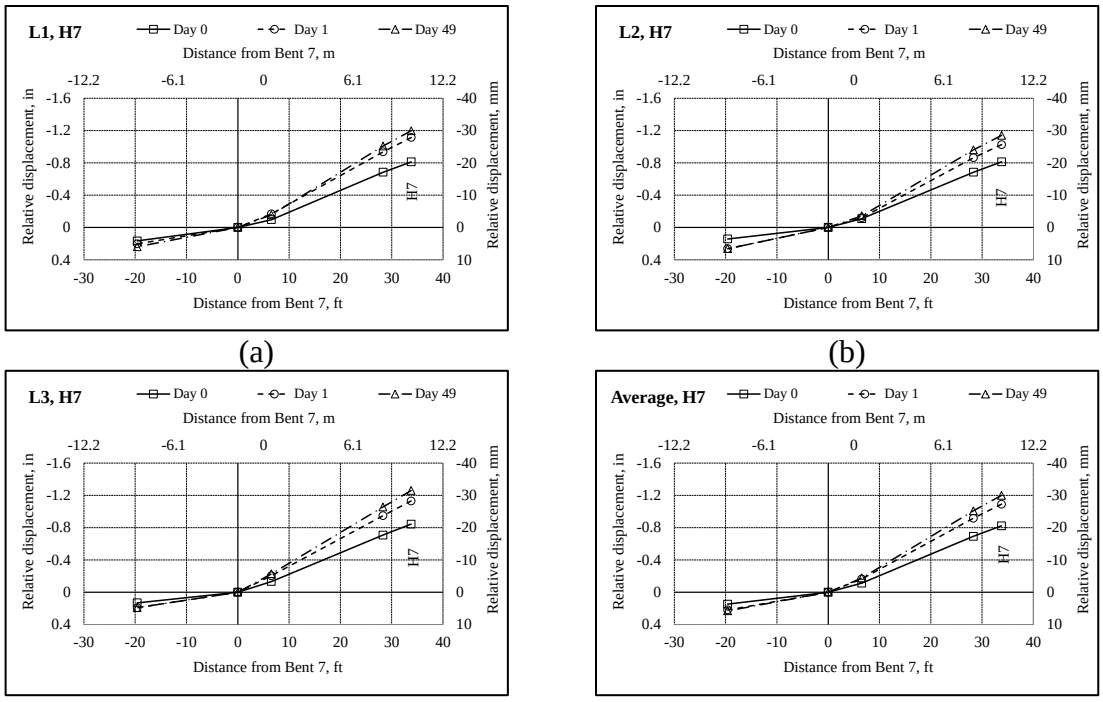


Figure 4-9 Time-dependent deformation before load transfer at H7, Bridge 1: (a) L1 response; (b) L2 response; (c) L3 response; (d) Average response

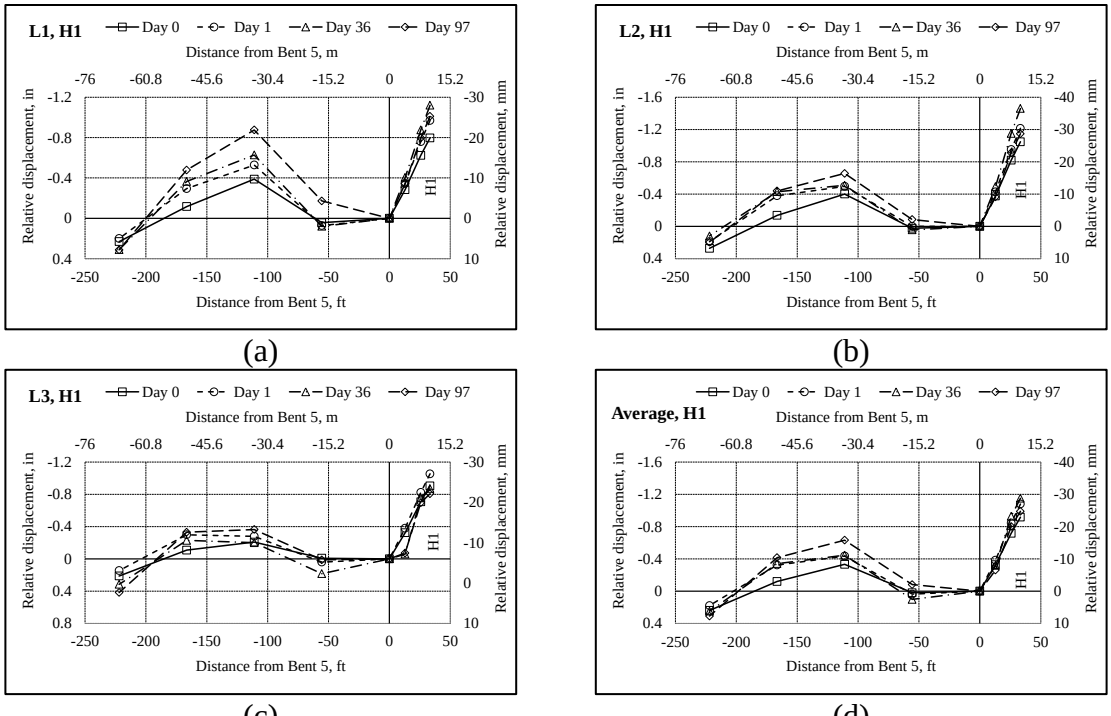


Figure 4-10 Time-dependent deformation before load transfer at H1, Bridge 2: (a) L1 response; (b) L2 response; (c) L3 response; (d) Average response

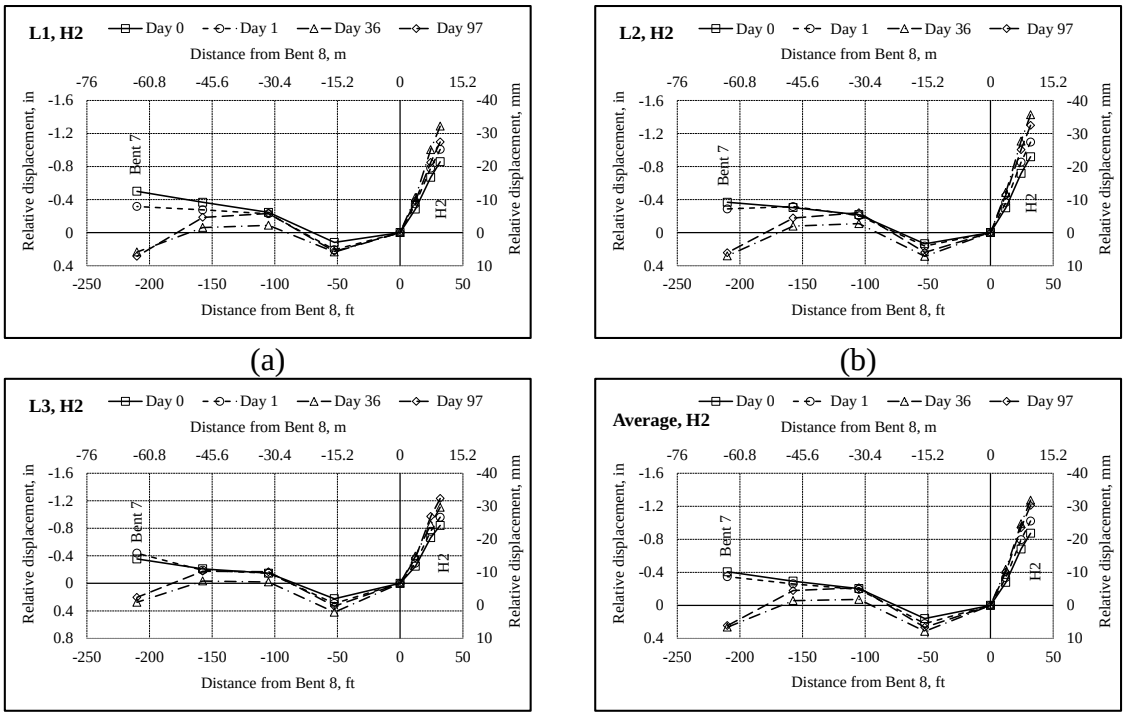


Figure 4-11 Time-dependent deformation before load transfer at H2, Bridge 2: (a) L1 response; (b) L2 response; (c) L3 response; (d) Average response

Figure 4-12 Self-supporting outrigger bent (Bent 7) after falsework removal

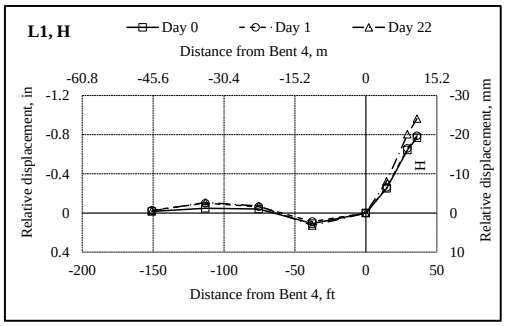


(a)

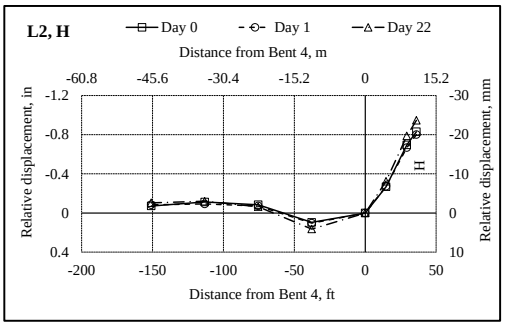


(b)

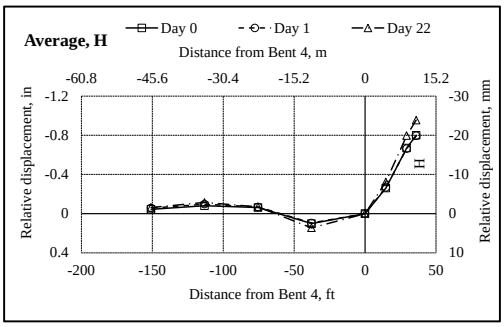


(c)

Figure 4-13 Time-dependent deformation before load transfer at H, Bridge 3: (a) L1 response; (b) L2 response; (c) Average response

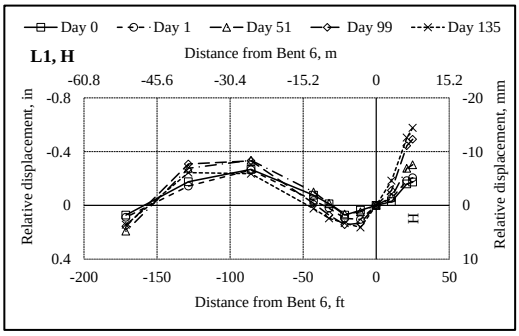


(a)

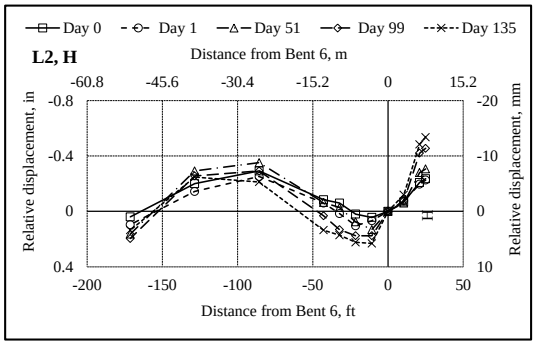


(b)

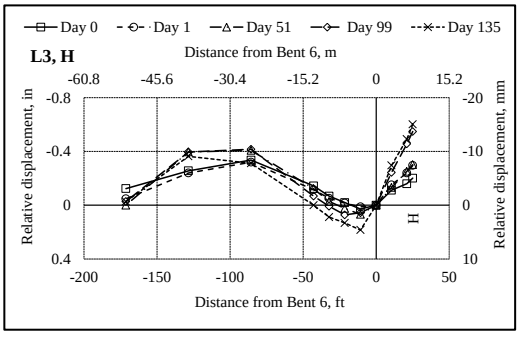


(c)

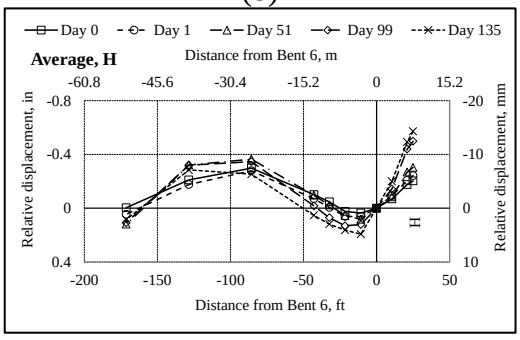


(d)

Figure 4-14 Time-dependent deformation before load transfer at H, Bridge 4: (a) L1 response; (b) L2 response; (c) Average response

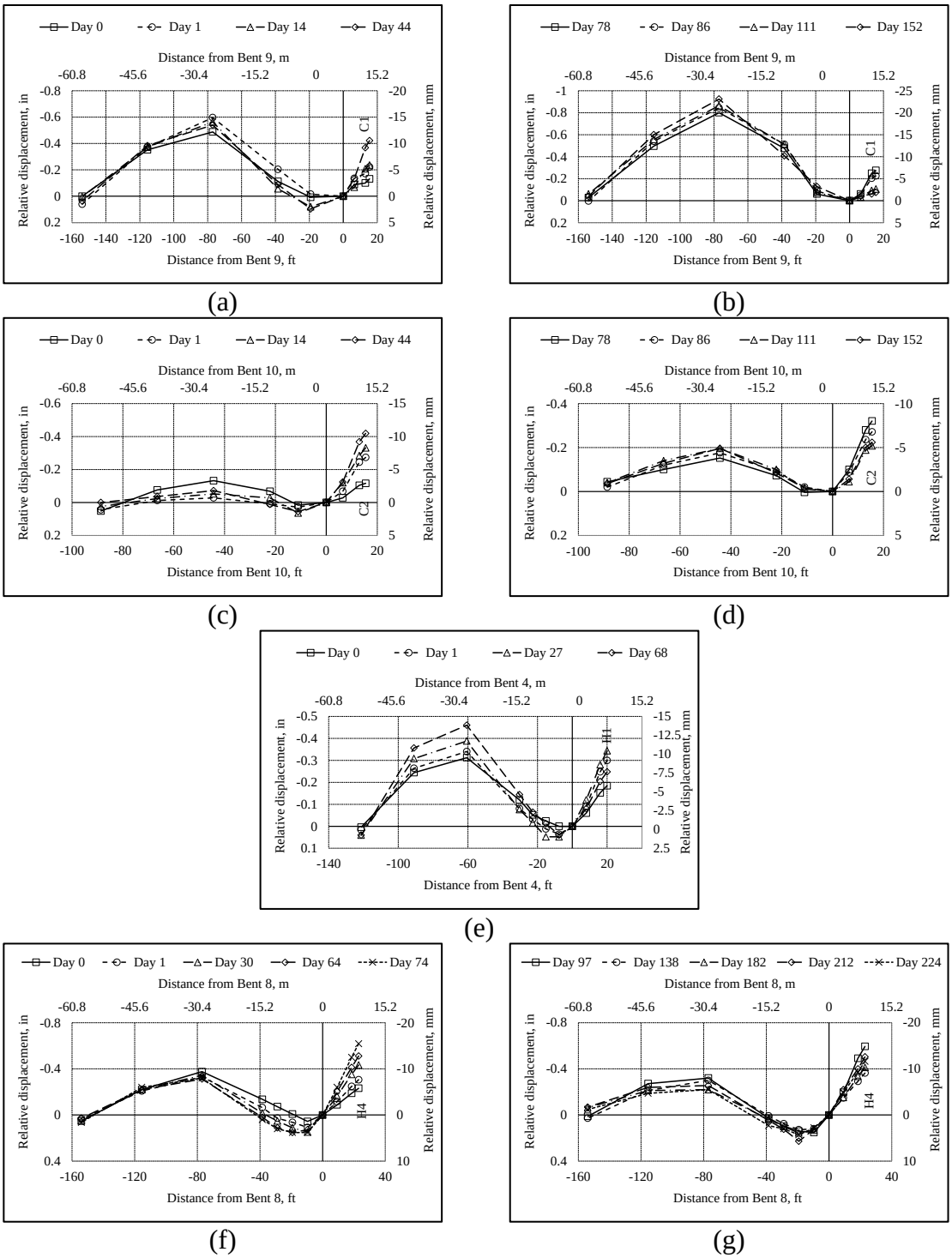


Figure 4-15 Time-dependent deformation before load transfer at the P/S hinges, Bridge 5: (a) C1 before lowering the drop-in span; (b) C1 after lowering the drop-in span; (c) C2 before lowering the drop-in span; (d) C2 after lowering the drop-in span; (e) H1; (f) H4 before casting top ledge; (g) H4 after casting top ledge

Figure 4-16 Completion of the hinge closure and long cantilever of H1 on Day-68

(a)

(b)

Figure 4-17 Four 1200mm cubic concrete blocks placed on the short cantilever of H4: (a) Short cantilever view; (b) Hinge view

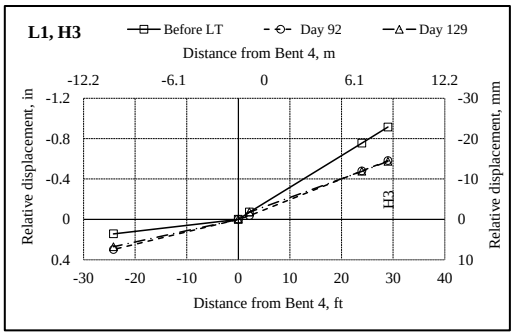


(a)

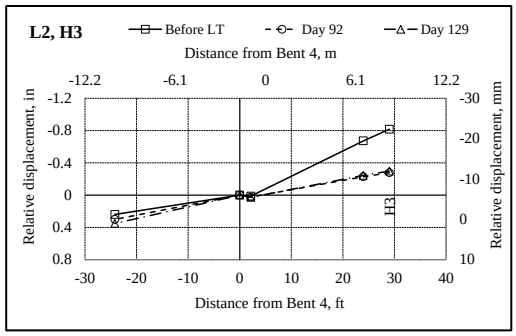


(b)

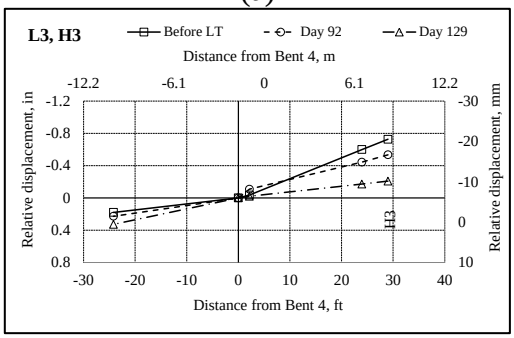


(c)

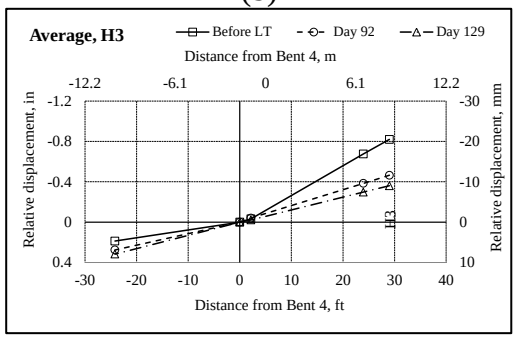


(d)

Figure 4-18 Time-dependent deformation after load transfer at H3, Bridge 1: (a) L1 response; (b) L2 response; (c) L3 response; (d) Average response

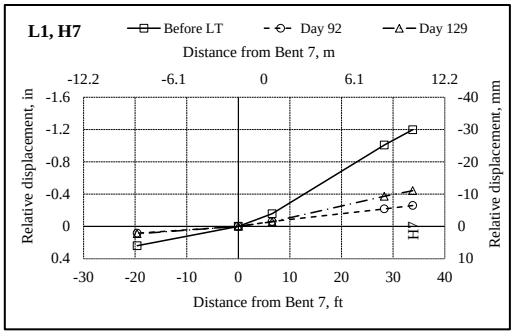


(a)

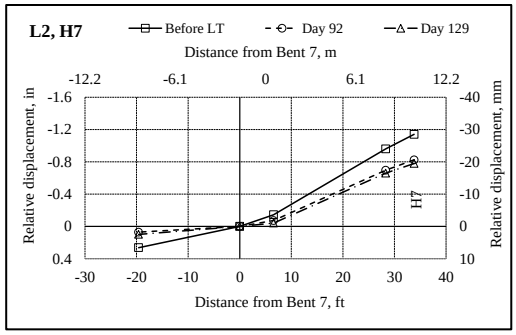


(b)

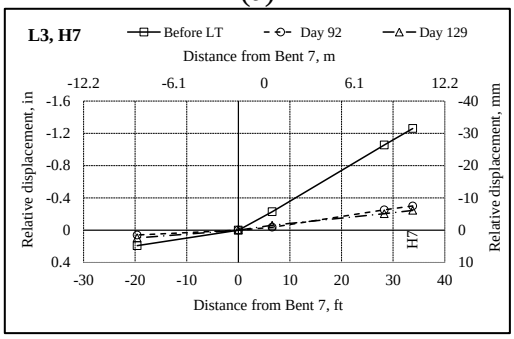


(c)

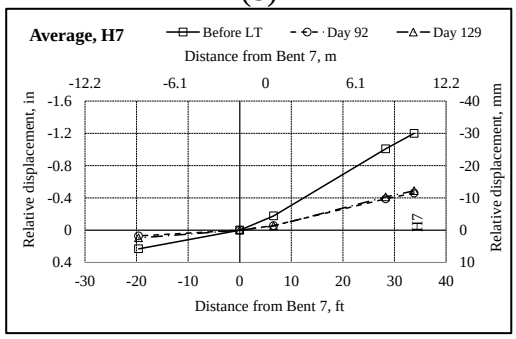


(d)

Figure 4-19 Time-dependent deformation after load transfer at H7, Bridge 1: (a) L1 response; (b) L2 response; (c) L3 response; (d) Average response

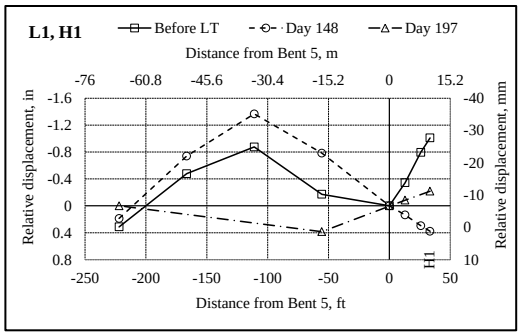


(a)

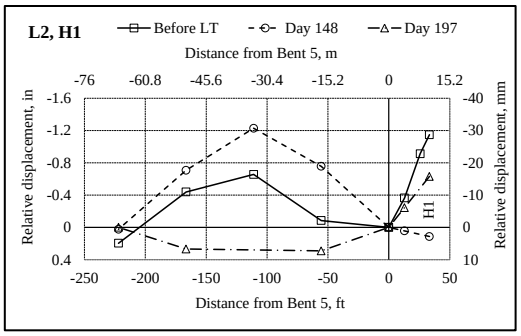


(b)

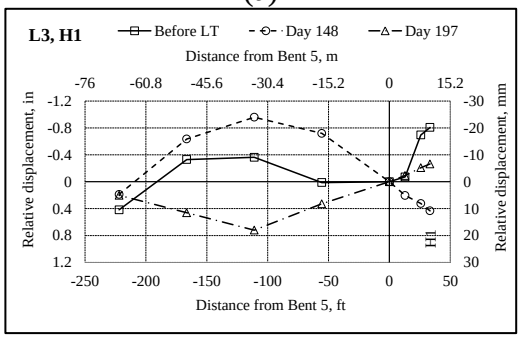


(c)

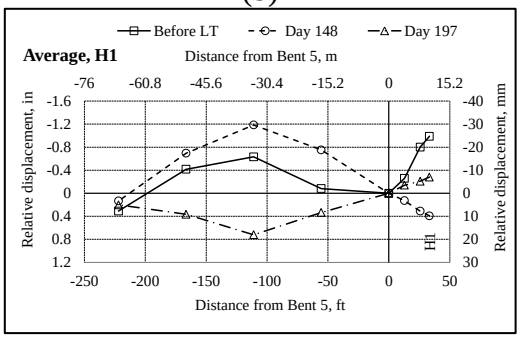


(d)

Figure 4-20 Time-dependent deformation after load transfer at H1, Bridge 2: (a) L1 response; (b) L2 response; (c) L3 response; (d) Average response

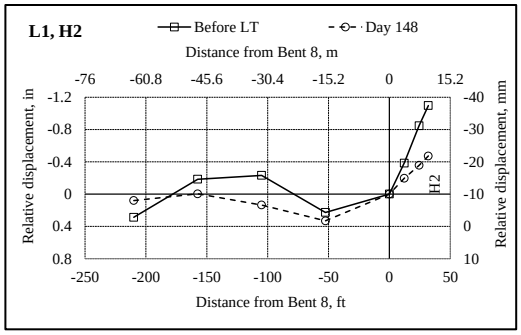


(a)

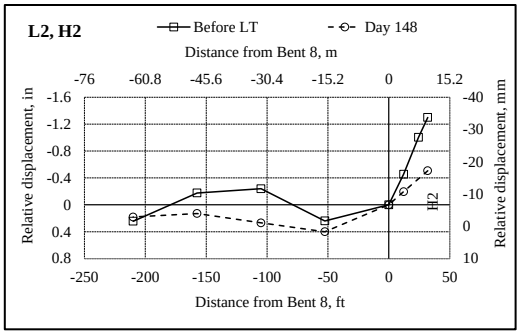


(b)

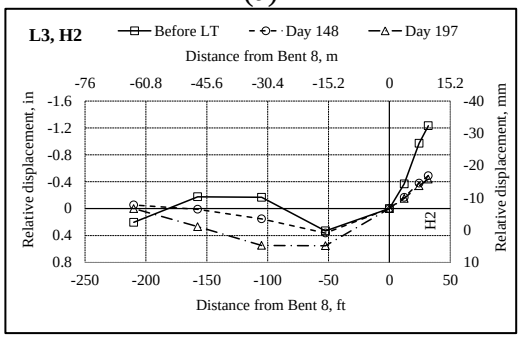


(c)

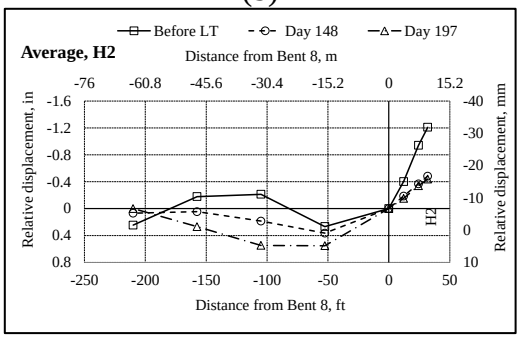


(d)

Figure 4-21 Time-dependent deformation after load transfer at H2, Bridge 2: (a) L1 response; (b) L2 response; (c) L3 response; (d) Average response

(a) (b)

Figure 4-22 Bridge deck grinding at hinge 2 area on Day-197: (a) Hinge 2 view; (b) Adjacent span view

Figure 4-23 Partial falsework removal in Frame 2 on Day 148

Figure 4-24 Complete falsework removal in Frame 2

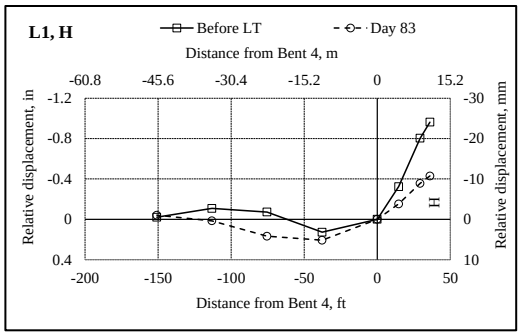


(a)

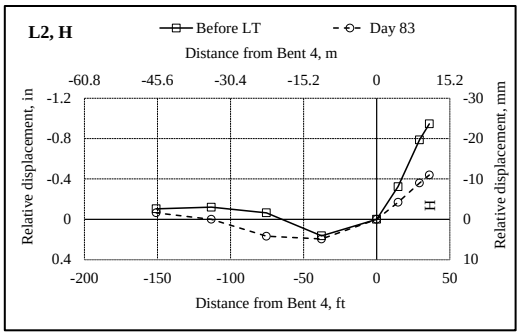


(b)

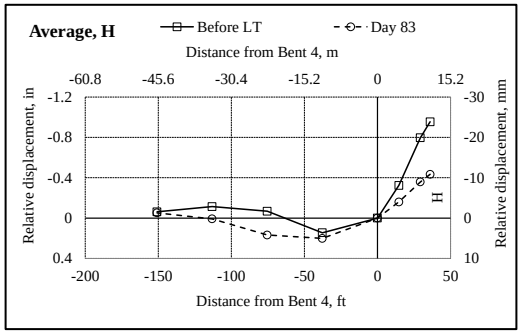


(c)

Figure 4-25 Time-dependent deformation after load transfer at H, Bridge 3: (a) L1 response; (b) L2 response; (c) Average response

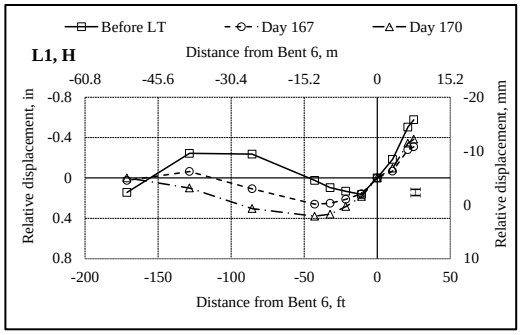


(a)

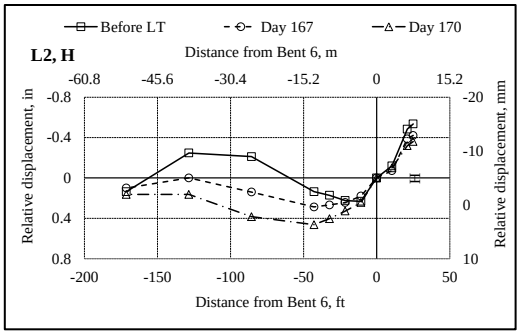


(b)

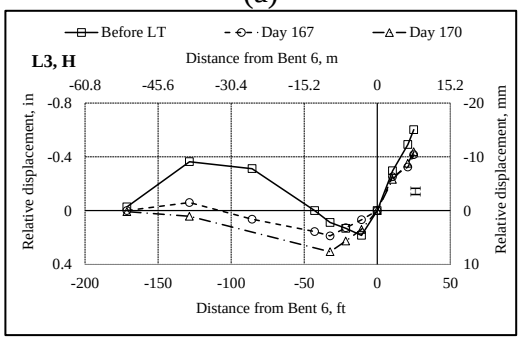


(c)

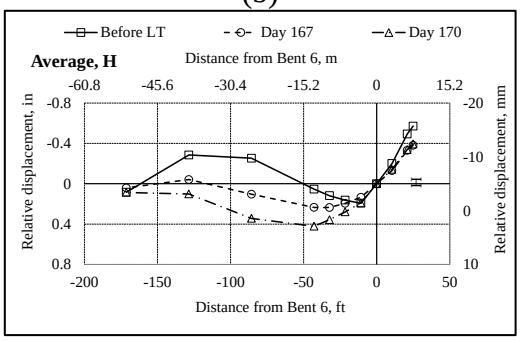


(d)

Figure 4-26 Time-dependent deformation after load transfer at H, Bridge 4: (a) L1 response; (b) L2 response; (c) L3 response; (d) Average response

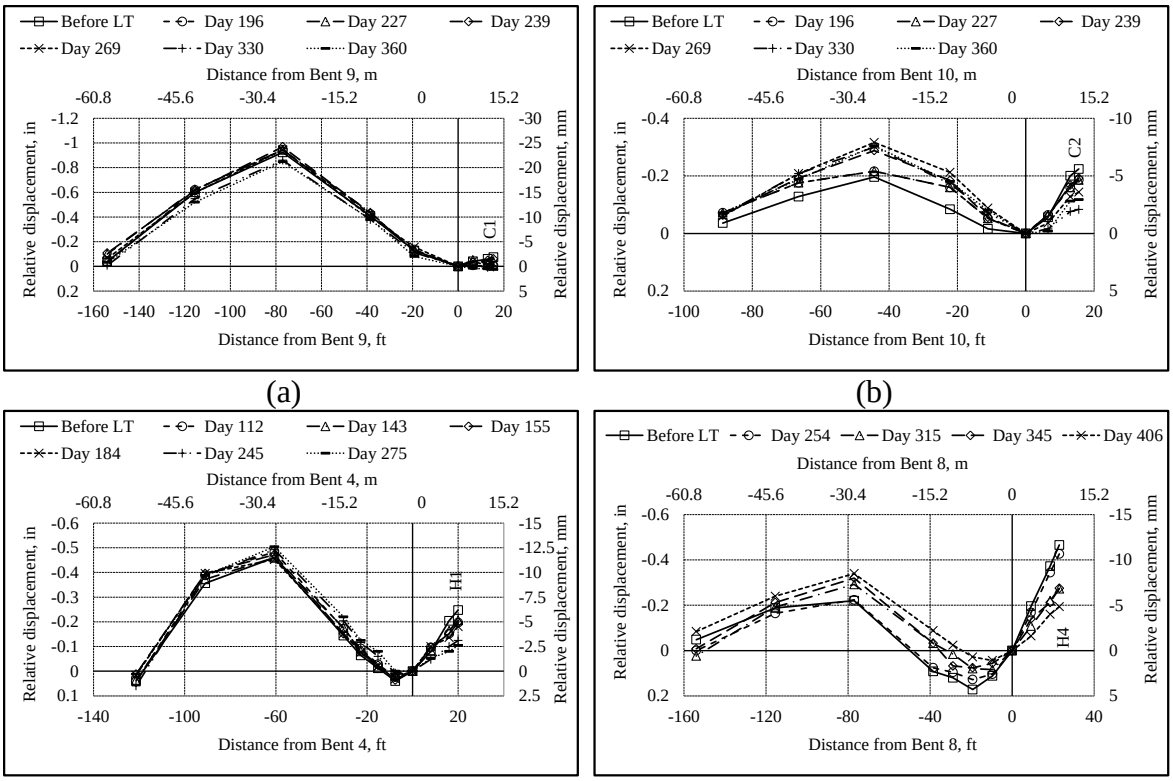


Figure 4-27 Time-dependent deformation after load transfer at the P/S hinges, Bridge 5: (a) C1, Bridge 5EB; (b) C2, Bridge 5EB; (c) H1, Bridge 5EB; (d) H4, Bridge 5WB

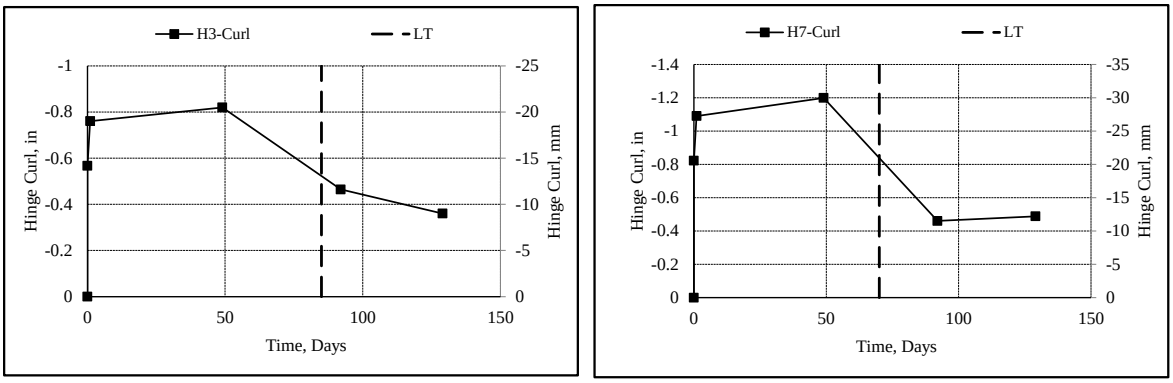


Figure 4-28 Hinge curl history of Bridge 1: (a) Hinge curl at H3; (b) Hinge curl at H7 (LT = load transfer)

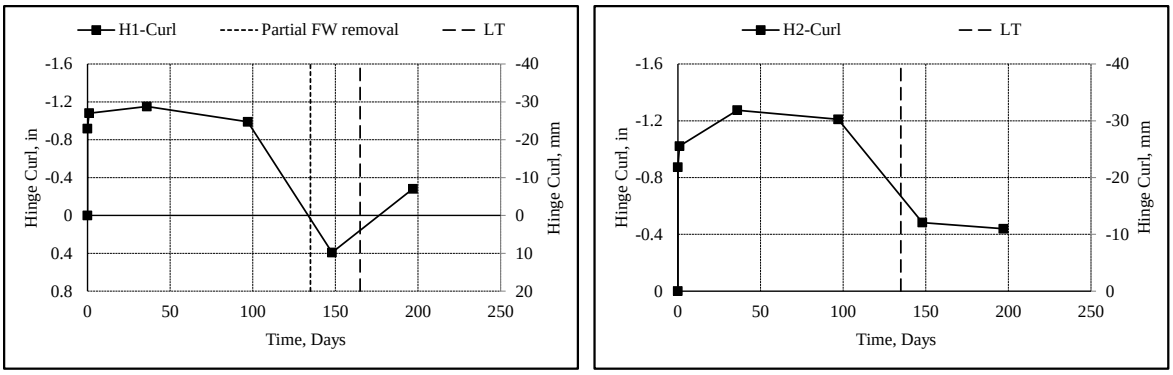


(a) (b)

Figure 4-29 Hinge curl history of Bridge 2 (LT = load transfer): (a) Hinge curl at H1; (b) Hinge curl at H2

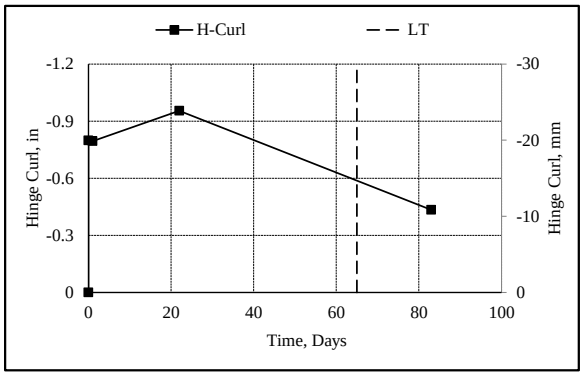


Figure 4-30 Hinge curl history at H, Bridge 3 (LT = load transfer)

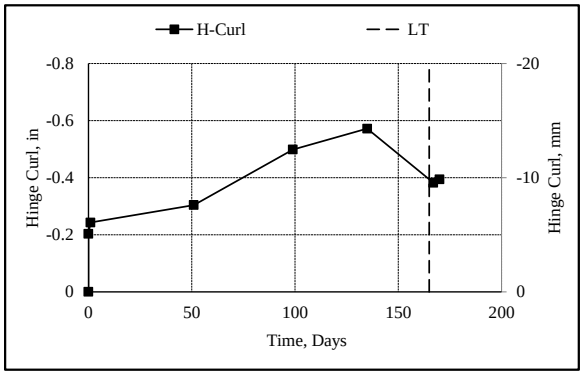


Figure 4-31 Hinge curl history at H, Bridge 4 (LT = load transfer)

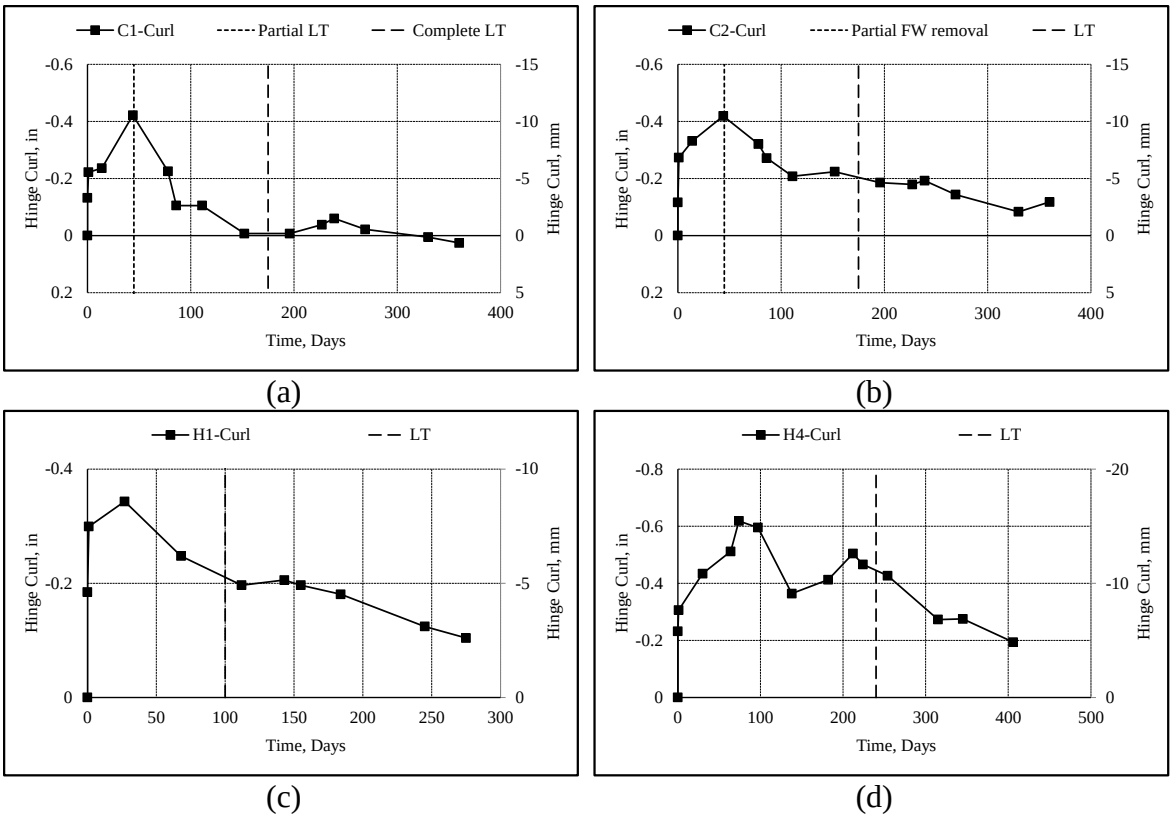


Figure 4-32 Hinge curl history of Bridge 5 (LT = load transfer): (a) Closure 1, Bridge 5EB; (b) Closure 2, Bridge 5EB; (c) Hinge 1 Bridge 5EB; (d) Hinge 4, Bridge 5WB

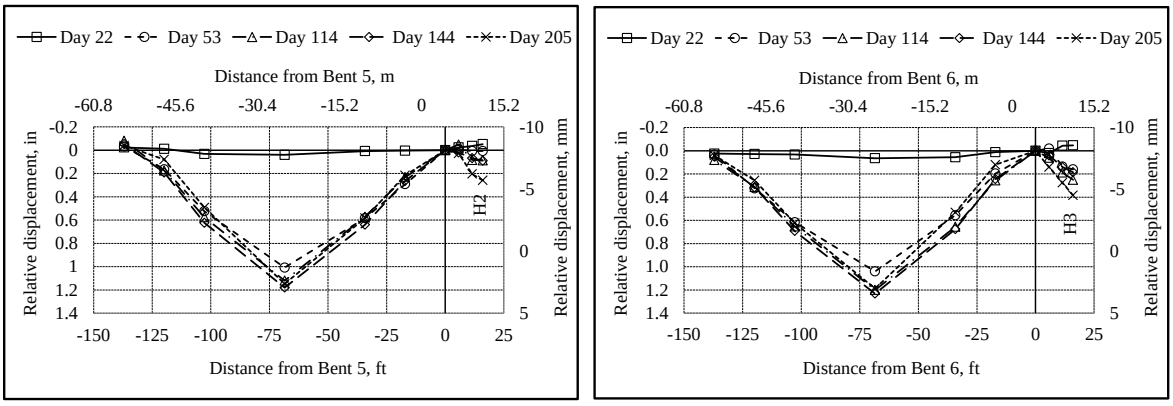


Figure 4-33 Time-dependent deformation at non-PS hinges, Bridge 5WB: (a) H2; (b) H3

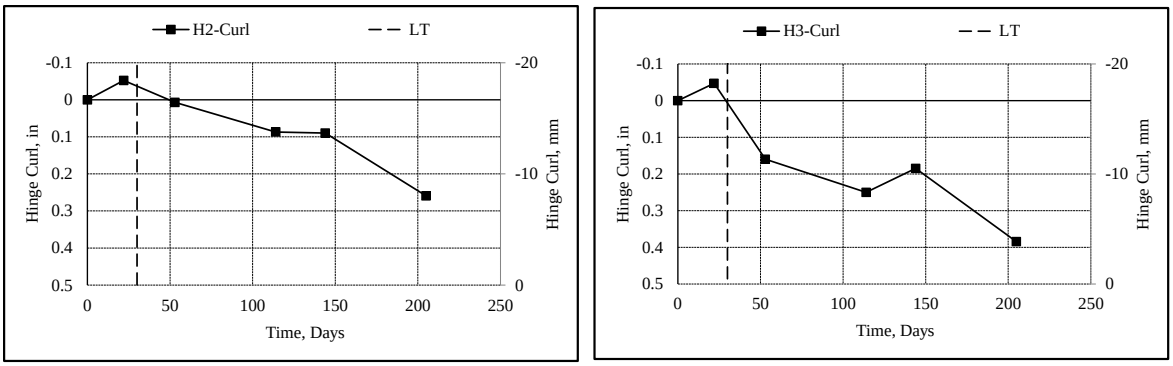


(a) (b)

Figure 4-34 Hinge deformation history of non-PS hinges, Bridge 5WB (LT = load transfer): (a) H2; (b) H3

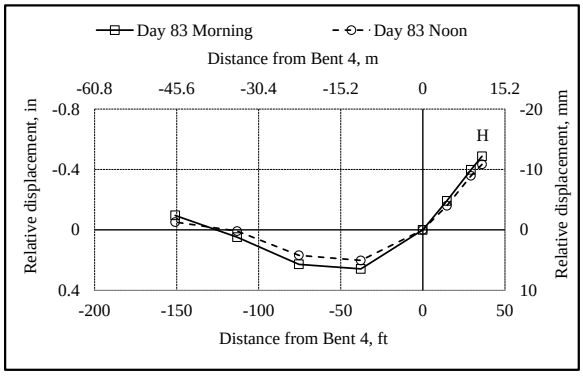


(a)

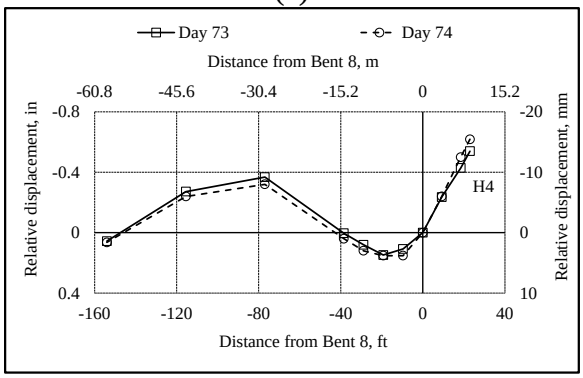


(b)

Figure 4-35 Influence of temperature and relative humidity change on deformation behavior: (a) H, Bridge 3; (b) H4, Bridge 5WB

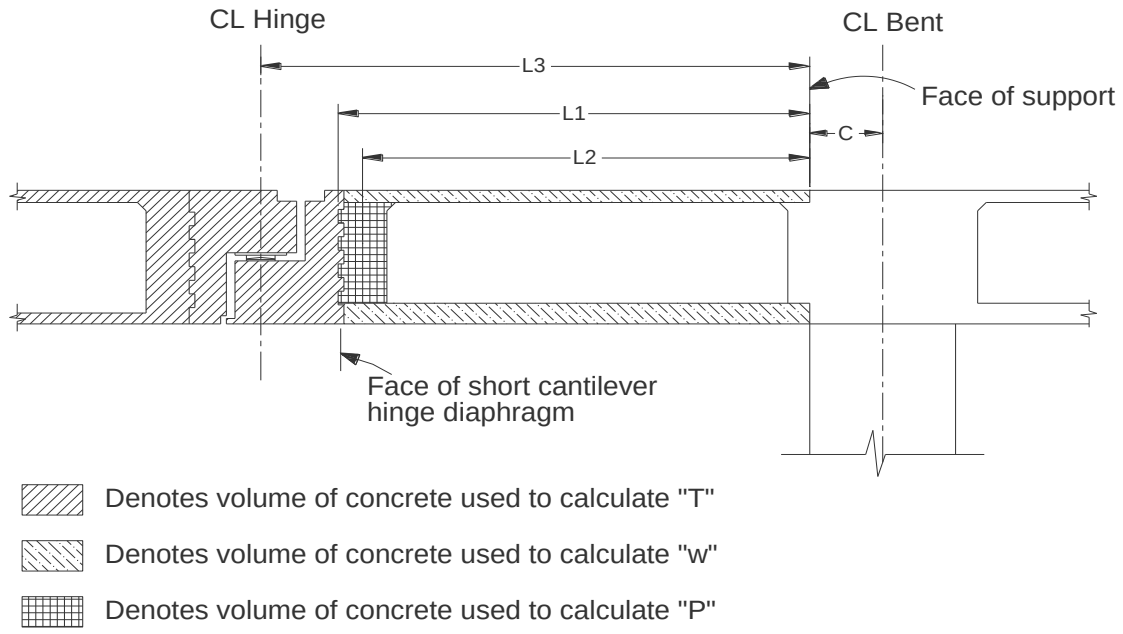


Figure 5-1 Parameters used in calculation of short cantilever deflection under dead load

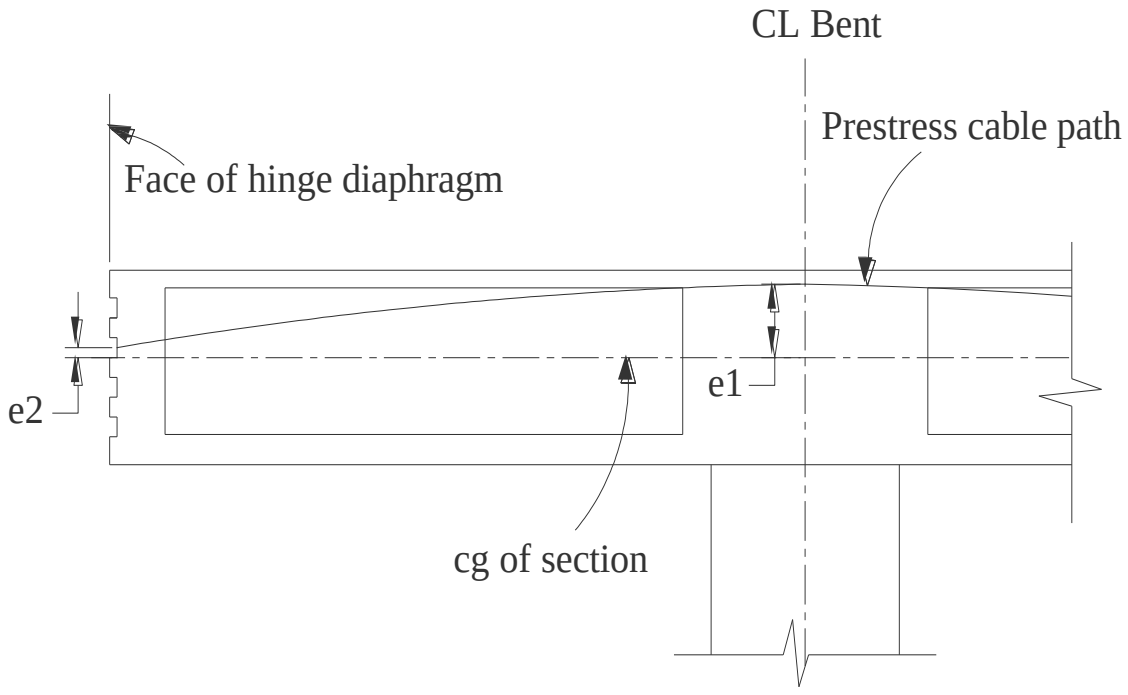


Figure 5-2 Prestress tendon path

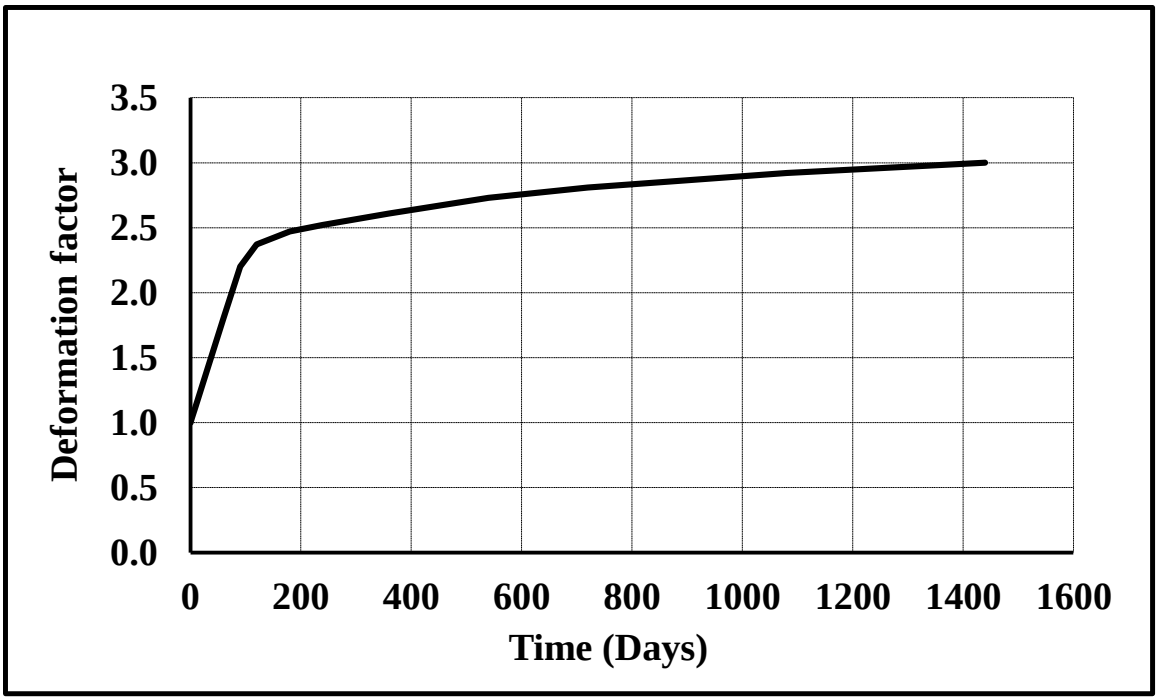


Figure 5-3 MTD 11-34 Deflection factor chart

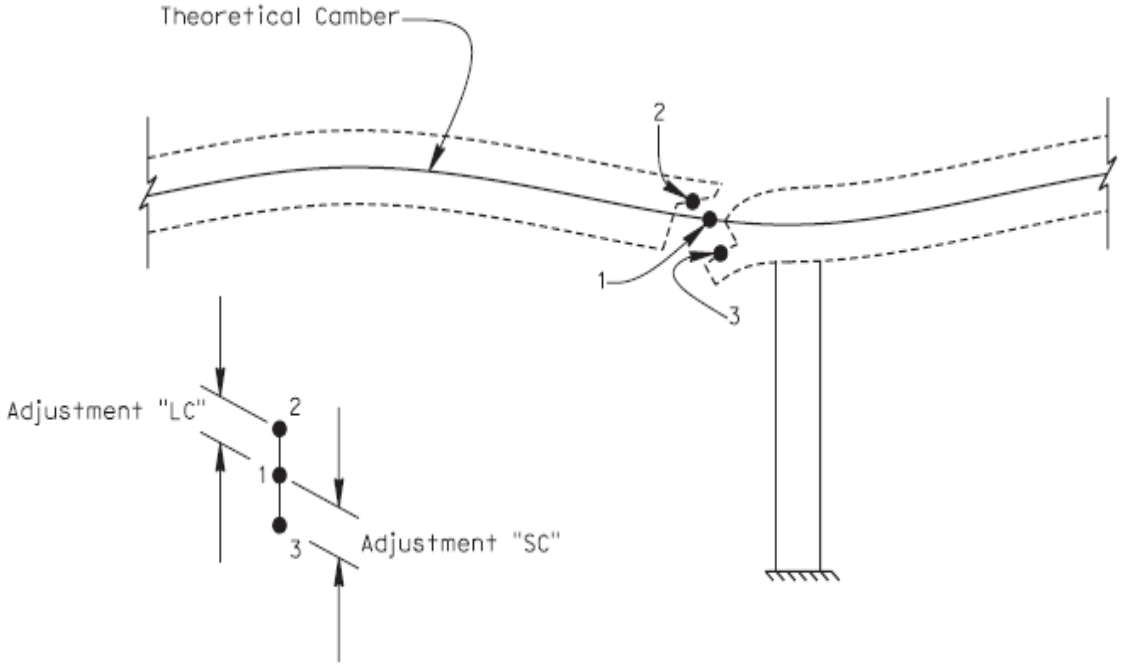


Figure 5-4 Adjustment to theoretical camber

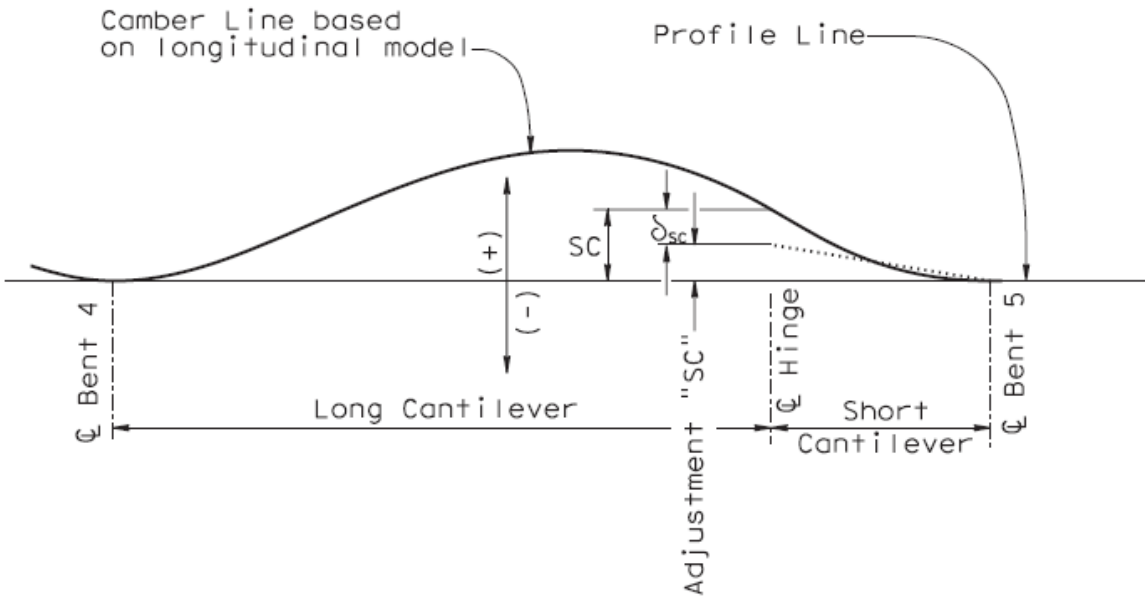


Figure 5-5 Short cantilever camber

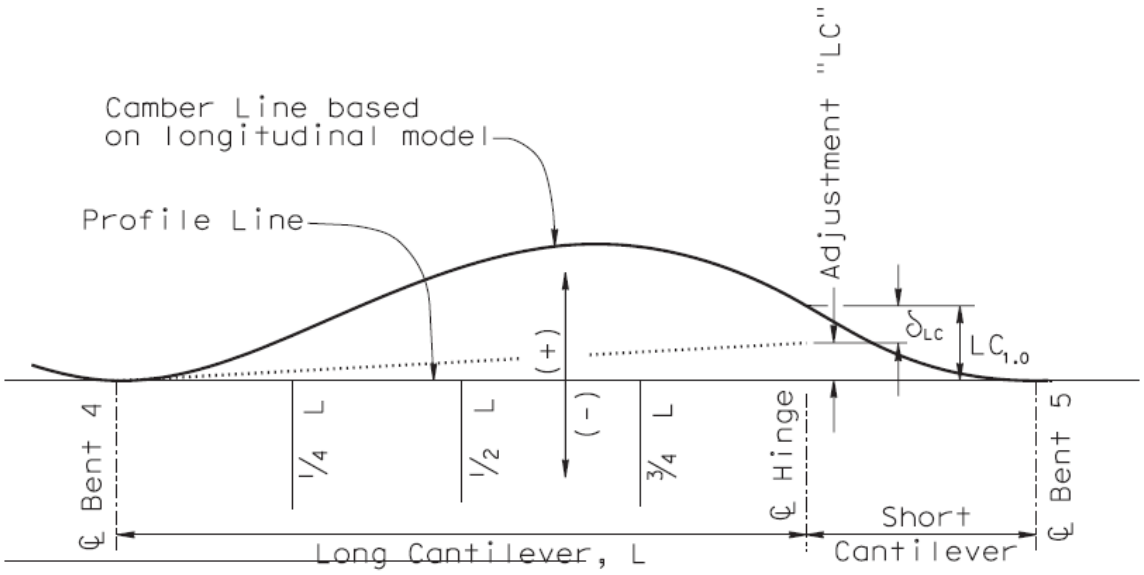


Figure 5-6 Long cantilever camber

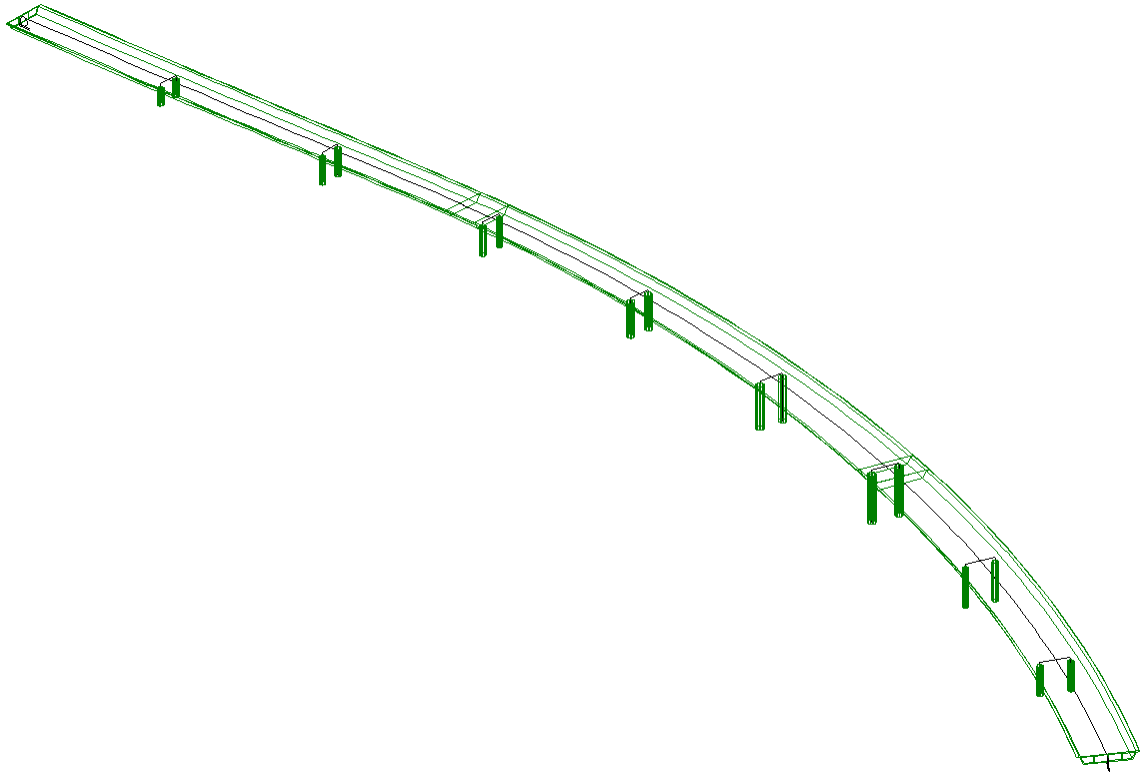

Figure 5-7 Perspective view of Bridge 1 model

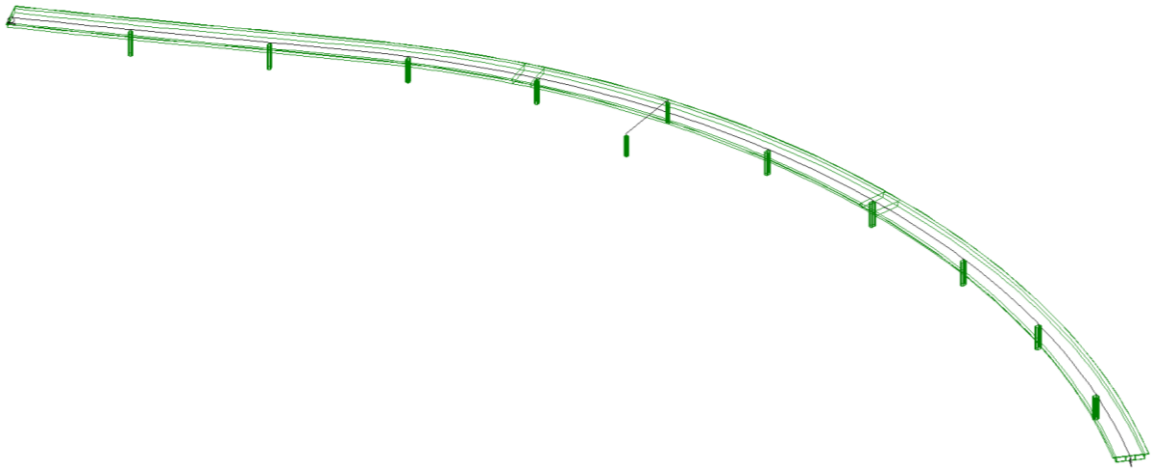

Figure 5-8 Perspective view of Bridge 2 model

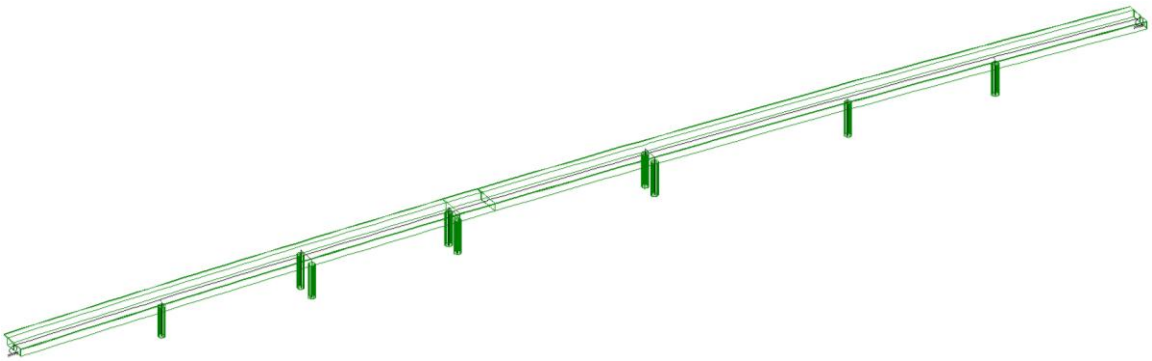

Figure 5-9 Perspective view of Bridge 3 model

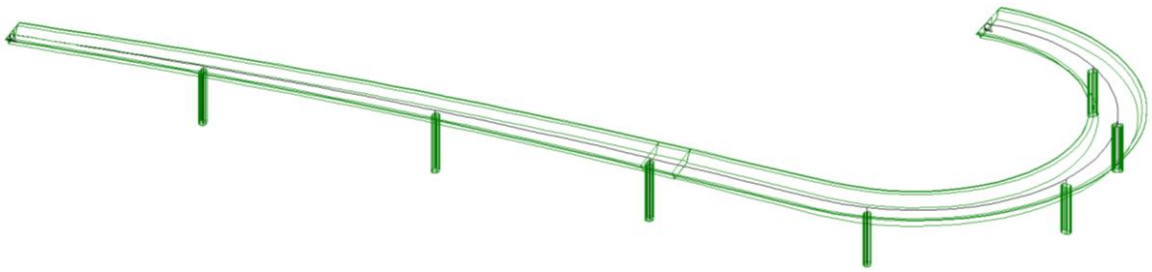

Figure 5-10 Perspective view of Bridge 4 model

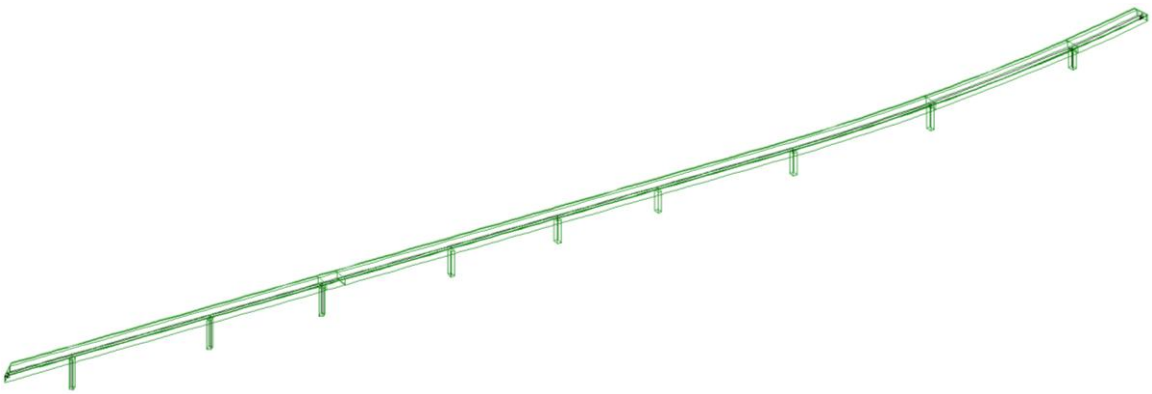

Figure 5-11 Perspective view of Bridge 5EB model

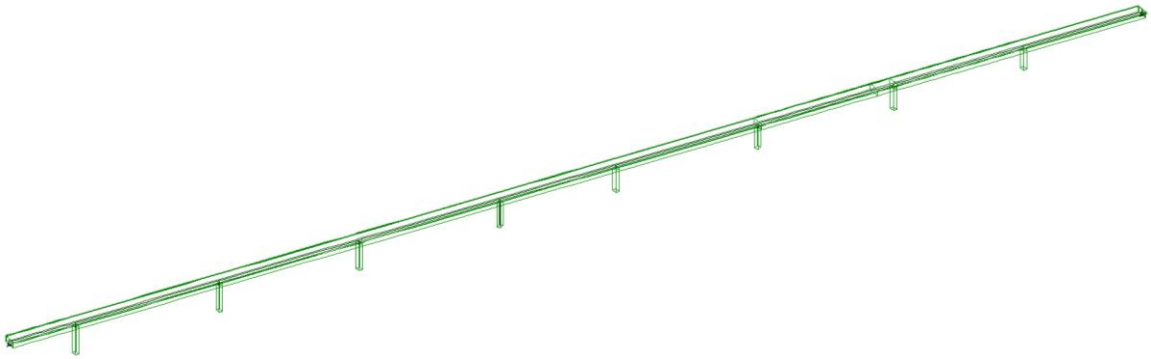

Figure 5-12 Perspective view of Bridge 5WB model

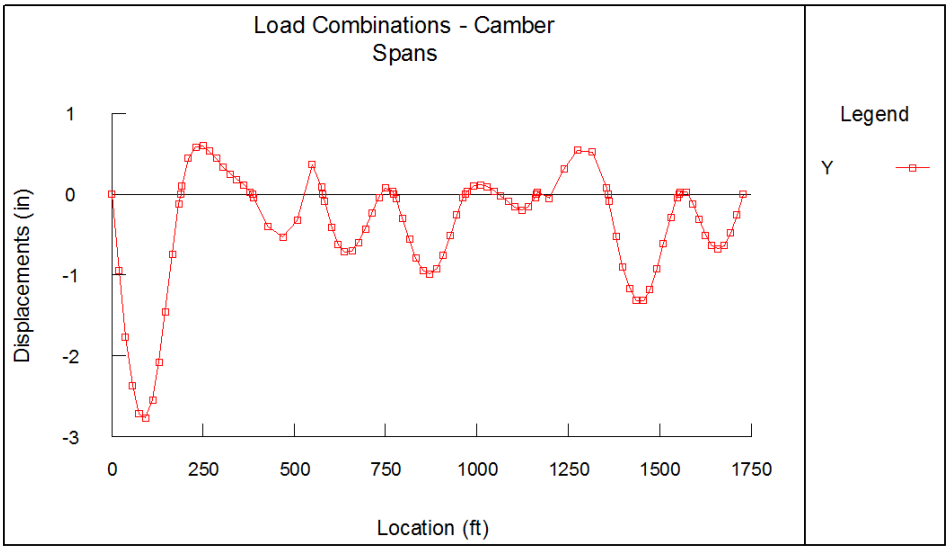


Figure 5-13 Theoretical camber diagram for Bridge 1

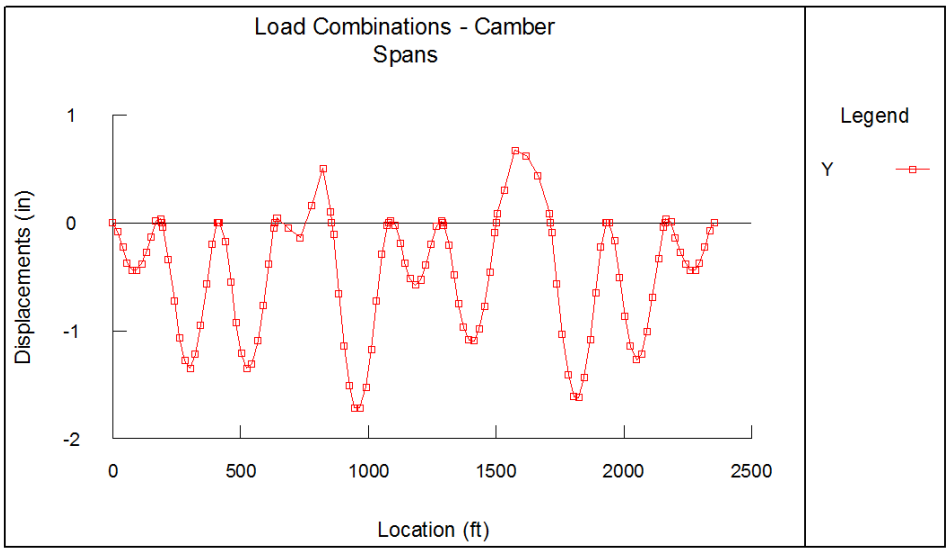


Figure 5-14 Theoretical camber diagram for Bridge 2

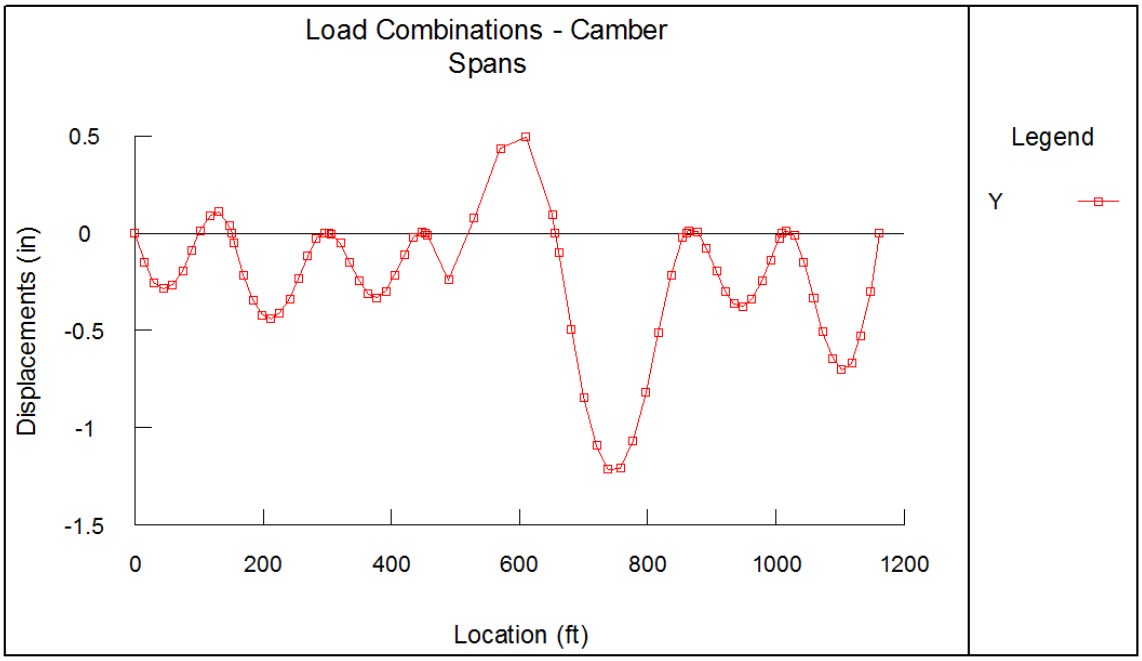


Figure 5-15 Theoretical camber diagram for Bridge 3

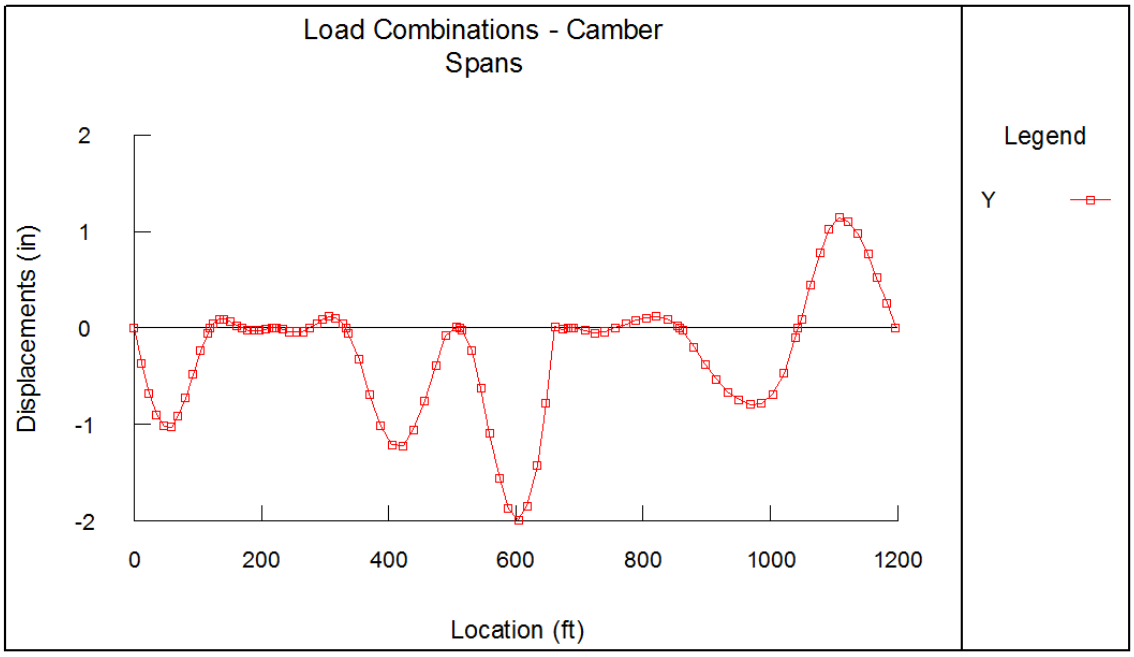


Figure 5-16 Theoretical camber diagram for Bridge 4

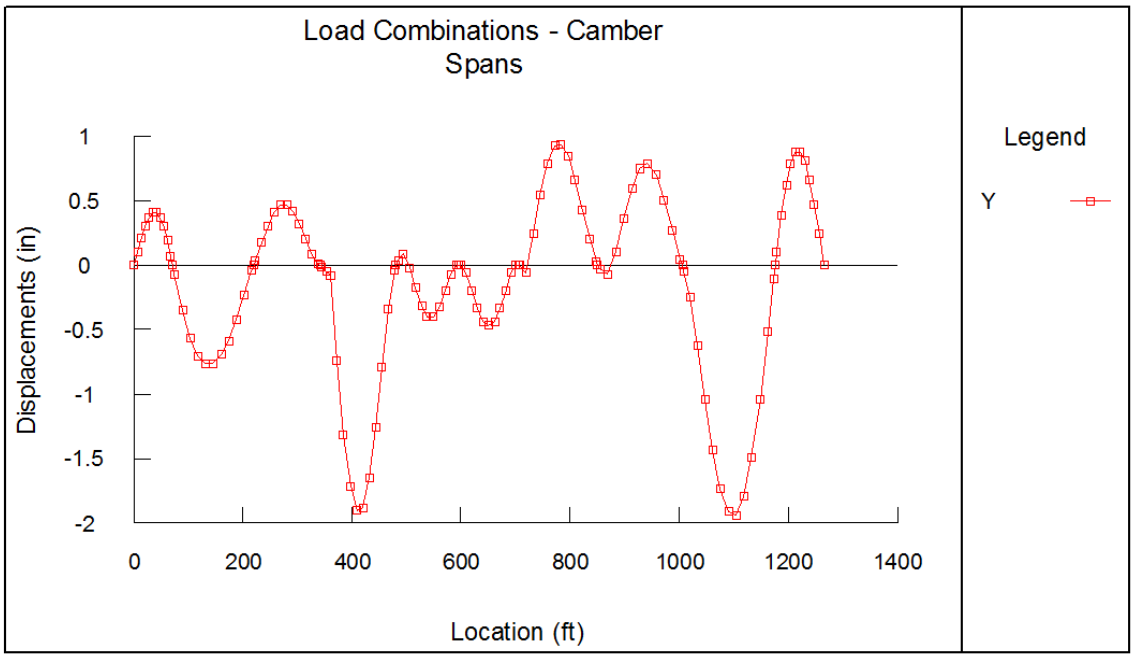


Figure 5-17 Theoretical camber diagram for Bridge 5EB

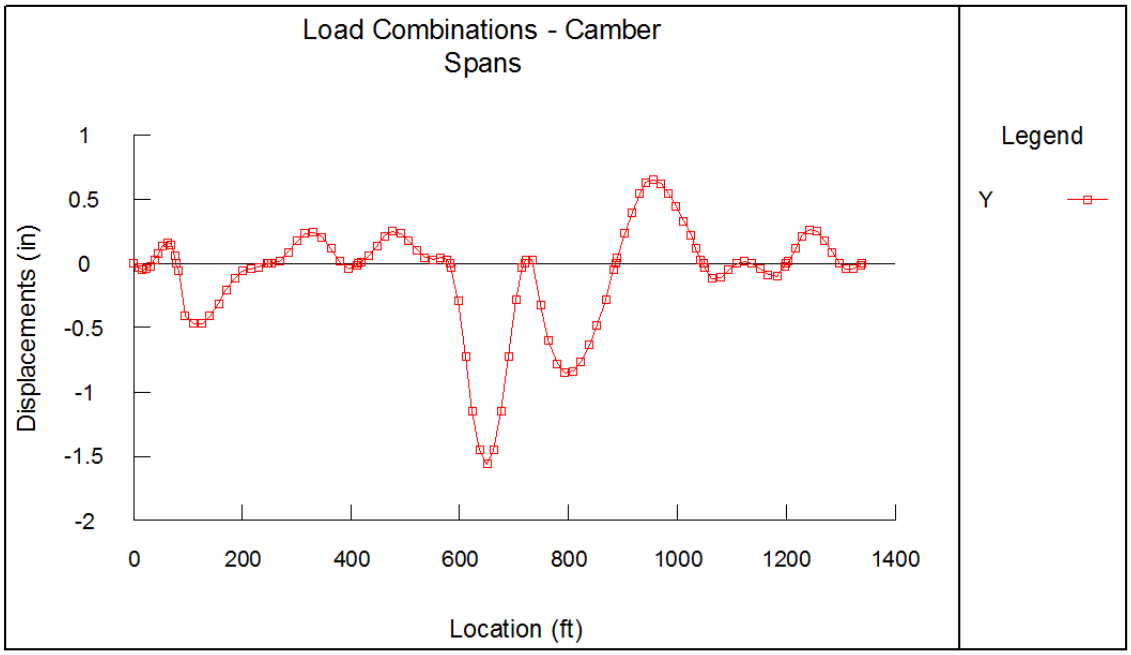


Figure 5-18 Theoretical camber diagram for Bridge 5WB

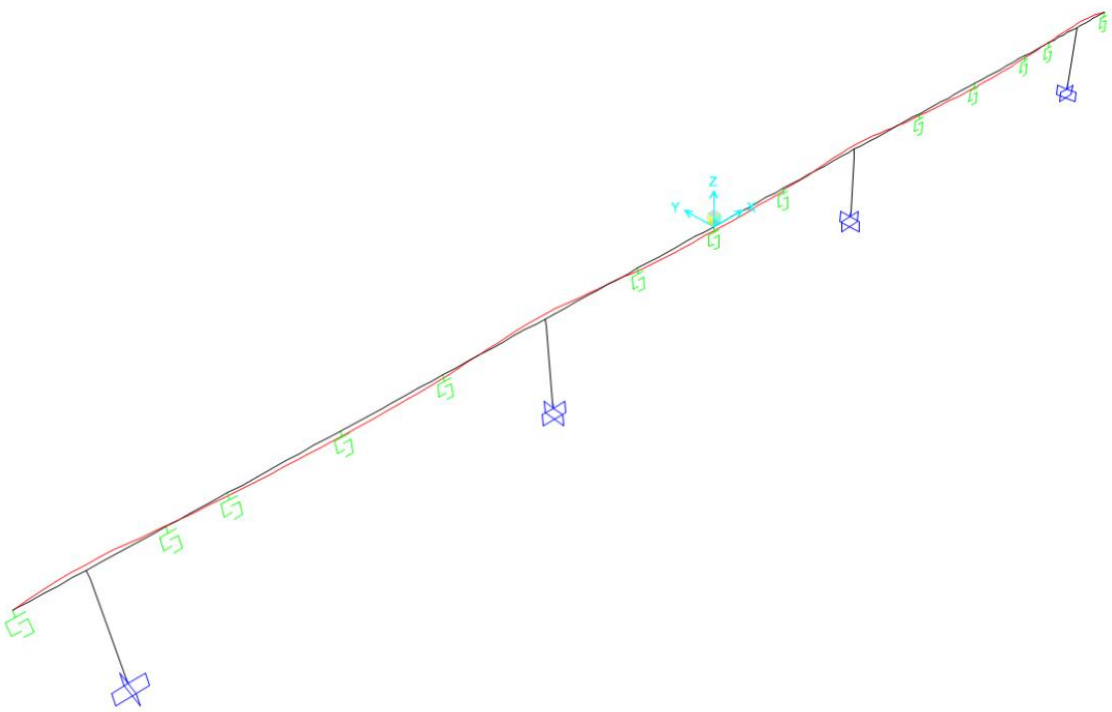


Figure 6-1 3-D view of SAP2000 model for Frame 2, Bridge 1

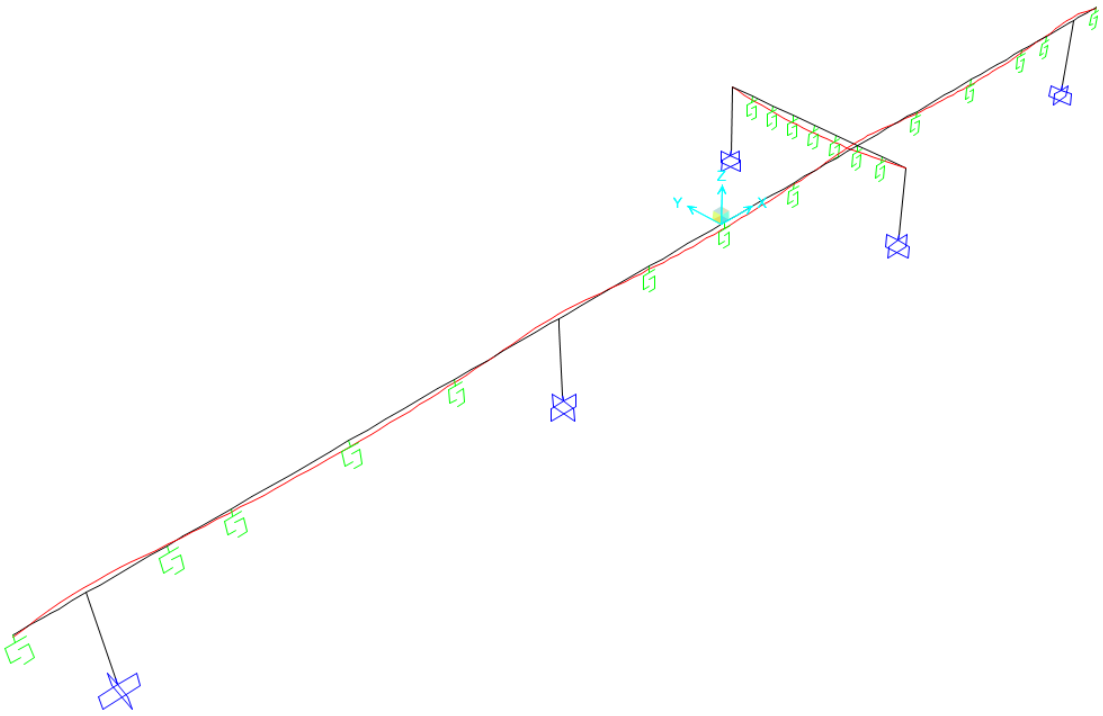


Figure 6-2 3-D view of SAP2000 model for Frame 2, Bridge 2

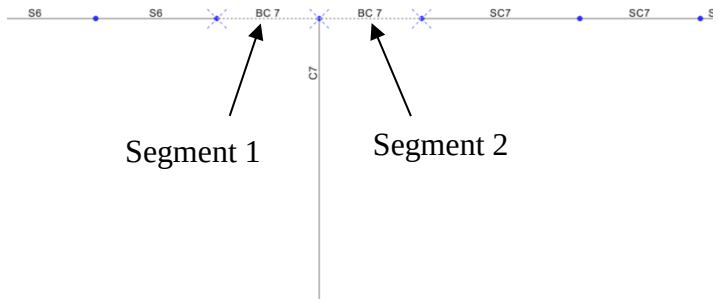


Figure 6-3 Bent cap modelling

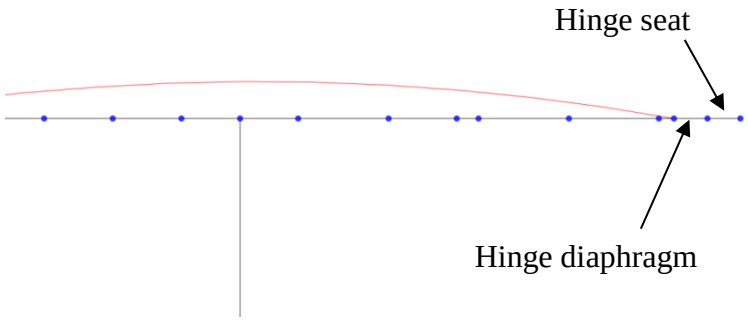


Figure 6-4 Modelling of an in-span hinge of a prestressed frame

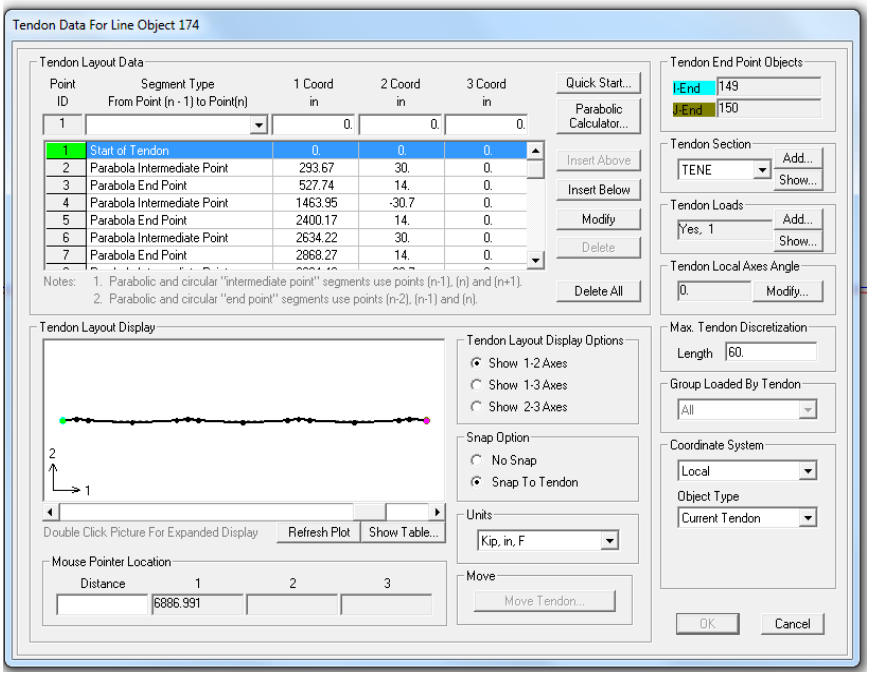


Figure 6-5 Typical tendon layout data in SAP2000


Figure 6-6 Typical pattern of falsework springs in a frame

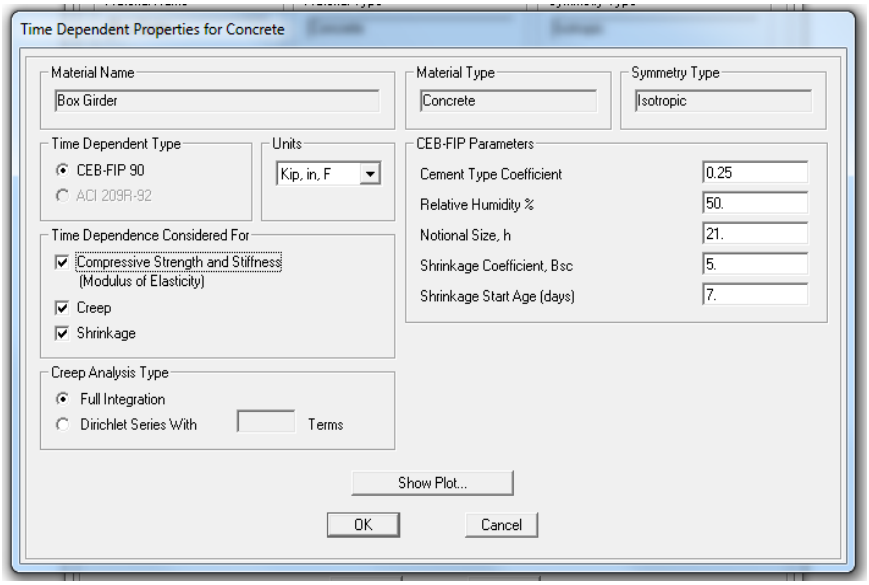


Figure 6-7 SAP2000 parameters for time-dependent properties of concrete

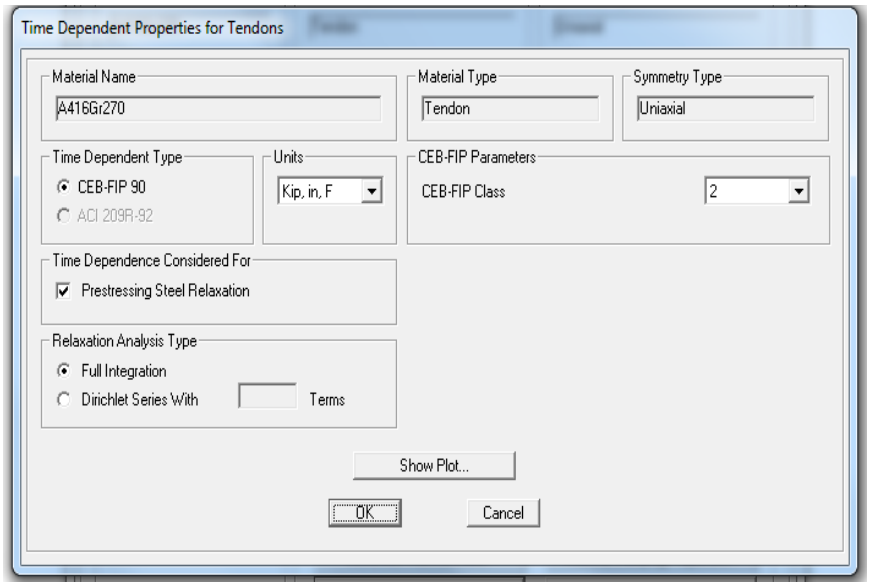


Figure 6-8 Time-dependent properties for prestressing steel

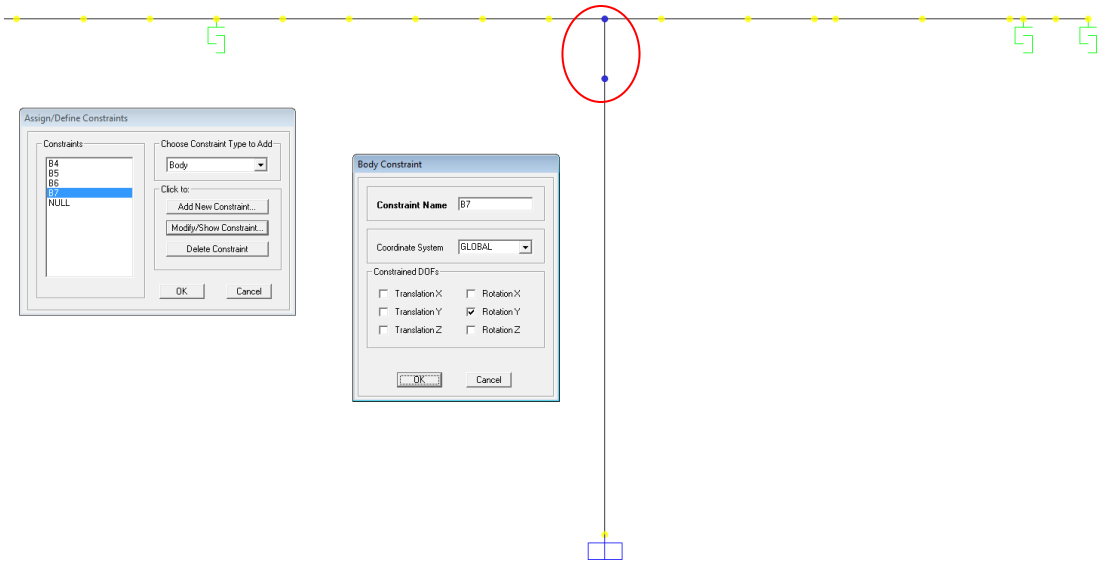


Figure 6-9 Body constraint at the column-cap beam connection

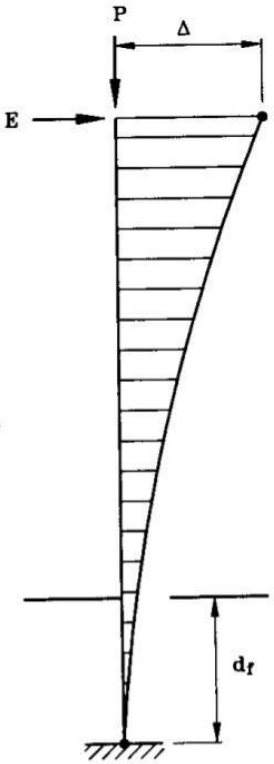


Figure 6-10 Equivalent Fixity Model (Caltrans 2014)

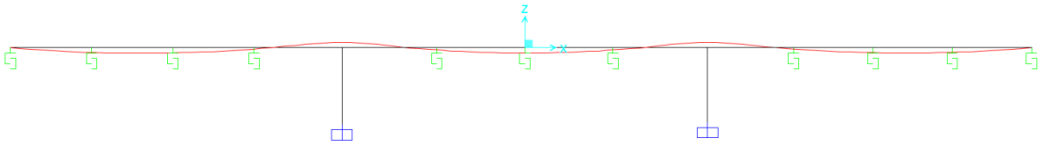

(a)

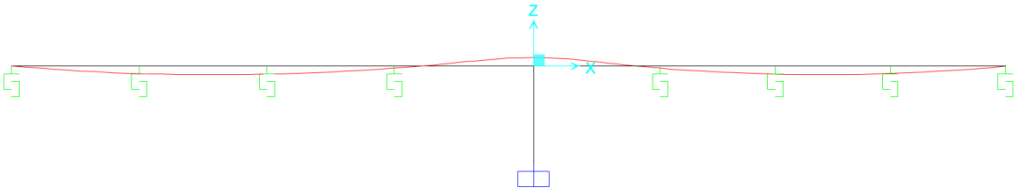

(b)

Figure 6-11 SAP models for prestressed frames including the long cantilevers : (a) Frame 2, Bridge 5WB; (b) Frame 4, Bridge 5WB

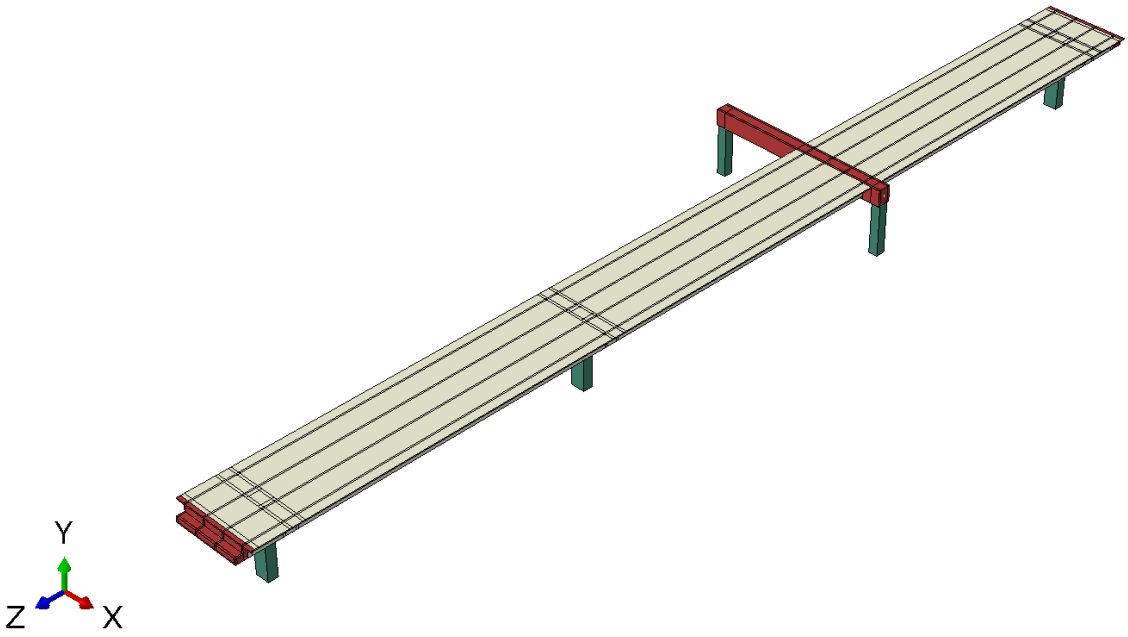


Figure 7-1 3D view of a typical ABAQUS model (Frame 2, Bridge 2)

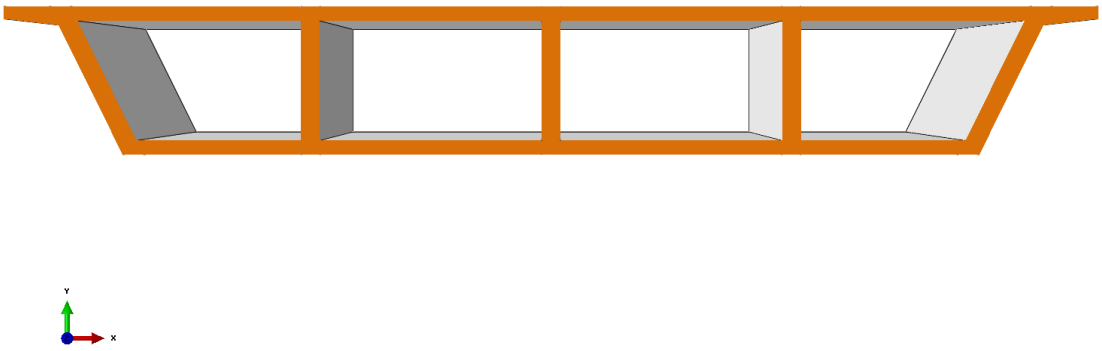

Figure 7-2 Perspective view of a typical box-girder cross-section modeled in ABAQUS

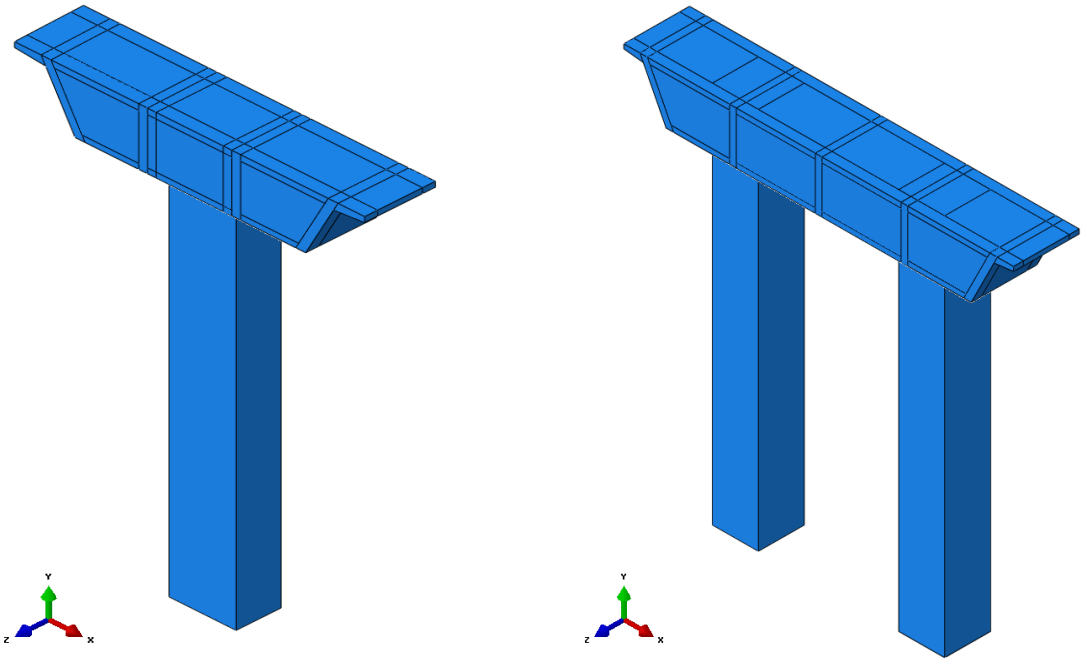

Figure 7-3 Single and two-column bents with equivalent  column sections

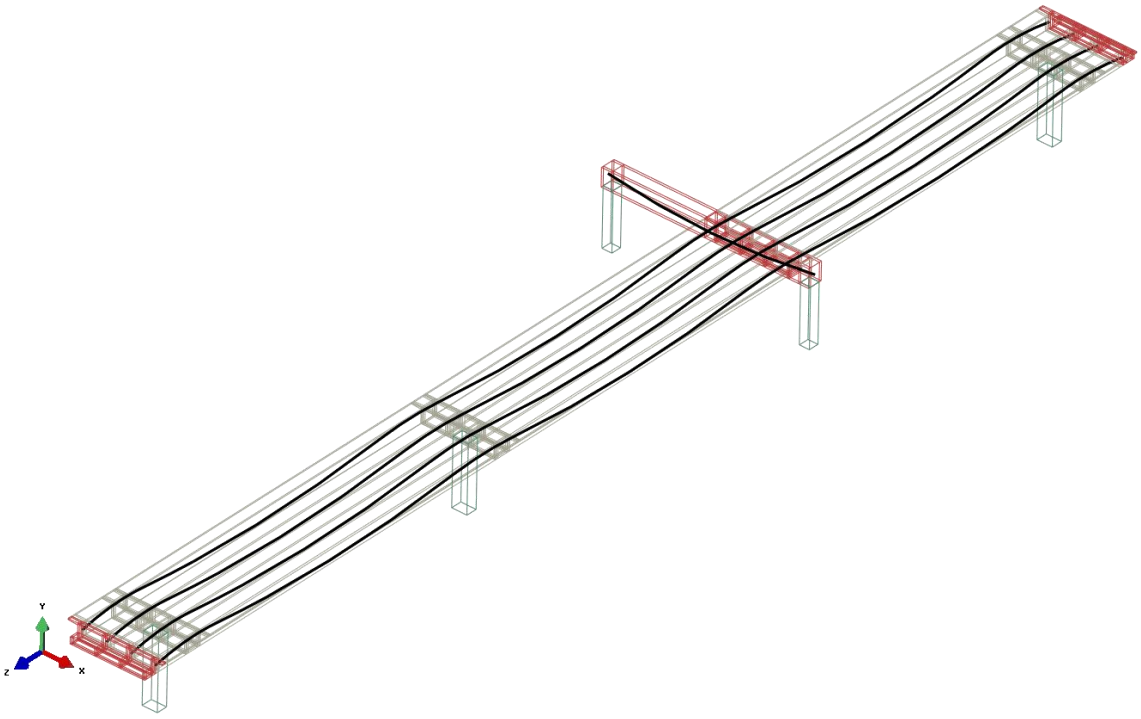

Figure 7-4 Longitudinal and transverse equivalent prestressing tendons within the superstructure

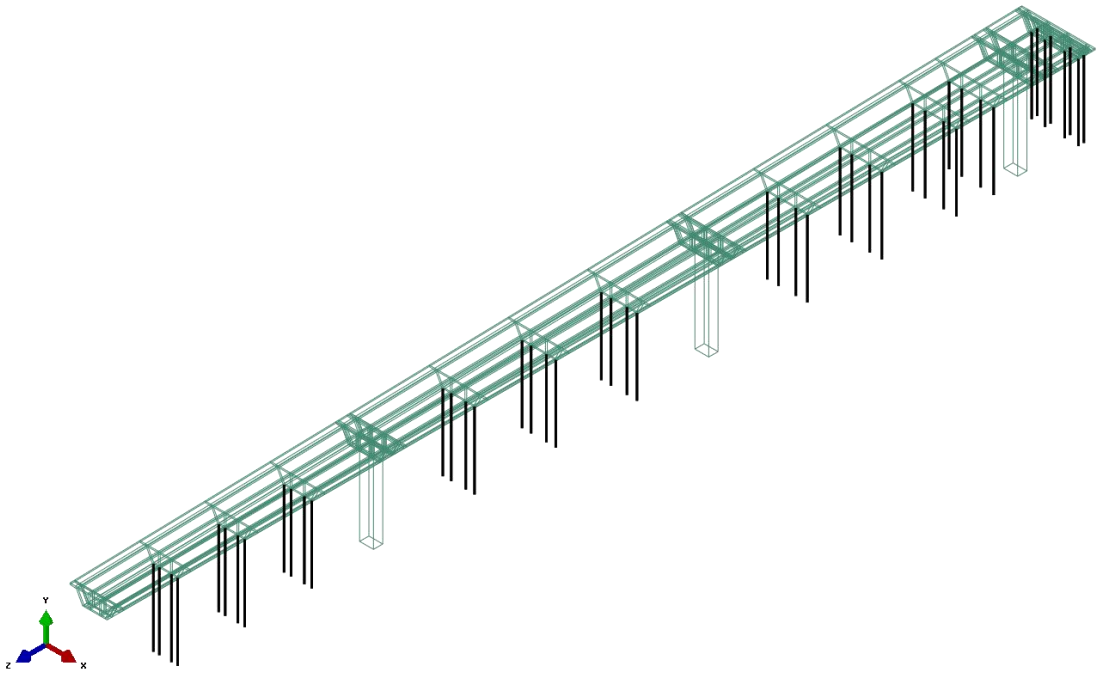

Figure 7-5 A typical pattern of falsework arrangement in FE models

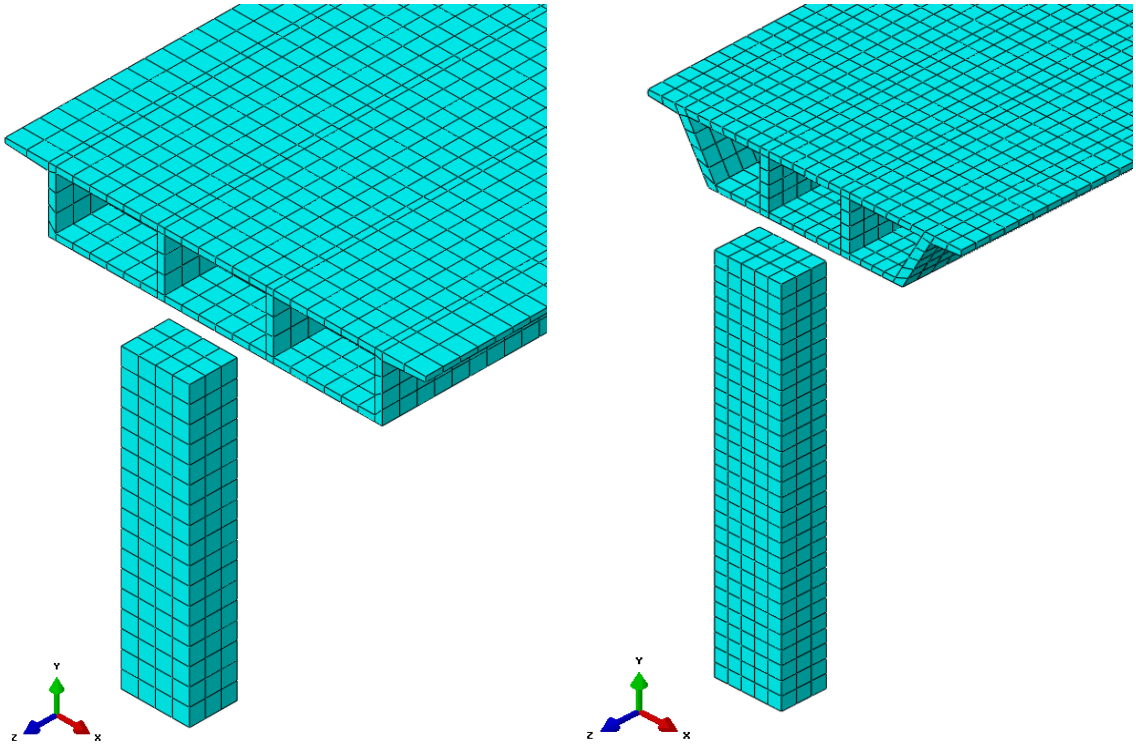

(a) (b)

Figure 7-6 Typical meshing schemes with mesh sizes: (a) 2.5 ft; (b) 1.67 ft

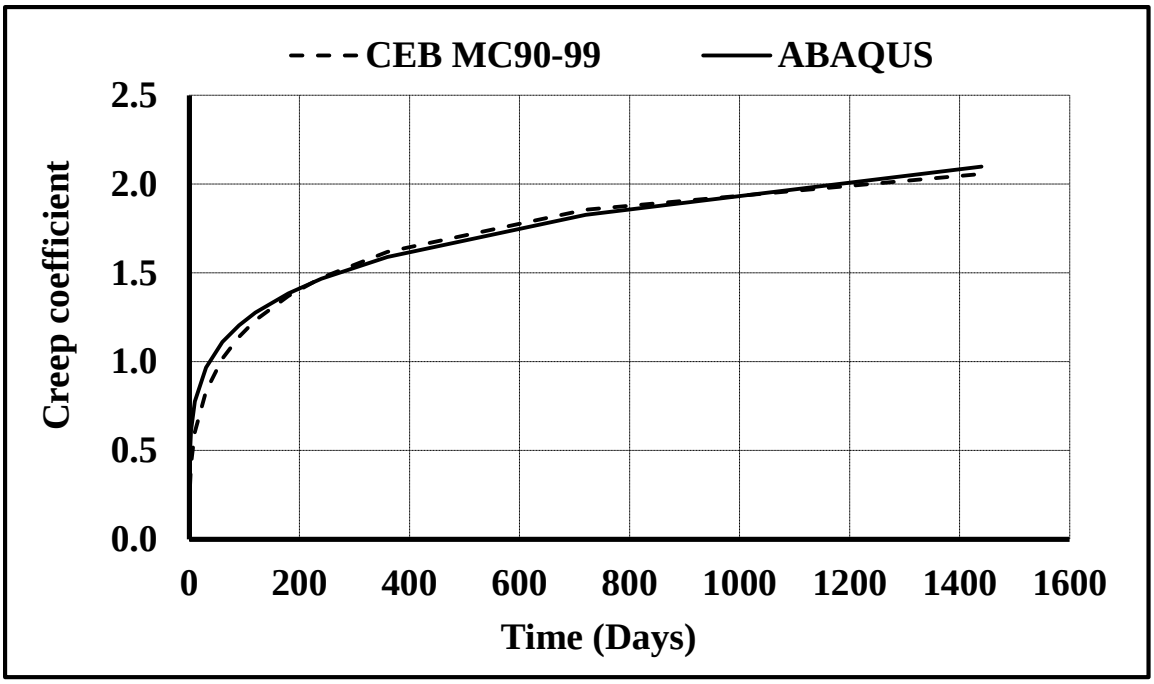


Figure 7-7 Curve fitting for creep coefficient predictions

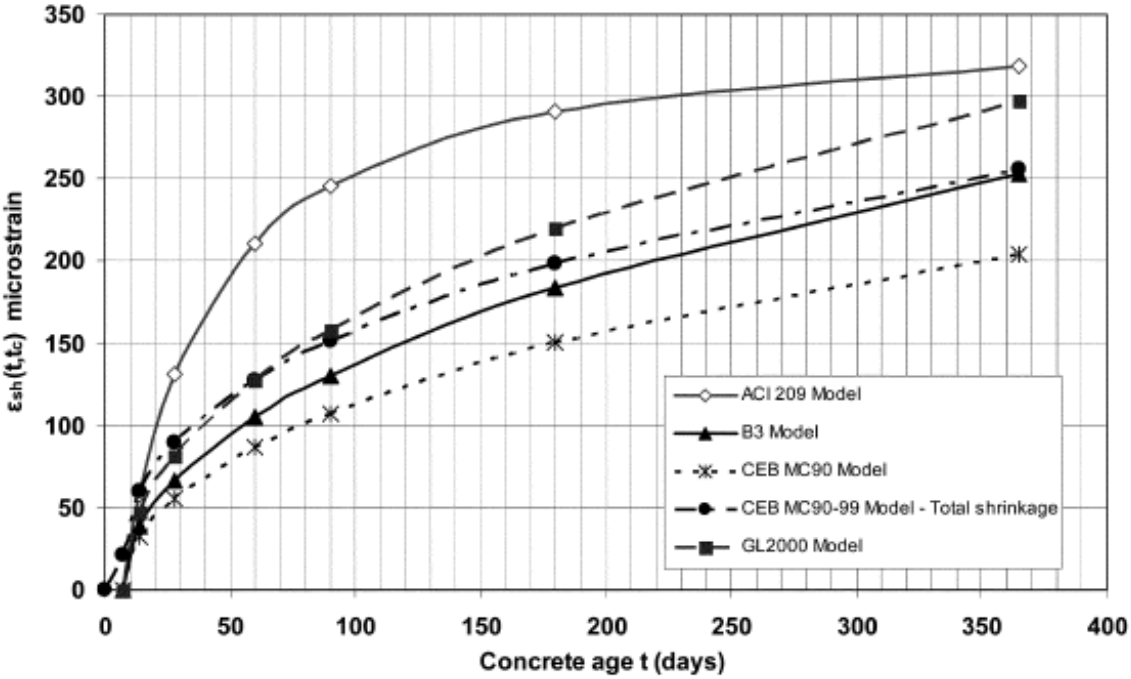


Figure 7-8 Shrinkage strain predictions using different models (ACI 2008)

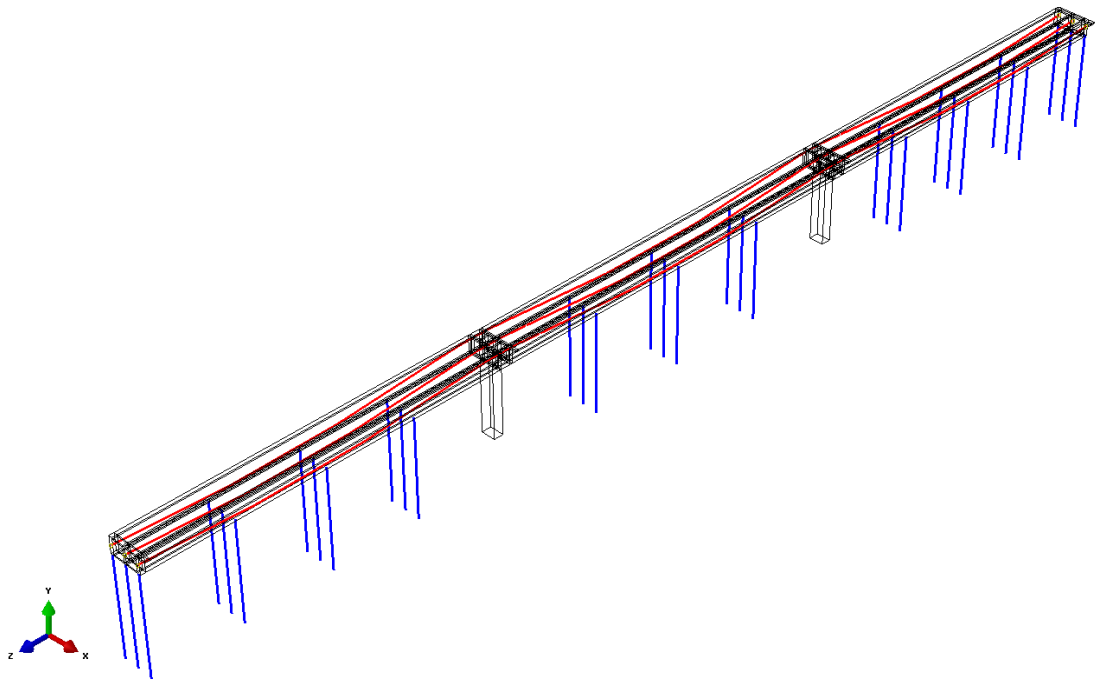

(a)

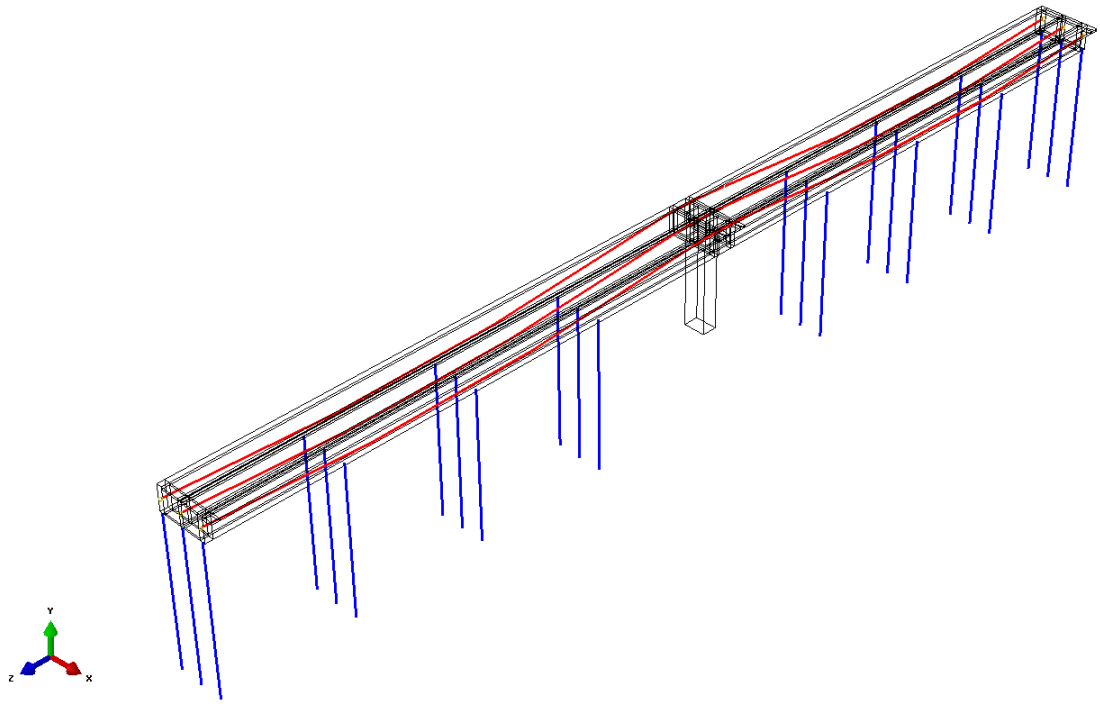

(b)

Figure 7-9 ABAQUS models for prestressed frames including the long cantilevers: (a) Frame 2, Bridge 5WB; (b) Frame 4, Bridge 5WB

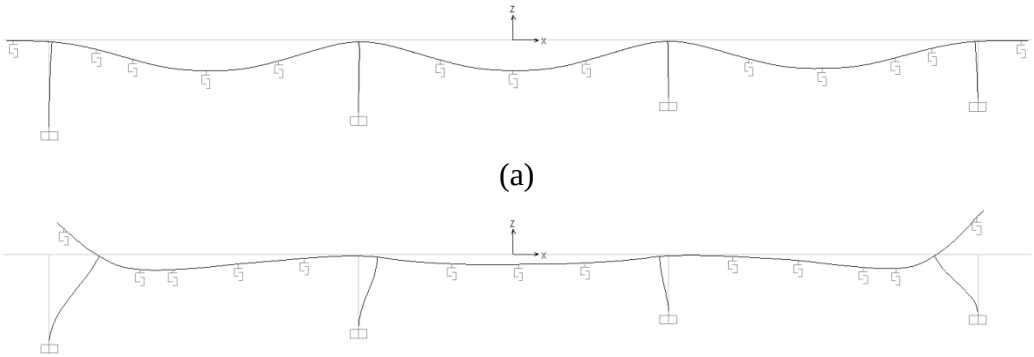

(a)

(b)

Figure 8-1 Deformed shapes of Frame 2, Bridge 1 (SAP2000): (a) Before stressing; (b) Immediately after stressing

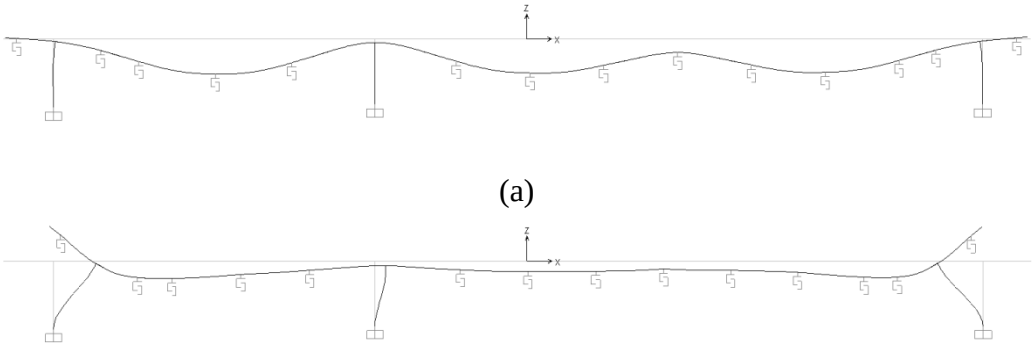

(a)

(b)

Figure 8-2 Deformed shapes of Frame 2, Bridge 2 (SAP2000): (a) Before stressing; (b) Immediately after stressing

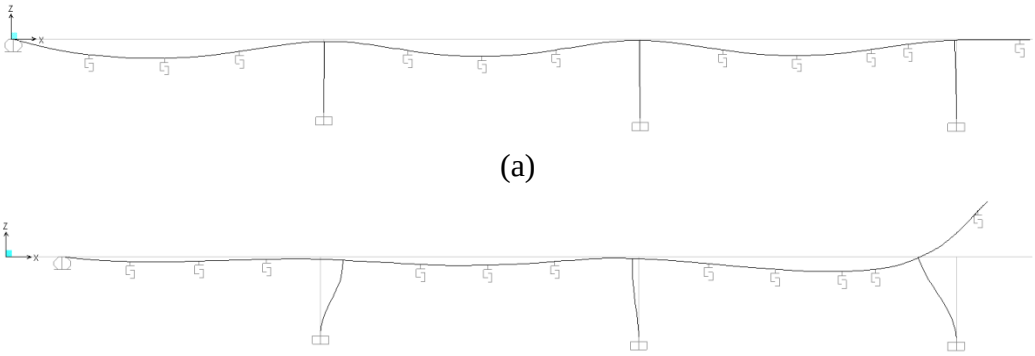

(a)

(b)

Figure 8-3 Deformed shapes of Frame 1, Bridge 3 (SAP2000): (a) Before stressing; (b) Immediately after stressing

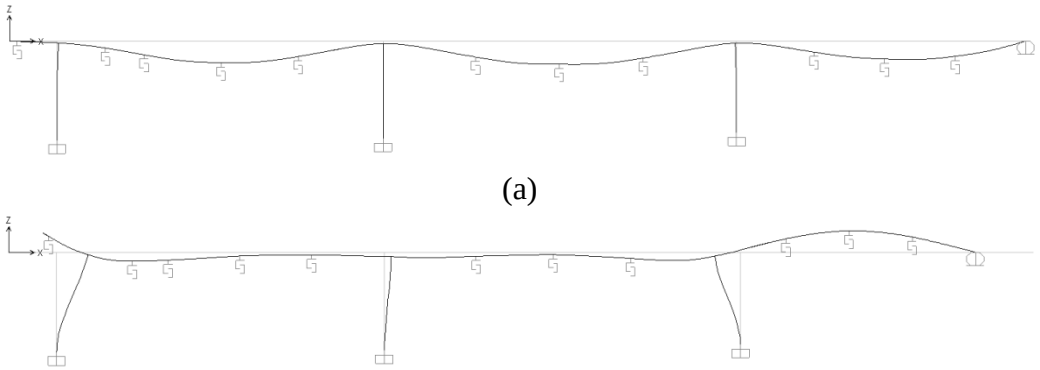

(a)

(b)

Figure 8-4 Deformed shapes of Frame 2, Bridge 4 (SAP2000): (a) Before stressing; (b) Immediately after stressing

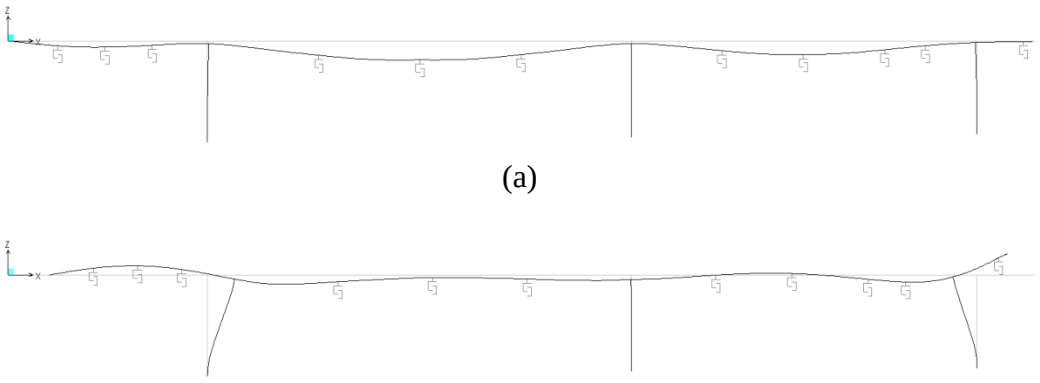

(a)

(b)

Figure 8-5 Deformed shapes of F1EB, Bridge 5 (SAP2000): (a) Before stressing; (b) Immediately after stressing

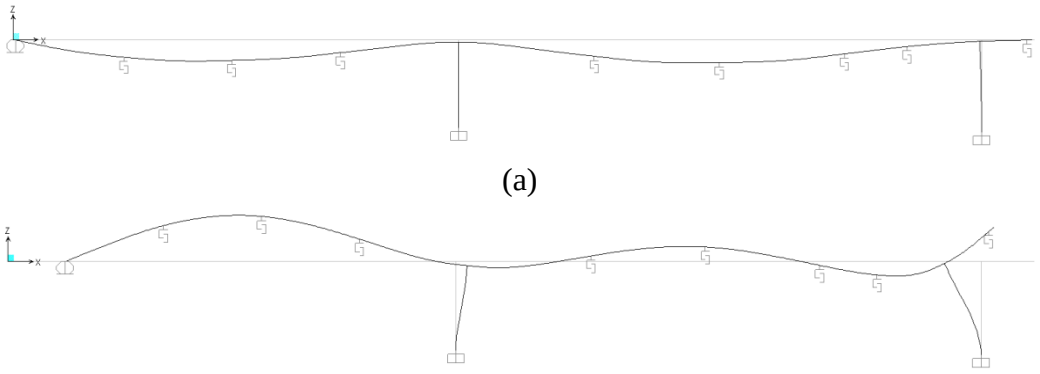

(a)

(b)

Figure 8-6 Deformed shapes of F3EB (Segment A), Bridge 5 (SAP2000): (a) Before stressing; (b) Immediately after stressing

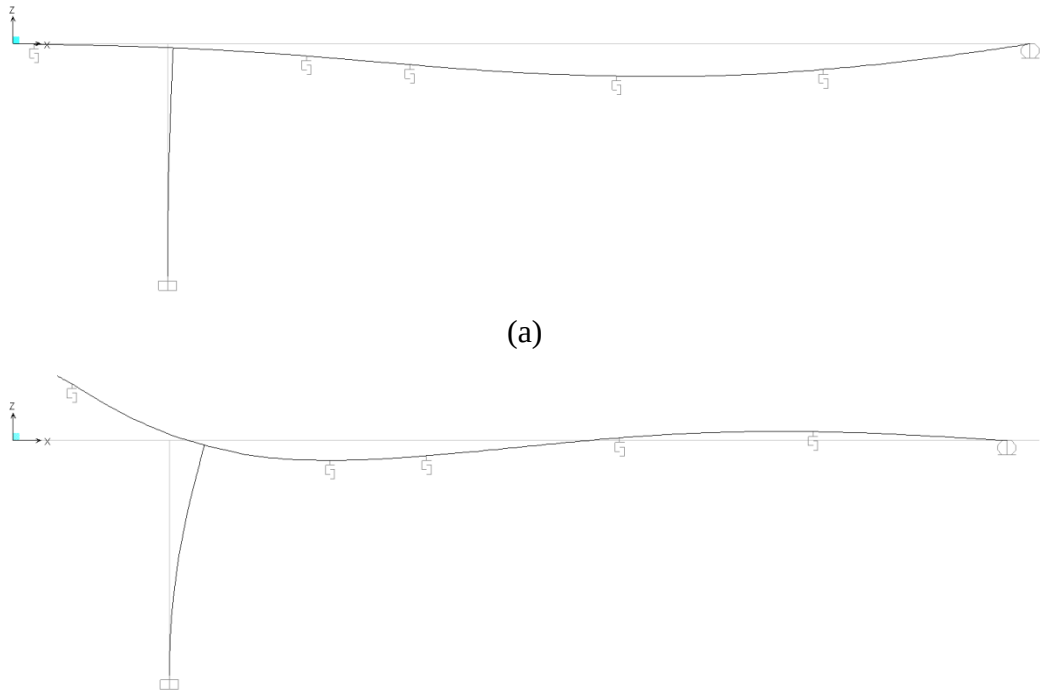

(a)

(b)

Figure 8-7 Deformed shapes of F3EB (Segment C), Bridge 5 (SAP2000): (a) Before stressing; (b) Immediately after stressing

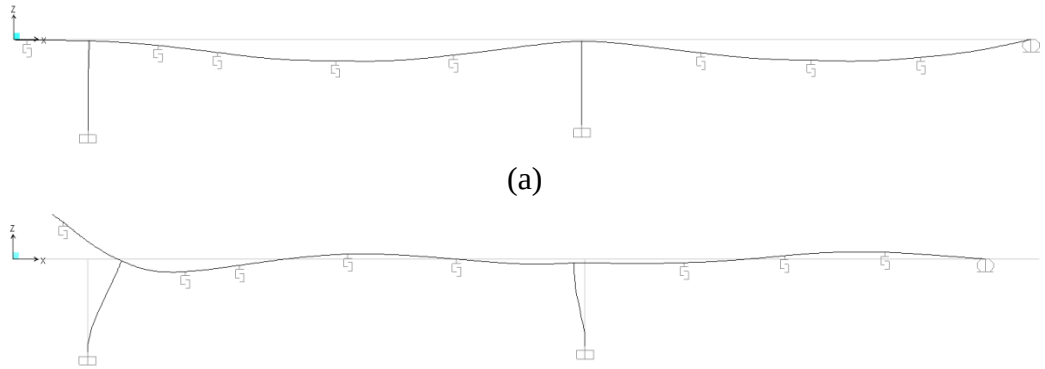

(a)

(b)

Figure 8-8 Deformed shapes of F5WB, Bridge 5 (SAP2000): (a) Before stressing; (b) Immediately after stressing

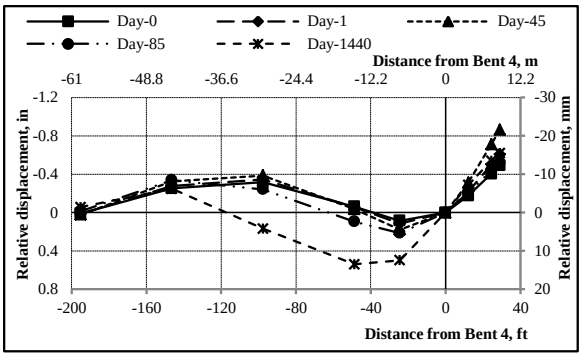


(a)

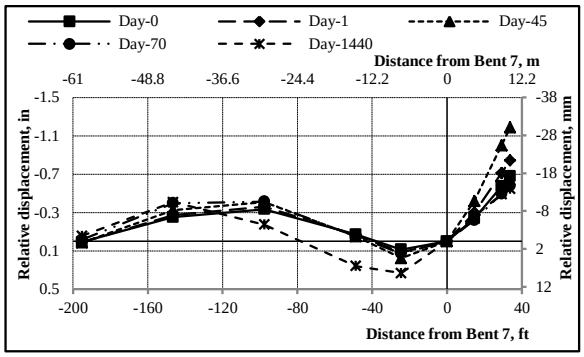


(b)

Figure 8-9 SAP2000 deflections of Bridge 1: (a) at H3; (b) at H7

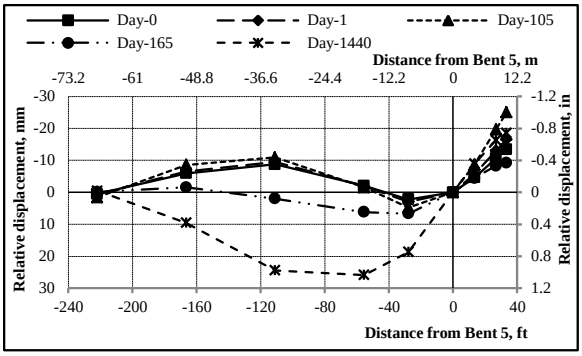


(a)

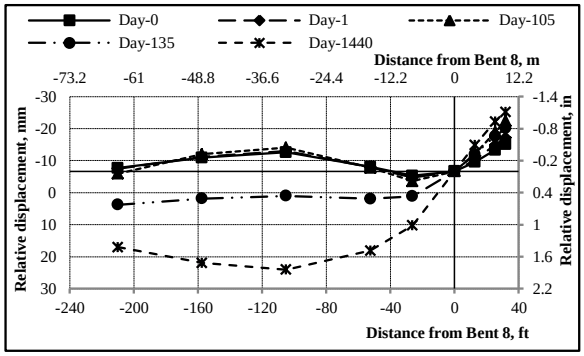


(b)

Figure 8-10 SAP2000 deflections of Bridge 2: (a) at H1; (b) at H2

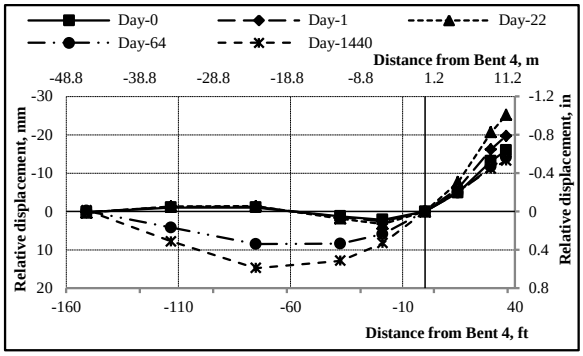


Figure 8-11 SAP2000 deflections of Bridge 3 at Hinge

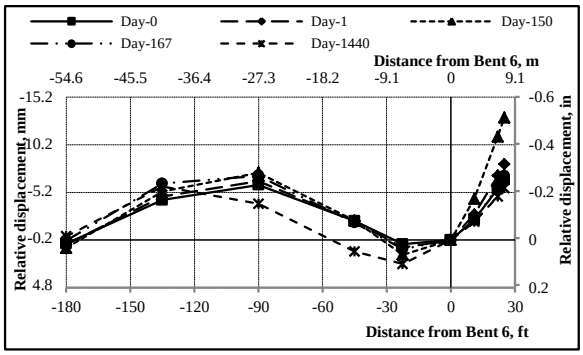


Figure 8-12 SAP2000 deflections of Bridge 4 at Hinge

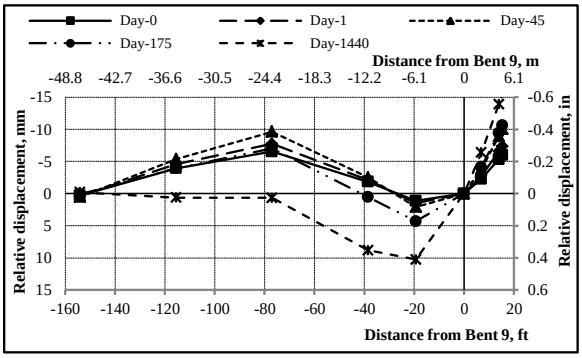


(a)

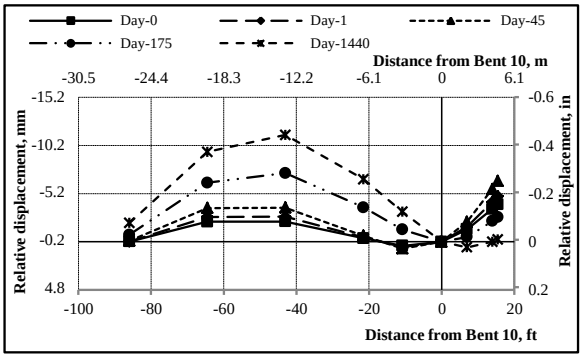


(b)

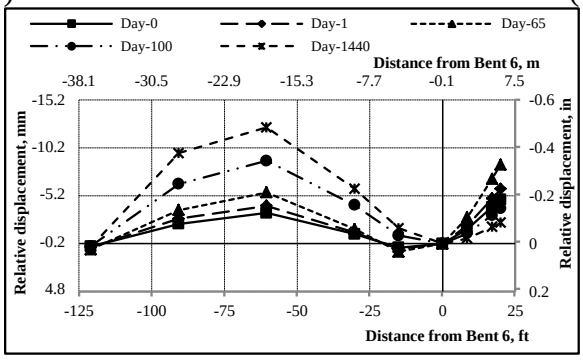


(c)

Figure 8-13 SAP2000 deflections of B5EB: (a) at C1; (b) at C2; (c) at H1

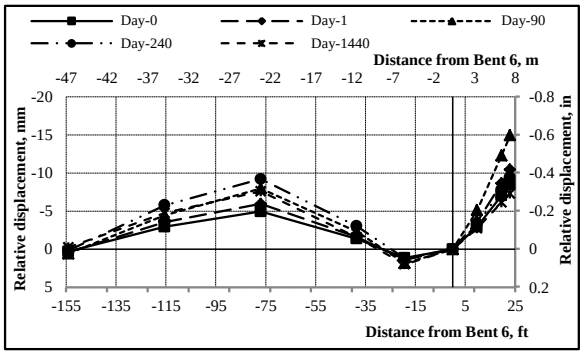


Figure 8-14 SAP2000 deflections of B5WB at H4

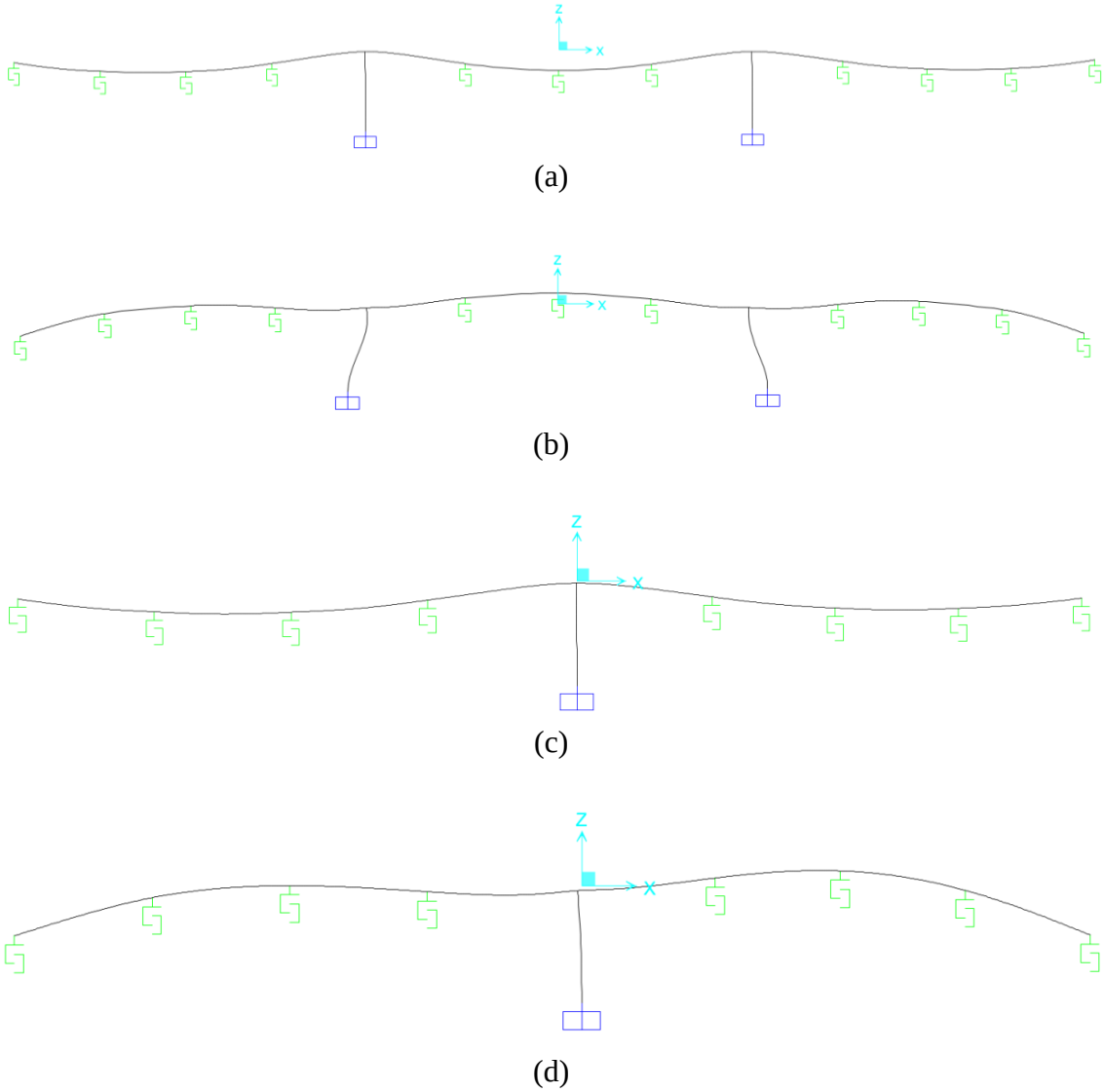


Figure 8-15 SAP2000 deflections of prestressed long cantilevers frames in Bridge 5WB: (a) Frame 2 (Day -1); (b) Frame 2 (Day 0); (c) Frame 4 (Day -1); (d) Frame 4 (Day 0)

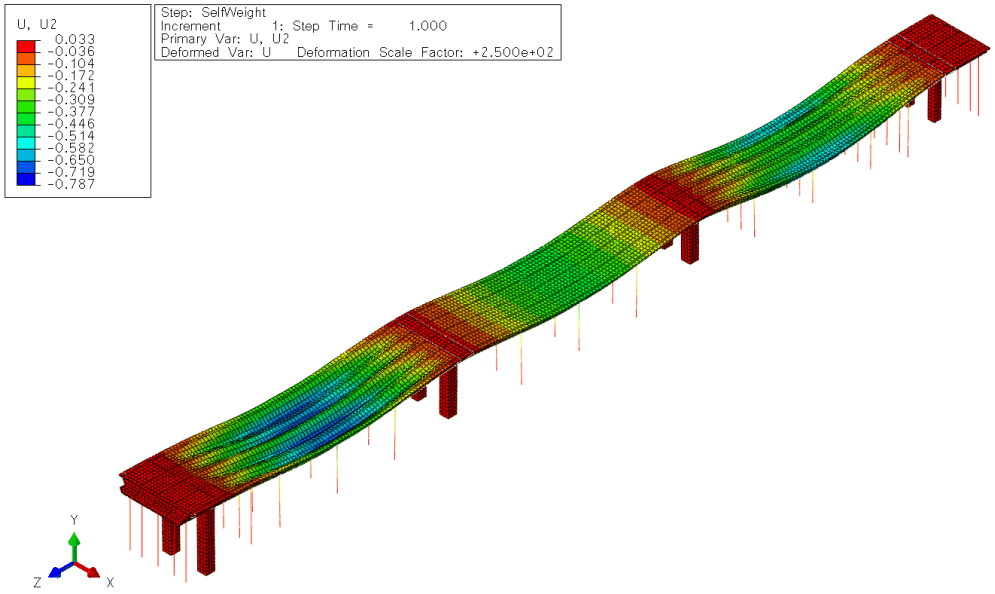


(a)

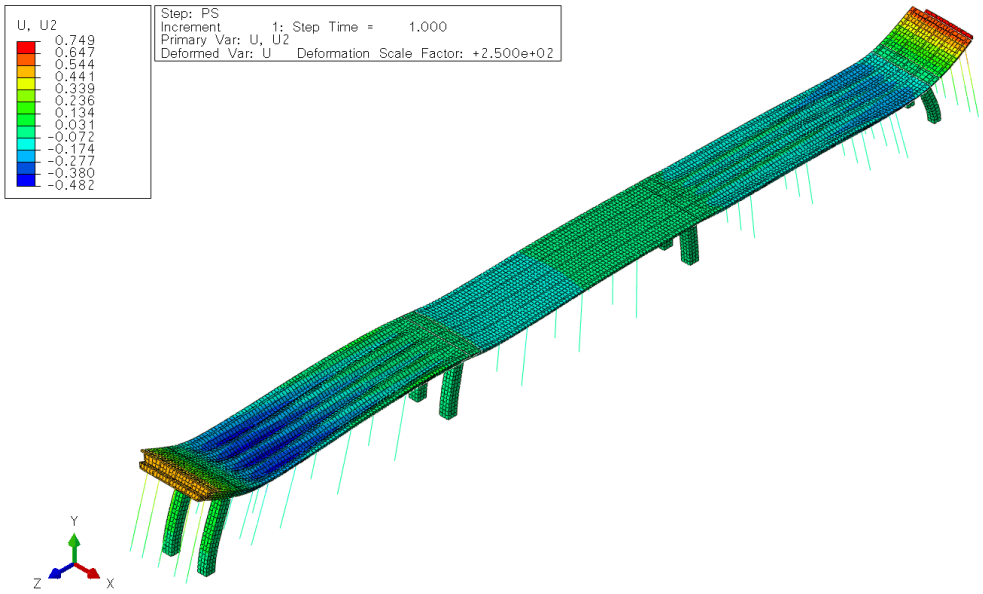


(b)

Figure 8-16 Deformed shapes of Frame 2, Bridge 1 (ABAQUS): (a) Before stressing; (b) Immediately after stressing

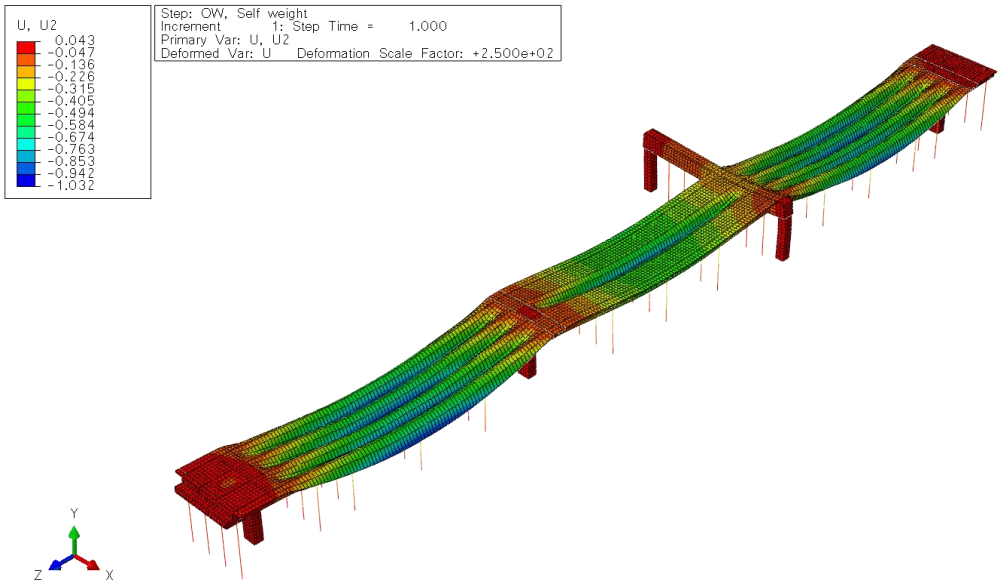


(a)

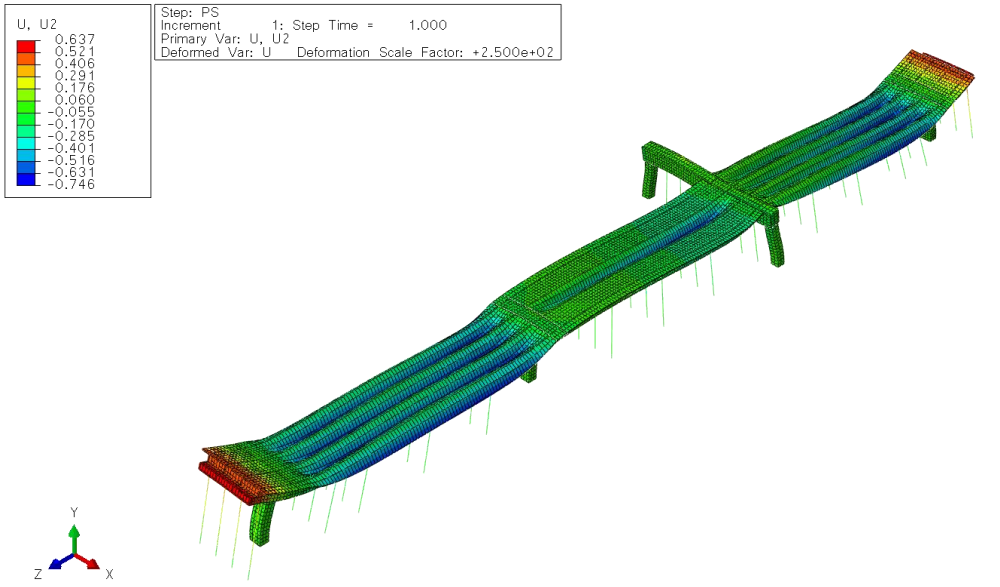


(b)

Figure 8-17 Deformed shapes of Frame 2, Bridge 2 (ABAQUS): (a) Before stressing; (b) Immediately after stressing

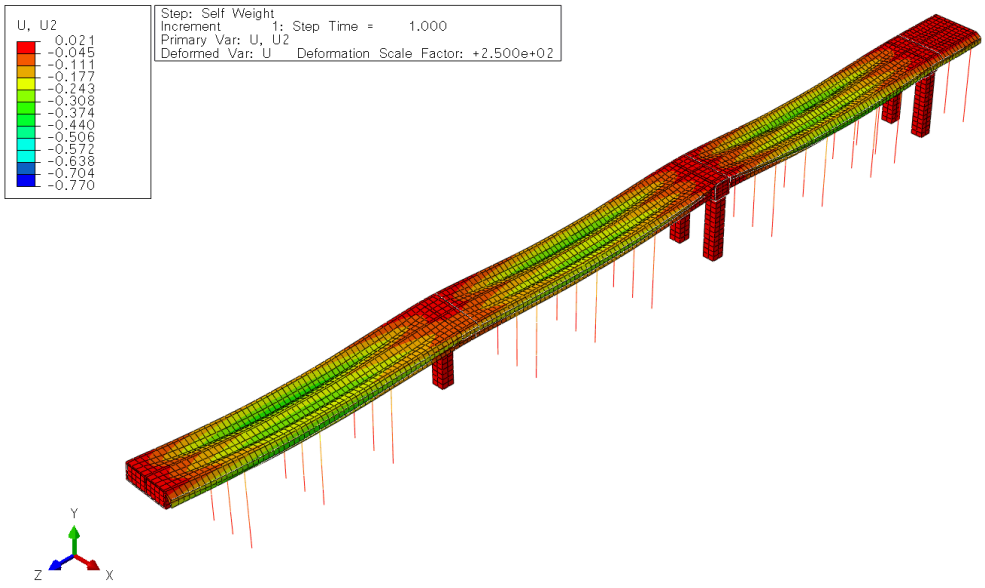


(a)

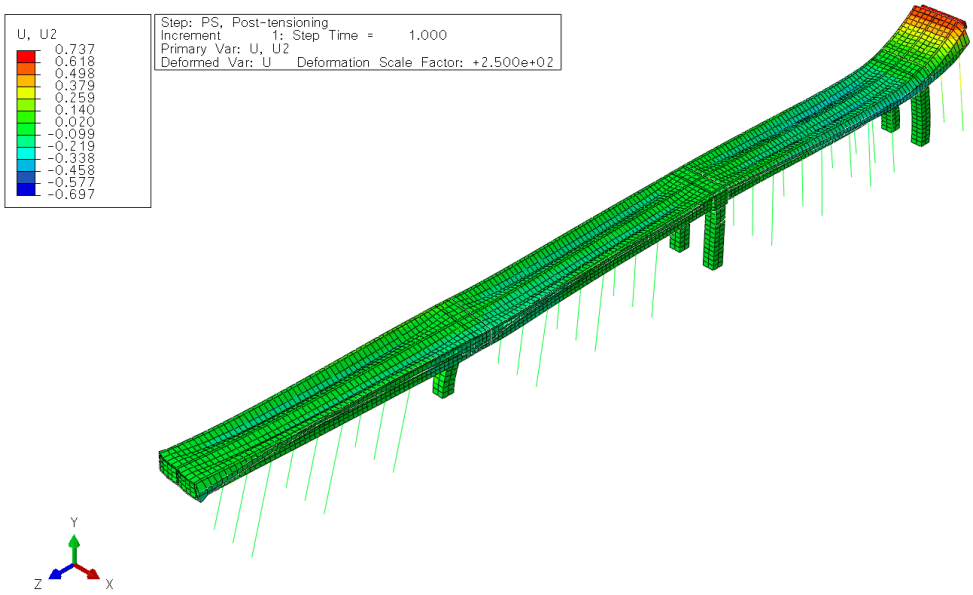


(b)

Figure 8-18 Deformed shapes of Frame 1, Bridge 3 (ABAQUS): (a) Before stressing; (b) Immediately after stressing

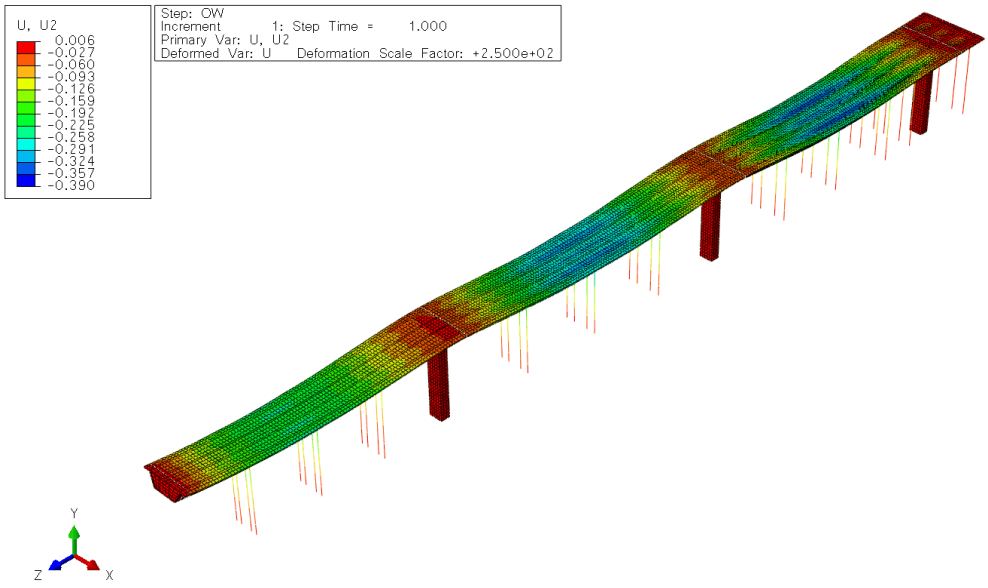


(a)

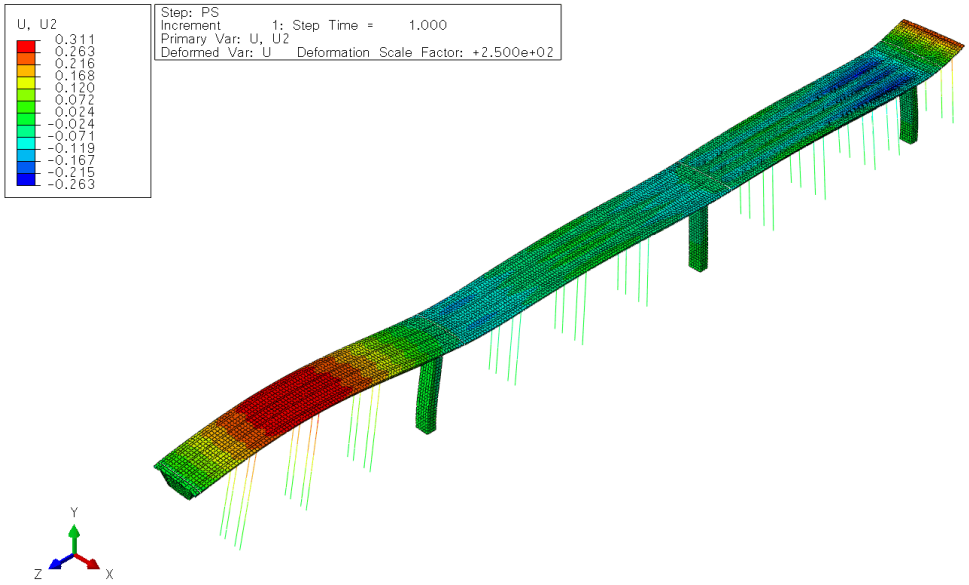


(b)

Figure 8-19 Deformed shapes of Frame 2, Bridge 4 (ABAQUS): (a) Before stressing; (b) Immediately after stressing

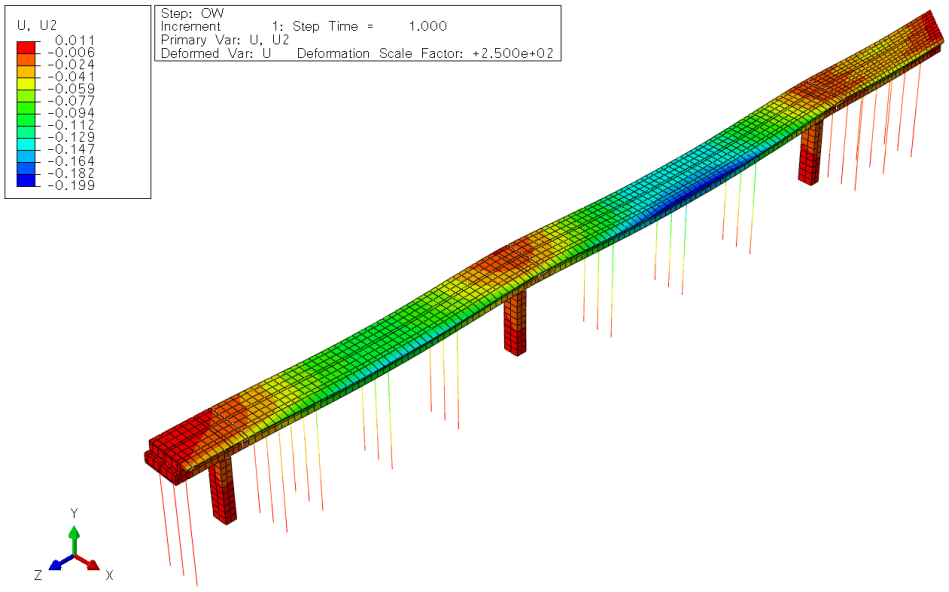


(a)

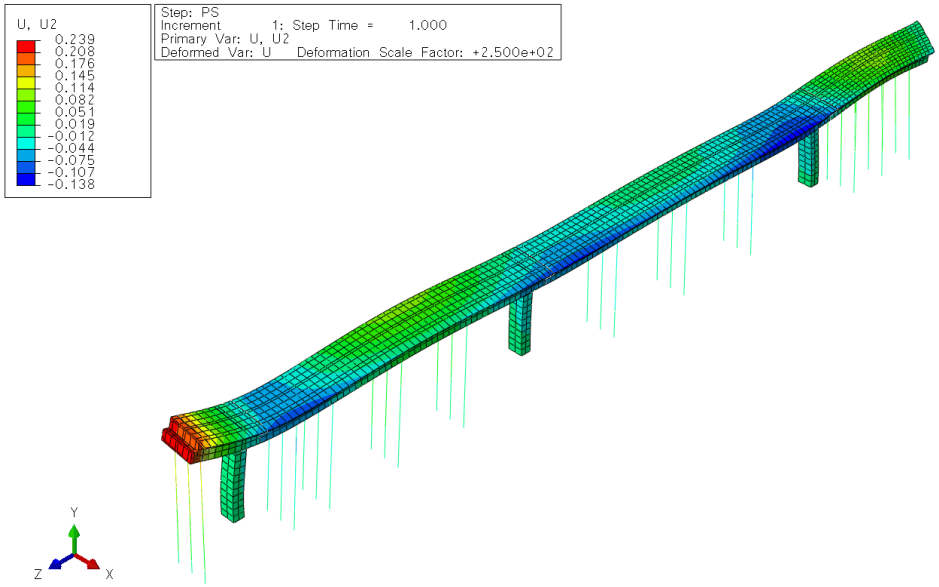


(b)

Figure 8-20 Deformed shapes of F1EB, Bridge 5 (ABAQUS): (a) Before stressing; (b) Immediately after stressing

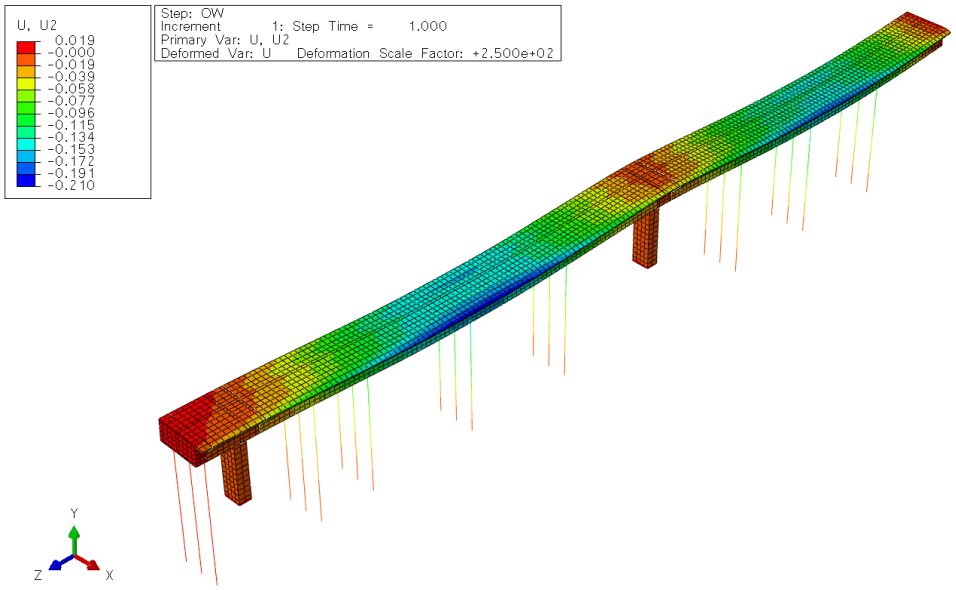


(a)

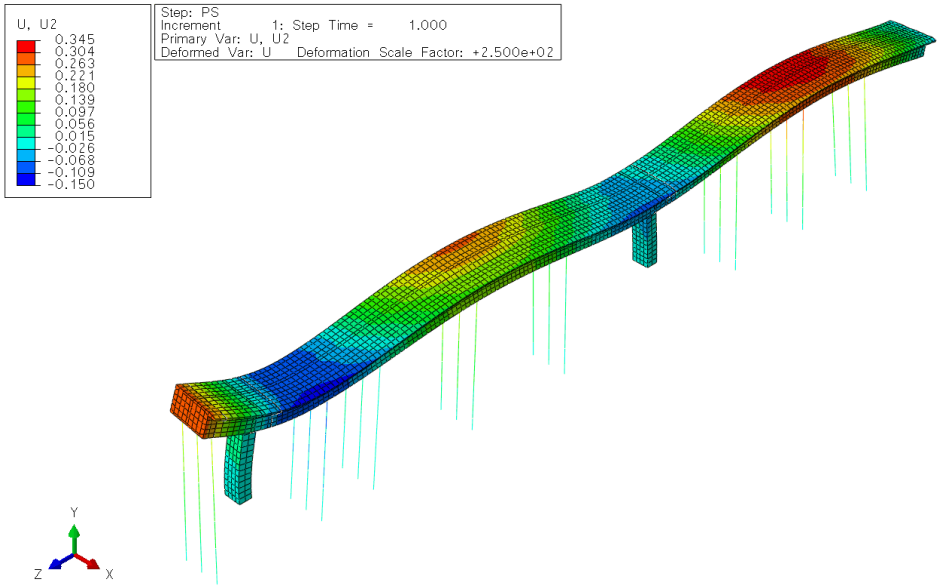


(b)

Figure 8-21 Deformed shapes of F3EB (Segment A), Bridge 5 (ABAQUS): (a) Before stressing; (b) Immediately after stressing

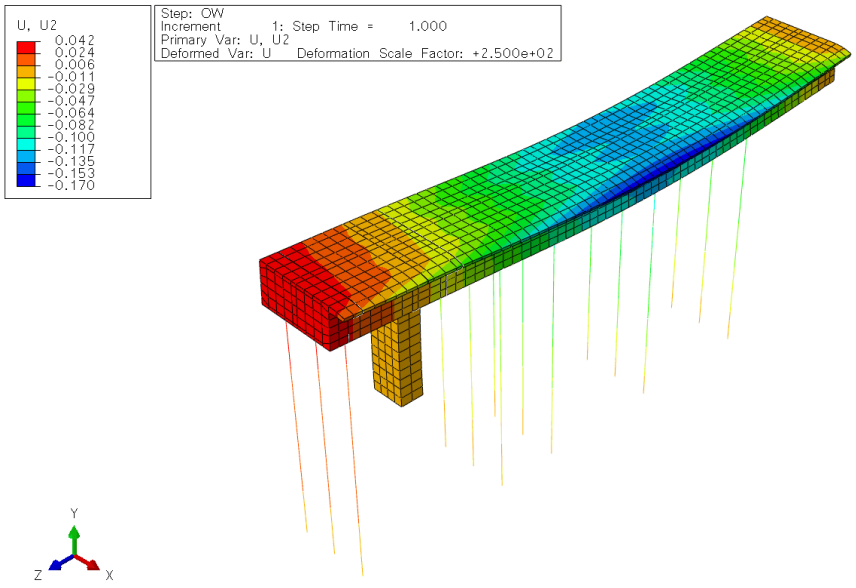


(a)

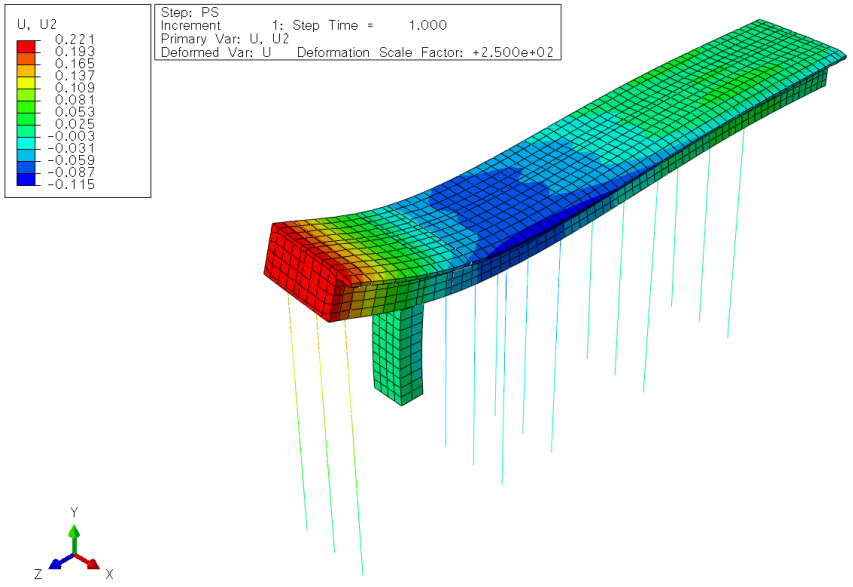


(b)

Figure 8-22 Deformed shapes of F3EB (Segment C), Bridge 5 (ABAQUS): (a) Before stressing; (b) Immediately after stressing

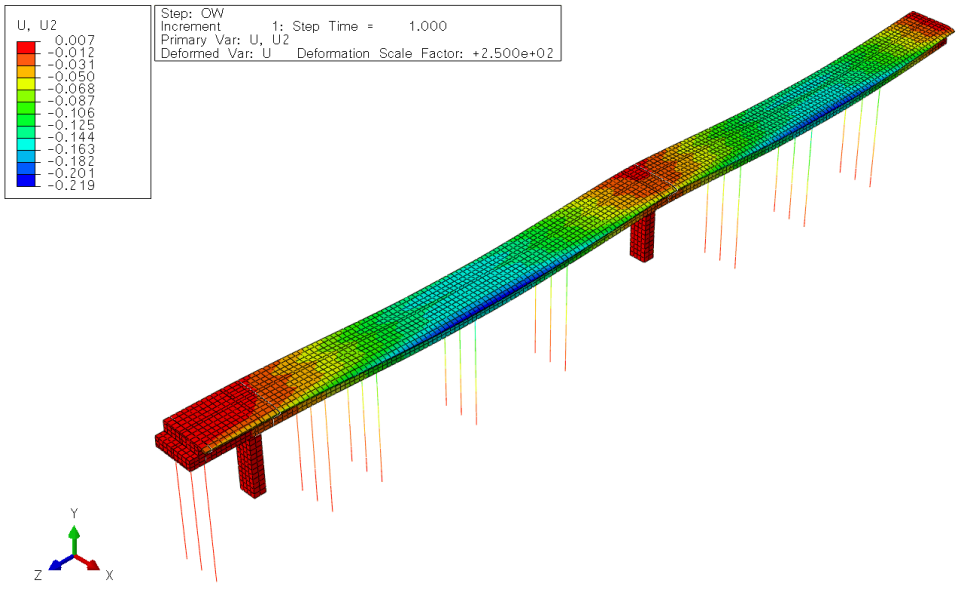


(a)

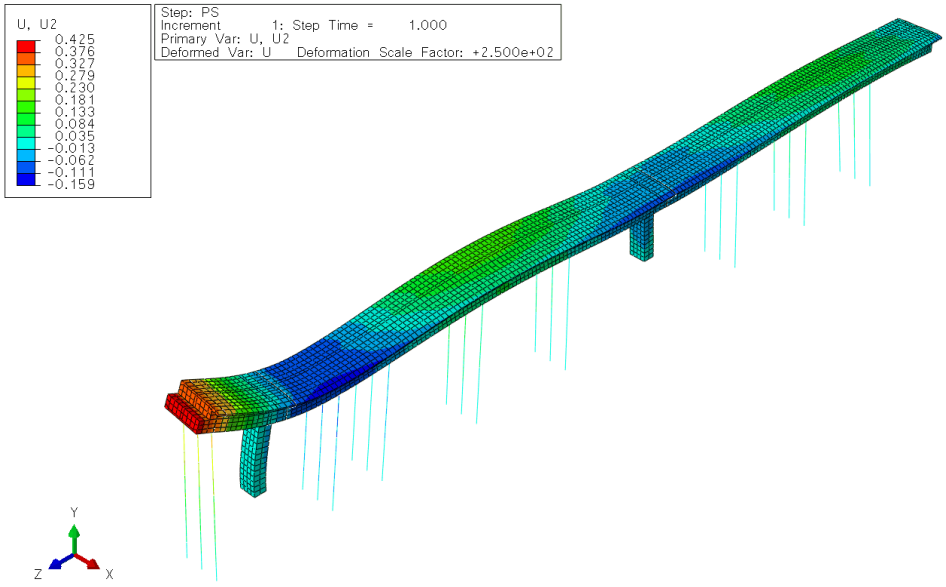


(b)

Figure 8-23 Deformed shapes of F5WB, Bridge 5 (ABAQUS): (a) Before stressing; (b) Immediately after stressing

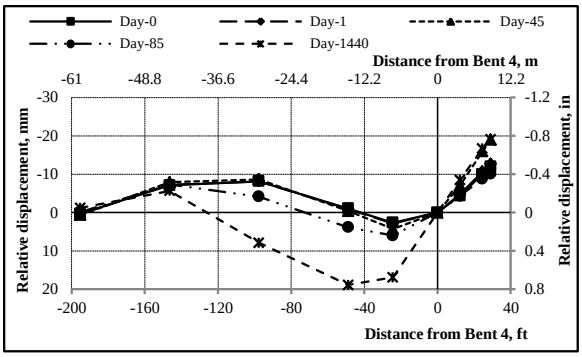


(a)

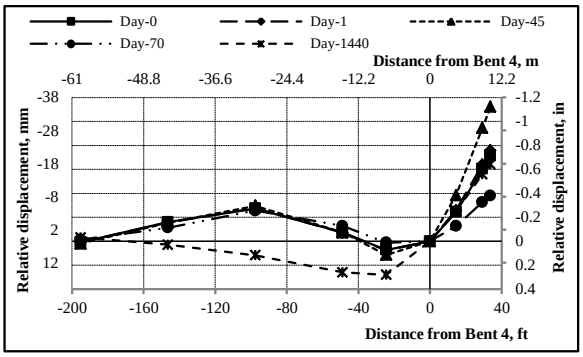


(b)

Figure 8-24 ABAQUS deflections of Bridge 1: (a) at H3; (b) at H7

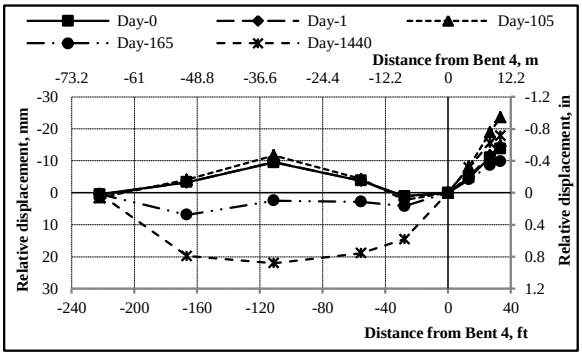


(a)

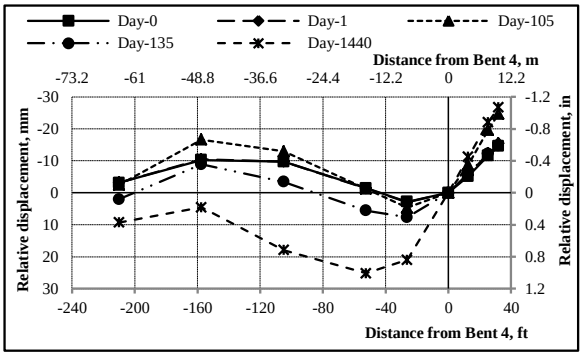


(b)

Figure 8-25 ABAQUS deflections of Bridge 2: (a) at H1; (b) at H2

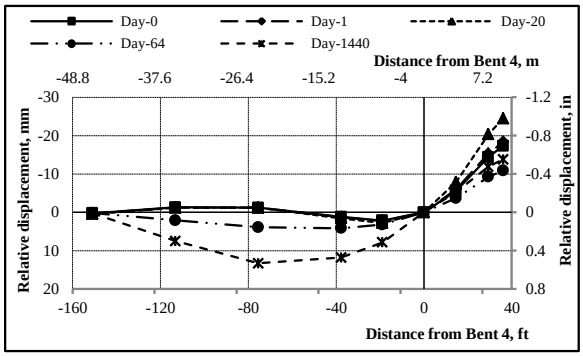


Figure 8-26 ABAQUS deflections of Bridge 3 at Hinge

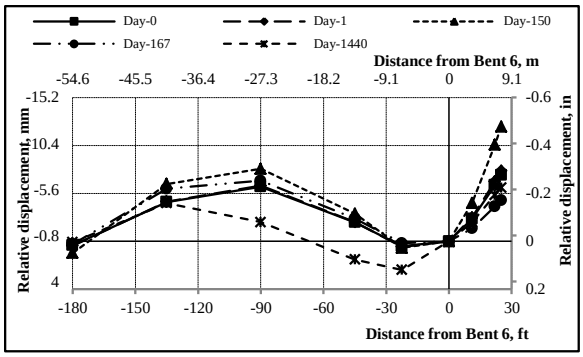


Figure 8-27 ABAQUS deflections of Bridge 4 at Hinge

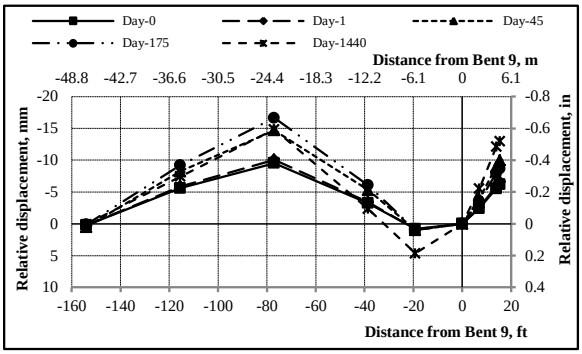


(a)

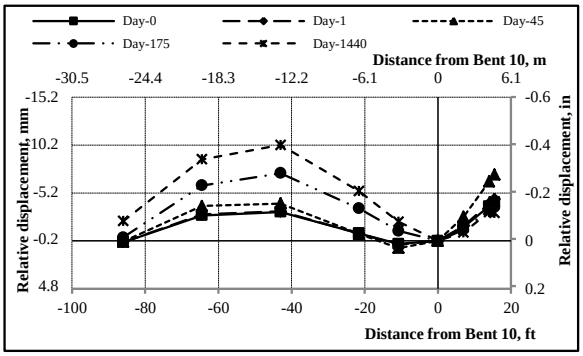


(b)

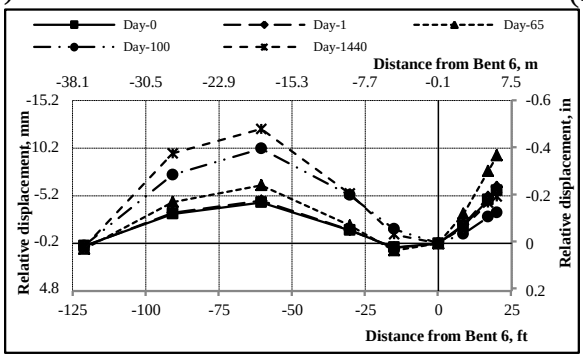


(c)

Figure 8-28 ABAQUS deflections of B5EB: (a) at C1; (b) at C2; (c) at H1

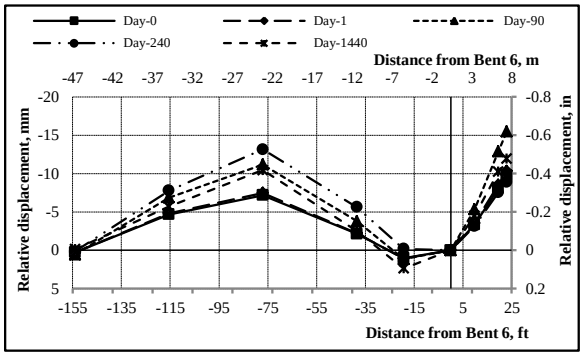


Figure 8-29 ABAQUS deflections of B5WB at H4

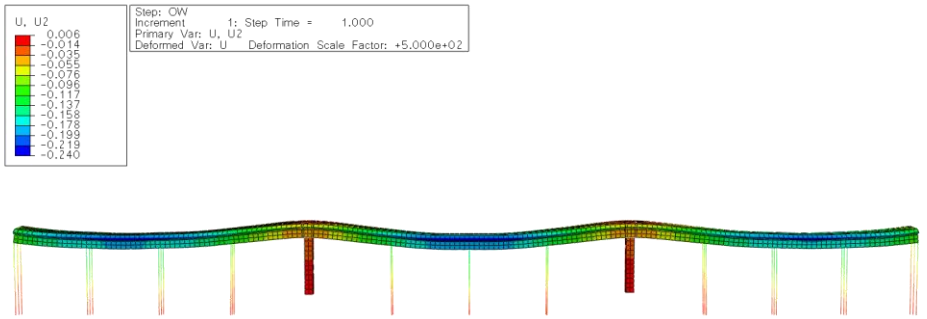


(a)

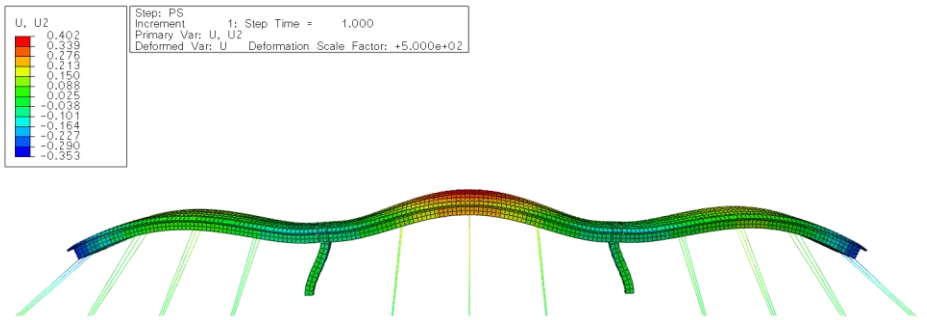


(b)

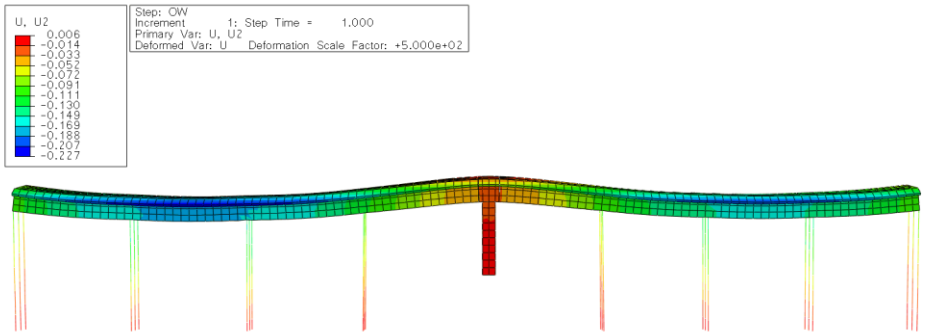


(c)

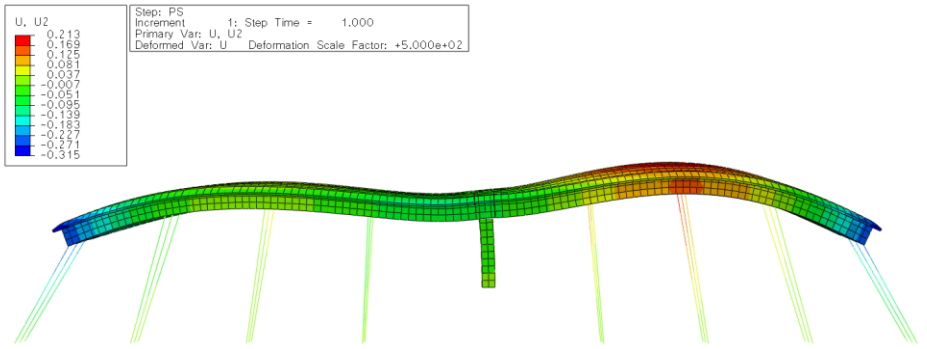


(d)

Figure 8-30 ABAQUS deflections of prestressed long cantilevers frames in Bridge 5WB: (a) Frame 2 (Day -1); (b) Frame 2 (Day 0); (c) Frame 4 (Day -1); (d) Frame 4 (Day 0)

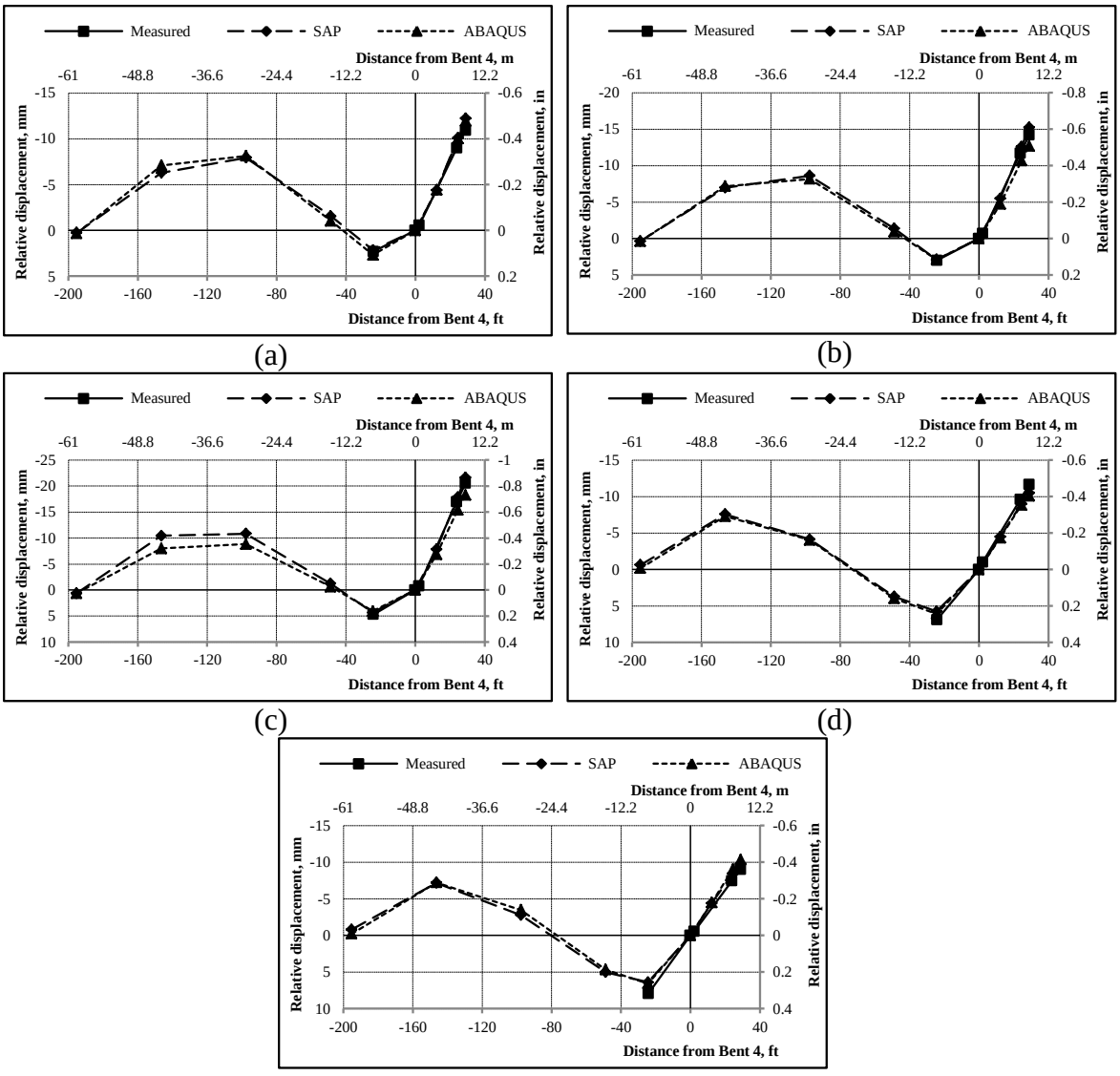


Figure 8-31 Measured and calculated deflections of Bridge 1 for H3: (a) Day 0; (b) Day 1; (c) Day 49; (d) Day 92; (e) Day129

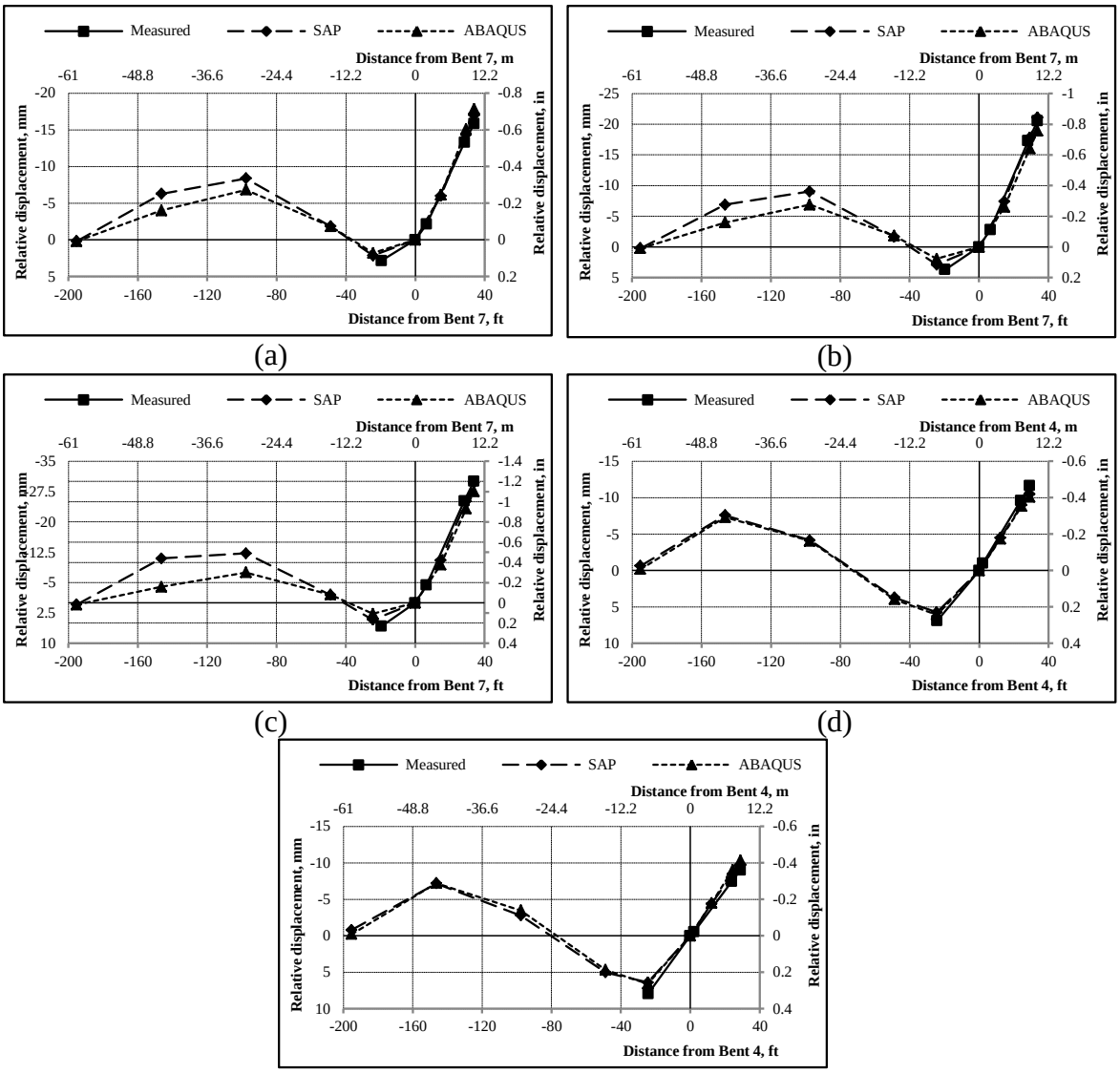


Figure 8-32 Measured and calculated deflections of Bridge 1 for H7: (a) Day 0; (b) Day 1; (c) Day 49; (d) Day 92; (e) Day129

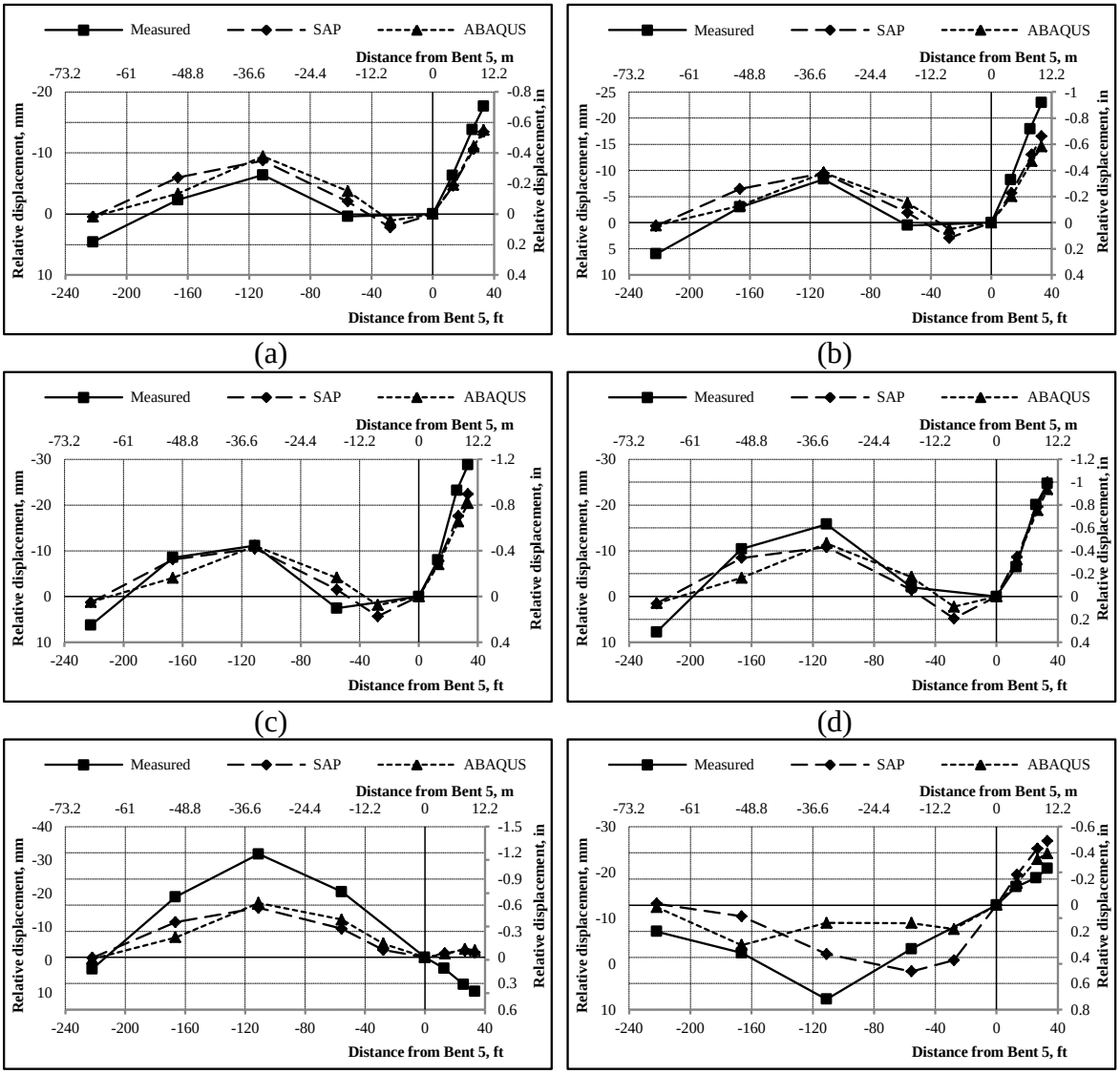


Figure 8-33 Measured and calculated deflections of Bridge 2 for H1: (a) Day 0; (b) Day 1; (c) Day 36; (d) Day 97; (e) Day 148; (f) Day 197

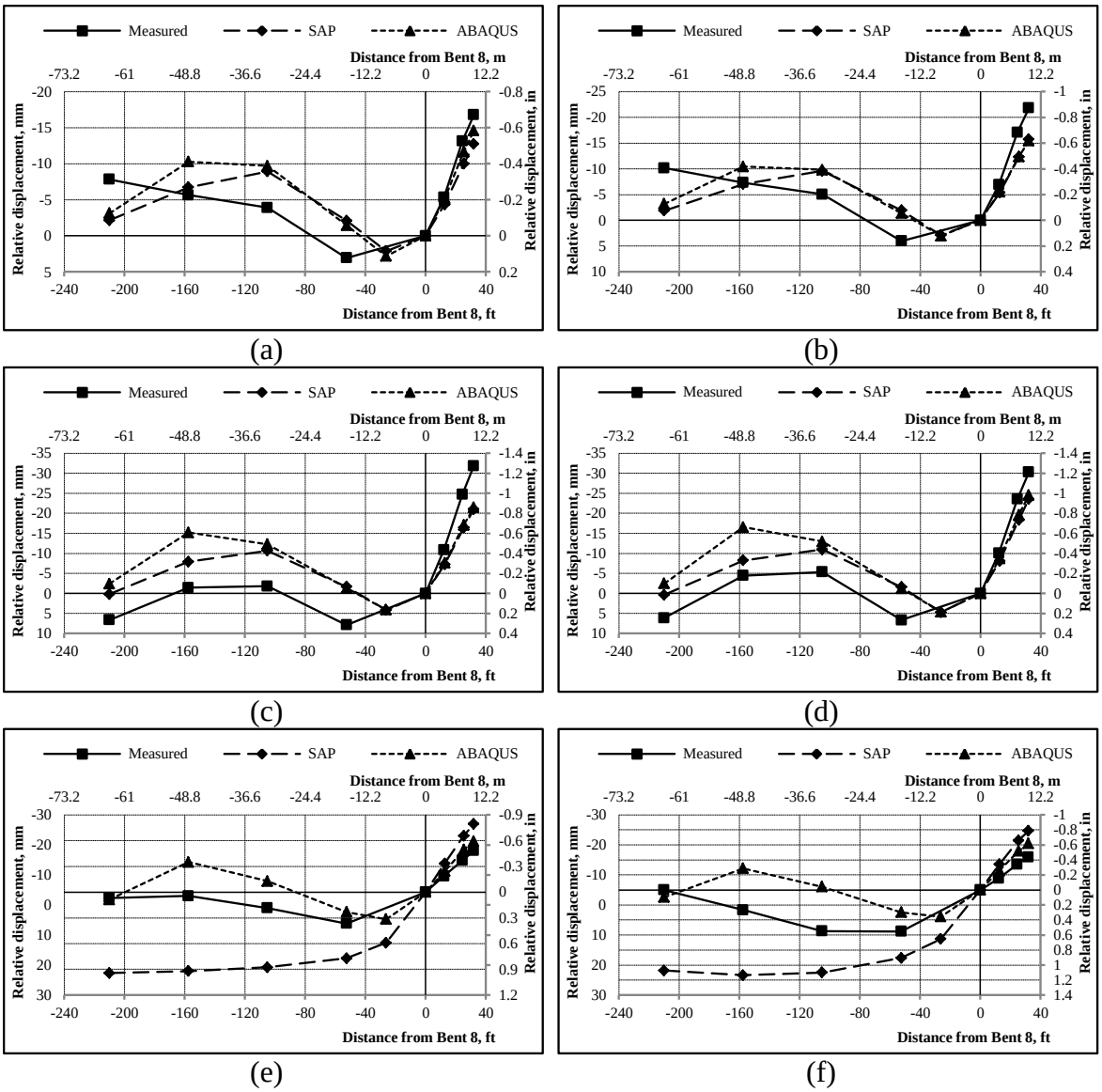


Figure 8-34 Measured and calculated deflections of Bridge 2 for H2: (a) Day 0; (b) Day 1; (c) Day 36; (d) Day 97; (e) Day 148; (f) Day 197

(a)

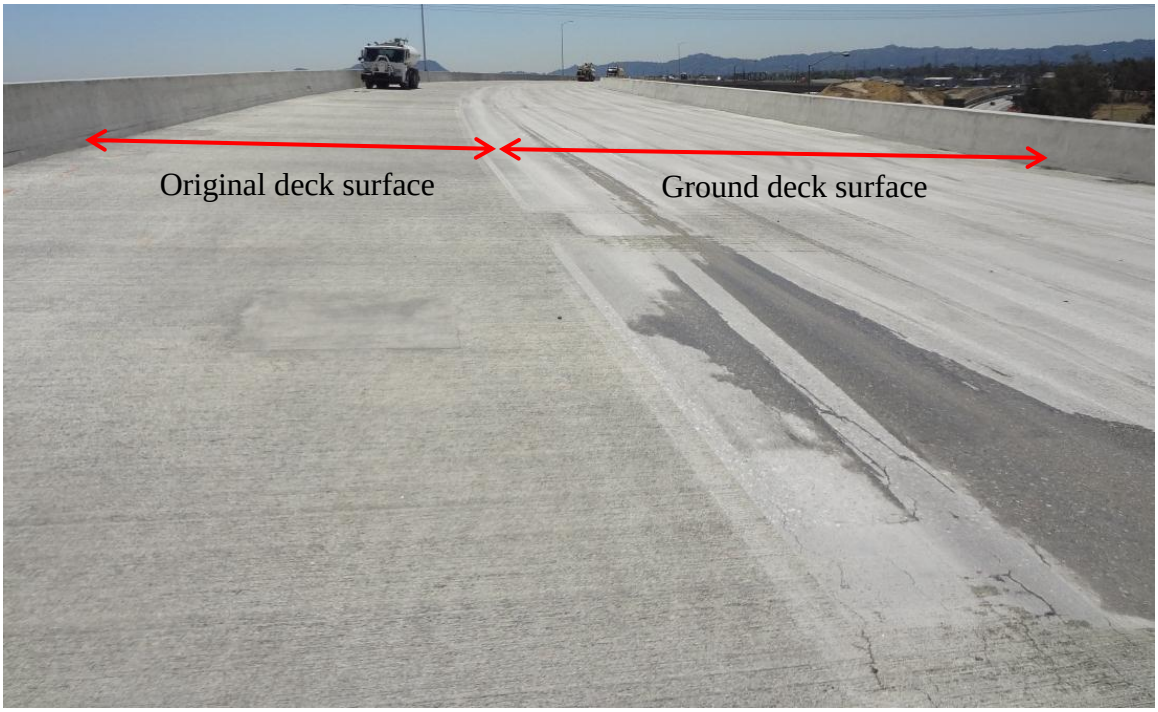


(b)

Figure 8-35 Concrete grinding work on Frame 2, Bridge 2: (a) Grinding equipment during the operation; (b) Deck surface after grinding half of it

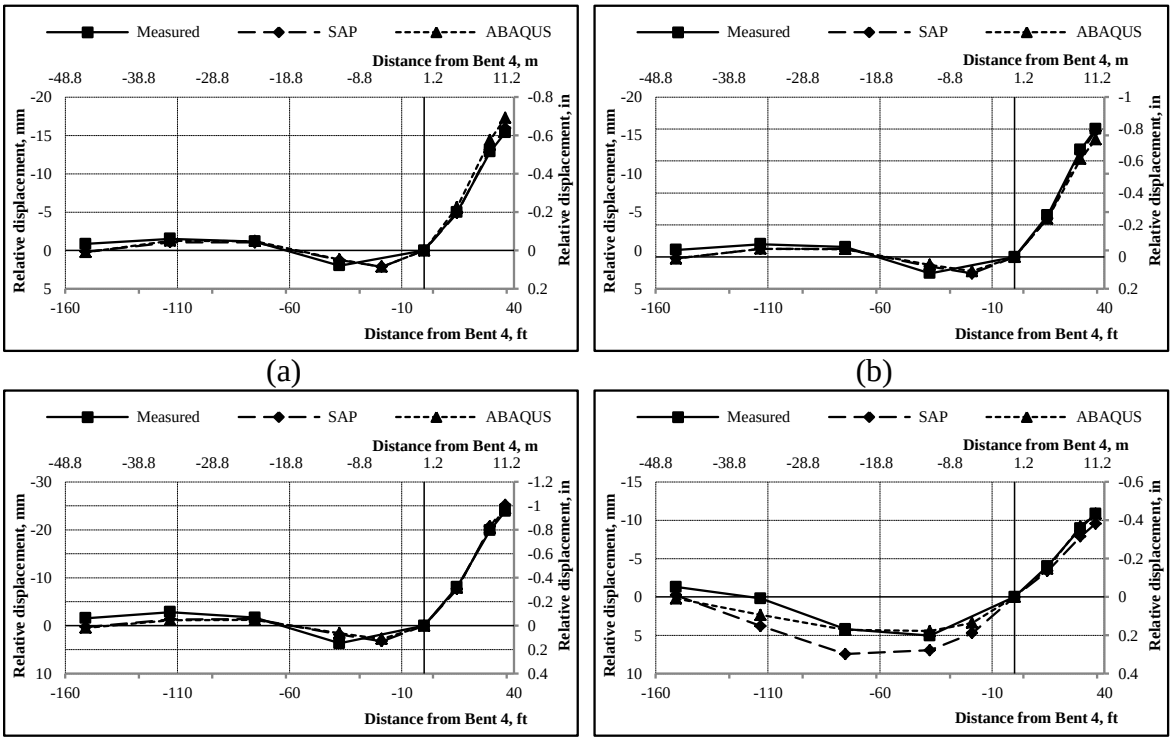


Figure 8-36 Measured and calculated deflections of Bridge 3 for H: (a) Day 0; (b) Day 1; (c) Day 22; (d) Day 83

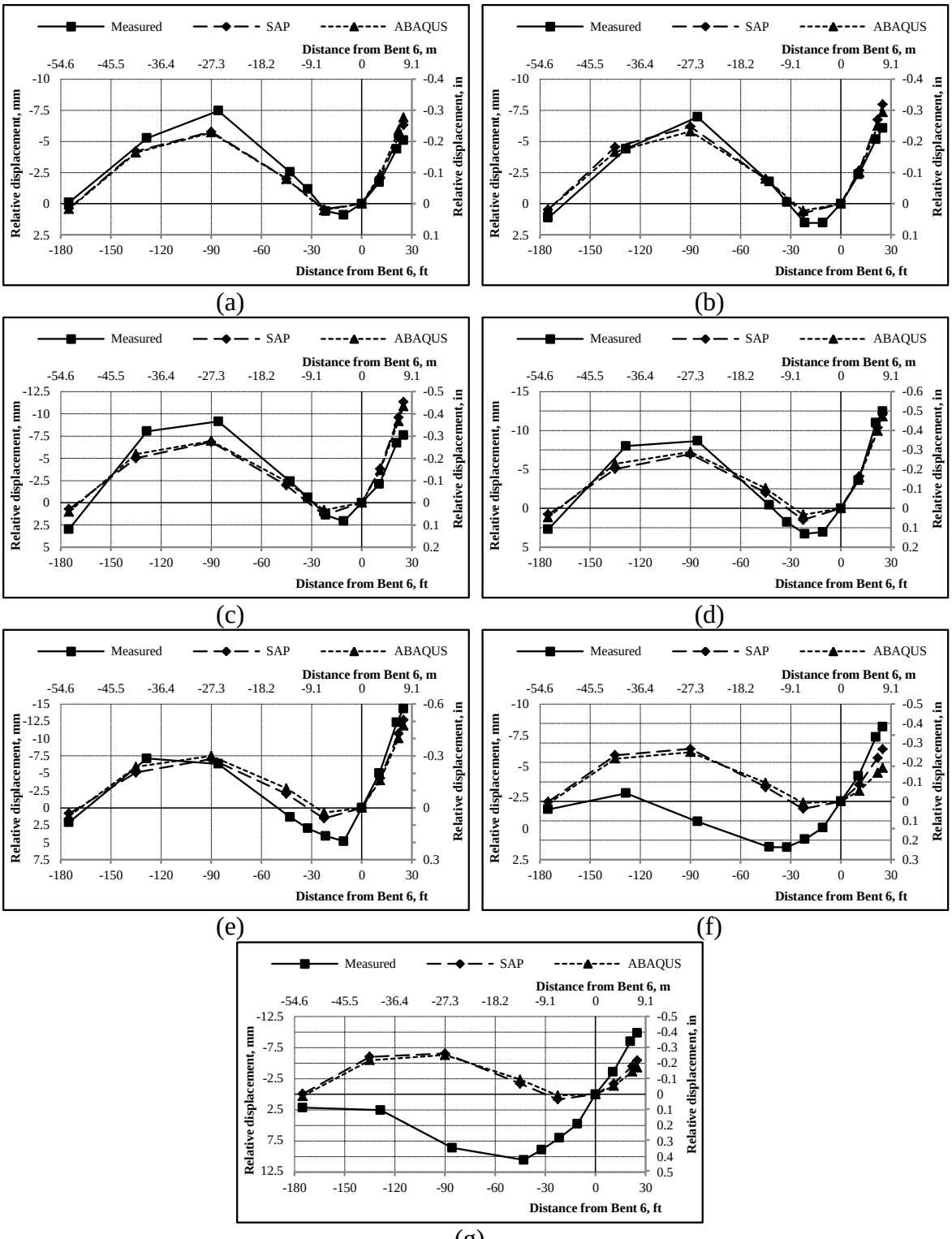


Figure 8-37 Measured and calculated deflections of Bridge 4 for H: (a) Day 0; (b) Day 1; (c) Day 51; (d) Day 99; (e) Day 135; (f) Day 167; (g) Day 170


Figure 8-38 Partial load transfer at H, Bridge 4

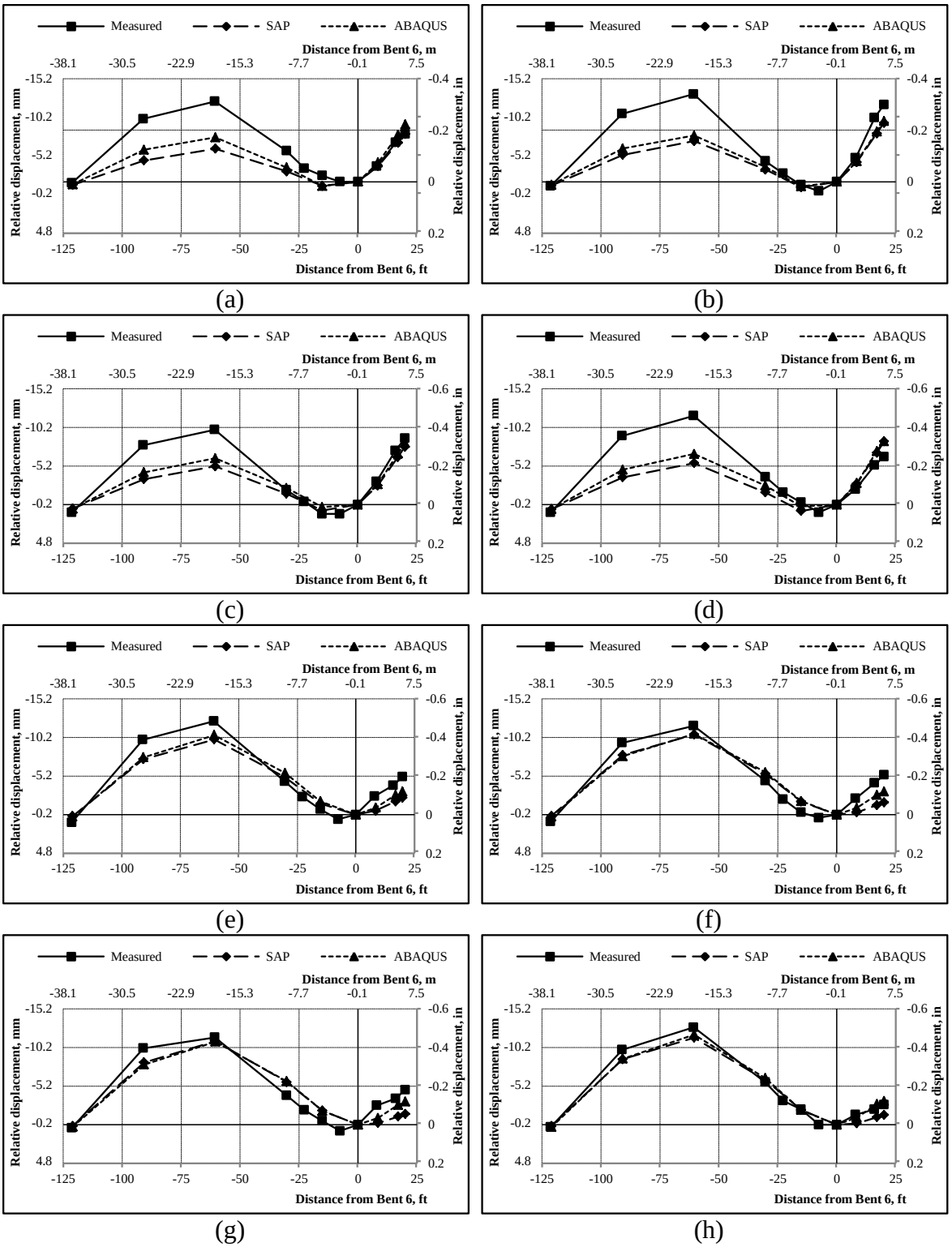


Figure 8-39 Measured and calculated deflections of B5EB for H1: (a) Day 0; (b) Day 1; (c) Day 27; (d) Day 68; (e) Day 112; (f) Day 143; (g) Day 184; (h) Day 275

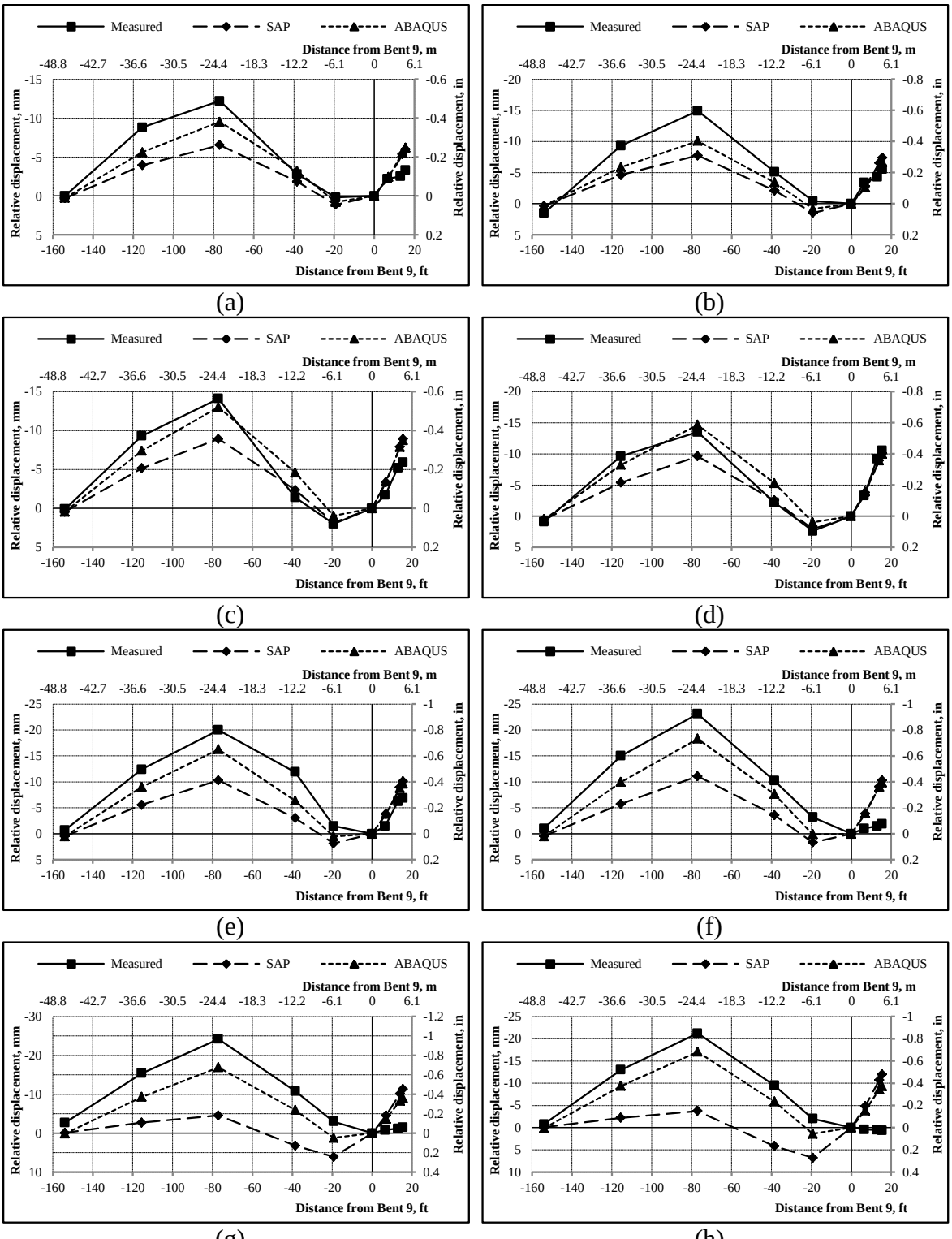


Figure 8-40 Measured and calculated deflections of B5EB for C1: (a) Day 0; (b) Day 1; (c) Day 13; (d) Day 45; (e) Day 78; (f) Day 152; (g) Day 239; (h) Day 360

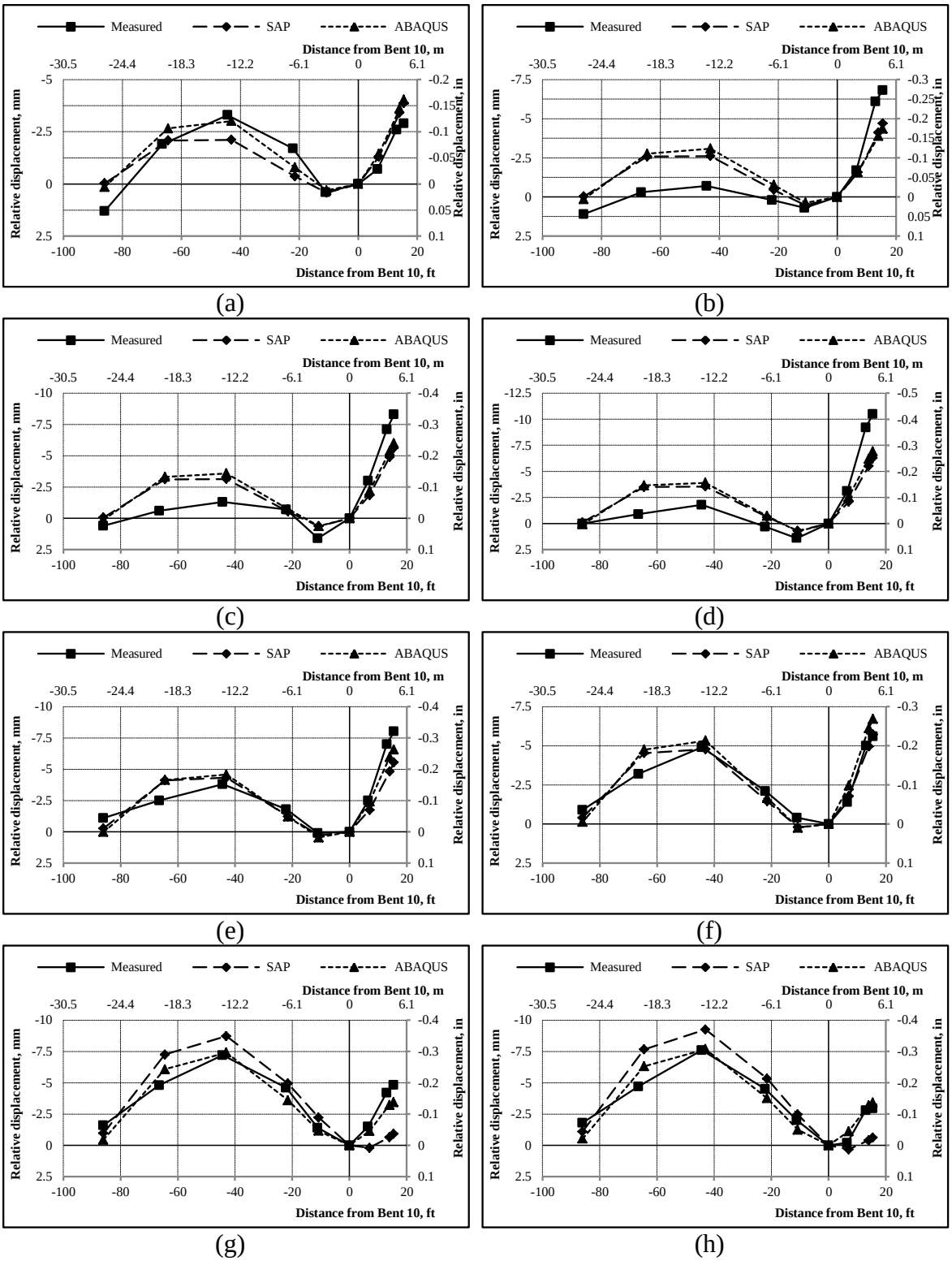


Figure 8-41 Measured and calculated deflections of B5EB for C2: (a) Day 0; (b) Day 1; (c) Day 13; (d) Day 45; (e) Day 78; (f) Day 152; (g) Day 239; (h) Day 360

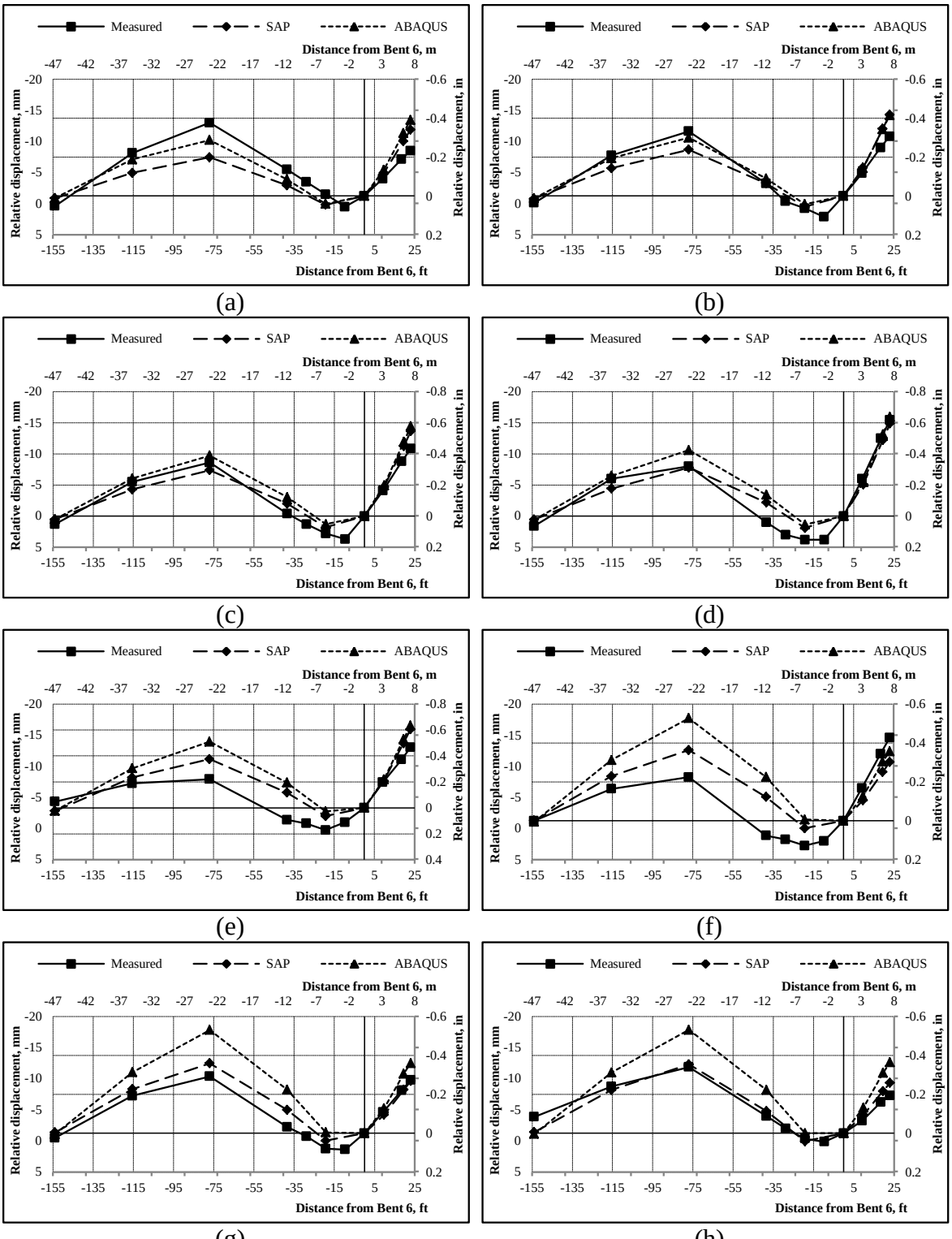


Figure 8-42 Measured and calculated deflections of B5WB for H4: (a) Day 0; (b) Day 1; (c) Day 30; (d) Day 74; (e) Day 224; (f) Day 254; (g) Day 315; (h) Day 406

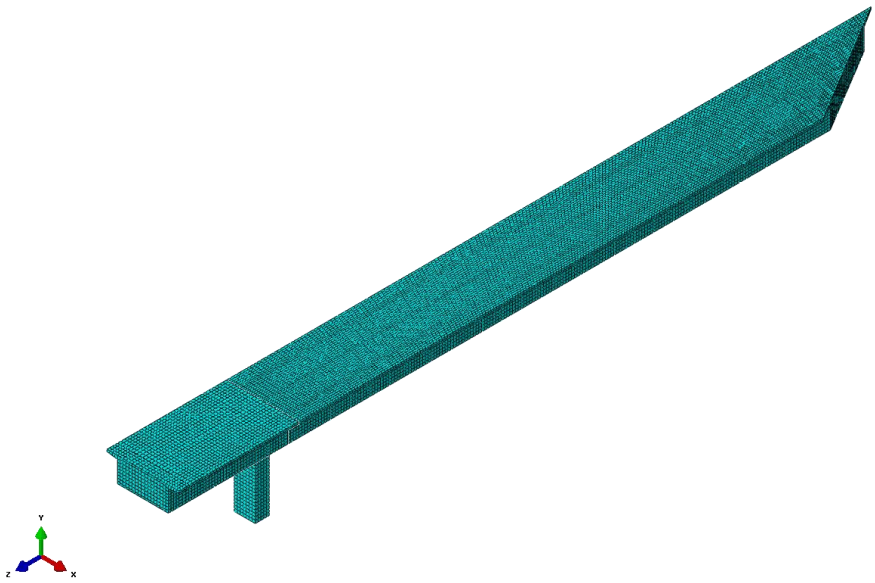

(a)

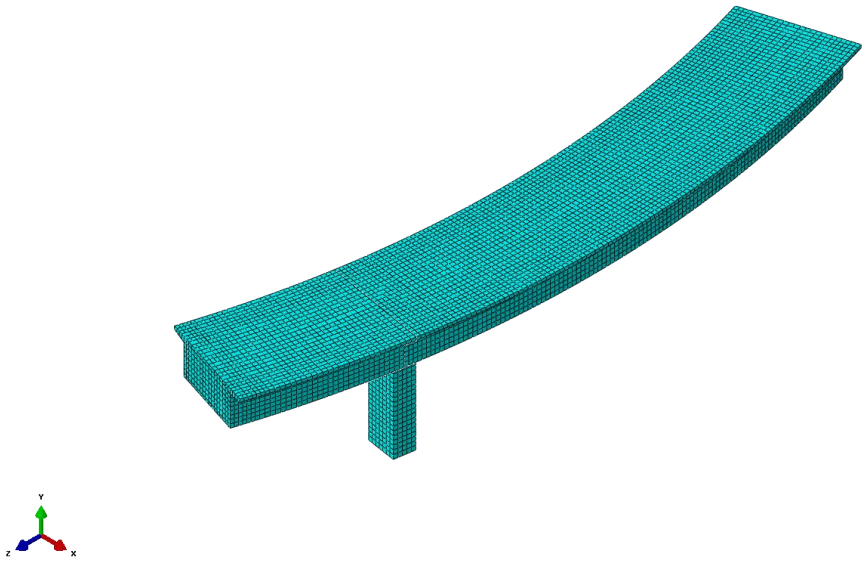

(b)

Figure 8-43 ABAQUS model samples used in the parametric study: (a) with 60-degree angle of skew abutment; (b) with 200 ft radius of horizontal curvature

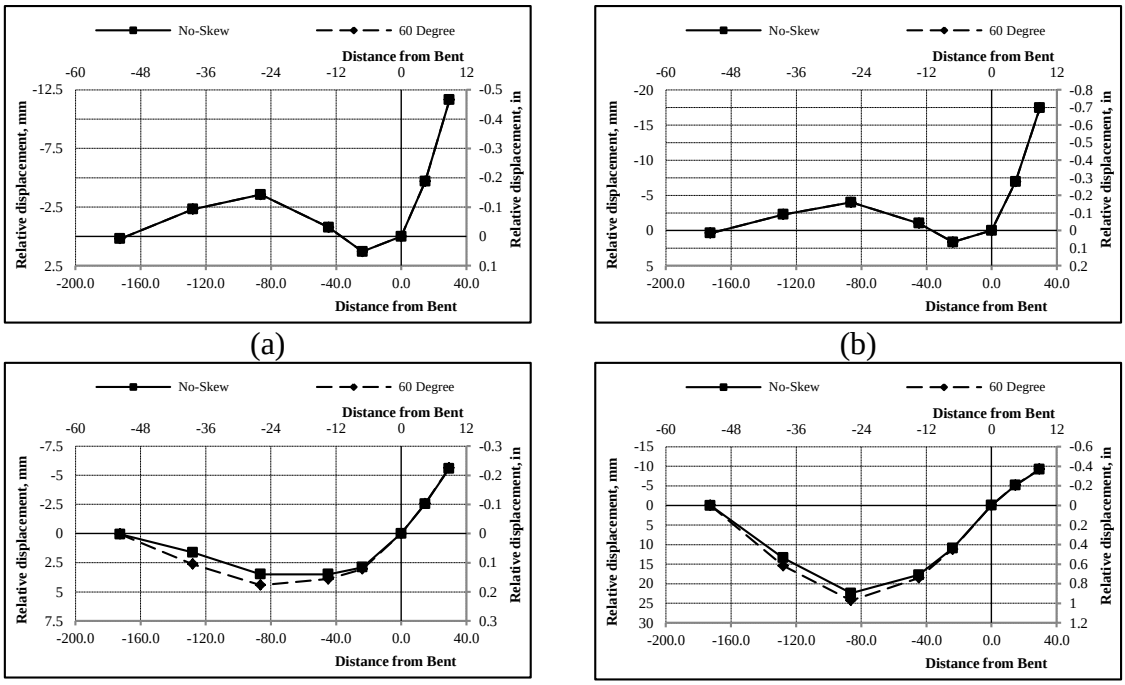


Figure 8-44 Effect of the abutment skew angle on the deformation behavior (group 1): (a) Day 0; (b) Day 30; (c) Day 60 (at Load Transfer); (d) Day 1440

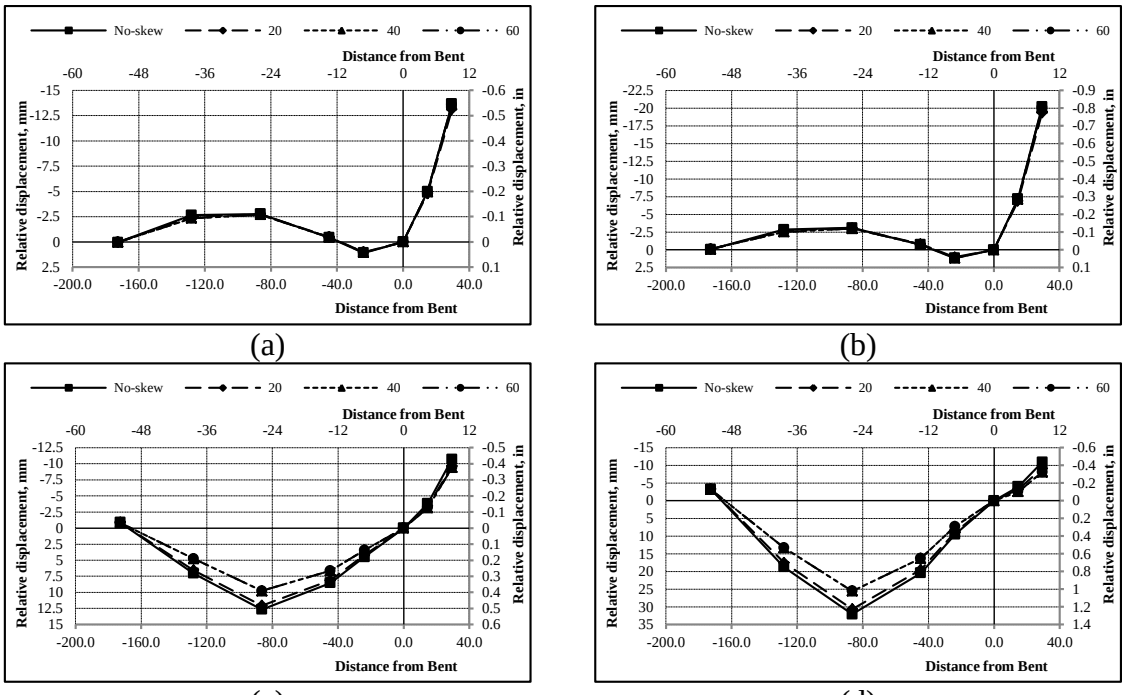


Figure 8-45 Effect of the abutment skew angle on the deformation behavior (group 2): (a) Day 0; (b) Day 30; (c) Day 60 (at Load Transfer); (d) Day 1440

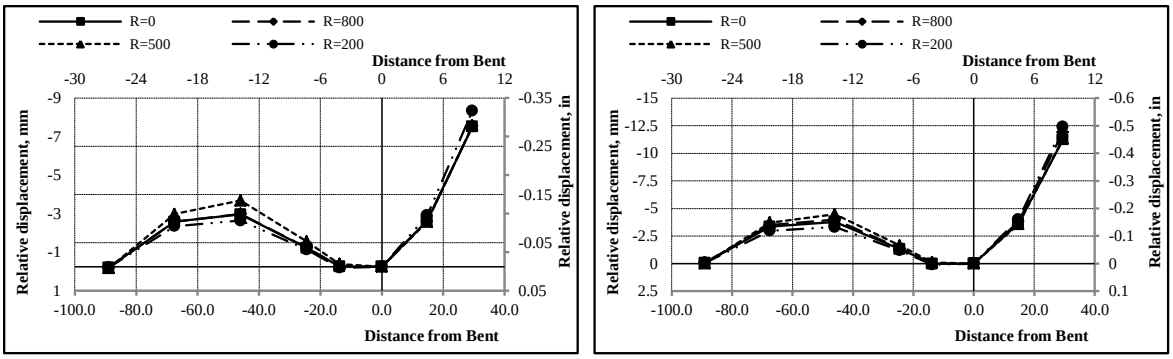


Figure 8-46 Effect of the radius of horizontal curvature on the deformation behavior: (a) Day 0; (b) Day 30; (c) Day 60 (at Load Transfer); (d) Day 1440

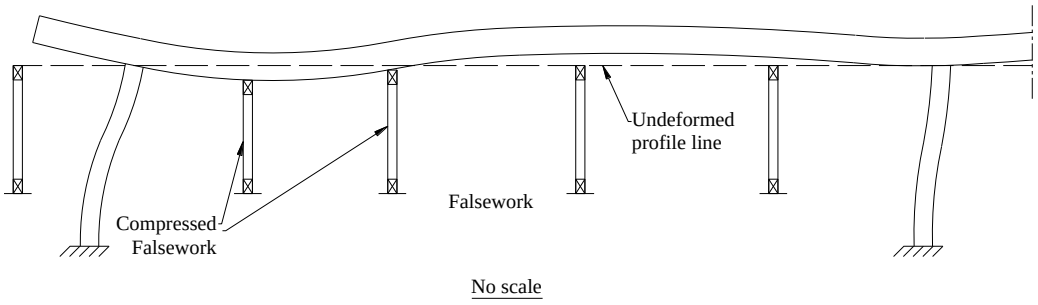


Figure 9-1 Typical deformation behavior after stressing

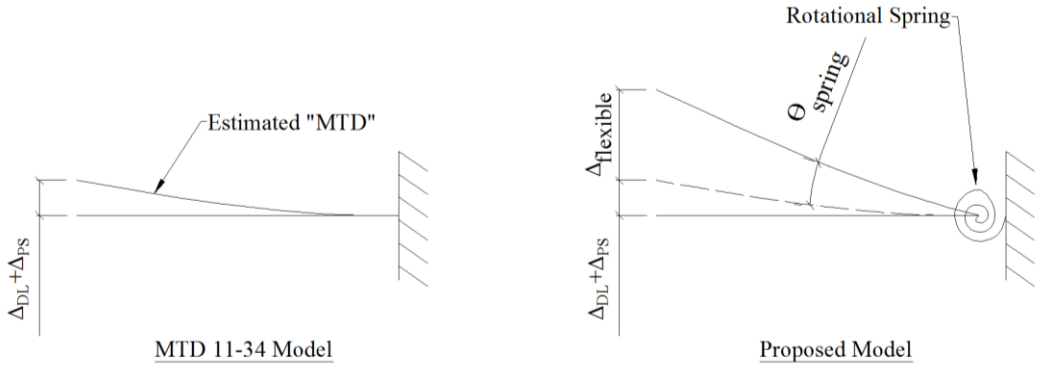


Figure 9-2 Hinge curl models

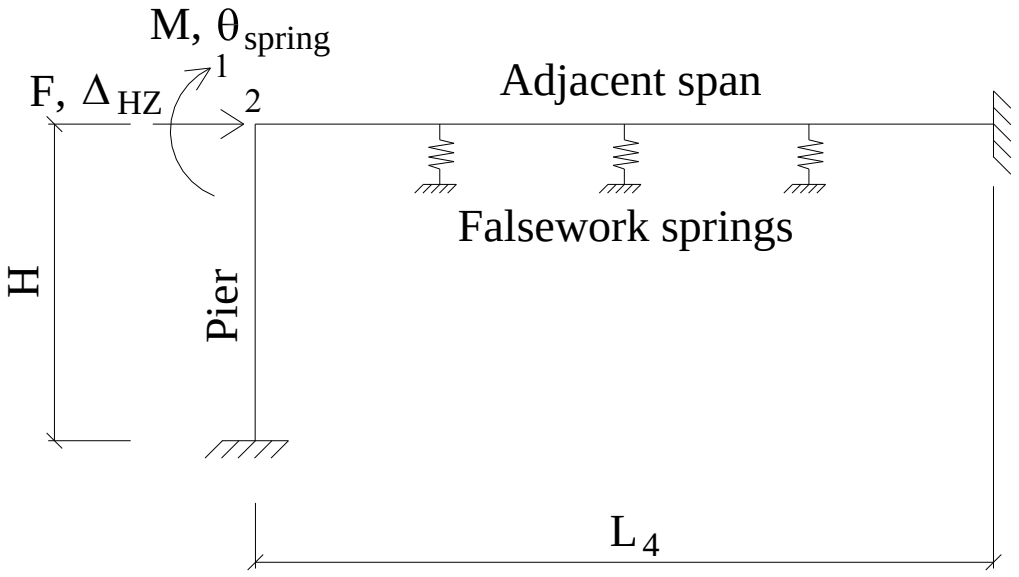


Figure 9-3 Equivalent nodal loads and DOF's

Figure 9-4 Falsework in Bridge 4

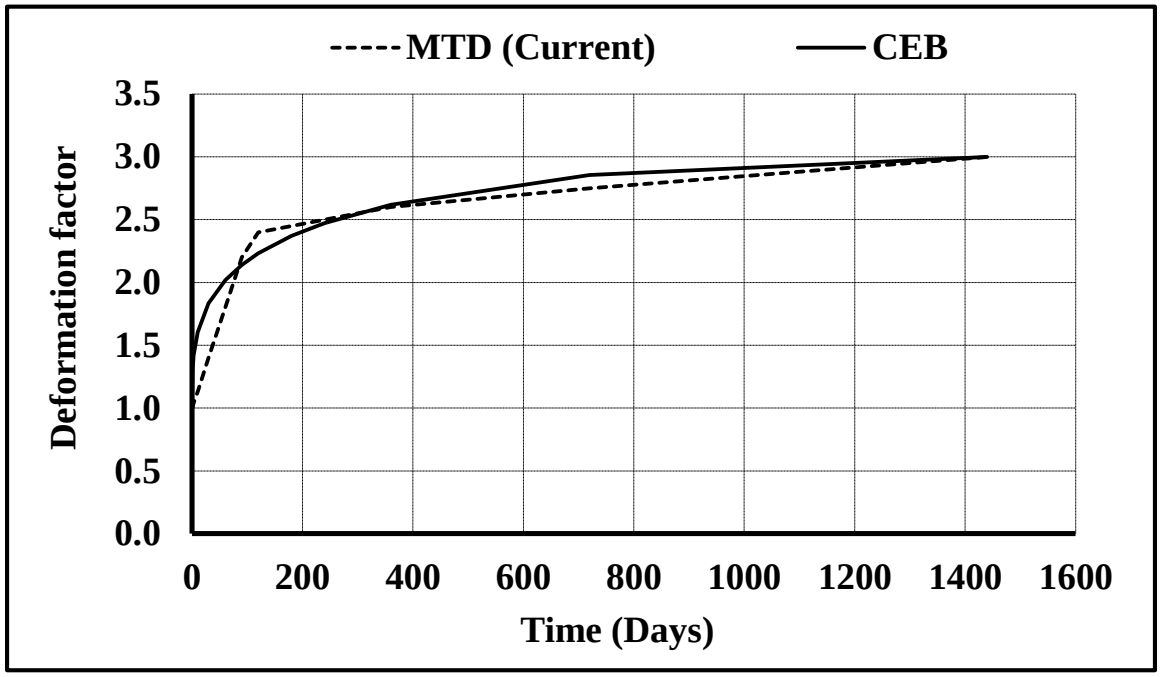


Figure 9-5 Deflection factor charts

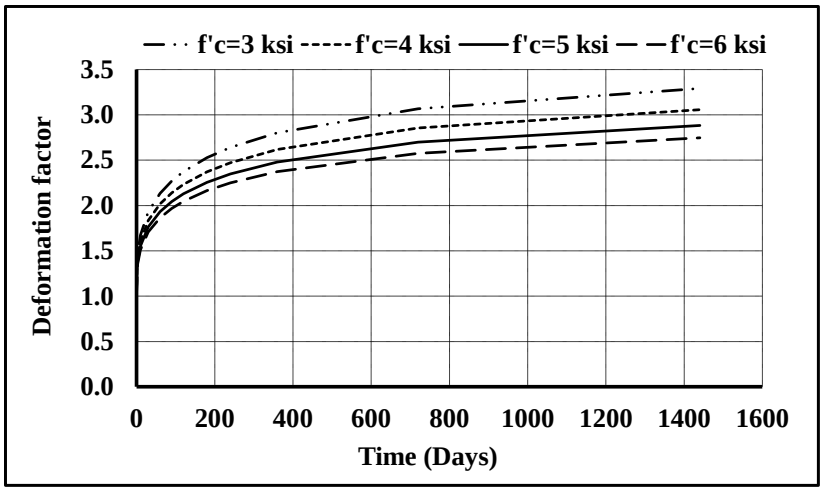


(a)

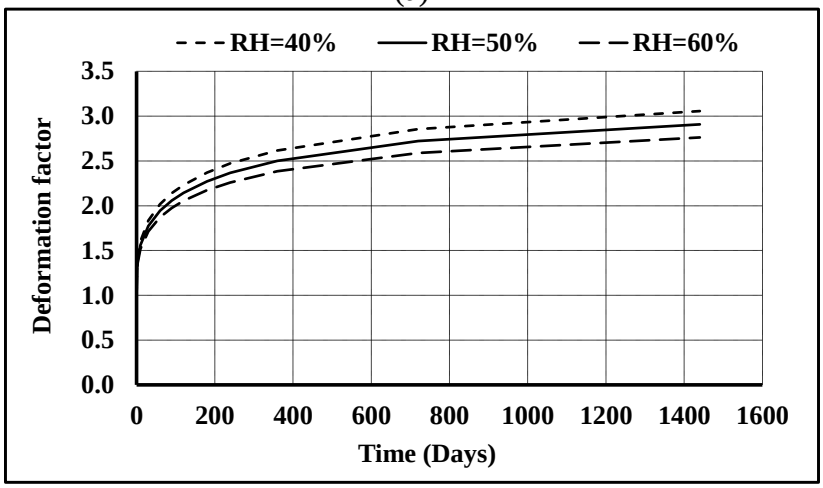


(b)

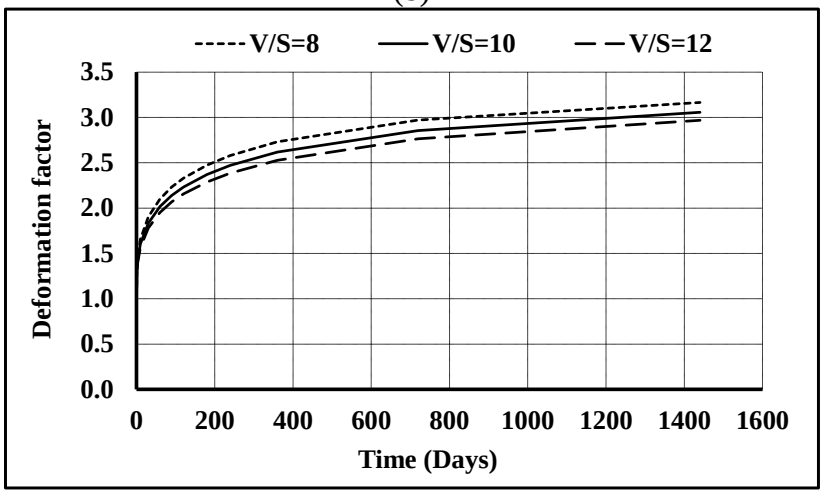


(c)

Figure 9-6 Sensitivity of CEB creep model due to change of: (a) Concrete strength ($f_{cm28}$); (b) Relative humidity (RH); (c) Volume-surface ratio (V/S)

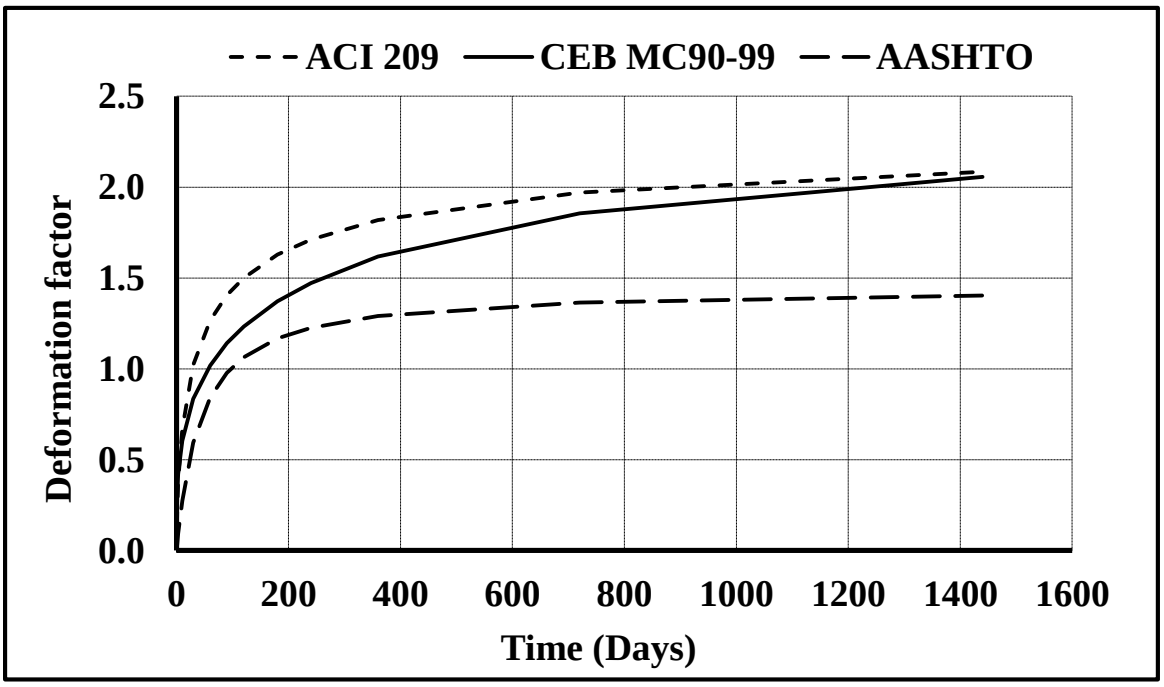


Figure 9-7 Creep coefficient predictions

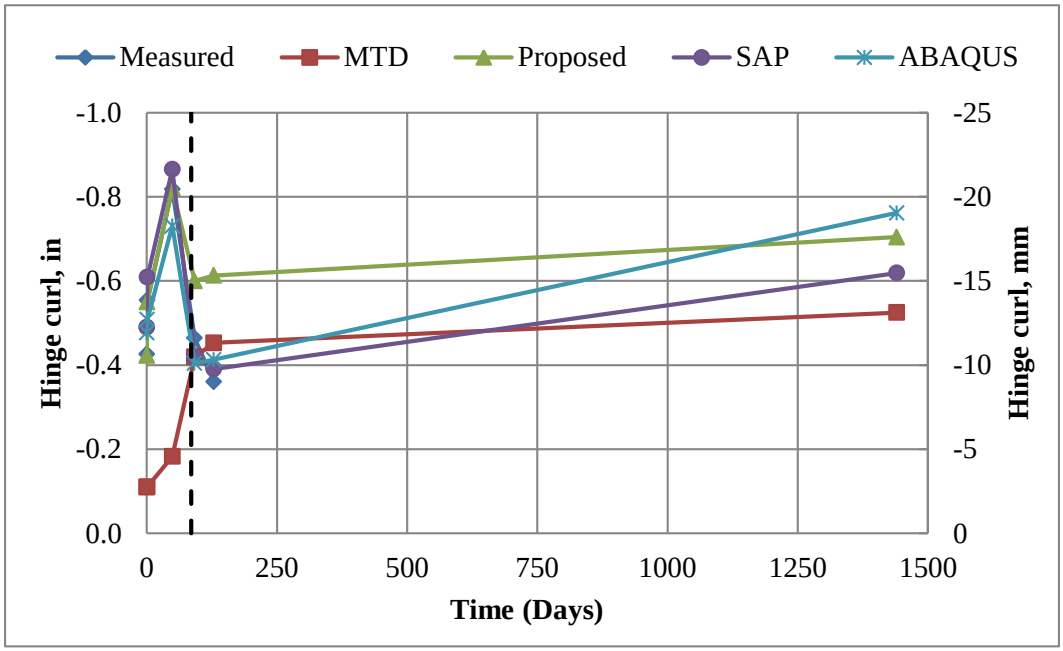


Figure 9-8 Comparison of measured and calculated hinge curl for H3, Bridge 1

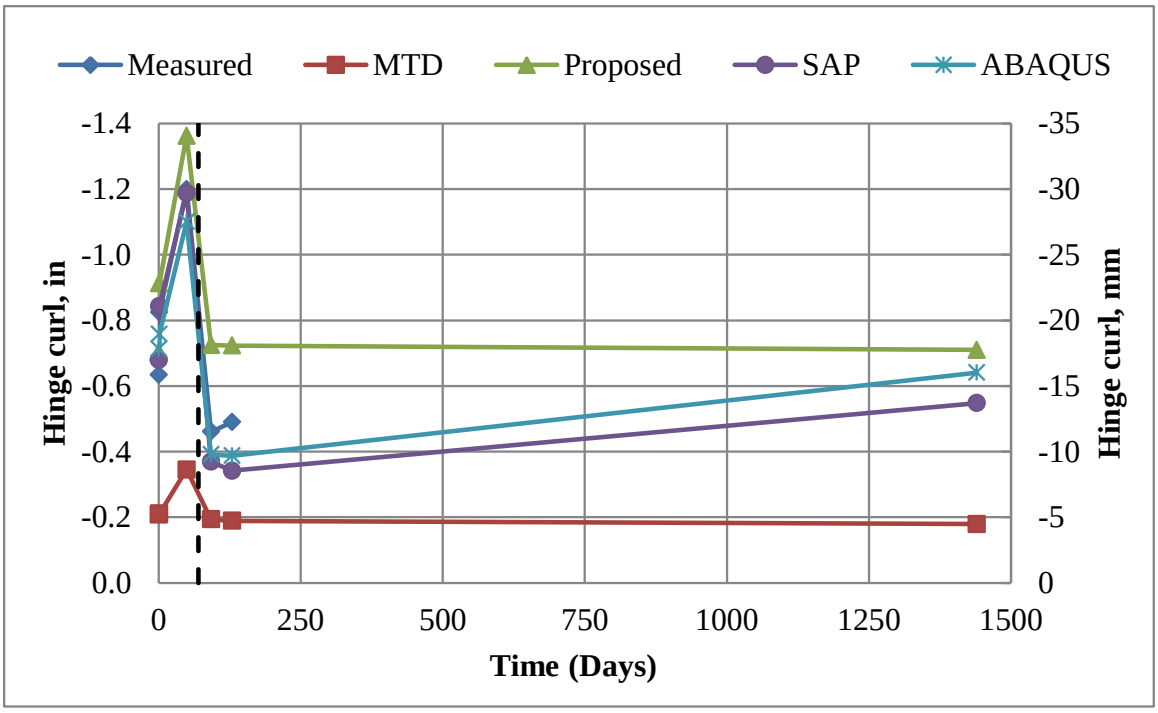


Figure 9-9 Comparison of measured and calculated hinge curl for H7, Bridge 1

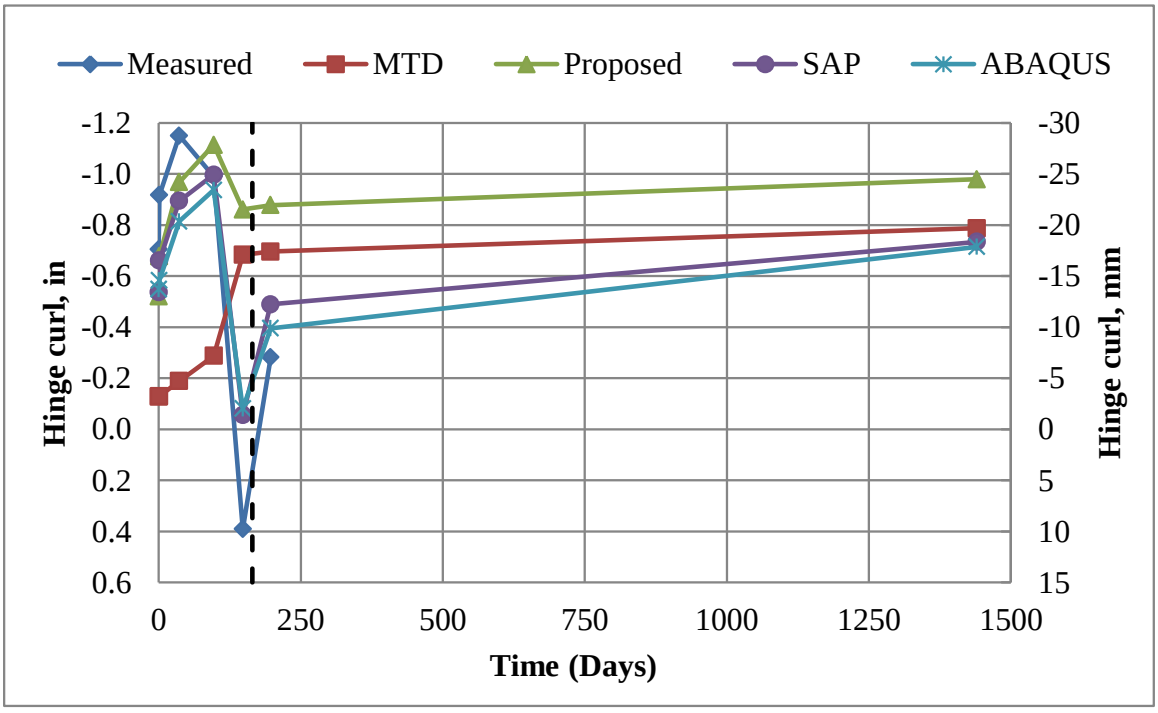


Figure 9-10 Comparison of measured and calculated hinge curl for H1, Bridge 2

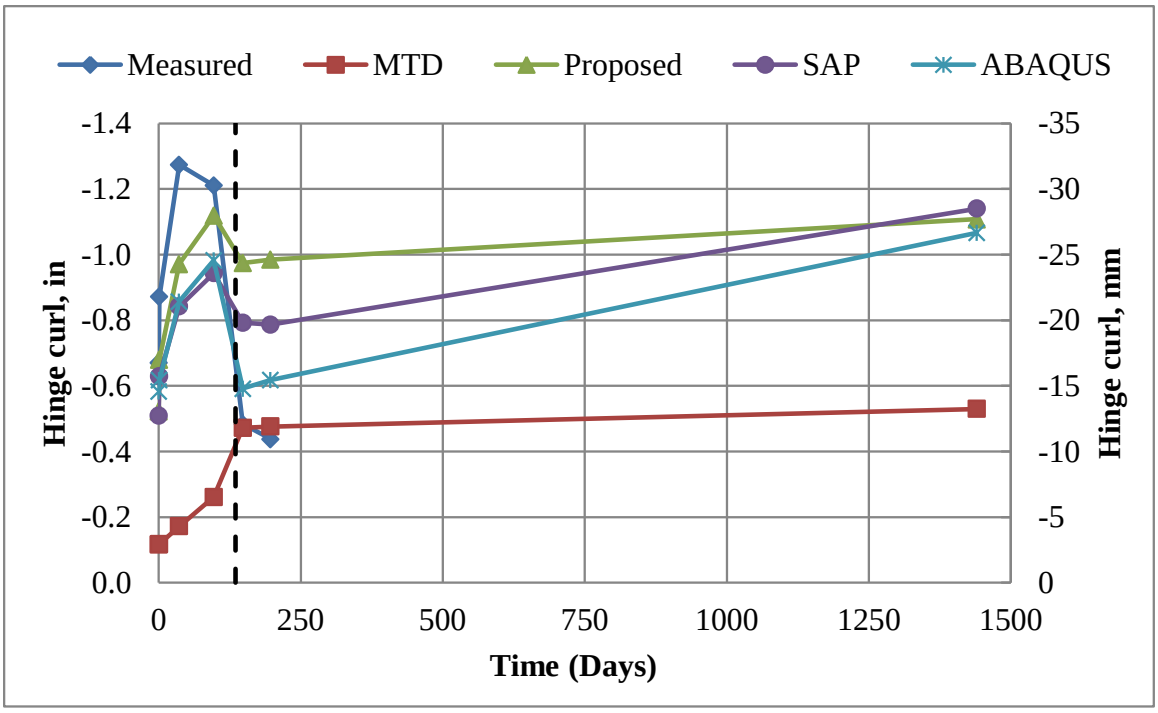


Figure 9-11 Comparison of measured and calculated hinge curl for H2, Bridge 2

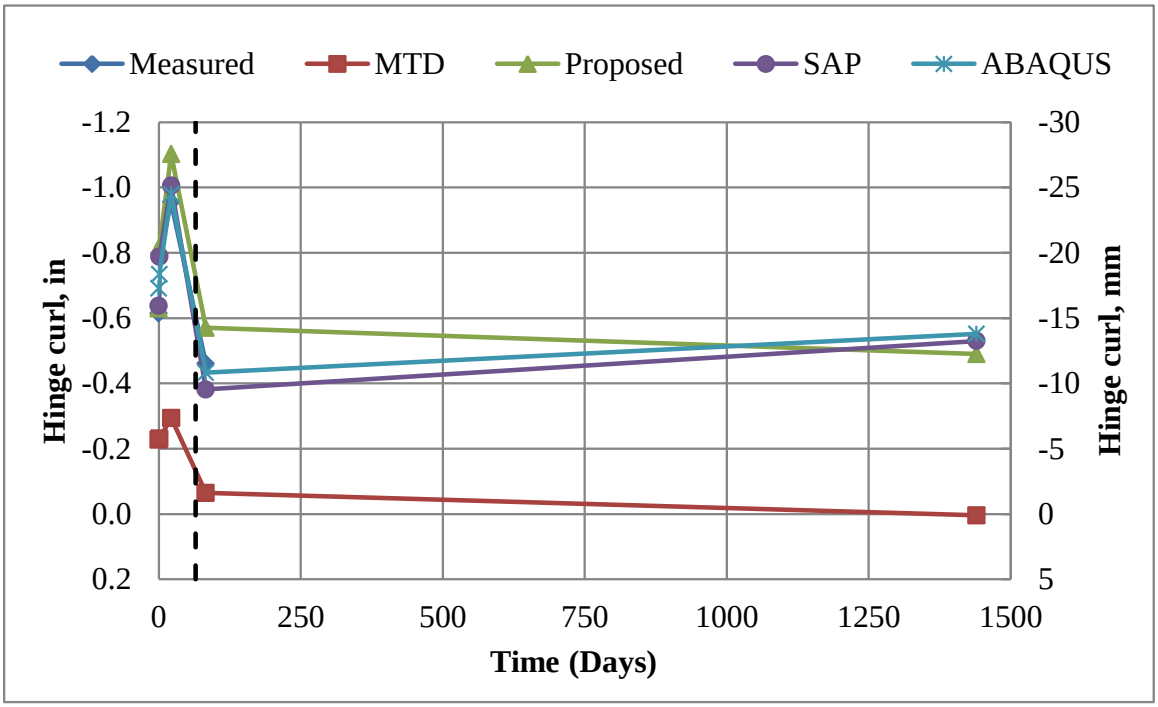


Figure 9-12 Comparison of measured and calculated hinge curl for H, Bridge 3

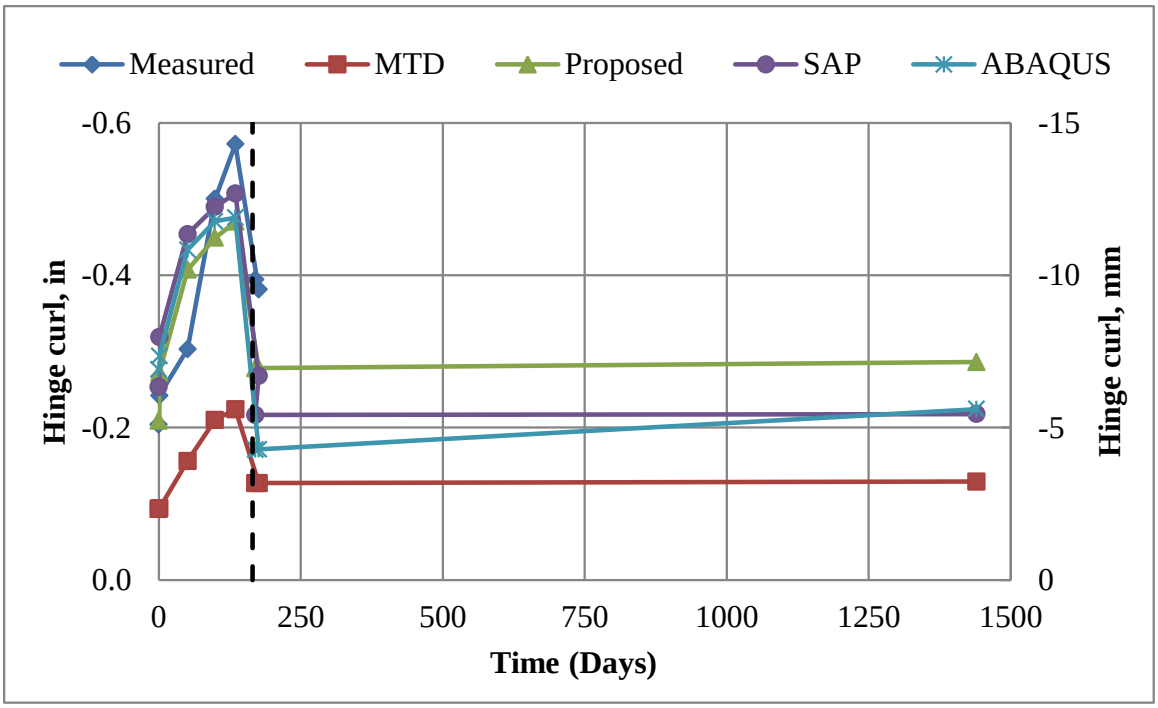


Figure 9-13 Comparison of measured and calculated hinge curl for H, Bridge 4

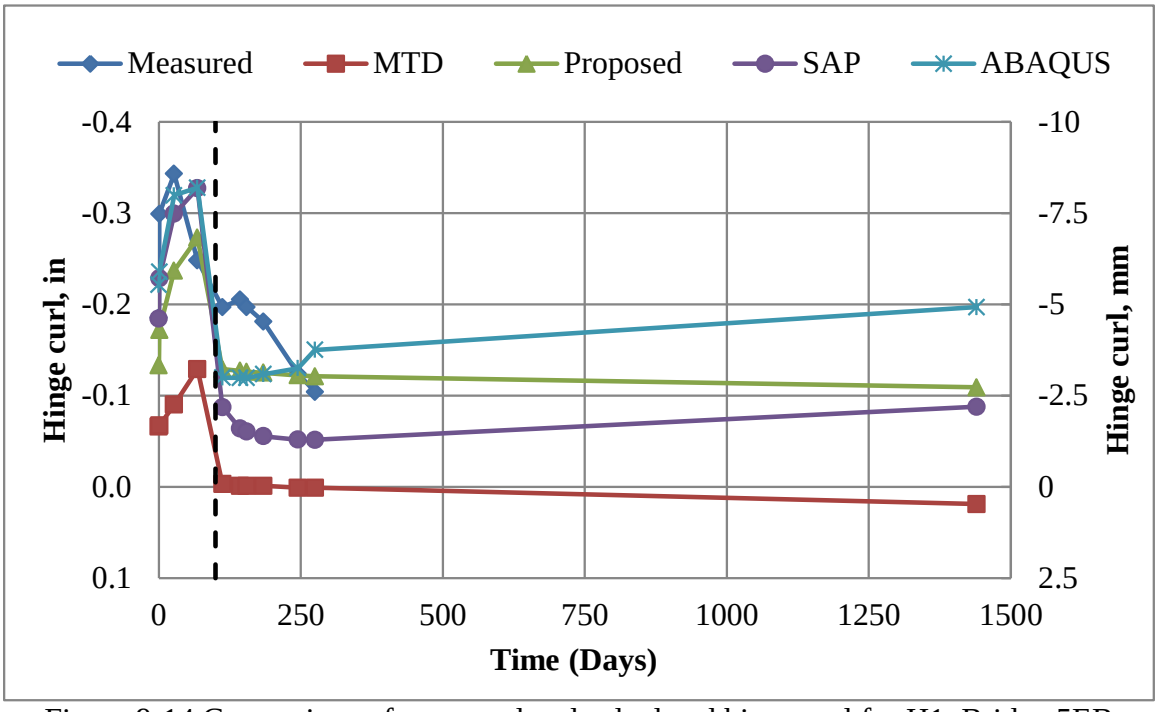


Figure 9-14 Comparison of measured and calculated hinge curl for H1, Bridge 5EB

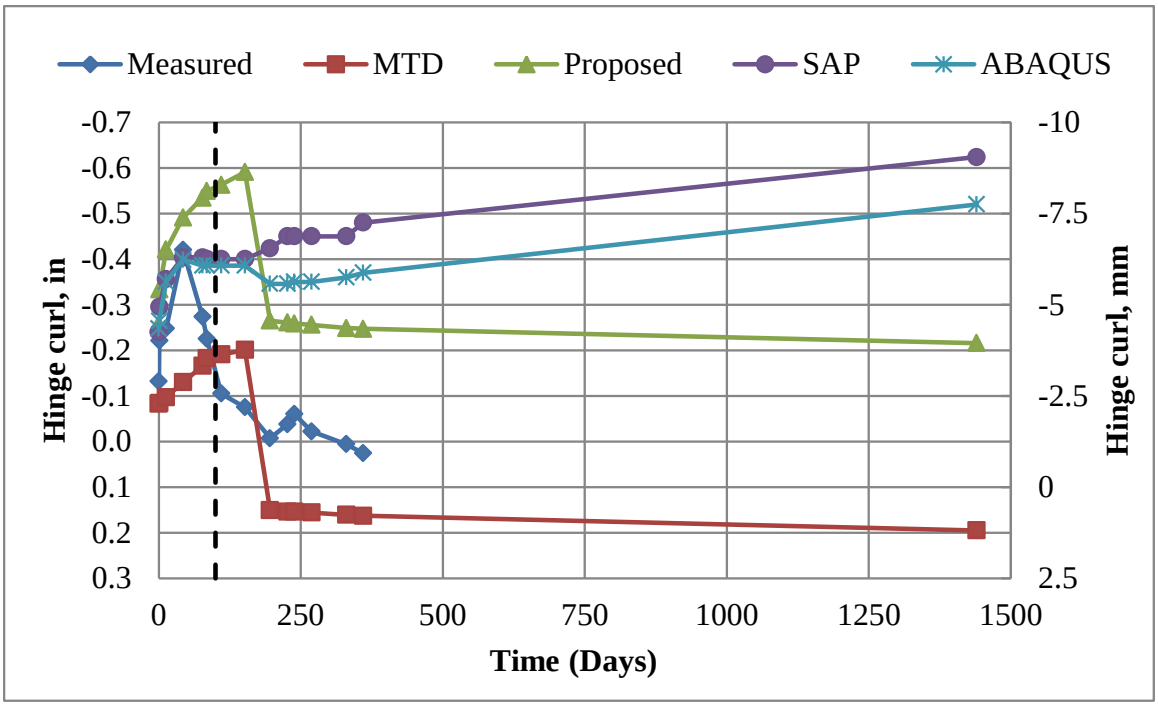


Figure 9-15 Comparison of measured and calculated hinge curl for C1, Bridge 5WB

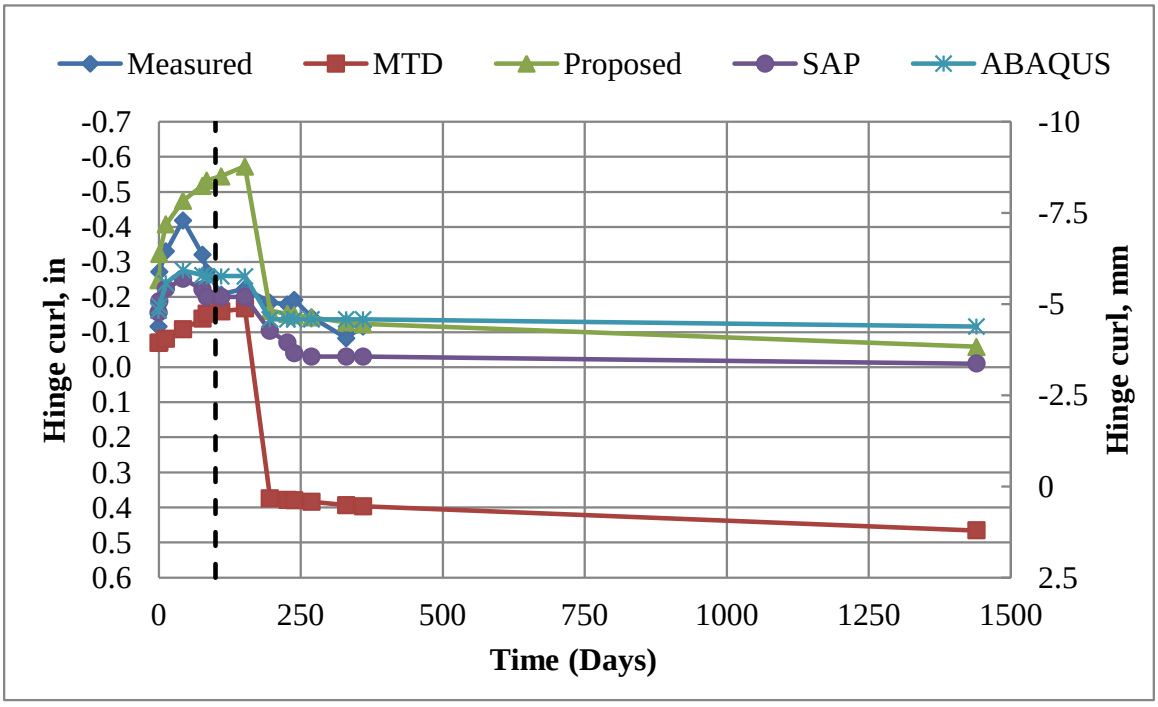


Figure 9-16 Comparison of measured and calculated hinge curl for C2, Bridge 5WB

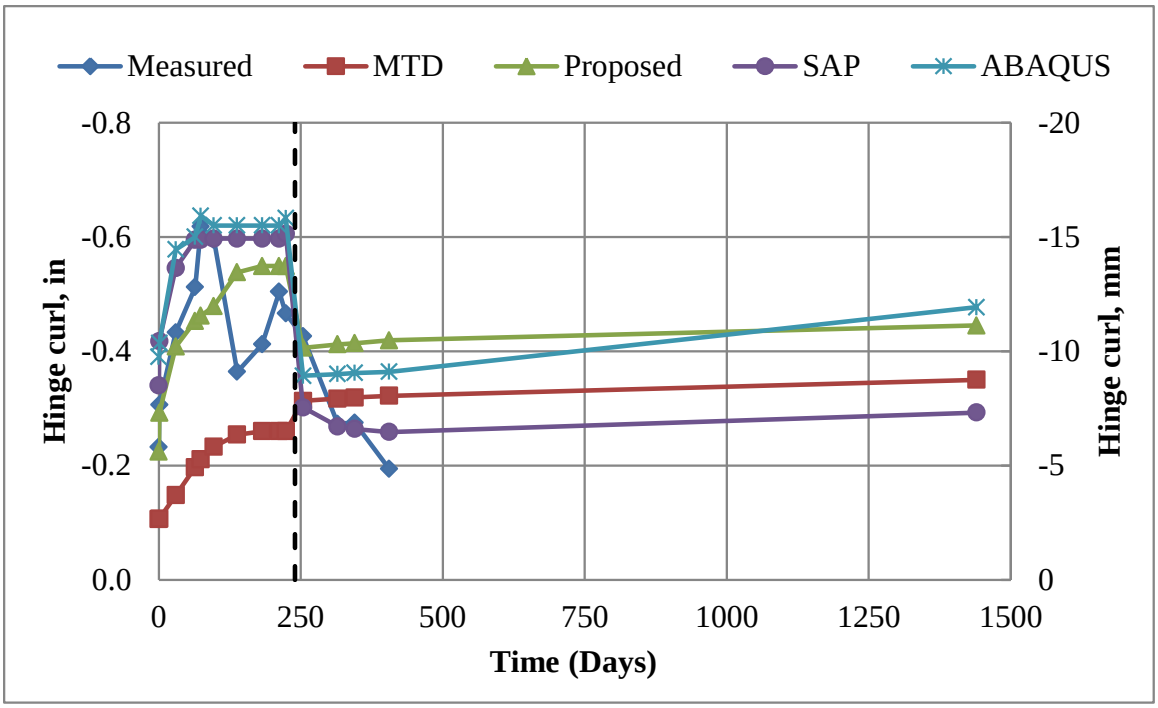


Figure 9-17 Comparison of measured and calculated hinge curl for H4, Bridge 5WB

# APPENDIX A

This appendix presents a sample data sheet used in field measurements.

**Date:** **Temp.:**

**Time:** **RH %:**

| | | L1 | L2 |
|---|---|---|---|
| Short Cantilever | T1 | | |
| | | | |
| | | | |
| | Avgerage | | |
| | T2 | | |
| | | | |
| | | | |
| | Avg. | | |
| | T3 "Bent 4" | | |
| | | | |
| | | | |
| | Avgerage | | |
| Adjacent Span | T4 | | |
| | | | |
| | | | |
| | Avgerage | | |
| | T5 | | |
| | | | |
| | | | |
| | Avgerage | | |
| | T6 | | |
| | | | |
| | | | |
| | Avgerage | | |
| | T7 "Bent 3" | | |
| | | | |
| | | | |
| | Avgerage | | |

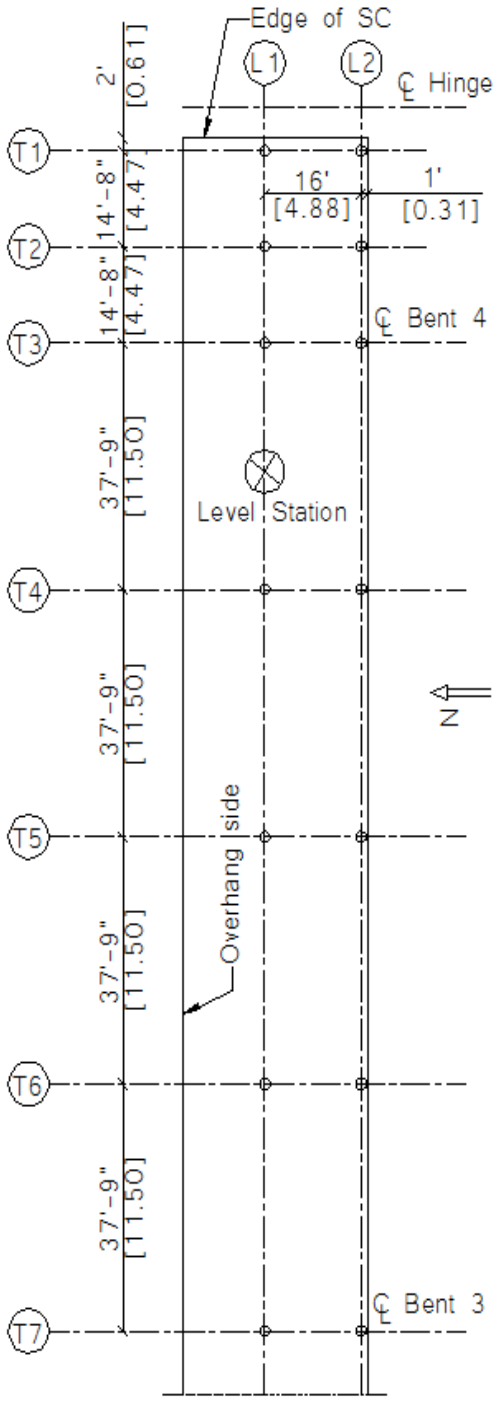


Figure A-1 Data collection sheet of Hinge, Bridge 3

# APPENDIX B

This appendix presents the draft new version of MTD 11-34 and a numerical example.

# 11-34 HINGE CURL

## Introduction

This memo discusses the deformation behavior of in-span hinges (Figure 1) for cast-in-place prestressed concrete box girder bridges. This behavior consists of the upward deflection of the unloaded short cantilever of the box girder bridge, as well as the downward deflection of the short cantilever when it is loaded by the long cantilever. This deformation behavior is commonly referred to as "hinge curl."

The designer is reminded that there is a variable period of time, usually between 30 and 180 days, in which the short cantilever remains unloaded after it has been stressed. Experience indicates that the duration over which the prestressed short cantilever is left unloaded influences the final location of the hinge. In general, shorter durations would produce a final deflection that is downward from its initial formed location, while longer durations may result in a final deflection that is upward from its initial formed location. This period of time and the extent of the deformation cannot be predicted until the contractor's schedule is finalized. Therefore, a table of values is typically provided in the plans that describes the amount of anticipated deflection, or more specifically, anticipated camber values relative to the duration in which the short cantilever is left unloaded.

The procedure and an example for estimating hinge curl are presented in this memo. The procedure simplifies a complicated analysis process by using deflection factors instead of using the time-dependent changes in concrete modulus of elasticity, creep, shrinkage, and steel relaxation. The procedure described in this memo provides the design engineer with a method for predicting the "hinge curl" deflections in order to provide the associated camber values on the contract plans. The procedure assumes that falsework will remain in the adjacent spans until the load is transferred to the hinge. This assumption is based on the requirements of the standard specifications.

After stressing, the short cantilever and the adjacent span deflect (Figure 2). Although the falsework remains in the adjacent span, the pier-superstructure connection rotates after stressing due to the flexibility of the columns, the adjacent span, and the falsework supporting the adjacent span. If the hinge span length and the adjacent span length are not equal, the connection rotates more after falsework removal due to the effect of unbalanced spans. The rotation of pier-superstructure connection before and after falsework removal is included in the hinge curl calculation using the procedure presented in this memo.

Should it be desirable to remove falsework prior to load transfer, the procedure presented in this memo should not be used. Instead, consideration should be given to either tying down the short cantilever or producing the camber values using an elaborate time-dependent analysis. Both alternatives are beyond the scope of this memo.

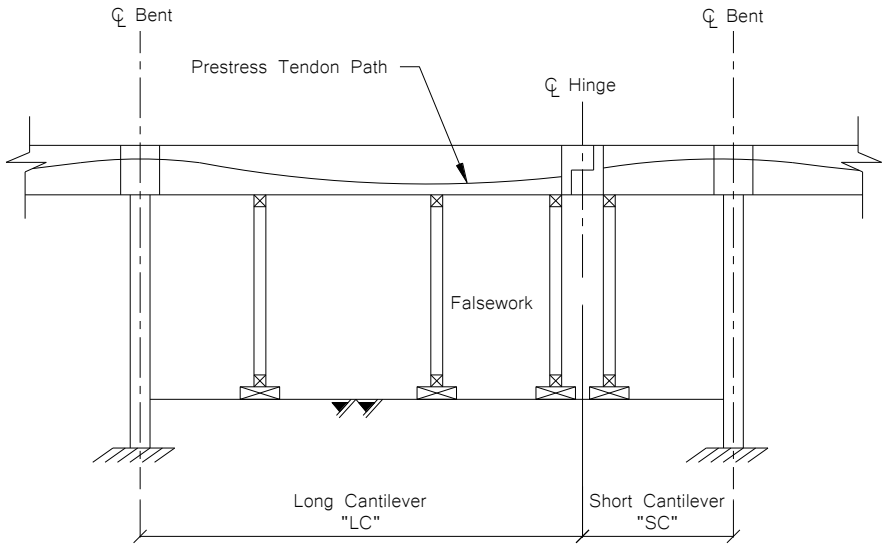


**Figure 1: Typical span of a hinge**

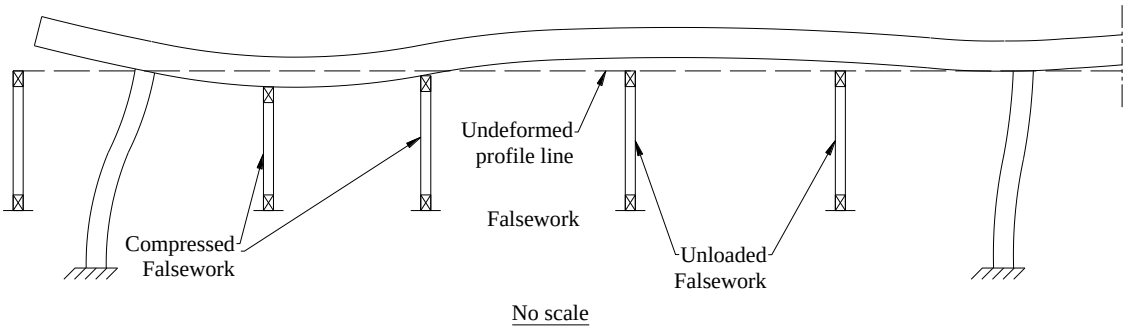


**Figure 2: Deformed shape of the short cantilever and the adjacent span after stressing**

## Sign Convention

It is important to note that deflection and camber carry opposite sign conventions. Specifically, **a downward deflection is considered positive and corresponds to a positive camber in the upward direction**. Positive camber requires setting screed line elevations higher than profile grade.

## Method of Calculation

1. Approximate the deflection of the short cantilever at the centerline of hinge due to dead load (Figure 3).

$$\Delta_{DL} = \underbrace{\frac{wL_1{}^3}{24EI}(4L_3 - L_1)}_{(1)} + \underbrace{\frac{PL_2{}^2}{6EI}(3L_3 - L_2)}_{(2)}$$

Where
(1) = Deflection of short cantilever due to the self-weight (in)
(2) = Deflection of short cantilever due to the weight of short cantilever portion of the hinge diaphragm (in)
w = Uniform self-weight of the prismatic section of the short cantilever (kips/in)
P = Weight of the portion of the hinge diaphragm that fills the voids of the prismatic section; short cantilever side only (kips)
$L_1$ = Length of short cantilever measured from the face of the hinge diaphragm to the face of support (in)
$L_2$ = Length of short cantilever measured from the face of support to the centroid of the short cantilever hinge diaphragm (in)
$L_3$ = Length of short cantilever measured from the face of support to the centerline of the hinge (in)
E = Concrete modulus of elasticity based on $f'_c$ (ksi)
I = Average moment of inertia of short cantilever span ($in^4$)

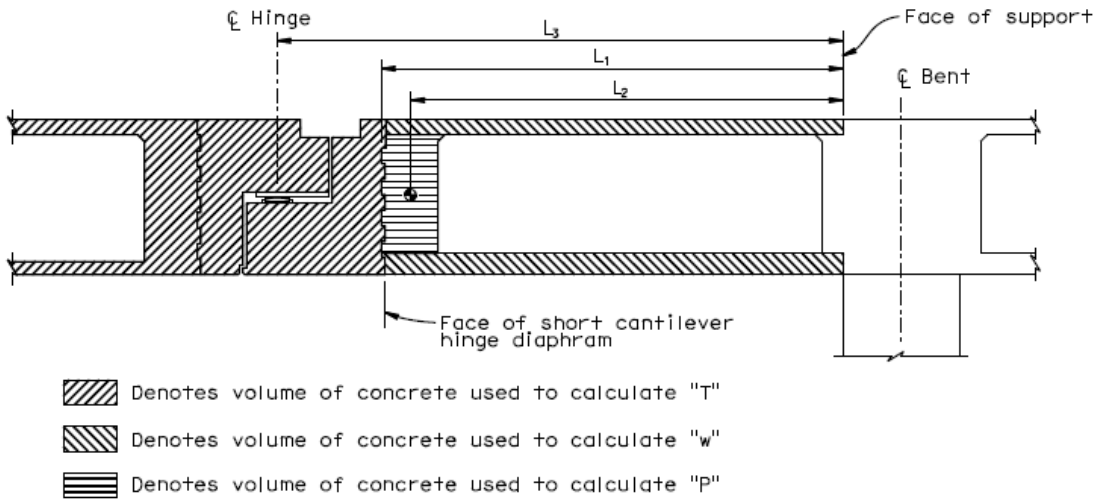


**Figure 3: Dead load for short cantilever**

2. Approximate the deflection of the short cantilever at the centerline of hinge due to prestressing force (Figure 4).

$$\Delta_{PS} = \frac{-P_j L_1 FC}{12EI}[e_1(8L_3 - 3L_1) + e_2(4L_3 - 3L_1)]$$

Where,
$P_j$ = Design jacking force (kips)
FC = Average initial force coefficient at time of stressing in the short cantilever (unitless)
$e_1$ = Eccentricity at centerline of bent, positive up (in).
$e_2$ = Eccentricity at anchorage in hinge diaphragm, positive up (in).

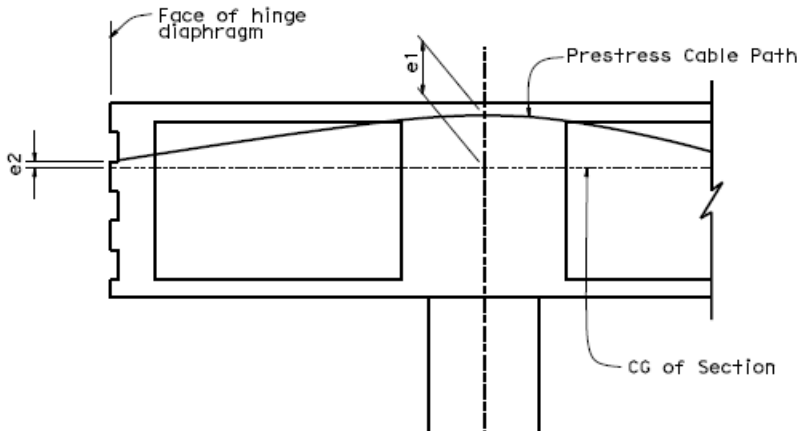


**Figure 4: Prestress cable path**

3. Approximate the deflection of the short cantilever due to flexibility of the support (Figure 5).

$$\Delta_{\text{flexible}} = -\theta_{\text{spring}} * \left(L_3 + \frac{C}{2}\right)$$

Where,
C = Column width in the bridge longitudinal direction
$\theta_{\text{spring}}$ = The rotation angle due to support flexibility and calculated as follows:

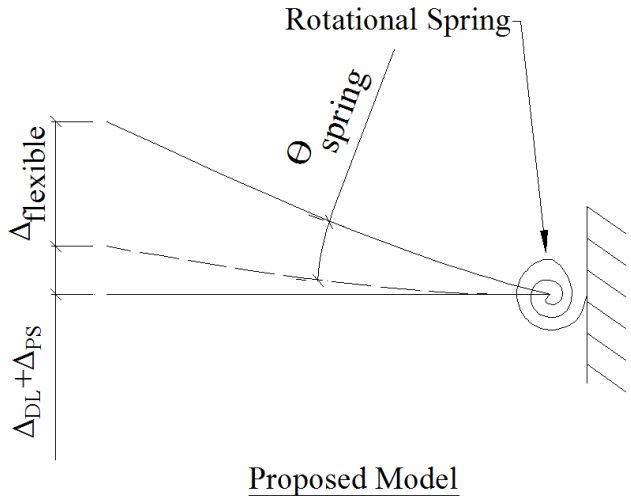


**Figure 5: Initial deflection of the short cantilever after stressing**

$$\theta_{\text{spring}} = \frac{K_1(M_{SC} - M_{\text{adjacent}}) - K_2(P_j FC)}{K_1 K_3 - {K_2}^2}$$

where

$M_{SC}$ = the moment acting at the short cantilever support due to post-tensioning and self-weight and calculated as follows:

$$M_{SC} = P_j FCe_1 - w\left(L_1 + \frac{C}{2}\right)^2/2 - P\left(L_2 + \frac{C}{2}\right)$$

$M_{adjacent}$ = the fixed end moment at the end of the adjacent span close to the hinge due to span weight, prestress force, and falsework reactions and calculated as follows:

$$M_{adjacent} = \frac{W_u(L_4)^2}{12} * Z$$

Where

$W_u$ = the equivalent falsework upward reaction on the adjacent span, assumed to be 5 k/ft for typical falsework (Figure 6)
Z = factor to account for the end support condition in the adjacent span away from the hinge, 1 for moment connection and 1.5 for simple support
$L_4$ = center to center adjacent span length

$$K_1 = \left(\frac{EA_{adj}}{L_4}\right) + \left(\frac{12EI_{col}}{H^3}\right)$$

$$K_2 = -\left(\frac{6EI_{col}}{H^2}\right)$$

$$K_3 = \left(\frac{KEI_{adj}}{L_4}\right) + \left(\frac{4EI_{col}}{H}\right)$$

Where

K = Coefficient to account for the end support condition in the adjacent span away from the hinge, 4 for moment connection and 3 for simple support
H = Clear column height
$I_{adj}$ = Average moment of inertia for the adjacent span
$I_{col}$ = Column gross moment of inertia
$A_{adj}$ = Average cross-section area for the adjacent span
E = Modulus of elasticity of concrete in the adjacent span and the adjacent column

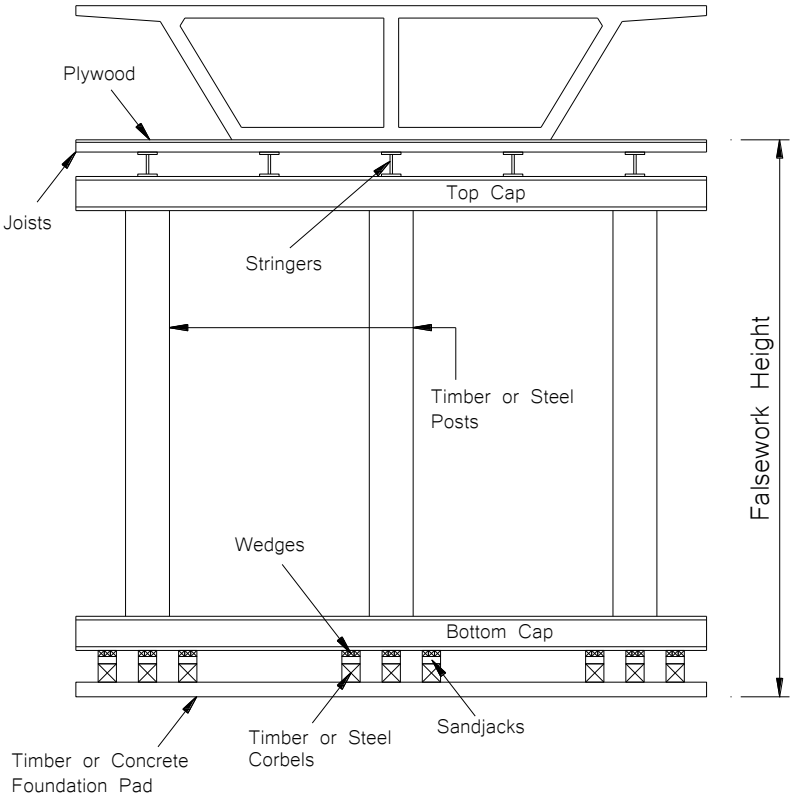


**Figure 6 (a) Bridge falsework; (b) Typical falsework bent**

4. Calculate $\Delta_{curl}$

$$\Delta_{curl} = \Delta_{DL} + \Delta_{PS} + \Delta_{flexible}$$

5. Approximate the deflection of the short cantilever due to load transfer from the long cantilever (Figure 3).

$$\Delta_{reaction} = \frac{TL_3^3}{3EI}$$

Where
T = Transfer load from long cantilever; dead load and prestressing load only. "T" includes the weight of the cast-in-place hinge ledges. The transfer load may be estimated from the longitudinal model as the shear demand at the face of the short cantilever hinge diaphragm.

6. Calculate Adjustment "SC" and Adjustment "LC" using the following formulas:

**Adjustment "SC" -** Profile adjustment required for Short Cantilever (can be positive or negative value).

0 day value = $3.00\Delta_{reaction} + 3.00\Delta_{curl}$ (theoretical; included here for illustrative purposes only.)
30 day value = $2.17\Delta_{reaction} + 3.00\Delta_{curl}$
60 day value = $1.98\Delta_{reaction} + 3.00\Delta_{curl}$
90 day value = $1.86\Delta_{reaction} + 3.00\Delta_{curl}$
120 day value = $1.77\Delta_{reaction} + 3.00\Delta_{curl}$
180 day value = $1.63\Delta_{reaction} + 3.00\Delta_{curl}$
240 day value = $1.53\Delta_{reaction} + 3.00\Delta_{curl}$
360 day value = $1.38\Delta_{reaction} + 3.00\Delta_{curl}$
720 day value = $1.14\Delta_{reaction} + 3.00\Delta_{curl}$
1440 day value = $1.00\Delta_{reaction} + 3.00\Delta_{curl}$ (theoretical; included here for illustrative purposes only.)

**Adjustment "LC" -** Profile adjustment required for the Long Cantilever (can be positive or negative value)

0 day value = $3.00\Delta_{reaction} + 3.00\Delta_{curl}$ (theoretical; included here for illustrative purposes only.)
30 day value = $2.17\Delta_{reaction} + 1.17\Delta_{curl}$
60 day value = $1.98\Delta_{reaction} + 0.98\Delta_{curl}$
90 day value = $1.86\Delta_{reaction} + 0.86\Delta_{curl}$
120 day value = $1.77\Delta_{reaction} + 0.77\Delta_{curl}$
180 day value = $1.63\Delta_{reaction} + 0.63\Delta_{curl}$
240 day value = $1.53\Delta_{reaction} + 0.53\Delta_{curl}$
360 day value = $1.38\Delta_{reaction} + 0.38\Delta_{curl}$
720 day value = $1.14\Delta_{reaction} + 0.14\Delta_{curl}$
1440 day value = $1.00\Delta_{reaction} + 0.00\Delta_{curl}$ (theoretical; included here for illustrative purposes only.)

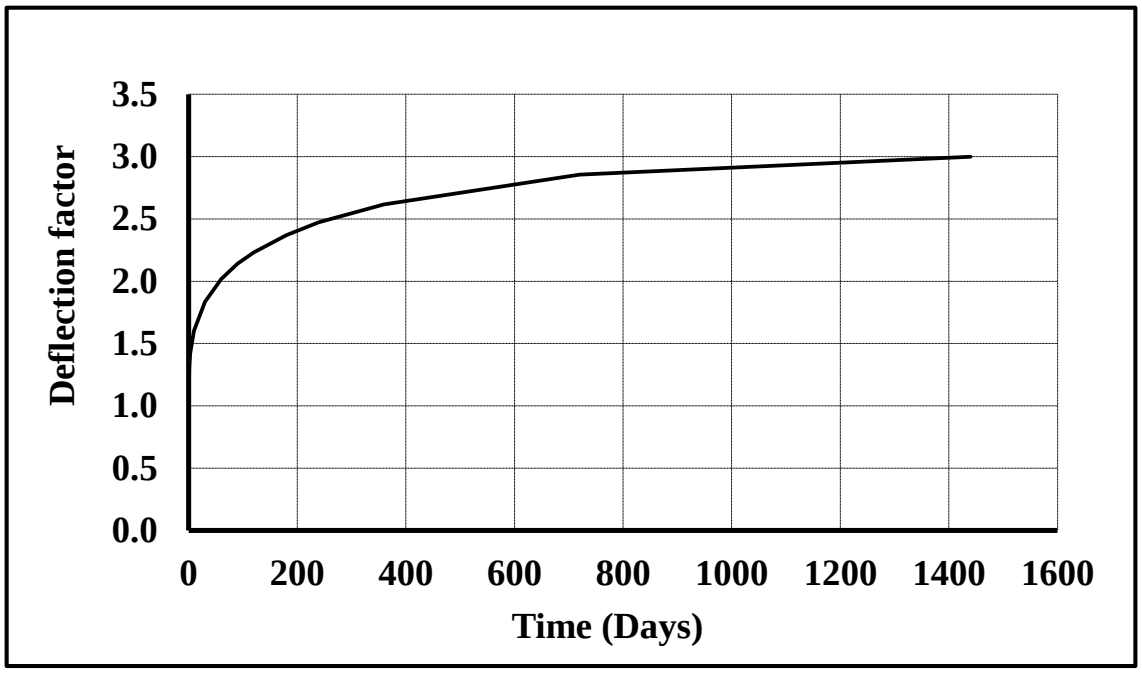


**Figure 7: Deflection factor chart**

The long term effects that are incorporated into the Adjustment "SC" and Adjustment "LC" calculations are derived from the deflection factor chart (Figure 7). The deflection factor curve represents the total amount of deflection a cast-in-place prestressed concrete element undergoes with respect to time. Table 1 lists the time-dependent deflection factors. The long term deflection including creep and shrinkage is assumed to be three times the immediate elastic deflection and this will occur over a four year period. The curve starts at a value of 1.00 since it represents immediate elastic deflection for a given load at Day 0. Also, day "0" is considered the day that the short cantilever is prestressed.

**Table 1: Deflection factors**

| Time (Days) | Deflection factor |
|---|---|
| 0 | 1.00 |
| 1 | 1.30 |
| 3 | 1.42 |
| 10 | 1.60 |
| 30 | 1.83 |
| 60 | 2.02 |
| 90 | 2.14 |
| 120 | 2.23 |
| 180 | 2.37 |
| 240 | 2.47 |
| 360 | 2.62 |
| 720 | 2.86 |
| 1440 | 3.00 |

The Deflection Factor chart may be used thus:

On Day 0:
$\Delta_{total,\ day\ 0}=1.00\Delta_{elastic}$

If the given load is left for 60 days after Day 0, the deflection factor grows to 2.02, thus:

On Day 60:
$\Delta_{total,\ day\ 60}=2.02\Delta_{elastic}$

Adjustment "SC" and Adjustment "LC" utilize the deflection factor graph in the same manner as described. The difference is that the adjustment calculations capture a change in the loading condition sometime after the initial loading condition. The initial loading condition is the prestressing and self-weight of the short cantilever, and the change in loading condition pertains to the addition of the transfer load from the long cantilever. The time value is the elapsed time between the initial loading condition and the time that the long cantilever load is transferred to the short cantilever. Each loading component results in an elastic deflection ($\Delta_{curl}$ and $\Delta_{reaction}$), and each deflection component is multiplied by a deflection factor associated with the time that the load is applied.

For example, the Adjustment "SC" at Day 30 is: $2.17\Delta_{reaction} + 3.00\Delta_{curl}$. The deflection factor of 3.00, applied to $\Delta_{curl}$, represents the notion that the short cantilever will be loaded by its self-weight and prestressing immediately after it is cured sufficiently, therefore the maximum deflection factor of 3.00 is applied. The $2.17\Delta_{reaction}$ represents the notion that 30 days has elapsed since the initial load, and the component of the deflection factor representing creep and shrinkage, in the amount of 0.83 (1.83-1.00), has already occurred in the short cantilever. Thus, the transfer load component, $\Delta_{reaction}$, will only be subjected to the remaining deflection factor of 2.17 (3.00-0.83).

Accordingly, Adjustment "LC" for the Day 30 value is: $2.17\Delta_{reaction} + 1.17\Delta_{curl}$. Adjustment "LC" signifies the amount of camber correction that the long cantilever needs in order to match the location of the short cantilever when the load is transferred. The factor 1.17, applied to $\Delta_{curl}$, represents the notion that at Day 30, the short cantilever has already undergone $1.83\Delta_{curl}$ of deflection, and what remains is $(3.00\text{-}1.83)\Delta_{curl}$. The $2.17\Delta_{reaction}$ signifies that the transfer load component, $\Delta_{reaction}$, will only be subjected to the remaining deflection factor of 2.17 (3.00-0.83). In short, Adjustment "LC" results in the contact of Points 2 and 3 (Figure 8) when the transfer load from the long cantilever occurs on the anticipated schedule.

The factors used for Adjustment "SC" and Adjustment "LC", and the calculation methods presented herein, may be adjusted if more accurate site-specific and material-specific deflection curves can be generated.

## Development of the Plan Camber Diagram

This step involves incorporating the Adjustment "SC" and Adjustment "LC" values with the theoretical camber of the hinge span. Once the Adjustment values are added to the theoretical camber of the span, we refer to the values as Camber "SC" and Camber "LC". Load transfer from the long cantilever will usually occur sometime in the period of 30 to 180 days after prestressing the short cantilever span. Thus, tabulated camber values shall be shown on the plans. The designer may optionally provide camber values for up to 720 days.

Figure 8 shows the relationship between Adjustment "SC", Adjustment "LC", and the theoretical camber of the span.

**Point 1 -** Represents the theoretical adjustment to theoretical camber if load transfer is immediate.

**Point 2 -** Represents the adjustment to theoretical camber, up or down, at the end of the long cantilever, which is dependent on the time of load transfer (Adjustment "LC")

**Point 3** – Represents the adjustment to theoretical camber up or down at the end of the short cantilever (Adjustment "SC").

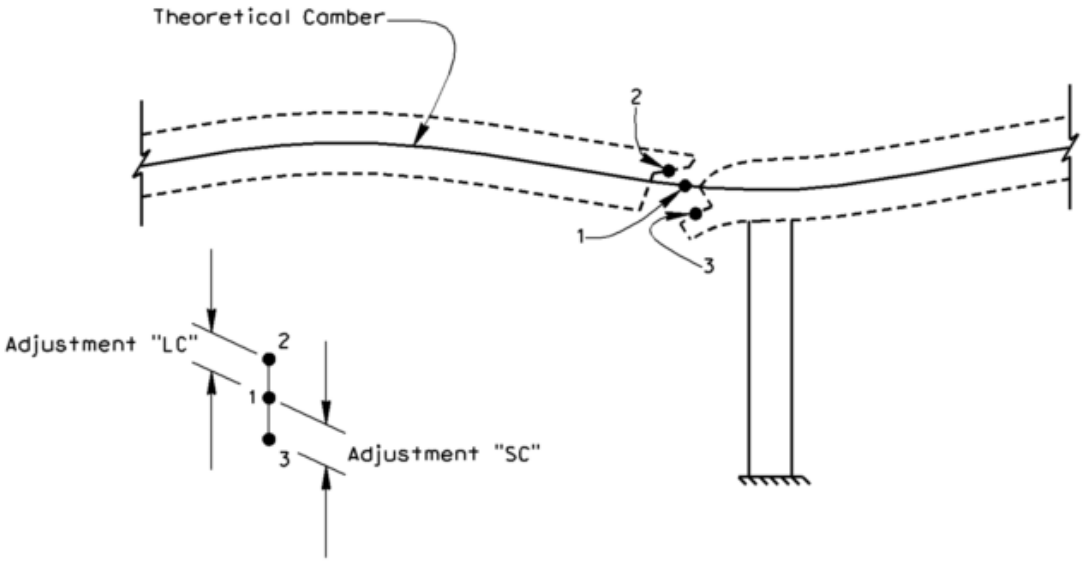


**Figure 8: Adjustment to Theoretical Camber**

The generation of tabulated camber values and the camber diagram is illustrated in an example. The example below shows the steps involved in calculating the Adjustment "SC" and Adjustment "LC" values, as well as incorporating them with the theoretical camber to generate time-dependent Camber "SC" and Camber "LC" values.

**Example**

In this example, the time-dependent cambers were calculated using the procedure presented in this memo. The example problem consists of one in-span hinge as shown in Figure 9. The short cantilever length is 20 ft, and the adjacent span is 121 ft.

**Given:**

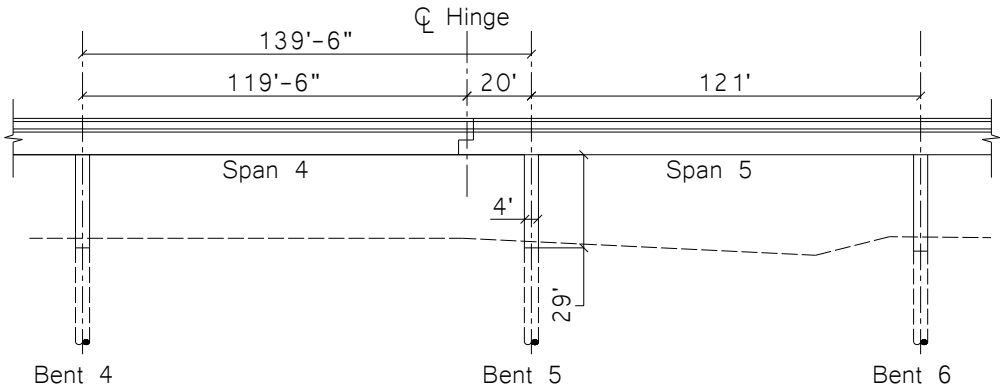


**Elevation**

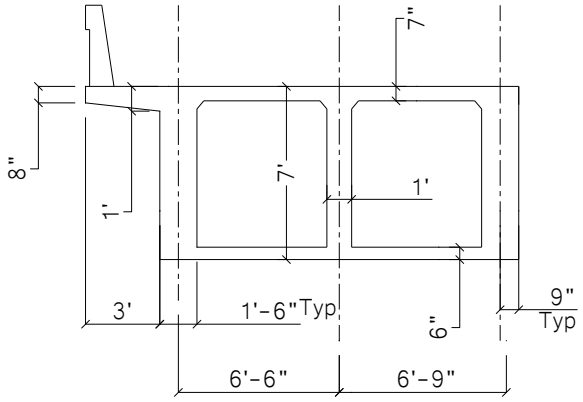


**Typical Section**

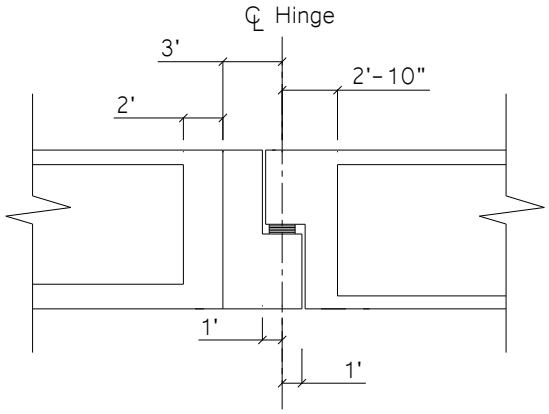


**Hinge Section**

**Figure 9: Example bridge**

**Short cantilever**

$A_{SC}$ = 48 ft$^2$

$A_{voids}$ = 60 ft$^2$

$I_{SC}$ = 301 ft$^4$

E = 3834 ksi

$e_1$ = 29 inch = 2.42 ft

$e_2$ = 0

$P_j$ = 3600 kips

FC = 0.85 (average force coefficient along length of short cantilever)

$t_{hinge\ diaph}$ = 2 ft

$L_1$ = 15 ft

$L_2$ = 14 ft

$L_3$ = 18 ft

$A_{adj}$ = 41 ft$^2$

$I_{adj}$ = 258 ft$^4$

E = 3834 ksi

$L_4$ = 121 ft

**Column**

$I_{col}$ = 32 ft$^4$

E = 3637 ksi

H = 29 ft

C = 4 ft

**Step 1 – Calculate $\Delta_{DL}$**

$$\Delta_{DL} = \frac{wL_1^{\,3}}{24EI}(4L_3 - L_1) + \frac{PL_2^{\,2}}{6EI}(3L_3 - L_2)$$

$$w = 48\ \text{ft}^2 \times 0.15\frac{\text{kip}}{\text{ft}^3} = 7.2\frac{\text{kip}}{\text{ft}}$$

$$P = A_{voids} \times t_{hinge\ diaph} \times 0.15\frac{\text{kip}}{\text{ft}^3} = 60\ \text{ft}^2 \times 2\ \text{ft} \times 0.15\frac{\text{kip}}{\text{ft}^3} = 18\ \text{kip}$$

E = 3834 ksi

I = 301 ft$^4$

$\Delta_{DL}$ = 0.005 in

**Step 2 – Calculate $\Delta_{PS}$**

$$\Delta_{PS} = \frac{-P_j L_1 FC}{12EI}[e_1(8L_3 - 3L_1) + e_2(4L_3 - 3L_1)]$$

E = 3834 ksi

I = 301 $ft^4$

$\Delta_{PS}$ = -0.066 in

**Step 3 – Calculate $\Delta_{flexible}$**

$$K_1 = \left(\frac{EA_{adj}}{L_4}\right) + \left(\frac{12EI_{col}}{H^3}\right) = \left(\frac{(3834 \times 12^2) \times 41}{121}\right) + \left(\frac{12 \times (3637 \times 12^2) \times 32}{29^3}\right)$$
$$= (1.87E+05) + (8276) = (1.95E+05)\frac{kip}{ft}$$

$$K_2 = -\left(\frac{6EI_{col}}{H^2}\right) = -\left(\frac{6 \times (3637 \times 12^2) \times 32}{29^2}\right) = -(1.20E+05)\frac{kip}{ft}$$

$$K_3 = \left(\frac{KEI_{adj}}{L_4}\right) + \left(\frac{4EI_{col}}{H}\right) = \left(\frac{4 \times (3834 \times 12^2) \times 258}{121}\right) + \left(\frac{4 \times (3637 \times 12^2) \times 32}{29}\right)$$
$$= (4.71E+06) + (2.31E+06) = (7.02E+06)\ kip.\frac{ft}{rad}$$

$$M_{SC} = Fe_1 - \frac{w\left(L_1 + \frac{C}{2}\right)^2}{2} - P\left(L_2 + \frac{C}{2}\right)$$

$$M_{SC} = 3060 \times 2.42 - \frac{7.2\left(15 + \frac{4}{2}\right)^2}{2} - 18\left(14 + \frac{4}{2}\right) = 6156\ kip.ft$$

$$M_{adjacent} = \frac{W_u(L_4)^2}{12} * Z = \frac{5(121)^2}{12} * 1 = 6100\ kip.ft$$

$$\theta_{spring} = \frac{K_1(M_{SC} - M_{adjacent}) - K_2(P_j FC)}{K_1 K_3 - {K_2}^2}$$
$$= \frac{(1.95E+05) \times (6156 - 6100) - (-1.20E+05) \times (3600 \times 0.85)}{(1.95E+05) \times (7.02E+06) - (-1.20E+05)^2}$$
$$= 2.78E-04\ rad.$$

$$\Delta_{flexible} = -\theta_{spring} * \left(L_3 + \frac{C}{2}\right) = -(2.78E-04) * \left(18 + \frac{4}{2}\right) = -0.067\ in$$

**Step 4 – Calculate $\Delta_{curl}$**

$$\Delta_{curl} = \Delta_{DL} + \Delta_{PS} + \Delta_{flexible} = 0.005 + (-0.066) + (-0.067) = -0.128\ in$$

**Step 5 – Calculate $\Delta_{reaction}$**

T = 355 kips (transfer load from long span)

$$\Delta_{reaction} = \frac{TL_3^3}{3EI} = \frac{355(18^3)}{3(3834 \times 12^2)(301)}(12) = 0.05 \text{ in}$$

**Step 6 – Calculate Adjustment "SC"**

| | $\Delta_{reaction}$ | $\Delta_{curl}$ | |
|---|---|---|---|
| Day 0 = | 3.00(0.05) + | 3.00(-0.128) | = **-0.234"** |
| Day 30 = | 2.17(0.05) + | 3.00(-0. 128) | = -0.275" |
| Day 60 = | 1.98(0.05) + | 3.00(-0. 128) | = -0.285" |
| Day 90 = | 1.86(0.05) + | 3.00(-0. 128) | = -0.291" |
| Day 120 = | 1.77(0.05) + | 3.00(-0. 128) | = -0.295" |
| Day 180 = | 1.63(0.05) + | 3.00(-0. 128) | = -0.302" |
| Day 240 = | 1.53(0.05) + | 3.00(-0. 128) | = -0.307" |
| Day 360 = | 1.38(0.05) + | 3.00(-0. 128) | = -0.315" |
| Day 720 = | 1.14(0.05) + | 3.00(-0. 128) | = -0.327" |

**Step 7 – Calculate Adjustment "LC"**

| | $\Delta_{reaction}$ | $\Delta_{curl}$ | |
|---|---|---|---|
| Day 0 = | 3.00(0.05) + | 3.00(-0. 128) | = **-0.234"** |
| Day 30 = | 2.17(0.05) + | 1.17(-0. 128) | = -0.041" |
| Day 60 = | 1.98(0. 05) + | 0.98 (-0. 128) | = -0.027" |
| Day 90 = | 1.86(0. 05) + | 0.86(-0. 128) | = -0.017" |
| Day 120 = | 1.77(0. 05) + | 0.77(-0. 128) | = -0.010" |
| Day 180 = | 1.63(0. 05) + | 0.63(-0. 128) | = 0.001" |
| Day 240 = | 1.53(0. 05) + | 0.53(-0. 128) | = 0.008" |
| Day 360 = | 1.38(0. 05) + | 0.38(-0. 128) | = 0.020" |
| Day 720 = | 1.14(0. 05) + | 0.14(-0. 128) | = 0.039" |

**Step 8 – Obtain Long Cantilever Camber from CTBridge at ¼ points**

The camber at ¼ points includes a deflection factor of 3.0.

$LC_{0.25}$ (at 29.9') = 1.044"
$LC_{0.50}$ (at 59.8') = 1.872"
$LC_{0.75}$ (at 89.6') = 1.560"
$LC_{1.00}$ (at 119.5') = 0.084"
SC (at 119.5') = 0.084"

Where, $LC_{0.25}$ represents unadjusted camber at the quarter point along the length of the long cantilever calculated from the CTBridge program. SC is the unadjusted camber at the tip of the short cantilever. SC, by definition, is equal to $LC_{1.00}$. However, for a reverse configuration, in which the short cantilever is on the left side of the span, SC is equal to $LC_{0.00}$.

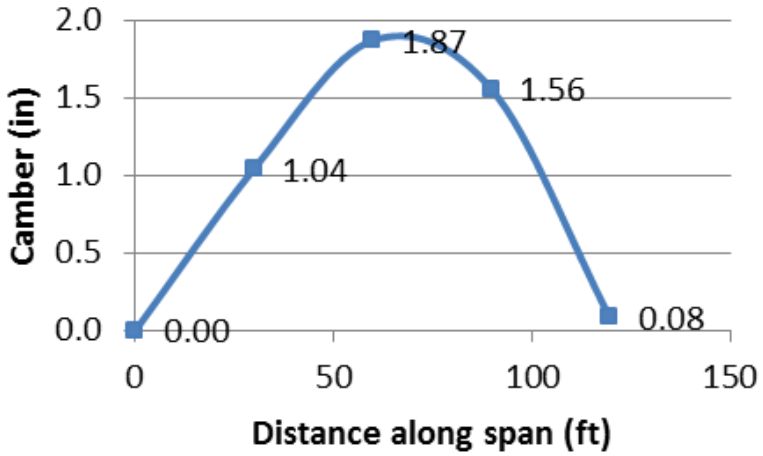


**Figure 10: Long cantilever camber**

## Step 8 – Adjust Short Cantilever Camber for Time-Dependent Correction

This step calculates Camber "SC" for the short cantilever. Because the calculation of $\Delta_{curl}$ assumes that the adjacent spans are supported on falsework, the joint rotation due to the effect of unbalanced spans is neglected. Generally, unbalanced spans will generate deflections that differ from the Adjustment "SC" values. Therefore, one can estimate the deflection due to joint rotation, $\delta_{SC}$, by calculating the difference between the camber determined by the longitudinal analysis program, CTBridge, and Adjustment "SC" at 0-day (Figure 11).

Adjustment "SC" at 0-day = -0.234" (from Step 5)
$\delta_{SC}$ = SC - Adjustment "SC" = 0.084" - (-0.234)" = **0.318"**

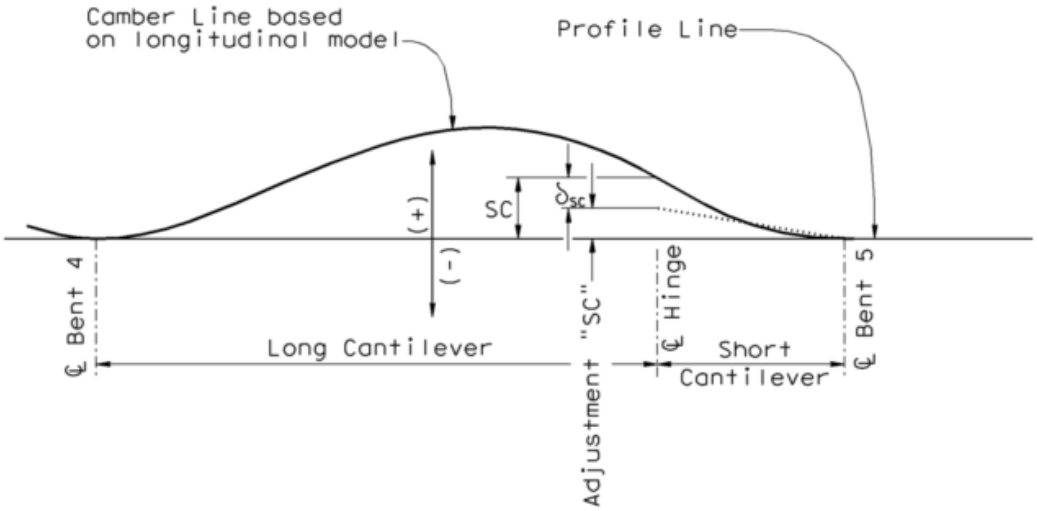


**Figure 11: Short cantilever camber**

Camber “SC” values are calculated as such:

Day 30 = Adjustment “SC” + 2.17×($\delta_{SC}$/3)
= -0.275” + 2.17×(0.318”/3) = -0.045”
Day 60 = -0.285” + 1.98×(0.318”/3) = -0.075”
Day 90 = -0.291” + 1.86×(0.318”/3)” = -0.094”
Day 120 = -0.295” + 1.77×(0.318”/3)” = -0.108”
Day 180 = -0.302” + 1.63×(0.318”/3)” = -0.129”
Day 240 = -0.307” + 1.53×(0.318”/3)” = -0.145”
Day 360 = -0.315” + 1.38×(0.318”/3)” = -0.168”
Day 720 = -0.327” + 1.14×(0.318”/3)” = -0.206”

**Step 9 – Adjust Long Cantilever Camber for Time-Dependent Correction**

Camber “LC” is calculated similarly to Camber "SC"

**At $LC_{1.00}$ (at hinge):**

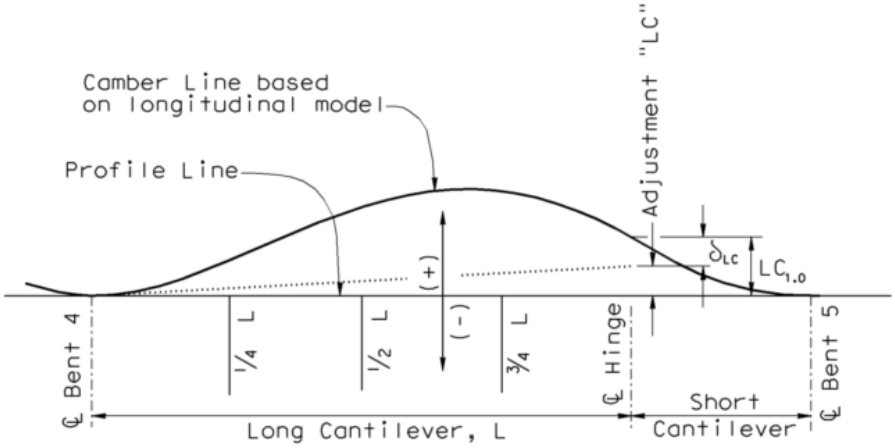


**Figure 12: Long cantilever camber**

Adjustment “LC” at 0-day = -0.234” (from Step 6)
$\delta_{LC1.0}$ = $LC_{1.00}$ – Adjustment “LC”
= 0.084” - (-0.234)”
= **0.318”**
Day 30 = Adjustment “LC” + 2.17×($\delta_{LC1.00}$/3)
= -0.041” + 2.17×(0.318”/3) = 0.189”
Day 60 = -0.027” + 1.98×(0.318”/3) = 0.183”
Day 90 = -0.017” + 1.86×(0.318”/3) = 0.180”
Day 120 = -0.010” + 1.77×(0.318”/3) = 0.177”
Day 180 = 0.001” + 1.63×(0.318”/3) = 0.173”
Day 240 = 0.008” + 1.53×(0.318”/3) = 0.171”
Day 360 = 0.020” + 1.38×(0.318”/3) = 0.166”
Day 720 = 0.039” + 1.14×(0.318”/3) = 0.160”

**At $LC_{0.75}$ (at ¾ point):**

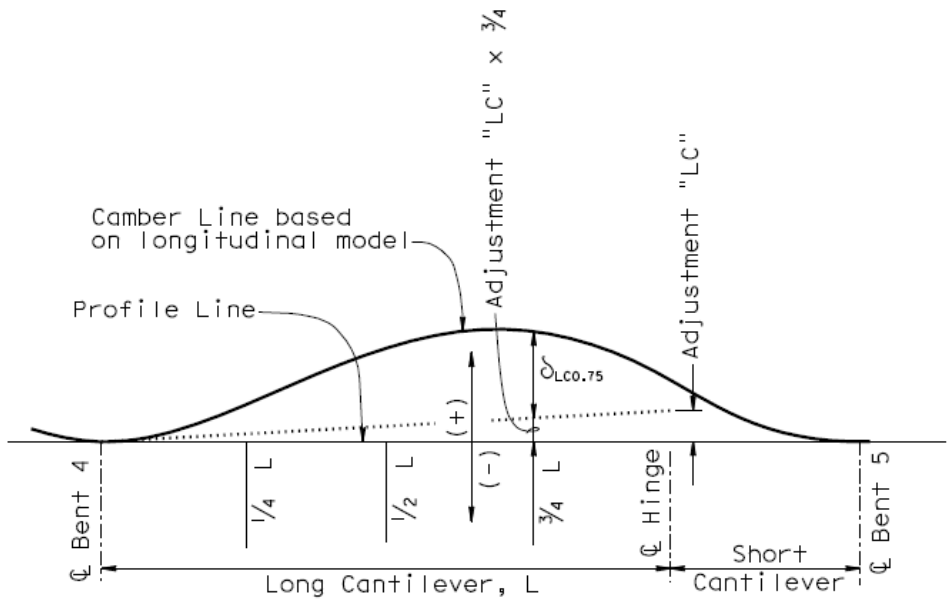


**Figure 13: Long cantilever camber at ¾ point**

At locations along the long cantilever, other than at the hinge, time-dependent camber values are adjusted by linearly interpolating Adjustment "LC". At the ¾L point, Adjustment "LC" is factored by ¾. Note that if the hinge span configuration is reversed, in which the short hinge is on the left, the factor applied to Adjustment "LC" at the ¾L point would be ¼ instead of ¾.

Adjustment "LC" at Day 0 = -0.234" × ¾ = -0.175"
$\delta_{LC0.75}$ = $LC_{0.75}$ – (Adjustment "LC" × ¾)
= 1.56" - (-0.175)"
= **1.735"**

Day 30= Adjustment "LC" × ¾ + 2.17×($\delta_{LC0.75}$/3)
= -0.041"(¾) + 2.17×(1.735"/3) = 1.224"
Day 60 = -0.027"(¾) + 1.98×(1.735"/3) = 1.125"
Day 90 = -0.017"(¾) + 1.86×(1.735"/3) = 1.063"
Day 120 = -0.010"(¾) + 1.77×(1.735"/3) = 1.016"
Day 180 = 0.001"(¾) + 1.63×(1.735"/3) = 0.943"
Day 240 = 0.008"(¾) + 1.53×(1.735"/3) = 0.891"
Day 360 = 0.020"(¾) + 1.38×(1.735"/3) = 0.813"
Day 720 = 0.039"(¾) + 1.14×(1.735"/3) = 0.689"

**At $LC_{0.50}$ (at ½ point):**

Adjustment "LC" at 0-day = -0.234" × ½ = -0.117"
$\delta_{LC0.50}$ = $LC_{0.50}$ – (Adjustment "LC" × ½)
= 1.872" - (-0.117)"
= **1.989"**

Day 30 = Adjustment "LC" × ½ + 2.17×($\delta_{LC0.50}$/3)
= -0.041"(½) + 2.17×(1.989"/3) = 1.418"
Day 60 = -0.027"(½) + 1.98×(1.989"/3) = 1.299"
Day 90 = -0.017"(½) + 1.86×(1.989"/3) = 1.225"
Day 120 = -0.010"(½) + 1.77×(1.989"/3) = 1.168"
Day 180 = 0.001"(½) + 1.63×(1.989"/3) = 1.081"
Day 240 = 0.008"(½) + 1.53×(1.989"/3) = 1.019"
Day 360 = 0.020"(½) + 1.38×(1.989"/3) = 0.925"
Day 720 = 0.039"(½) + 1.14×(1.989"/3) = 0.775"

**At $LC_{0.25}$ (at ¼ point):**

Adjustment "LC" at 0-day = -0.234" × ¼ = -0.058"
$\delta_{LC0.25}$ = $LC_{0.25}$ – (Adjustment "LC" × ¼)
= 1.044"- (-0.058)"
= **1.102"**

Day 30 = Adjustment "LC" × ¼ + 2.17×($\delta_{LC0.25}$/3)
= -0.041"(¼) + 2.17×(1.102"/3) = 0.787"
Day 60 = -0.027"(¼) + 1.98×(1.102"/3) = 0.721"
Day 90 = -0.017"(¼) + 1.86×(1.102"/3) = 0.679"
Day 120 = -0.010"(¼) + 1.77×(1.102"/3) = 0.648"
Day 180 = 0.001"(¼) + 1.63×(1.102"/3) = 0.599"
Day 240 = 0.008"(¼) + 1.53×(1.102"/3) = 0.564"
Day 360 = 0.020"(¼) + 1.38×(1.102"/3) = 0.512"
Day 720 = 0.039"(¼) + 1.14×(1.102"/3) = 0.429"

The camber diagram and time-dependent camber table for the hinge span are shown below (Figure 14)

| TIME-DEPENDENT CAMBER TABLE | | | | | |
|---|---|---|---|---|---|
| Elapsed time measured from prestressing the short cantilever until load transfer of long cantilever | Span Hinge 1 Hinge | | | | |
| | Long Cantilever Camber (mm) | | | Long Cantilever Camber "LC" (mm) | Short Cantilever Camber "SC" (mm) |
| | 1/4 LC | 1/2 LC | 3/4 LC | | |
| 30 days | 20 | 36 | 31 | 5 | -1 |
| 60 days | 18 | 33 | 29 | 5 | -2 |
| 90 days | 17 | 31 | 27 | 5 | -2 |
| 120 days | 16 | 30 | 26 | 4 | -3 |
| 180 days | 15 | 27 | 24 | 4 | -3 |
| 240 days | 14 | 26 | 23 | 4 | -4 |
| 360 days | 13 | 23 | 21 | 4 | -4 |
| 720 days | 11 | 20 | 17 | 4 | -5 |

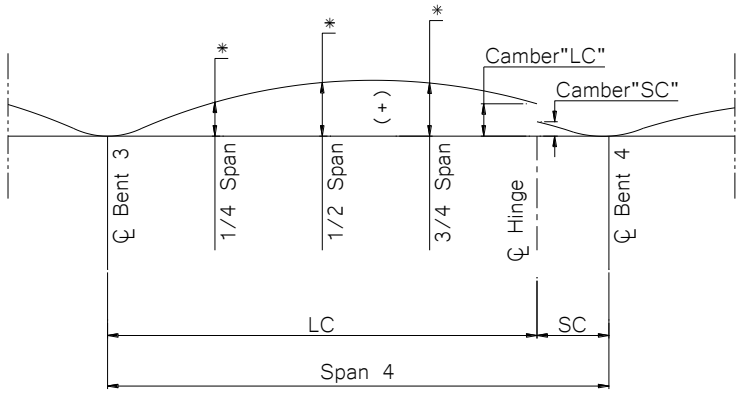


Camber Diagram
No Scale

Notes:

1. Camber diagram does not include allowance for falsework settlement.
2. For Camber "SC" and Camber "LC" vlaues, see "Time Dependent Camber Table".

* Denotes time dependent camber values along the long cantilever. See "Time Dependent Camber Table".

**Figure 14: Camber diagram and time-dependent camber table**

## Construction Details and Recommendations

Although efforts are made to provide accurate time-dependent camber adjustments for hinge spans, it is prudent to provide construction details that accommodate variations to the final product. Therefore, it is recommended that designers provide an additional 1" of concrete cover for the top deck reinforcement so that grinding can be performed if necessary. The additional cover should extend over a distance no less than the full length of the hinge diaphragm.

When the long cantilever is CIP/PS, it is recommended to provide an upward camber of 0.2" at the edge of the long cantilever in addition to the calculated camber value at $LC_{1.00}$ from the aforementioned procedure. This additional camber is to account for the potential immediate downward displacement at the hinge caused by the jacking force.

If an outrigger bent is located at the far end of the adjacent span of an in-span hinge, it is recommended to provide an additional camber at the hinge for both short and long cantilevers. The additional camber is downward corresponding to an upward camber of the outrigger and vice versa. The additional camber is calculated as follows:

$$\text{Camber "SC"}_{\text{additional}} = \text{Camber "LC}_{1.00}\text{"}_{\text{additional}} = \frac{\Delta_{\text{outrigger}}}{L_4}\left(L_3 + \frac{C}{2}\right)$$

Where,
$\Delta_{outrigger}$ = Camber of the outrigger beam at the center of the bridge